Establishing a flow-based system for repressing target gene expression in a microfluidic device using a glioblastoma spheroid model

Ines Hosni Ep Ben Daoud
Student number: 201851690

Supervisors: Prof John Greenman

Dr Mark Wade

A dissertation submitted in fulfilment of the requirements of a

PhD in Genetics & Molecular Biology

Hull University, Faculty of Health Sciences, Department of Biomedical Sciences

June 2022

Abstract

Glioblastoma (GBM) is a deadly disease with poor prognosis. The gold standard treatment is surgery followed by chemoradiotherapy almost always including Temozolomide. Despite extensive research for new therapeutic approaches relapse after treatment still occurs in approximately 80% of patients. The median survival, after first diagnosis, remains at 15 months, with a 5-year survival rate still less than 5%. Translationally-relevant models are urgently needed to allow reliable identification and validation of new potential therapeutic targets. The current study aims to establish a microfluidic flow-based system for identifying targets via gene knockdown in a GBM spheroid model.

Two genes, *PRMT2* and *RAB21*, were chosen as suitable targets for doing knockdown experiments, following a review of the literature and demonstration that both were expressed in the U87 GBM cell line. Gene knockdown was initially undertaken using lipofectamine based siRNA transfection of U87 cultured in monolayer, 3D static and 3D flowing systems. Gene expression was assessed by qPCR whereas western blotting and MTS assays were used to measure protein expression and cell proliferation, respectively. Accell™ siRNA, a chemically modified form of siRNA, were used to try and improve the gene repression levels. Finally, a comparison of the whole transcriptome profile between spheroids from three, independent, GBM cell lines was conducted both pre- and post-maintenance on the microfluidic device.

The microfluidic chip was demonstrated to successfully maintain GBM spheroids in a viable state for up to 7 days, during which the RNA yield was significantly higher compared to the 3D static conditions for three independent genes (*PRMT2*, *RAB21* and *FUS*). Respectively, *PRMT2* and *RAB21* siRNA silencing levels showed a gradual decrease from monolayer (75.66±5.13% vs 86.33±9.01%), to 3D static (43.00±24.75% vs 59.00±4.58%) and 3D flow system (26.33±2.51% vs 19.67±8.02%) using 5nM of siRNA. Gene repression of *PRMT2* and *RAB21* had no effect on the protein expression or on the proliferation rate. This study also showed that Accell siRNA was effective in inducing gene silencing in U87 spheroids maintained in static conditions (with 1%FBS, 49±0.09% of *FUS* knockdown level and 29.71±0.03% of protein depletion using 0.5µM of Accell siFUS).

Next Generation Sequencing analysis of the transcriptome of three GBM cell lines showed that the correlation in gene expression pattern was higher between two patient derived cells (PDCs) than between them and U87. Furthermore, PDCs presented a heterogeneity in activated and deactivated pathways similar to developing tumour tissues, compared to U87 which was characterised by a predominance of pro-proliferative pathways. In addition, gene ontology and Kyoto Encyclopedia of Genes and Genomes enrichment analysis demonstrated that GBM spheroids when cultured in the microfluidic system compared to the static conditions, exhibited a more *in vivo*-like profile by activating pathways considered as hallmarks of cancer. These included pathways and cellular functions involved in: proliferation, inflammation, metabolism dysregulation, senescence, necrosis, and invasion.

In conclusion, this study showed that siRNA mediated gene knockdown was successful in the 3D flowing microfluidic platform, however no effects were observed on protein expression or cell proliferation; this may be due to the half-life of mRNA and will require additional study. Furthermore, PDCs spheroids cultured in this flow system compared to static state, exhibited properties more comparable to that of *in vivo* tumour tissues. Further investigation using a range of other genes or comparing spheroids with primary human tissue would be likely to give additional evidence about the effectiveness of the current flow system for mimicking the *in vivo* microenvironment.

Thesis associated presentations

Ines Hosni; Victoria Green; Mark Wade; John Greenman (2022). siRNA gene knockdown and differential gene expression profiling of glioblastoma spheroids cultured in a microfluidic vs. static system. (Poster) Cancer Research UK Brain Tumour Conference London 2022

List of contents

Table of figures

Table of tables

Abbreviations

2D	Two dimensional
3D	Three dimensional
5- ALA	5- aminolevulinic acid
ANOVA	Analysis of variance
ATCC	American Type Culture Collection
ATP	Adenosine triphosphate
BBB	Blood brain barrier
BCL	B-cell lymphoma 2
BER	Base excision repair
BRCA	Breast cancer
BSA	Bovine Serum Albumin
CNS	Central nervous system
CO2	Carbon Dioxide
CRUK	Cancer Research UK
CSCs	Cancer stem cells
CSF	Cerebrospinal fluid
CXCR4	Chemokine (C-X-C motif) receptor 4
DDR	DNA damage response
DMEM	Dulbecco's Modified Eagle's Medium
DMSO	Dimethylsulphoxide
DNA	Deoxyribonucleic acid
dNTP	Deoxynucleoside triphosphates
DSB	Double strand break
DSBR	Double strand break repair
dsDNA	Double stranded DNA
EBV	Epstein Barr Virus
ECACC	European Collection of Authenticated Cell Cultures
ECM	Extra cellular matrix
EDTA	Ethylenediaminetetra Acetic Acid
EGFR	Epidermal growth factor receptor
EMT	Epithelial mesenchymal transition
ERBB2	V-erb-b2-erythroblastic leukaemia viral oncogene homolog 2
FBS	Foetal bovine serum
FDA	Food and Drug administration
GBM	glioblastoma
GBM58	G58
GBM63	G63
HEPES	4-(2-Hydroxyethyl) Piperazine-1-Ethanesulfonic Acid
HIF	Hypoxic inducible factor
HIF1α	Hypoxia inducible factor 1α
HNSCC	Head and Neck Squamous Cell Carcinoma
HR	Homologous recombination
HRP	Horse radish peroxidase
HUVECs	Human umbilical vein endothelial cells
IDH1	Isocitrate Dehydrogenase 1

IFN-γ	Interferon-gamma
IL	Interleukin
kDa	kilo Dalton
M	Molar
MGMT	O6-methylguanine-DNA methyltransferase
min	Minutes
miRNA	Micro Ribonucleic Acid
MMR	Mismatch repair
mol	Moles
mRNA	Messenger Ribonucleic Acid
MRP	Multidrug resistance protein
NADPH	Nicotinamide Adenine Dinucleotide Phosphate (Reduced)
NF1	Neurofibromin 1
NICE	National Institute of Clinical health Excellence
NK	Natural killer
NVU	Neurovascular unit
OS	Overall survival
PA	Pilocytic Astrocytoma
PARP	Poly (ADP-ribose) polymerase
PBS	Phosphate Buffered Saline
PCR	Polymerase chain reaction
PDGFR	Platelet derived growth factor receptor
PDMS	Polydimethylsiloxane
PEG	Polyethylene glycol
P-gp	P-glycoprotein
PIK3CA	Phosphoinositide-3-kinase catalytic alpha
PIK3R1	Phosphoinositide-3-kinase regulatory 1
PMMA	Polymethyl methacrylate
PTEN	Phosphatase and Tensin Homolog
PTPRD	Protein tyrosine phosphatase receptor type D
PVDF	Polyvinylidene fluoride
QALY	Quality adjusted life years
q-PCR	Real time polymerase chain reaction
RB1	Retinoblastoma 1
RNA	Ribonucleic Acid
RT-PCR	Real time polymerase chain reaction
SCC	Squamous Cell Carcinoma
SDS	Sodium dodecyle sulphate
SNP	Single Nucleotide Polymorphism
SSB	Single strand break
TBS	Tris-Buffered Saline
TBST	Tris buffered saline tween
TEMED	Tetramethylethylenediamine
TF	Tissue factor
TGF-β	Transforming growth factor beta
TIC	Tumour initiating cells
TLR	Toll-like receptor
TMZ	Temozolomide
TNF	Tumour Necrosis Factor
TP53	Tumour protein p53

ULA	Ultra-low attachment
VEGF	Vascular Endothelial Growth Factor
WHO	World Health Organization

Ethical approval

The majority of the work uses commercially available cell lines that were obtained from the European Collection of Authenticated Cell Cultures (ECACC). Human primary glial cells (GBM58) and (GBM63) were obtained from Dr Lucy Stead (University of Leeds); samples were taken with informed consent (NRES Ethical Approval Ref (15/YH/0080)) and transferred to Hull under a Technology Transfer Agreement.

Dedication

I would like to seize this opportunity to express my appreciation and gratefulness to all people that helped me to complete my PhD. I would like to dedicate this work to my Mum, Dad, my brother, and my sisters for their unlimited support during my PhD. I am extremely grateful to my sister Imen for her unconditional help and support she provided to me throughout my studies.

I further dedicate my work and give special thanks to my small family, my husband and my kids Yahya, Maryem and Nour. They all have been a great source of inspiration and motivation and for being my best cheerleaders.

Acknowledgements

I would like to express my special gratitude and thanks to my supervisors John Greenman and Mark Wade for their guidance and for imparting their knowledge and expertise in this study. My thanks and appreciations also go to Pedro Alvarez and Victoria Green for their helpful advice. I am very grateful to all members of the Brain Cancer research meeting for their valuable feedback and all lab members for their co-operation during my study period

Author's declaration

I declare that this work is original, and I am the sole author. Any passage(s) or diagram(s) been copied from academic papers, books, the internet, or any other sources, they are clearly recognized using quotation marks with fully cited reference(s). I certify that, this work does not breach the regulations of the University of Hull regarding plagiarism or academic conduct in examinations. I have read the Code of Practice on Academic Misconduct and confirm that this work does not contain any unacknowledged work from any other sources.

Chapter 1.
Introduction

1.1 Overview of Glioblastoma

Gliomas are the most common malignant primary brain tumour in adults, and they are classified according to their assumed cell of origin (Lapointe et al., 2018). They can be subdivided into: oligodendrogliomas, astrocytic tumours (astrocytoma, anaplastic astrocytoma and glioblastoma (GBM)), ependymomas, and mixed gliomas (Holland, 2000; Maher et al., 2001; Schwartzbaum et al., 2006; Agnihotri et al., 2013). Astrocytomas are the most frequently occurring tumours of the central nervous system (CNS), accounting for almost 80% of all malignant primary brain tumours (Schwartzbaum et al., 2006; Agnihotri et al., 2013; Messali et al., 2014). GBM is a malignant brain neoplasia occurring in the cells which are responsible for supplying O_2 and nutrients to the neurons, it is considered a grade IV astrocytoma due its aggressive and highly proliferative nature (Lukas et al., 2019), confirmed recently with the molecular characterization (Louis et al., 2021). GBM account for more than 60% of all brain tumours in adults (Taylor et al., 2019).

Glial cells had been considered as "non-functional glue" for neurons for decades (Garcia-Segura & McCarthy, 2004; Jäkel & Dimou, 2017). Until recently many functions of the different glial cells both under physiological and pathological circumstances remained unresolved (Jäkel & Dimou, 2017). However, a number of functions were reported relatively recently, including a role in the processes of neuroinflammation and brain injury in which they act as the first line defence of the central nervous system (Loane & Kumar, 2016). In addition to their contribution in the maintenance of blood brain barrier, these cells play critical roles in many physiological processes such as neurogenesis, transport of nutrients and elements essential for the function and survival of neurons as well as participating in synaptic transmission and plasticity (Garcia-Segura & McCarthy, 2004; Jessen, 2004; Perez-Catalan et al., 2021).

1.1.1 Glial cells

There are two major cell types in the CNS: neurons and glial cells. Glial cells are the most abundant in the nervous system forming nearly half of the volume of the brain (Gosselin et al., 2010). Until 2009, glial cells were considered to be outnumbering neurons in human brain with glia:neuron ratio of 10:1. New data using an isotropic fractionator counting method revised this figure to a ratio of glia to neurons of 1:1; with a range of 40 –130 billion glial cells in total (Herculano-Houzel & Lent, 2005; Bartheld et al., 2016; Neves et al., 2019).

Glial cells in the CNS are divided into two main groups, micro- and macroglia; they differ functionally and phenotypically as illustrated in (**Figure 1.1)**.

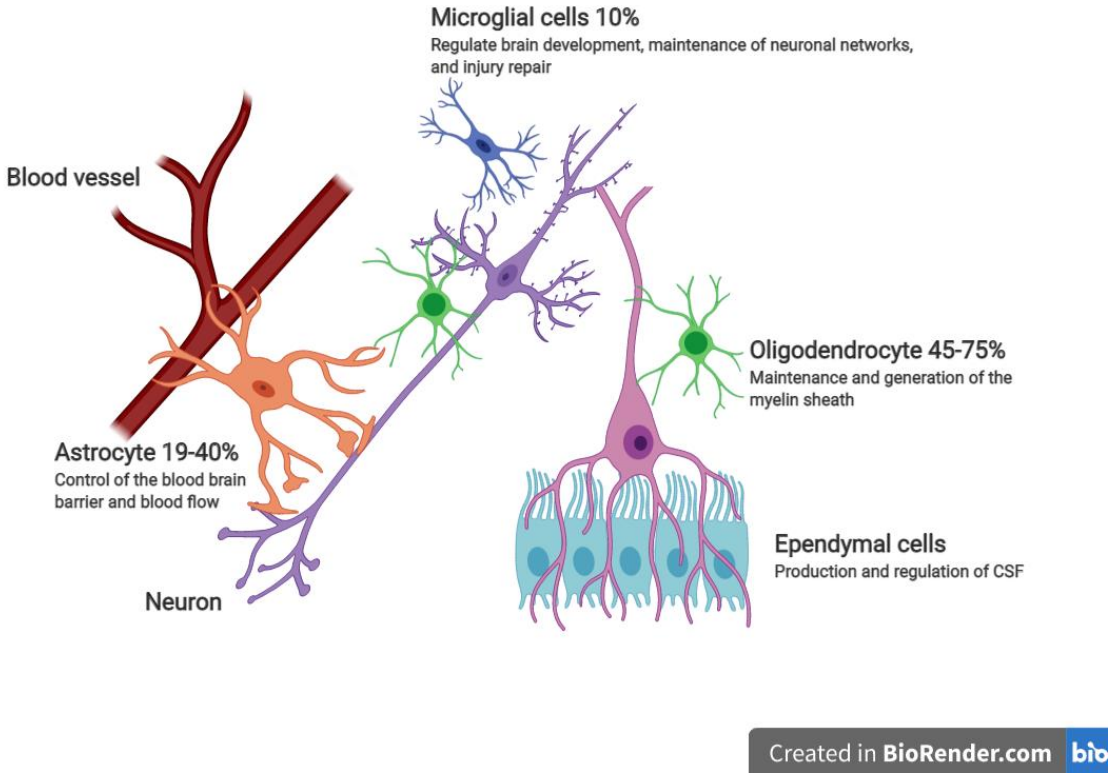

Figure 0.1 Different types of glial cells in the adult brain

Astrocytes make contacts with neurons and blood vessels and appear to be tightly associated with synapses. Microglial cells constantly scan the CNS *for plaques, damaged neurons, and unnecessary synaptic structures. Resting microglia show a characteristic ramified morphology whereas on activation exhibit a transformed, amoeboid-like, phenotype. Macroglia include ependymal cells, oligodendroglia, and astroglia. Glia cells ratios are according to Bartheld et al. (2016). Functions of different glial cells are reported from Jiménez et al., (2014); Colonna & Butovsky,(2017); Gordon & Woodruff, (2017) and Kim et al., (2019). CSF: cerebrospinal fluid. Image created in Biorender.com.*

1.1.2 The Microglial Cell

Microglia, constitute around 10% of CNS glia (Hanisch & Kettenmann, 2007; Soulet & Rivest, 2008). It was well demonstrated that microglial cells arise from yolk sac (YS)-primitive macrophages (Ginhoux & Prinz, 2015). They are derived from erythromyeloid -progenitors and enter the vertebrate CNS early in development at the onset of neurogenesis where they proliferate and migrate to colonise the spinal cord and entire brain (Ginhoux & Prinz, 2015). Two key functional characteristics define microglia: first immune defence (Lehnardt, 2010) secondly maintenance of CNS homeostasis (Blank & Prinz, 2013).

Recent *in vivo* time-lapse imaging has revealed dynamic interactions between microglia and neurons in the brain following lesion or injury. Detection of signals of external danger from invading pathogens mediated by pathogen associated molecular patterns (PAMP) which bind to Toll-like receptors (TLRs) (Davalos et al., 2005; Nimmerjahn et al., 2005; Lehnardt, 2010), or internal danger signals generated locally by damaged or dying CNS cells releasing endogenous molecules (such as HSP60) which binds to TLR expressed on microglial cells (Bessis et al., 2007; Hanisch & Kettenmann, 2007) initiate microglial activation. These cells proliferate, change shape, and become phagocytic in order to try and resolve the injury or protect the CNS from the effects of the inflammation, and support tissue repair and remodelling (Goldmann & Prinz, 2013).

Even though these cells represent an important component of the CNS, it is believed that their activity can be neurotoxic and potentially result in long term damage. Proinflammatory cytokines (such as TNFα), as well as nitric oxide released upon activation of microglial cells have been demonstrated to have toxic and deleterious effect on neurons (Bachiller et al., 2018). In parallel, many studies have reported that media taken from primary microglial cultures are neurotoxic to cultured neurons. These studies demonstrated that molecules responsible for neuronal cell death include small-molecular-weight microglial neurotoxin such as nitric oxide and glutamate (Yuste et al., 2015; Haroon et al., 2017; Almeida et al., 2020). For this reason, medical intervention in response to brain injury often involves factors that inhibit microglial activity (Fu et al., 2018). Molecules targeting microglial activation and neuroinflammation include microglial inhibitors, and other molecules targetting TLR, ATP receptors, cytokines, and MAP kinases. Although effective, these drugs may have side effects such as increased rates of infection, especially after long term treatment (Chen et al., 2018).

1.1.3 The Macroglial Cell

Macroglia include ependymal cells, oligodendroglia, and astroglia in the CNS and Schwann cells and satellite cells in peripheral nervous system (PNS). Here the focus will be on macroglial cells in the CNS.

Ependymal cells are epithelial, multi-ciliated, cells lining the cavities of the CNS including the cerebro-spinal fluid (CSF)-filled ventricles in the brain and the central canal of the spinal cord (Silva-Alvarez et al., 2005). According to their location, ependymal cells display structural differences, such as the bi- and uni-ciliated ependymal subtypes that have been found in the third ventricle floor (Mirzadeh et al., 2017). Ependymal cells (choroid

plexus) are involved in the creation and secretion of CSF and help circulate it by beating their cilia. They participate also in the creation of the blood brain barrier (BBB) and the blood-cerebrospinal fluid barrier (BCB) (Lukas et al., 2019). Genzen et al., (2009) reported that the maintenance of a proper ependymal layer in both physiological and pathological conditions, is performed by astrocytes through a repair mechanism probably stimulated by purinergic signalling.

Oligodendroglias are morphologically like astrocytes, but they are smaller in size and with fewer, less branched, processes (Jauregui-Huerta et al., 2010). The main function of these cells is the formation and maintenance of the myelin sheaths of the CNS. While Schwann cells serve this role in the peripheral nervous system, oligodendrocytes are found to extend out from the brain to the proximal segments of the cranial nerves (and even covering the entire optic nerve) (Luca et al., 2018). While one Schwann cell forms myelin for a single axon, oligodendrocytes can provide myelin for up to 50 axons (Baumann & Pham-Dinh, 2001). Oligodendrocytes are characterized by a high iron content, and they are highly vulnerable to low oxidant level (oxygen species). However, it was demonstrated that once mature, oligodendrocytes are relatively unable of myelinating axons (Bradl & Lassmann, 2010).

In addition, studies have demonstrated that oligodendroglia synthesize and provide trophic signals to nearby neurons, suggesting their importance in the regulation of proliferation, differentiation, and survival of neurons (Fields & Stevens-Graham, 2002). More recently, it was reported that oligodendrocytes represent the majority of glial cells in the cortical grey matter, as in the white matter, not astrocytes (Pelvig et al., 2008; Bartheld et al., 2016).

A detailed study of the cellular content of the grey matter of the human cerebral cortex demonstrated that astrocytes only comprise19-40% of the glial cells (Bartheld et al., 2016). According to their morphology, location, and function, classical neurohistologists divided astrocytes into two main classes. Fibrillary (or fibrous) astrocytes, which have long, slender arms that branch less frequently, are located primarily in the white matter in contact with nodes of Ranvier. In comparison the protoplasmic astrocytes, which have thick projections with lots of branches, are found in the grey matter closely associated with synapses (Stevens, 2003; Tabata, 2015). Protoplasmic grey-matter astrocytes secrete the extracellular matrix (ECM) proteins (synaptogenic factor: thrombospondins) TSP1 and -2

whereas, the subventricular zone and fibrous white matter astrocytes secrete TSP4 (Chung et al., 2015).

Brain performance is highly dependent on astrocytes. Malfunctioning of these cells can lead to many brain diseases including Nijmegen breakage syndrome (NBS) (Meshulam et al., 2012; Barzilai, 2013; Siracusa et al., 2019a). Astroglia make direct contact with blood vessels, neurons, and other glial cell types and astrocytic processes may extend beyond a 50μm radius; allowing them to exert loco-regional control. However, the activity of distant neurons integrated in different neuronal circuits is affected by the propagation of Ca^{2+} waves through networks of astrocytes, which release signalling molecules such as ATP (Araque et al., 1999; Araque et al., 2001; Guerra-Gomes et al., 2018).

It was demonstrated that astrocytes release their own transmitters that act on adjacent neurons and regulate their function, suggesting a bidirectional signalling pathway between astrocytes and neurons (Kurosinski & Götz, 2002; Matejuk & Ransohoff, 2020). Furthermore, astrocytes perform many other functions regulating synaptogenesis, cerebral microcirculation, extracellular pH and ion concentration, haemostasis and synaptic networks (Araque et al., 2001; Caudle, 2006; Siracusa et al., 2019b).

1.1.4 World Health Organisation (WHO) Grading and Classification

Brain tumours, like all other malignancies, can be subdivided into different stages, considering the size of the tumour, the level of penetration and spread to the adjacent lymph nodes or distant organs. The TNM staging system is most commonly used, where 'T' stands for tumour, 'N' for lymph nodes and 'M' for metastasis. Thus far, five stages have been described (Galon et al., 2012; Lapointe et al., 2018) (**Table 1**).

Table 0.1 Median age at diagnosis, average 5- and 10-year survival rate of selected primary brain tumours in adults

	Median age at diagnosis (years)	5-year survival rate*	10-year survival rate*
Pilocytic astrocytoma (WHO I)	12	94%	>90%
Oligodendroglioma (WHO II)	43	81%	65%
Diffuse astrocytoma (WHO II)	48	50%	40%
Anaplastic oligodendroglioma (WHO III)	50	57%	43%
Anaplastic astrocytoma (WHO III)	53	30%	20%
Glioblastoma (WHO IV)	64	5·5%	NA
Ependymoma (WHO I-III)	45	83%	Close to 80%

(Lapointe et al., 2018) *TNM, tumour-node-metastasis.

The current international standard for the grading of gliomas is the World Health Organization (WHO) classification (Vigneswaran et al., 2015). It classifies gliomas into grade I to IV based on the level of malignancy determined by the histopathological criteria. Grade I gliomas refer to lesions that have low proliferative ability and these are usually cured by surgical procedure, while grade II to IV gliomas are highly malignant and invasive. GBM is the most aggressive, invasive, and undifferentiated type of tumour and has been defined as Grade IV astrocytoma by WHO (Jovcevska et al., 2013; Hara et al., 2019). Recently, Louis et al., (2021), reported that CNS WHO grading system is no longer restricted to histological characteristics. Molecular parameters such as IDH status are critical, thus now in some cases of GBM they are designated as grade IV due to gene status, even though they appear histologically of a lower grade.

The word "multiforme" that used to be added to the name of glioblastoma, refers to the heterogeneity of this kind of cancer regarding clinical presentation, pathology, genetic signature, and response to treatment (Iacob & Dinca, 2009). The term is no longer use in nomenclature for GBM, but it has been reused in the twenty-first century in regard to the genotypic diversity of this neoplastic entry (Stoyanov et al., 2018). GBM can arise *de novo* (primary) or from a lower-grade tumour (secondary), (Bralten & French, 2011). The most common are the primary GBM which occur usually in patients aged over 50 years and commonly show the following genetic aberrations: deletion of phosphatase and tensin (PTEN) homologue genes on chromosome 10, p16 deletion, and loss of heterozygosity on chromosomes 10q and 17p (Yoshida, 1996, Zhang et al., 2019).

Although most cases are primary GBM with a higher prevalence in elderly people (Minniti et al., 2019), secondary GBM are more common among younger patients (mean age 40) (Tamimi & Juweid, 2017). They arise as low-grade tumours and they progress to full-blown GBM; these are commonly associated with mutations in the p53 tumour suppressor gene, abnormalities in the p16 and retinoblastoma pathways and aberrations in the DNA copy number (Mansouri et al., 2017).

Molecular profiling has allowed for more refinement of GBM classification and is now a fundamental part of the diagnosis of malignant glioma (Louis et al., 2001; Vigneswaran et al., 2015; Zhang, Pei et al., 2020). Patients are classed into one of three subgroups based on the absence or presence of mutations in the isocitrate dehydrogenase *IDH1* or *IDH2* genes (Lukas et al., 2019). Primary GBM which are *IDH* wild-type, account for more than 90% of cases (Ohgaki & Kleihues, 2007), with secondary glioblastoma bearing

IDH-mutations accounting for the remaining 10% of patients and can harbour a mutation in either *IDH1* or *IDH2* genes (Lukas et al., 2019). IDH mutation analysis is now adopted as a routine method to classify gliomas and an independent prognostic marker, and especially *IDH1* in combination with *p53* is now considered as an extremely helpful markers for differential diagnosis of reactive gliosis and low-grade astrocytoma (Geramizadeh et al., 2021).

Primary and secondary glioblastomas were regarded in the past as the same clinical entity. However, recent studies indicate that IDH-mutated glioblastomas have a more protracted natural course. As such, secondary glioblastomas are to be categorized as a distinct biological and molecular subgroup for which different treatment strategies are being investigated (Lukas et al., 2019). Recent study shows that *IDH1* mutation may not be a prognostic factor for survival of patient with GBM (Tabei et al., 2021).. This study report that the median overall survival between mutant and wild type *IDH1* groups was not statistically significant at the first progression (10.1 vs 10.5 months) and become significantly different at initial diagnosis (47.5 vs. 18.3 months, respectively)

1.1.5 Epidemiology

CNS cancer is responsible for 227,000 deaths around the world with an age-standardised death rate of 3.24 per 100,000 person-years. This rate has not changed significantly between 1990 and 2016. CNS cancer was responsible for 7.7 million disability-adjusted life-years (DALYs) globally, with an age-standardised rate of 105.05 DALYs per 100,000 person-years. DALYs are calculated by adding years lived with disability (YLD) to years of life lost (YLL). YLL is calculated by taking away the current age from the years of life expectancy. The age-standardised DALY rate for CNS cancer between 1990 and 2016 decreased by 10%, which was not considered significant (GBD 2016 Brain and Other CNS Cancer Collaborators, 2019). In England, for comparison, the age-standardised rate of DALYs per 100,000 person in 2017 for breast, kidney and pancreatic cancer are respectively 297.6, 78.1 and 162.4 (GBD 2017 DALYs and HALE Collaborators et al., 2018).

East Asia was the region with the highest number of cases of CNS cancer for both sexes in 2016 (108,000), followed by Western Europe (49,000), and South Asia (31,000). According to the same study, the three countries with the highest number of cases were China, the USA, and India (GBD 2016 Brain and Other CNS Cancer Collaborators, 2019).

As was said previously GBM is mostly diagnosed at an older age with a median age of 64 years at diagnosis (Ostrom et al., 2013; Ladomersky et al., 2019). The frequency increases with age reaching a peak at 75–84 years and then drops (Ostrom et al., 2013). At diagnosis, the age is likely to be higher for primary GBM (mean age of 55) than for secondary GBM (mean age of 40 years; Wilson et al., 2014). GBM is uncommon in children and its incidence is higher in males than in females with a mean male to female ratio varying from 1.0 to 1.9 (Ostrom et al., 2013; Das & Kumar, 2017; Tian et al., 2018).

In the UK, there are every year about 12,100 new brain, other CNS, and intracranial tumour cases: about 33 every day. This kind of tumour is the 9th most common cancer in the UK, accounting for 3% of all new malignancies. Rates in males have increased by 8%, and rates in females have risen by around approximately 25%. Frequencies for brain tumours are projected to continue to rise by 6% in the UK between 2014 and 2035, to 22 cases per 100,000 individuals by 2035. Survival for brain cancer in England is highest for younger people diagnosed aged under 40 years old. For this age range, around 60 % of patients in England diagnosed with brain cancer survive their disease for five years or more, compared with only 1% of people diagnosed aged 80 and over. Overall, each year around 130 children and young people (aged 0-19) in the UK lose their lives to a brain tumour. In adults just 15% survive for five years or more after the diagnosis of a malignant brain tumour (Cancer Research UK, 2021). It is estimated that over 55,000 people are currently living with a primary brain tumour in the UK (Thebraintumourcharity.org, 2020; Cancer Research UK, 2021; Hu et al., 2020).

1.1.6 Aetiology of GBM

As compared with other cancer types, there is relatively little known about the aetiology of brain tumours, and no fundamental carcinogenic causes have been reported (Hanif et al., 2017). So far, exposure to high doses of ionizing radiation is the only confirmed risk factor (Inskip et al., 2001; Bondy et al., 2008; Ohgaki, 2009). Large retrospective cohort data also shows a higher risk of glioma in younger populations after exposure to intracranial radiation for therapeutic reasons, where both patient age- and radiation dose/volume- are critical factors to be considered (Prasad & Haas-Kogan, 2009; Davis, 2016a; Lanese et al., 2018). Data in adults are more limited but show increased risk in certain groups exposed to radiation such as exposure of the Japanese population in Nagasaki and Hiroshima to atomic bomb irradiation (Douple et al., 2011).

However, information about the link between Chernobyl radiation emission and brain cancer is not so well established. This could be related to the protracted nature of this exposure where the main radioisotope responsible for contamination (Caesium-137) has a half-life of 30 years, and brain tumours can present 20 to 30 years after first exposure (Chia et al., 2017). In 2013, Dmytriw & Pickett, (2013) reported a case of GBM in a 39-year-old man 24 years after initial exposure to radiation emission in Chernobyl. In a relatively recent communication of Society for Neuro-Oncology and Oxford University Press, Chernobyl was considered as a relevant geo-historical factor of the increasing incidence of brain and CNS tumours population in England originating from Poland (neighbouring country to Ukraine where the Chernobyl accident happened, Chia et al., (2017)).

On the other hand, there is no conclusive correlation between GBM and environmental factors such as dietary risk factors, cell phone use or electromagnetic fields, occupational risk factors, severe head injury or pesticide exposure (Inskip et al., 2001; Ohgaki, 2009; Adamson et al., 2009; Agnihotri et al., 2013; Li et al., 2016). Recently, in a nationwide population-based cohort study, Ahn and colleagues demonstrated that smoking is associated with an increased risk of developing malignant glioma in a dose-dependent manner (Ahn et al., 2020).

Prognostic factors that can have an impact on the survival of GBM patients comprise the respectability of the tumour, its size, location, older age of the patient, as well as multifocality, comorbidities, and the patient's general condition (Nieder et al., 2005). Tumours in the brainstem or diencephalon are shown to be less amenable to surgical intervention and thus carry worse prognosis than supratentorial and cerebellar tumours (Coffey et al., 1988; Davis, 2018). Survival time of patients with unresectable tumours falls to a median time of only three months (Beauchesne et al., 2010), which was increased significantly with the improvement of clinical management and the introduction of targeted therapy. The use of targeted immunotherapy with durvalumab following platinum-based CRT has led to the improvement of progression free survival of unresectable stage III NSCLC patient from 5.6 to 16.8 months (Hansen et al., 2020).

The prognosis of glioma patients differs between histological subtypes and grades. For instance, patients with grade II have the longest survival (median survival 11.5 years) compared with patients with GBM (grade IV), have a median survival of only 4.9 months (Ohgaki & Kleihues, 2005). Pilocytic astrocytomas have the most favourable prognosis with approximately 96% five-year survival, (Ohgaki & Kleihues, 2005; Ostrom et al., 2015). Even

with greater understanding and modern therapies GBM remains a deadly disease with poor prognosis. The average survival time of GBM patient is short with a 1-year survival rate of only 37.2%, and a 5-year survival rate of 5.1% (Ostrom et al., 2015); median survival is ~10 months (Zhu et al., 2017).

Previous studies showed a positive prognosis with a prolonged postoperative survival in young patients diagnosed with GBM. The age of 40 is reported to be critical for GBM patients where 34 % of patients aged under 40 survived more than five years compared to only 6% for patients aged 40 years and older (Korshunov et al., 2005; Kleinschmidt-Demasters et al., 2006; Tamimi & Juweid, 2017). Moreover, an aggressive and multimodal treatment (not tolerated by older patients) is usually prescribed to younger GBM patients and thus the prognosis and survival rate are directly correlated with the age of patient at diagnosis (Walid, 2008). Despite the fact that age was considered a negative prognostic factor for high grade gliomas, a recent study demonstrated that when treated with extensive tumour resection associated to intraoperative multimodal imaging protocol, there was no statistically significant difference between elderly (>65 years) and younger (<65 years) patients (Barbagallo et al., 2020). This was explained by the improvement in new surgical strategy and technology which allow for extended safe resection and lower level of postoperative complications.

Marko et al., (2008) demonstrated that among 1478 differentially expressed genes between long-term and short-term GBM survivors, only 43 of them distinguished survival phenotypes and thus these were considered as a "fingerprint''. Moreover, *EGFR* amplification, loss of 9p21, and gain of chromosome 9 were associated with good prognosis for patients under the age of 40, whereas gain of chromosome 7 and loss of 10q23/*PTEN* were reported to have clinical significance only for patients aged 40 years and older (Aldape et al., 2015). Furthermore, cytogenetic and molecular genetic studies on GBM patients demonstrate a strong correlation between the presence of specific gene mutations and prognosis. Specifically, Burton's group reported that long term survival from GBM patients (>3 years) was characterised by the expression of *p53* gene while overexpression of the E3 Ubiquitin-Protein Ligase Mdm2 (*MDM2*) gene characterised patients with short term survival (<3years) (Burton et al., 2002).

A more recent study, analysing the transcriptome of 7 patients with GBM reported that decreased expression of Chitinase 3 Like 1 (*CHI3L1*), Fibulin 4 (*FBLN4*), Epithelial Membrane Protein 3 (*EMP3*), Insulin Like Growth Factor Binding Protein 2 (*IGFBP2*),

Insulin Like Growth Factor Binding Protein 3 (*IGFBP3*), Galectin 3 (*LGALS3*), Monoamine Oxidase B (*MAOB*), Podoplanin (*PDPN*), Serpin Family G Member 1 (*SERPING1*) and *TIMP* Metallopeptidase Inhibitor 1 (*TIMP1*) genes were all associated with prolonged survival (Jovcevska, 2019).

Research data shows that the adult human forebrain contains an abundant source of neural stem cells (Sanai et al., 2004) and that human GBM contain tumourigenic neural stem-like cells, suggesting that neural stem and/or progenitor cells are a plausible origin for human gliomas (Galli et al., 2004; Ignatova et al., 2002; Singh et al., 2004). These findings have given rise to hypothesis that more effective therapies could be based on approaches designed to target the stem cell-like component of GBM (Alves et al., 2021). Recent studies demonstrate that glioblastoma stem cells (GSCs) niches are formed as a copy of hematopoietic stem cell (HSC) niches in bone marrow. This similarity provides a basis for novel therapy strategy to sensitise GSCs by forcing them out from their niche in a similar way to that used against HSCs in acute myeloid leukemia (AML). In AML recent clinical trials have shown promising results with the removal of leukemic stem cells from HSC niches causing differentiation and proliferation, rendering them sensitive to chemotherapy (Hira et al., 2020).

1.1.7 Clinical Presentation

More than 50 % of the patients with GBM usually show a short clinical history which ranges between 3-6 months, nevertheless if the tumour develops from a low-grade astrocytoma, the clinical history can span several years (Hanif et al., 2017). Sometimes if symptoms develop rapidly, they may be misdiagnosed as a stroke (Omuro & DeAngelis, 2013) as there are similarities in presentation. Three different mechanisms are known to produce the different signs and symptoms present in patients with GBM.

First, there is the direct effect, in which the brain tissue is damaged as a result of necrosis giving rise to symptoms like focal neural deficit (eg. loss of speech, vision, and hearing up to 40-60%) and cognitive impairments. The regions of the brain which are affected by the tumour will characterize the signs and symptoms produced by the malignancy. For instance, patients showing visual and hearing problems indicate that a tumour is located in the temporal lobe area, whereas 20-40% patients present with a personality change as a consequence of tumour located in their frontal lobe, therefore impairing cognitive functions. If the tumour is large with considerable mass, it can give rise to imbalance in gait and incontinence (Faivre et al., 2015).

The increase in tumour size and oedema surrounding the tumour, can lead to an amplification of intracranial pressure and a shift of intracranial content. These physical changes in the intracranial environment result in headaches which are assumed as a hallmark feature in 30-50% of GBM patients (Hanif et al., 2017). Headaches are usually localized unilaterally with progressive severity, but with no specific pain pattern. These headaches may also be associated with other symptoms such as vomiting and papilledema, which are less aggressive if the disease is detected at an earlier stage (Omuro & DeAngelis, 2013). Generally, signs and symptoms of GBM tumours comprise cerebral oedema, seizures, osteoporosis, gastrointestinal tract disturbances, cognitive impairment, venous thromboembolism, and mood disorders (Thier et al., 2016). Finally, 20-40% of the cases may also present with seizures usually with a focal onset, which could be, depending on the tumour location, simple partial, complex partial or generalised seizures (Hanif et al., 2017).

1.1.8 Macroscopic and Histological Features of GBM

Macroscopically GBM presents as a heterogeneous mass which includes multifocal haemorrhage, necrosis, and cystic and gelatinous areas (Smith & Ironside, 2007; Agnihotri et al., 2013). Another characteristic feature of GBM is the variation in the appearance of the tumour from one region to the other. As a result of tissue necrosis, some of the regions appear as soft and yellow in colour, while some of the tumour areas appear firm and white and some other regions show remarkable cystic degeneration and haemorrhage **(Figure 1.2,** Hanif et al., (2017)). The tumour is usually characterized by a single, relatively large, unusual, shaped lesion which generally arises in the white matter (Nelson & Cha, 2003). GBM, histologically, resembles an anaplastic astrocytoma. These tumours show a pleomorphic cell population which varies from tiny, poorly differentiated, cancer cells to larger multinucleate cells with ‘’pseudopalisading’’ nuclei with multifocal necrosis and prevalent mitotic activity (Nelson & Cha, 2003). A major distinguishing feature is the association of endothelial cell proliferation with glomeruloid structures (Smith & Ironside, 2007; Agnihotri et al., 2013).

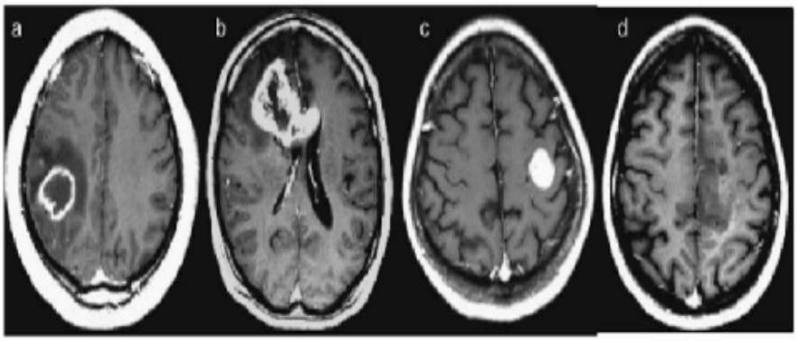

Figure 0.2 Anatomical heterogeneity of 4 different lesions for patients with GBM
Contrast-enhanced axial T1-weighted (TR, 600 msec; TE, 14 msec) MRI images show (a) rim-enhancing mass with central necrosis in the right parietal lobe with surrounding edema; (b) irregularly enhancing mass that crosses the corpus callosum; (c) well-circumscribed homogeneously enhancing mass in the left frontal lobe with no associated edema; (d) infiltrative mass in the left medial frontal lobe with no appreciable necrosis. Taken from Hanif et al., (2017).

1.1.9 Brain tumour locations

Regarding tumour location, data show that most gliomas are found in the cerebral lobes (86.0%). Gliomas located in the frontal lobe account for 40.0% of malignancies, temporal lobe for 29.0%, parietal lobe for 14.0%, and occipital lobe for 3.0% of the cases. Moreover, 6.4% were located primarily in the deep structures of the cerebrum, 2.2% in the ventricles, 1.5% in the cerebellum, and 4.1% in the brainstem (Larjavaara et al., 2007). Therapeutic approaches are affected by the tumour location as surgery is not an option in some areas of the brain (**Section 5.1**). Additionally, brain tumours are characterised by the presence of obstacles that limit the efflux of drugs to tumour cells, such as the BBB.

1.2 The Blood Brain Barrier

1.2.1 Basic brain anatomy

The brain is a highly organised organ in the human body. Its complex structure contains millions of neurons and their specialized projections called dendrites and axons. These terminals are supported by different cell types (oligodendrocytes, astrocytes, etc). The brain is divided into 2 principal regions, the cerebrum, and the cerebellum. The cerebrum is the largest part and is made up 2 hemispheres with 4 lobes: frontal, parietal, occipital and temporal **(Figure 1.3A).** Connected to the brainstem, the cerebellum is situated underneath the cerebrum. Filled with CSF, the ventricular system is a communicating network of cavities and located within the brain parenchyma (**Figure 1.3B)**.

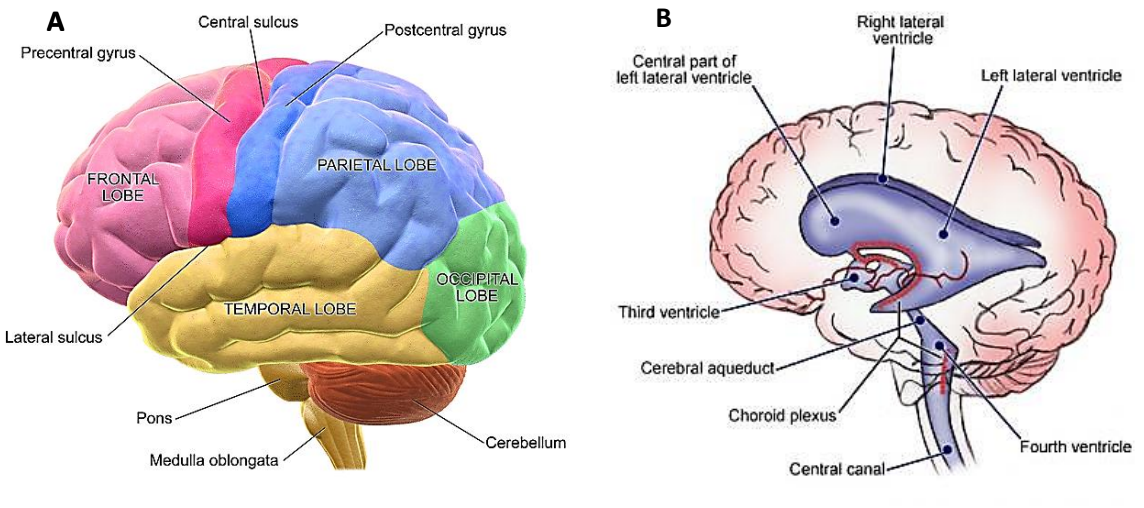

Figure 0.3 Basic anatomy of human Brain
A) a lateral view of the brain showing different lobes. B) the ventricular system of the brain. The choroid plexuses produce CSF and fills the ventricles and subarachnoid space (Figure adapted: 1.3A, from sciencetrends.com; and 1.3B from emedicine.medscape.com).

The brain is protected from physical injury by three structures: a 7 mm thick skull, meninges, and the CSF. It is also protected from disease-causing pathogens and toxins in the blood stream by the BBB. The BBB is represented by microvasculature of the CNS, including the BBB-endothelial cells, astrocyte end-feet, and pericytes (PCs) (Ballabh et al., 2004).

1.2.2 BBB - the security system of the brain

As stated above, the brain is a mixture of different types of neural cells (neurons) and non-neural cells (glial cells) as well as endothelial and immune cells, each with their own unique properties. These properties allow them to tightly regulate the exchange of molecules, ions, and cells from the blood to the CNS and vice versa (Zlokovic, 2008). All these cells are crucial for a normal functioning of the brain (Mota & Herculano-Houzel, 2014). In the CNS there are two main "gateways" for accessing the brain parenchyma: the blood and the CSF circulation (Chen & Liu, 2012). The exchange between blood and CNS is regulated through 3 major interfaces, the BBB, blood–CSF barrier and the arachnoid barrier (**Figure 1.4)**.

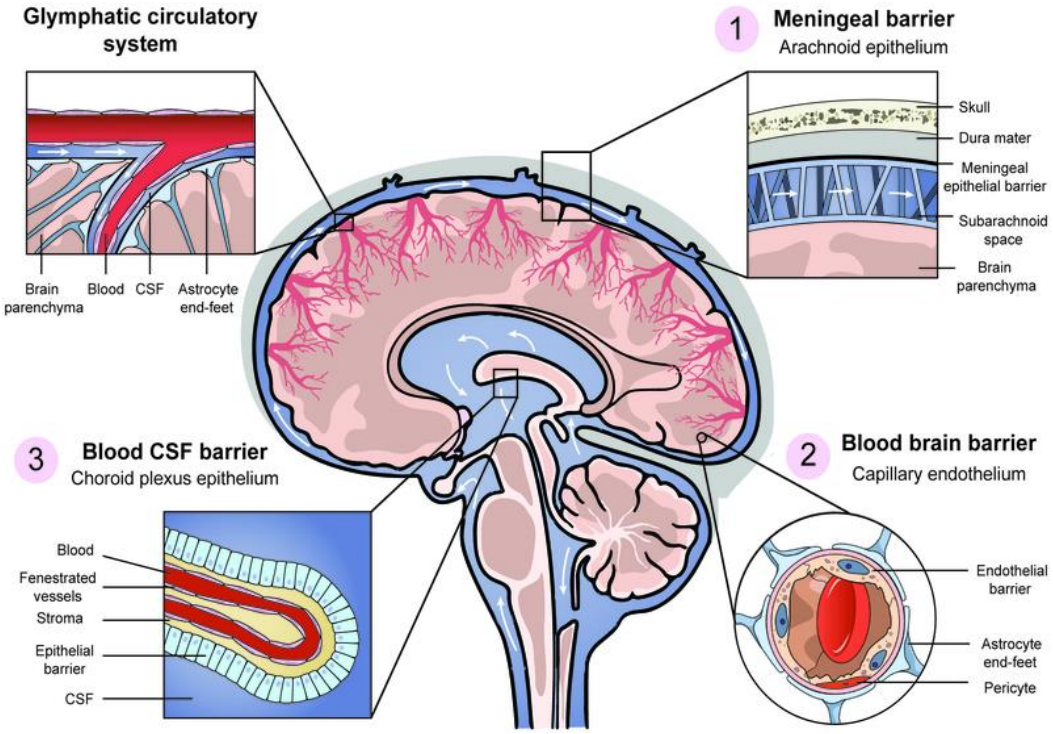

Figure 0.4 Central nervous system barriers
The three main zones of exchange between blood and brain each have a distinct barrier structure.(1) Meningeal barrier (arachnoid barrier) is an avascular multi-layered epithelium containing tight junctions forming an effective seal in the inner layer. (2) The BBB consist of tight junctions between cerebral vessels endothelial cells. (3) The blood–CSF barrier exists at the choroid plexuses in the brain ventricles (lateral, third and fourth ventricles) and consists of tight junctions formed between epithelial cells at the apical surface of the epithelium (CSF-facing surface). Taken from Ariel et al., (2017).

Since the first identification of the presence of a barrier between the CNS and the blood by Humphrey Ridley (Humphrey, 1695) and the seminal work of Lina Stern and collaborators in 1929 (Vein, 2008) to recent advances (Liddelow, 2011; Saunders et al., 2014; Bauer & Traweger, 2016; Haseloff et al., 2015), it has become clear that the BBB is the principal site for the exchange between these two body systems via its extensive branches of blood capillary networks (Chen & Liu 2012).

With the concept of neurovascular unit (NVU) adopted by (Hawkins & Davis, 2005), the BBB no longer only consists of endothelial cells but also includes pericytes, vascular smooth muscle cells, astrocytes, microglia and neurons (Lo & Rosenberg, 2009; Zlokovic, 2008; Segura et al., 2009; Daneman, 2012) (**Figure 1.5)**.

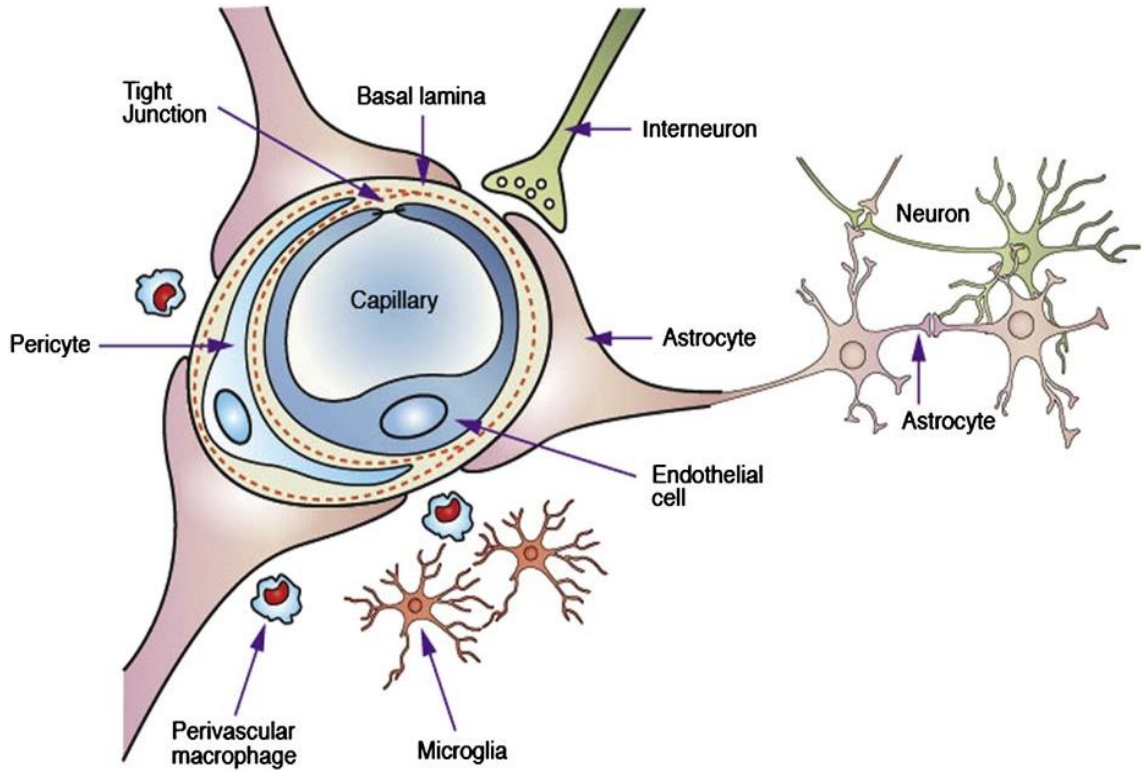

Figure 0.5 Neurovascular unit (NVU)

It includes endothelial cells of the central nervous system, pericytes, vascular smooth muscle cells, astrocytes, microglia, and neurons. Reproduced from Chen & Liu (2012).

1.2.3 Biological characteristics of the BBB

The highly selective permeability to molecules, represents the principal characteristic of the BBB. This feature can be attributed to its unique biological structures which includes: the absence of fenestration of endothelial tissue, the presence of tight junctions and the expression of transporter proteins.

1.2.4 The absence of fenestration of endothelial tissue

Endothelial tissue of the cerebral arterioles, especially at the BBB, is formed by a single layer of endothelial cells (EC) folded onto itself to form the lumen of the vessel (Aird, 2007). These EC are attached closely together by tight junctions (TJs), thus acquiring the characteristic of lack of fenestration which limits the paracellular flux of solutes (Westergaard & Brightman, 1973). The CNS EC undergo extremely low rates of vesicle-mediated transport of solutes (transcytosis) compared with peripheral EC, and the former also possess very few pinocytotic vesicles (Coomber & Stewart, 1985). This EC barrier consists of polarised cells with different luminal and abluminal membrane compartments allowing a

controlled movement of molecules using a regulated cellular transport properties (Betz & Goldstein, 1978; Betz et al., 1980).

Two categories of transporters are expressed on the CNS EC (**Figure 1.6)**. The first is on the luminal surface where the efflux transporters are responsible for the transport of different lipophilic molecules towards the blood (Cordon-Cardo et al., 1989; Löscher & Potschka, 2005; Thiebaut et al., 1989). The second represent the nutrient transporters which are highly selective transporters that facilitate the passage of specific nutrients to the CNS and the removal of waste products from the CNS into the blood (Mittapalli et al., 2010). It was reported that EC of CNS are highly metabolically active as they contain a greater number and volume of mitochondria compared to other EC of non-neural tissues (Daneman & Prat, 2015; Eelen et al., 2018).

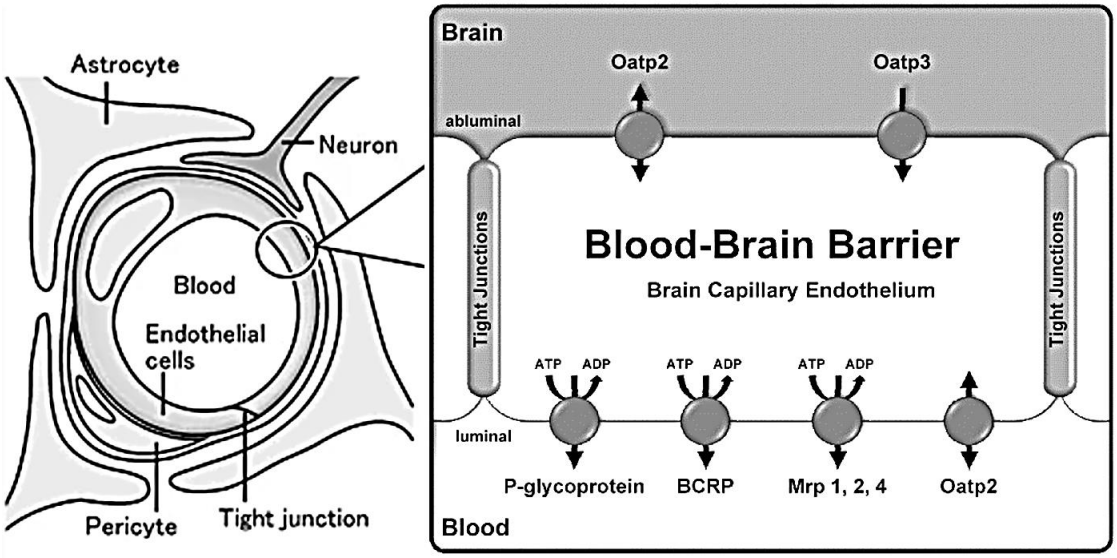

Figure 0.6 Schematic representation of endothelial cells of the blood brain barrier
The surface of the brain capillary endothelium cells facing the brain (abluminal) has different characteristics of that facing the blood (luminal) with expression of distinct transporters. Thus, creating a polarized cell and contributing to maximise the control of the exchange between the blood and the brain. The efflux and influx of product is shown by an arrow. Active transporters are marked with ATP/ADP hydrolysis. P-glycoprotein, Mrp 1, 2, and 4, and BCRP are expressed in the luminal membrane whereas the organic anion-transporting polypeptide 3 (Oatp3) has been detected only in the abluminal membrane. Oatp2 exist on both. Modified from Miller et al. (2008) and Ohtsuki & Terasaki (2007).

1.2.5 The presence of tight junctions (TJ)

TJ of CNS EC consist of two groups of membrane proteins. The first includes the transmembrane proteins (junctional adhesion molecule-1, occludin, and claudins) and the second includes the cytoplasmic accessory proteins (zonula occludens-1 and -2, cingulin, AF-6, and 7H6). Both groups are linked directly to the actin cytoskeleton (Hawkins & Davis,

2005), contributing thereby to the maintenance of structural and functional integrity of the endothelium. The presence of interaction of glial cells (astrocytes and pericytes) with CNS EC confer additional strength and maintenance for TJ (Persidsky et al., 2006).

1.2.6 The expression of transporter proteins

A group of various transporters is expressed on different effector cells of the BBB. Some of them contribute to the influx into the brain while others contribute to the efflux between the blood and the CNS conferring therefore a selective permeability of the BBB. Several key molecules include: GLUT1 glucose carrier, amino acid carrier LAT1, transferring receptors, insulin receptors, lipoprotein receptors and ATP belongs to a family of efflux transporters such as p-glycoprotein (P-gp) and multidrug resistance-related proteins MRPs (Rip et al., 2009; Abbott et al., 2006).

1.2.7 The immune system in brain

In his review, Wekerle and colleagues reported that the CNS is characterised by the absence of lymphatic drainage, and lack of major histocompatibility complex (MHC) antigens (Wekerle, 2002). It was demonstrated later that the BBB has a highly selective permeability for immune cells, especially for lymphocytes (Daneman & Rescigno, 2009). On the other hand, CNS EC express an extremely low level of leukocyte adhesion molecules (such as Activated leukocyte cell adhesion molecule (ALCAM)) thereby limiting the number of immune cells entering the CNS (Daneman et al., 2010; Lécuyer et al., 2017). It was demonstrated recently that glial cells are functioning as the immune system of the CNS, which can be activated in two different ways producing either cytotoxic or neuroprotective effects (Ronaldson & Davis, 2020; Huang et al., 2021).

1.2.8 Functions of CNS barriers

The BBB facilitates the entrance to the CNS of nutrients and oxygen and prevents neurotoxic products circulating in the blood from getting to the brain. The BBB regulates the CNS ionic composition maintaining it at levels optimal for synaptic signalling functions, through the action of a combination of specific ion channels and transporters (Kadry et al., 2020). It was demonstrated that despite changes of potassium concentration that can occur in plasma (naturally or experimentally) its concentration in mammalian plasma is maintained higher than in CSF and brain ISF by active astrocyte reuptake (around 4.5 mM and 2.5 to 2.9 mM respectively). Neurons undergo apoptosis when potassium concentration is kept at higher levels than normal in CSF (Hansen, 1985; Ghaffari et al., 2020). On the other hand,

Abbott et al., (2006) and Bernacki et al., (2008) have demonstrated that the BBB helps to keep the central and peripheral neurotransmitter pools separate, minimising "cross-talk".

The BBB function is also crucial in preventing many macromolecules from entering to the CNS and thereby providing a "safe" environment for the CNS cells. This is clear when comparing the protein content of CSF and the plasma (**Table 1.2)** as the CSF generally has a much lower protein content. Factor Xa and tissue plasminogen activator present in the brain convert pro-thrombin to thrombin and plasminogen to plasmin respectively. Thrombin and plasmin once in ISF, can induce seizures, glial activation, glial cell division and scarring, and cell death (Gingrich & Traynelis, 2000). Cystatin-C which is a serine protease inhibitor is highly concentrated in CSF (see **Table 1.2**) and is considered as a protective measure against micro-leaks in the BBB occurring continually and spontaneously (Reiber, 2001).

ATP-binding cassette transporters are one of the energy-dependent efflux transporters in the CNS. These transporters actively pump many of neurotoxic substances out of the brain. An increased access of neurotoxins into the brain could be lethal (Lim et al., 2007). Finally, it is interesting to note that the BBB has low passive permeability even for water-soluble nutrients and metabolites required by nervous tissue. Therefore, as it was explained above in **Figure 1.4,** the BBB express different specific transport systems to ensure an adequate supply of nutrients and metabolites. It was demonstrated that transporters facilitate the intake of nutrients including glucose and amino acids, whereas larger molecules including insulin, leptin, and iron transferrin are transferred to the brain via receptor-mediated endocytosis (Pardridge, 1999; Zhang & Pardridge, 2001). Polarity of CNS EC is a good example of regulation and establishment of concentration gradient (Abbott et al., 2006; Wolburg et al., 2009).

Table 0.2 Typical plasma and cerebrospinal fluid concentrations for some selected solutes

SOLUTE	UNITS	PLASMA	CSF	RATIO
NA^+	mM	140	141	~ 1
K^+	mM	4.6	2.9	0.63
CA^{2+}	mM	5.0	2.5	0.5
MG^{2+}	mM	1.7	2.4	1.4
CL^-	mM	101	124	1.23
HCO_3^-	mM	23	21	0.91
OSMOLARITY	mOsmol	305.2	298.5	~ 1
PH		7.4	7.3	
GLUCOSE	mM	5.0	3.0	0.6
TOTAL AMINO ACID	μM	2890	890	0.31
LEUCINE	μM	109	10.1–14.9	0.10–0.14
ARGININE	μM	80	14.2–21.6	0.18–0.27
GLYCINE	μM	249	4.7–8.5	0.012–0.034
ALANINE	μM	330	23.2–32.7	0.07–0.1
SERINE	μM	149	23.5–37.8	0.16–0.25
GLUTAMIC ACID	μM	83	1.79–14.7	0.02–0.18
TAURINE	μM	78	5.3–6.8	0.07–0.09
TOTAL PROTEIN	mg/ml	70	0.433	0.006
ALBUMIN	mg/ml	42	0.192	0.005
IMMUNOGLOBULIN G	mg/ml	9.87	0.012	0.001
TRANSFERRIN	mg/ml	2.6	0.014	0.005
PLASMINOGEN	mg/ml	0.7	0.000025	0.00004
FIBRINOGEN	mg/ml	325	0.00275	0.000008
A2-MACROGLOBULIN	mg/ml	3	0.0046	0.0015
CYSTATIN-C	mg/ml	0.001	0.004	4.0

(Reiber, 2001)

1.2.9 Structures in the brain that lack the BBB

Some regions of the brain lack BBB structure. These regions include area postrema, median eminence, neurohypophysis, pineal gland, subfornical organ, and lamina terminalis (**Figure 1.7**). The vascular endothelium in these areas is characterised by the presence of fenestration that permit passage of molecules across the vessel wall. Interestingly, these areas of the brain control the autonomic nervous system and endocrine glands of the human body (Ballabh et al., 2004). Notably, choroid plexus has a slight difference from the BBB in molecular composition of TJ in respect to claudins-2 and -5 (Wolburg et al., 2009).

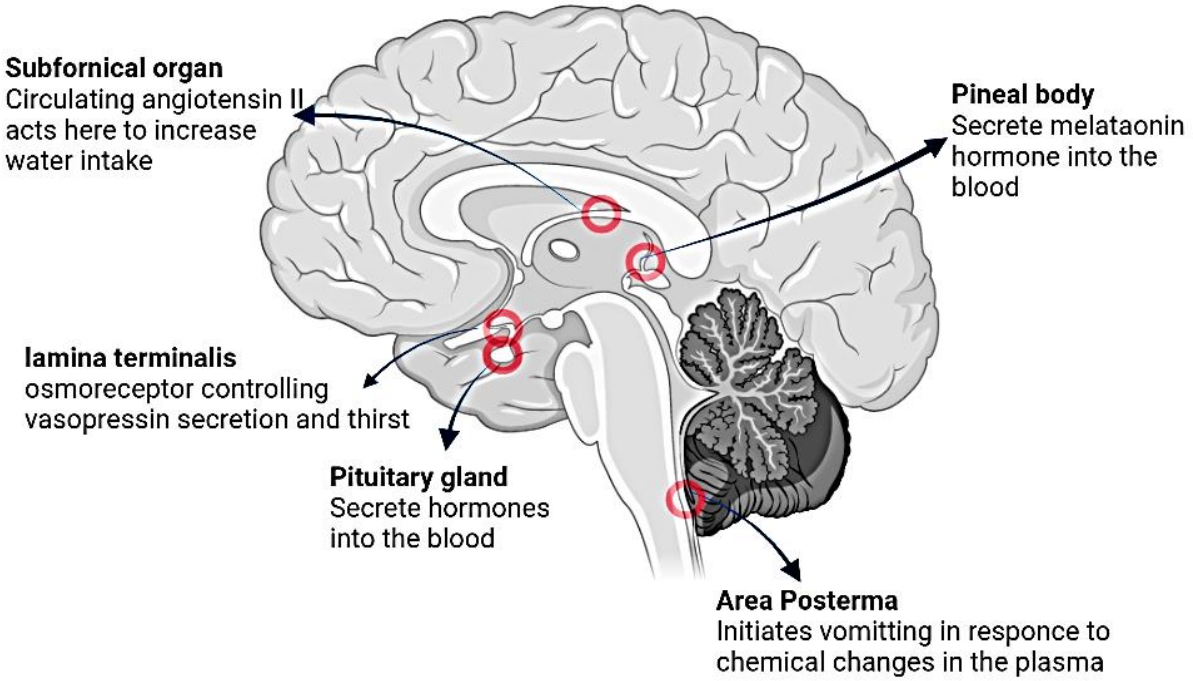

Figure 0.7 Regions of the brain that lacks the BBB structure and principal functions
Diagram created in Biorender.com.

1.3 Diagnosis of glioblastoma

The preliminary diagnosis of GBM is achieved by neuroimaging, followed by biopsy or resection of tumour tissue to ultimately diagnose, grade, and characterise the tumour (Müller Bark et al., 2019). Presently, tissue biopsies are the gold-standard procedure for GBM diagnosis. Nevertheless, resection or biopsy from a brain tumour can present risks to the patients, like potential brain swelling within and around the tumour mass or may possibly even affect neurological functions (Shankar et al., 2017). Additionally, some tumours might be inaccessible due to their location (Brill et al., 2005; Müller Bark et al., 2020). In summary, diagnosis of glioblastoma is done in three steps, first neurological exam followed by an

imaging test and finally tissue biopsy analysis before or during surgery (Silantyev et al., 2019).

1.3.1 Current Treatment Options

The main challenges in therapy of GBM are associated with the location of the tumour and its complex and heterogeneous biology (Kesari, 2011). Advances in surgical approaches, radiotherapy, and adjuvant chemotherapy have shown minimal improvements in survival and quality of life of the GBM patients and the prognosis is still disappointing.

The therapeutic strategy of newly diagnosed GBM usually involves a four-pronged approach. The initial approach for GBM is surgery, where maximal resection is associated with extended progression-free survival (PFS) and overall survival (OS) (Allahdini et al., 2010). In fact, resection alone is not usually a curative approach; hence, patients also undergo radiotherapy and chemotherapy as an adjunct (Vogelbaum, 2012) and recently in the USA a treatment of alternating electrical fields is approved to be used in combination with TMZ. The use of continuous alternating electric fields is approved by US Food and Drug Administration (FDA) under the name of "optune system" for the treatment of primary recurrent GBM (Branter et al., 2018; Lukas et al., 2019). The present standard of care for high-grade gliomas patients which is currently temozolomide in combination with radiotherapy in UK (Rominiyi et al., 2021), involves not only therapeutic standard management (i.e. anti-tumour therapy) but is also inclusive of giving effective supportive care to the patient (Renovanz et al., 2018).

1.3.1.1 Surgery

Surgery is the principal component of standard care (Ohka et al., 2012). Depending on the tumour type surgery can accomplish many things including reduction of tumour burden, control of seizures, reversal of neurological deficit, introduction of local therapeutic agent and improvement in quality of life (Hanif et al., 2017). The extent of surgical resection depends upon the site and extent of the brain area involved. Nevertheless, due to the invariably invasive nature of the tumour, even "complete" resection is not curative (Iacob & Dinca, 2009), and despite maximal surgical resection and adjuvant chemoradiation, relapse occurs in approximately 80% of cases usually within 2-3 cm of the margin of the original lesion and within 10 months in many cases. Recurrence after resection could also be due to the development of resistance to temozolomide mediated by resident cancer stem cells (Manrique-Guzmán et al., 2017).

However, in the case of newly diagnosed patients the extent of surgical resection holds prognostic worth (Scott et al., 2011), but again tumours that reside in sites like the cortex, brain stem or basal ganglia are not amenable to surgical intervention and these patients usually have worse prognosis (Mrugala, 2013).

Resection of GBM tumours is not limited to the area of enhancement, similarly to low-grade glioma, and it is extended to the area of increased T2/fluid-attenuated inversion recovery (FLAIR) signal. The durability of the effect of cytoreduction and whether it leads to a survival benefit, is likely related to the rate of tumour cell proliferation and the non-linear growth of tumour cells seen in glioblastoma which can quickly regenerate the tumour burden (Bette et al., 2017).

The tumour location can also reflect the underlying biology and influence the natural history of the disease. Resectable tumours, such as fronto-polar tumour, are present in "silent areas of the brain" (Friedlein et al., 2015). Tumours in these areas usually have *IDH1* mutations. On the other hand, unresectable tumours (midline/diencephalic or brainstem tumour), often carry H3K27 mutations, which reveal an overall more aggressive biology and a worse prognosis (Beiko et al., 2014; Chung et al., 2020).

To maximize the extent of resection safely, many technological advances have been developed with availability and usage greatly variable (reviewed in Lukas et al., 2019). These technologies are divided in three categories, as follows. The first is "intraoperative navigation technology" which involves the use of volumetric imaging (eg, CT scan or MRI). This technology is used as a reference to locate anatomical structure within the surgical field and allows real-time visualization of tools within the images. Even though the referenced images are not updated as resection progresses, the use of intraoperative ultrasound during surgery is easy to use, dynamic, and affordable alternative for real-time imaging (Napolitano et al., 2014; Fan et al., 2017).

The second technique is "electrophysiological monitoring and functional brain mapping". It is also called awake brain mapping and it was introduced to routine use by George Ojemann, Hugues Duffau, Mitchell Berger, and others. This technology based on monitoring motor, sensory, and language area functions, has greatly improved the surveillance of biological function of the brain by enabling them to be mapped and preserved (Ojemann et al., 2008; Sanmillan et al., 2017).

The third technique consist of the use of 'fluorescent markers' to maximize the tumour visualization. This is helpful, as tumour tissue is often very difficult to be distinguished from surrounding tissues under normal light conditions. The use of 5-aminolevulinic acid (5-ALA) in a phase III trial has demonstrated an improvement in OS compared with conventional microsurgery with white light (Stummer et al., 2006). The same result was obtained with fluorescein (Bowden et al., 2018). According to the national institute for health and care excellence (NICE) in UK, since July 2018, 5-ALA - known as the "pink drink" is recommended to be taken by patients prior to brain surgery (NICE, 2018).

1.3.1.2 Radiation therapy

Radiotherapy is the second step following surgical treatment, to kill remaining tumour cells. It has been shown to play a key role in treatment and improving survival in GBM (Scott et al., 2011). Chang and colleagues reported that the two main alternatives, brachytherapy and stereotactic radiosurgery, to be equally effective therapies against relapsed GBM (Chang et al., 2007) but not with newly diagnosed GBM where the effective standard of care is the surgical resection followed by concomitant radiotherapy and TMZ (Domingo-Musibay & Galanis, 2015). Later, Iacob & Dinca (2009) identified some limitations that could be associated with radiation therapy including the invasive nature of GBM, radiation-induced permanent neuronal damage, radiation necrosis and radio-resistance of some tumours.

The timing and type of radiation therapy the patient may receive, are determined by the type of glioma, its grade and other prognostic factors (Hartgerink et al., 2019). Radiation therapy options include:

- **Using computers to ensure delivery** of radiation treatment to the right location of the brain tumour. Techniques include 3D conformal radiation therapy and intensity-modulated radiation therapy.
- **Using protons rather than X-rays as a source of radiation. This technique is termed** conformal proton beam therapy. It delivers radiation only once proton beams reach the tumour. It causes less damage to surrounding tissue than X-rays.
- **Using multiple beams of radiation. This is to give a highly concentrated form of** radiation treatment. Despite its name, **stereotactic radiation therapy (radiosurgery),** this technique does not involve surgery in the traditional sense.

Side effects of radiotherapy depend on the type and dose of radiation the patient receive. Common side effects during or immediately following radiation include cognitive

deterioration, fatigue, headaches, and scalp irritation (Brown et al., 2016). These side effects are not unique to the GBM patients and though can generally be medically managed (Davis, 2016b). Many studies investigated the impact of timing of radiotherapy initiation on survival after surgery, but the results remain controversial (Noel et al., 2012; Sun et al., 2015). This is because this kind of study suffers from considerable bias such as the difficulty of finding homogeneous patient populations, following standardised treatment protocols, and ensuring tumours are of the same location

Recently, (Katsigiannis et al., 2019) conducted a study on newly diagnosed patients with GBM treated with the same therapeutic scheme. Patients were trichotomized based on the time interval from surgery until initiation of RT (< 28 days, 28–33 days, > 33 days). This study ended with the conclusion that timing of RT within a timeframe of up to 48 days postoperatively is not associated with worsened survival, rather a delay beyond this timeframe could be associated with worse OS. They suggest that RT should start promptly as soon as the patient has recovered from surgery.

In the UK and Western Europe GBM is treated with a cumulative absorbed dose of 60 Gy, spread as a daily dose of 1.8 to 2.0-Gy fractions for a total treatment that lasts approximately 6 weeks. Studies conducted with doses less than 60 Gy or up to 75 Gy have failed to demonstrate improved outcomes and could even lead to significantly worse survival (Keime-Guibert et al., 2007). Because of the risk of toxicity as a side effect of radiation, recent studies have demonstrated that abbreviated courses could be safely and effectively combined with concurrent chemotherapy. The study also denotes the absence of direct comparison between the association of full course of chemotherapy with short and long full course of radiotherapy (Minniti et al., 2017). This includes for instance, the employment of single-fractions doses of 13–28 Gy and of 12–14 Gy for pituitary adenomas and acoustic neuromas respectively.

1.3.1.3 Systemic therapy

Treatment for GBM was revolutionised on publication of the results of a 2005 trial, when a large, international, randomized, phase III trial of newly diagnosed glioblastoma patients, demonstrated that daily temozolomide (TMZ) chemotherapy (75 mg/m^2 daily × 40–49 days) added concomitantly to radiotherapy followed by 6 cycles of administration of TMZ (150–200 mg/m^2 × 5/28 days) led to prolonged survival. Based on this trial the above treatment regimen has become considered the worldwide standard of care for patients with newly diagnosed GBM (Stupp et al., 2005; Stupp et al., 2009). TMZ (**Figure 1.8**) is a DNA-

alkylating chemotherapy agent that can readily cross the BBB to reach therapeutic concentrations in the brain.

1.3.2 TMZ as a standard therapy for GBM

TMZ is a triazene analogue of dacarbazine with anti-neoplastic activity. It is a cytotoxic alkylating agent that at physiologic pH is converted to the short-lived, active, compound, monomethyl triazeno imidazole carboxamide (MTIC). The cytotoxicity of MTIC is the result of methylation of DNA at the O6 and N7 positions of guanine, leading to inhibition of DNA replication. The difference between dacarbazine and TMZ, is that the former molecule is metabolized to MITC only in the liver, whereas the latter is metabolized to MITC in all organs of the body. Usually, TMZ is prescribed to be administered orally and it penetrates efficiently into the CNS.

Figure 0.8 Chemical formula and structure of temozolomide
Figure taken from Pedraza et al., (2021).

Concerning the side effects of this chemotherapy, TMZ has been associated with a low level of serum enzyme increases during treatment, and with few cases of clinically apparent acute liver injury. It was reported that hepatotoxicity is uncommon and when they have been observed, the injury was mainly seen as transient increases in serum aminotransferase levels. These changes are usually mild and self-limiting and not usually requiring adjustment or drug discontinuation (Grant et al., 2013). However, in rare cases treatment with TMZ has been associated with reactivation of chronic hepatitis B in patients who are positive for hepatitis B surface antigen at the start of chemotherapy. This reactivation is usually marked by increases in HBV DNA levels and mild jaundice; such patients commonly have a positive response to hepatitis B antiviral therapy which allows TMZ administration to be recommenced. No cases of death were reported after reactivation, whilst hepatitis B reactivation with jaundice in general, has a mortality rate in excess of 10% (Purchiaroni et al., 2014).

1.3.2.1 Mechanism of action of TMZ

The prodrug TMZ, is an imidazole derivative (4-methyl-5-oxo-2,3,4,6,8-pentazabicyclo [4.3.0] nona-2,7,9-triene-9-carboxamide), with a molecular weight of 194.15g. As part of a rational drug development initiative TMZ, a second-generation alkylating chemotherapy factor, was developed in the 1980s. Because it is lipophilic, it crosses the BBB efficiently and is bioavailable to the CNS. It is stable at acidic pH (< 5), but rapidly hydrolyses at neutral and alkaline pH (>7) values to the active MTIC intermediate. Once in contact with the slightly basic physiologic pH of blood, TMZ is transformed to the active compound that transfers the methyl group to DNA bases (methyldiazonium ion; Denny et al., 1994; Tentori & Graziani, 2009) (**Figure 1.9**). As a highly reactive cation, methyldiazonium is principally responsible for the methylation of DNA guanine residues at the N7 (70% of its activity), O6 positions (5% of its activity) as well as adenine at the N3 position (9% of its activity; **Figure 1.10,** Barciszewska et al., (2015)).

Despite its low yield, the O6 methylguanosine pathway is currently recognized as the main mechanism of TMZ action. The resulting O-6-methylguanine adduct (O6-meG) appears to be the most genotoxic due to its subsequent nucleotide mispairing with thymine instead of cytosine during DNA replication. The generation of single- and double-strand DNA breaks, when mismatch repair (MMR) enzymes attempt to cleave the offending adduct, induces G2/M phase cell cycle arrest, leading to apoptosis and autophagy that ultimately results in tumour cell death (Alexander et al., 2012; Kanzawa et al., 2004).

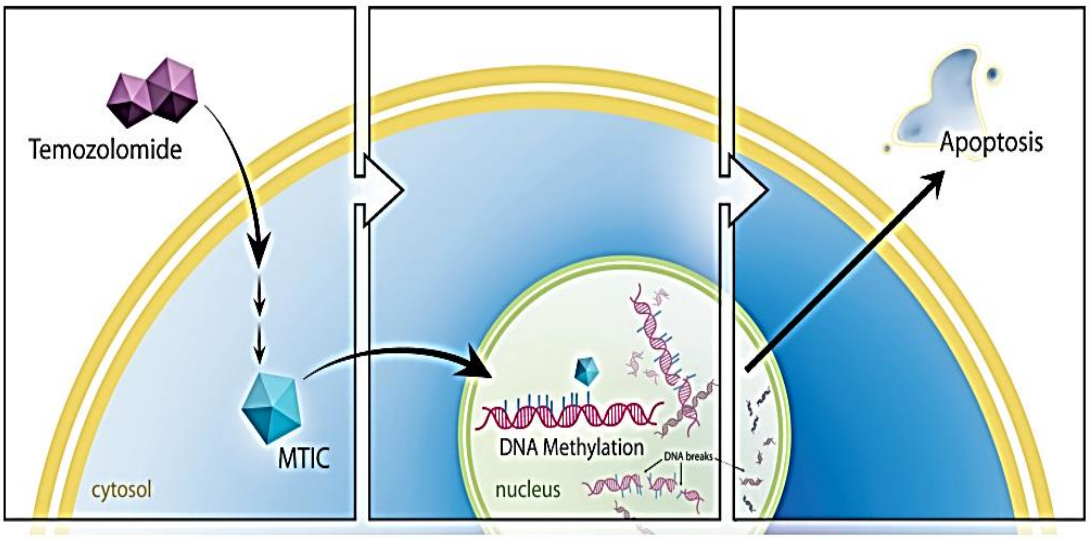

Figure 0.9 Schematic illustration of the proposed mechanism of temozolomide
Temozolomide is converted intracellularly into MTIC, which methylates DNA. Cellular repair mechanisms cannot adjust, resulting in DNA nicks and ultimately apoptosis (Wesolowski et al., 2010).

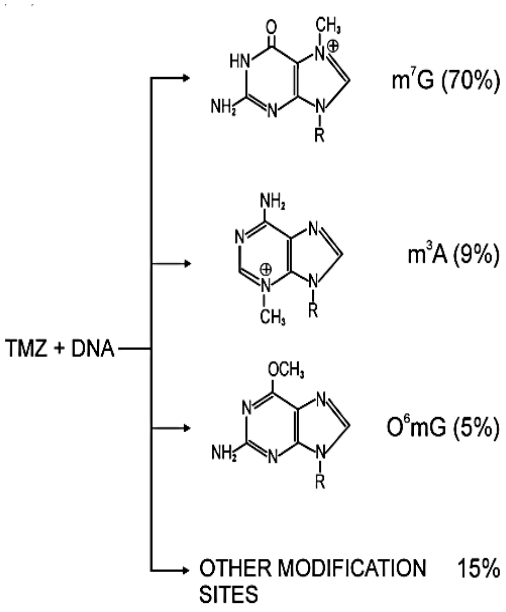

Figure 0.10 Site specific DNA methylation with temozolomide
The main product of DNA reaction with TMZ is 7- methylguanosine (m7G). Methylation of O6 guanosine is thought to be the main mechanism of TMZ action but takes place in only 5% of its activity (Barciszewska et al., 2015).

1.3.2.2 Blood-Brain Barrier (BBB) and penetration of TMZ

The presence of the BBB represents a major obstacle in GBM therapy. As detailed above the BBB prevents the passage of most substances from the blood to the brain and consequently limits the therapeutic efficiency of most chemotherapy drugs. One possible method to improve BBB permeability is the temporal disruption of the BBB using chemical or physical stimuli, but this is associated with a high risk of CNS toxicity and dysfunction (Obermeier et al., 2013; Upadhyay, 2014). Additionally, other trials, such as the administration of a drug directly into the brain, were found to be invasive and usually presented an unacceptably high risk of brain damage and require special devices (de Boer & Gaillard, 2007; Mitragotri et al., 2014; Lu et al., 2014).

Currently the BBB prevents the passage of 98% of drugs on the market (small molecules and most macromolecules) (Pardridge & William, 2005). Some proteins such as low-density lipoproteins, transferrin and lactoferrin can cross the BBB through receptor-mediated transcytosis (RMT) (Tsuji & Tamai, 1999; Pardridge, 1999; Fillebeen et al., 1999). Taking advantage of this pathway of natural endocytosis, many protein-based delivery systems have been developed, also known as protein shuttles but unfortunately have only achieved limited success (Kreuter et al., 2007; Pan et al., 2004; Oller-Salvia et al., 2016). Nevertheless, researchers have not given up, rather there has been an extensive focus on developing peptide-based delivery systems (Islam et al., 2020).

The two most commonly applied receptors in BBB-related drug development are (LRP1) a low-density lipoprotein receptor-related protein-1 and a glutathione transporter (Demeule et al., 2008; Gaillard et al., 2012; Lee et al., 2014; Ruan et al., 2018). LRP1 receptor is found to be over expressed in GBM, which makes it an ideal target as a solution brain cancer therapy and has been chosen in many studies as the target receptor for drug development (Maletínská et al., 2000). Previous studies showed that the Kunitz domain (conserved domain of LRP1 receptor) peptide mimics helped to LRP1 binding and BBB penetration (Régina et al., 2008; Demeule et al., 2008; Jiang et al., 2018; Rodrigues et al., 2021).

Recently Chen et al., (2019) have identified a specific peptide (from a peptide display phage library) that facilitated the passage of phage into the brain (**Figure 1.11**). It was demonstrated that this peptide had successfully crossed both the BBB and the BBTB required for tumour therapy. Using this peptide, the group have synthesized a peptide–drug conjugates which has been used for the treatment of glioma and breast cancer brain metastases (BCBM). Results from this study reported that one specific peptide–drug conjugates showed good efficacy in both tumour models. Additionally, it exhibited a synergistic effect when used with TMZ in a combination therapy with paclitaxel in mouse model (Chen et al., 2019).

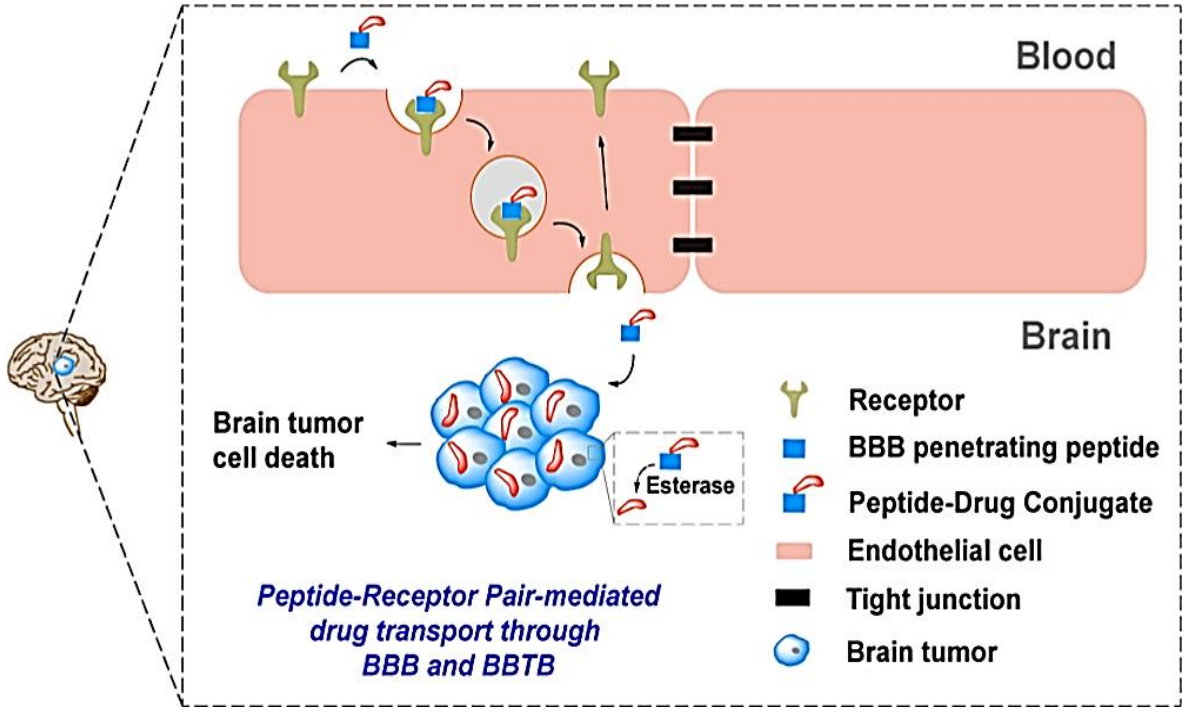

Figure 0.11 Passage of peptide drug into brain
Molecules enter tumour cells through receptor on endothelial cells surrounding the tumour tissue and representing the blood brain barriers: the blood–brain barrier (BBB) and the blood–brain tumour barrier (BBTB). Taken from Chen et al., (2019).

1.3.3 Temozolomide: Mechanisms of Resistance

Since the seminal clinical trial in 2005, TMZ has been considered the standard-of-care for newly diagnosed GBM (Stupp et al., 2005). The use of TMZ as a treatment for GBM patients is subjected to reaching a plateau where the activity of the drug is practically reduced to nothing and patients who initially responded to TMZ will inevitably relapse. This is due to resistance to TMZ developing after prolonged use by GBM patients. The process of TMZ resistance has been extensively studied and it is thought that 7 principal parameters contribute to the mechanism.

1.3.3.1 DNA damage repair mechanisms

1.3.3.1.1 Direct repair: O-6-methylguanine-DNA methyltransferase (MGMT)

MGMT gene is located on the chromosome 10q26. Despite its lower expression in brain tissue, this gene is constitutively expressed in different tissues. Its expression is variable between different individuals and even among tissues (Sharma et al., 2009). Many studies have reported that *MGMT* levels are about 4-6-fold less in primary glioma patients than those diagnosed with other tumours (Silber et al., 1996; Sharma et al., 2009). The physiological role of *MGMT* is in protecting cells from point mutations which are generated by environmental carcinogens. Interestingly, (Fujisawa et al., 2000) demonstrated that loss of heterozygosity on chromosome 10 is more extensive in primary *de novo* glioblastomas (65%–88% of tumours) than in secondary ones. Consequently, the MGMT protein is described as protecting cells from carcinogenesis and is a possible mediator of tumour chemoresistance in the case of GBM (Margison & Santibáñez-Koref, 2002). The expression of this gene is reduced as a result of methylation of CpG (cytosine–phosphate–guanine) islands in the promoter region leading to its silencing, which is the case in nearly 45% of newly glioma diagnosed patients (Esteller et al., 2000; Hegi et al., 2005).

Using a methylation-specific PCR (MSP) technique, the *MGMT* promoter methylation status was reported to be stable during the period of the disease in nearly 90% of GBM patients (Felsberg et al., 2011; Brandes et al., 2017). Despite this stability throughout the lesion (Grasbon-Frodl et al., 2007; Hamilton et al., 2011), some studies reported the epigenetic changes from methylated to unmethylated status of *MGMT* gene after TMZ exposure or on recurrence (Christmann et al., 2010; Jung et al., 2010; Brandes et al., 2017). Using multiplex ligation probe amplification technique, Park and colleagues reported a

decrease in methylation ratio after recurrence in about 75% of studied GBM cases, which could not be detectable using conventional techniques like MSP (Park et al., 2012).

In contrast to indirect multiprotein DNA repair mechanisms, direct repair relies only on MGMT, which removes TMZ induced DNA damage by eliminating the methyl group from O^6MeG (Jiang et al., 2012) (**Figure1.12)**. (Xu-Welliver & Pegg, 2002) also reported that MGMT protein undergoes inactivation with proteasomal degradation after alkylation without reconversion of its alkyl-cysteine residue 145. Thus, Bhattacharyya (1990) and Mitra (2007) demonstrated that MGMT acts on a stoichiometric reaction and described it as "not a true enzyme". Recently, Yu et al., (2019), reported that MGMT acts as a "suicide" DNA repair enzyme, where after repairing the normal base it forms a stable S-methylcysteine adduct, which inactivates the enzyme.

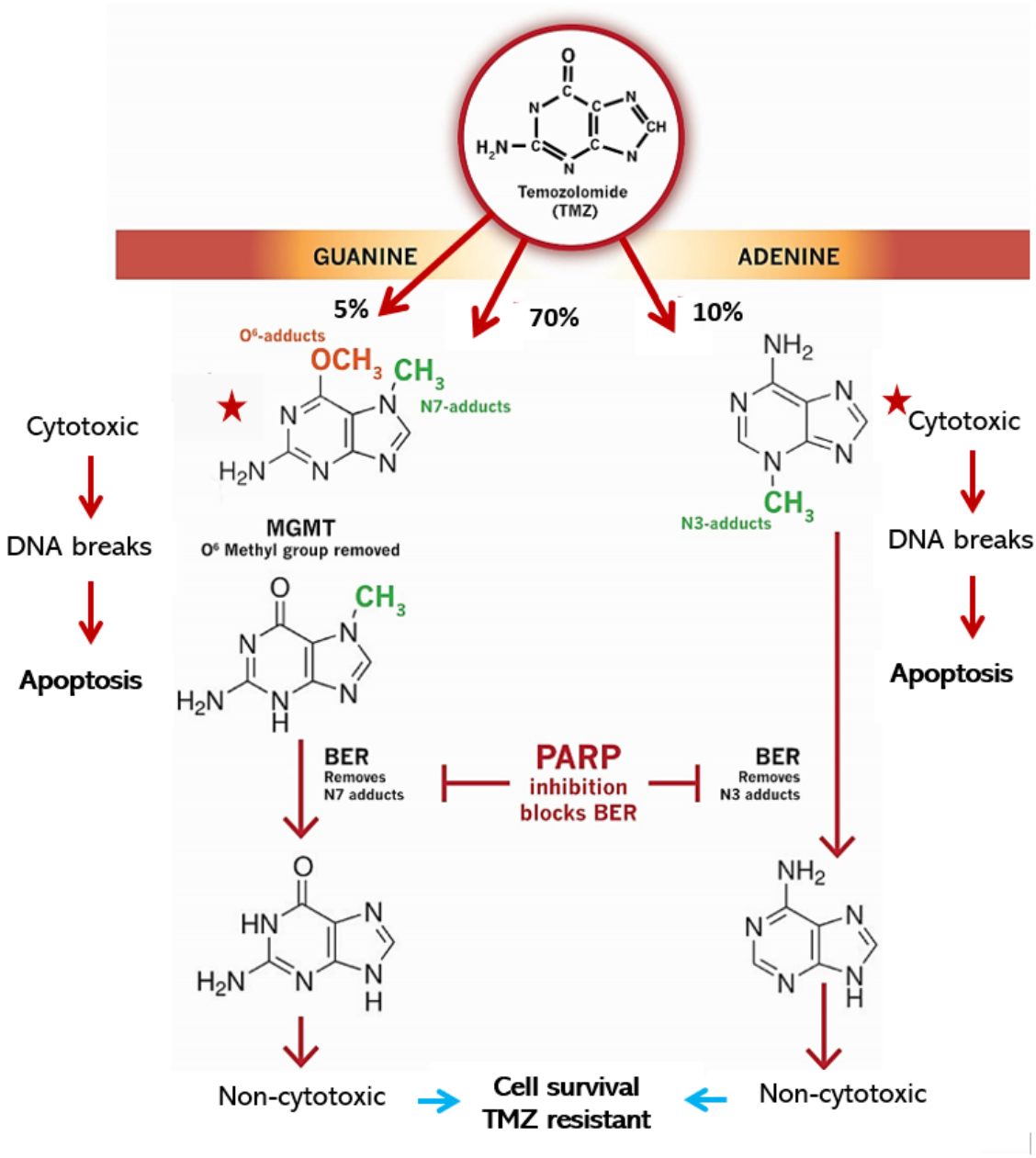

Figure 0.12 TMZ resistant phenotype induced by MGMT action
The most cytotoxic adduct is O6-methylguanine adducts which account for about 5% of lesions induced by TMZ. While O6-methylguanine is immediately repaired by MGMT, less toxic N7-methylguanine and N3-methyladenine are repaired by the base excision repair (BER) system. This DNA repair system result in TMZ resistant phenotype. The BER system could be inhibited using Poly (ADP-ribose) polymerase (PARP). Modified from Lawrence et al., (2015).

1.3.3.1.2 Indirect DNA repair: Mismatch repair

In addition to MGMT repair mechanism, many other DNA repair mechanisms have been reported to be involved in the mechanism of chemoresistance to TMZ; one of them is DNA MMR. The action of MMR consists of identifying and repairing mis-paired nucleotide bases. The repairing mechanism involves MutS protein homologs (MSH1 and MSH6) as a heterodimeric complex which bind to mis-paired nucleotide and activation of the MutL homolog-1/post-meiotic segregation increased 2 (MLH1/PMS2) protein heterodimer resulting in the replacement of the incorrect base (Alexander et al., 2012). In the case of cells treated with TMZ, where O^6-meG persists and mis-pairs with thymine, MMR initiates repetitive but ineffective cycles of thymine excision and reinsertion leading to accumulation of DNA breaks (single and double strand) and eventually to apoptotic cell death (Zhang et al., 2012).

Kim and co-workers demonstrated that TMZ resistance could be acquired because of disruption of the MMR repair system (Kim et al., 2015). Accordingly, *in vitro* studies reported an enhanced survival of glioma cells with knocked down *MSH6, MLH1,* and *PMS2* genes when given a dose of TMZ that previously induced cell cytotoxicity. TMZ sensitivity for these cells could be restored if MSH6 was re-expressed (Yip et al., 2009; Shinsato et al., 2013; Yuan et al., 2018). Paired patient studies (primary and recurrent glioblastomas) showed a significant decrease of MSH6, MLH1, and PMS2 protein expression in recurrent GBM after TMZ treatment compared with the original primary malignancy (Hunter et al., 2006; Cahill et al., 2007; Sun et al., 2018). These observations support the role that the MMR system has in acquired TMZ resistance, rather than glioma-genesis. Interestingly, in the Cancer Genome Atlas Research Network publication and in recent studies, shows that in TMZ treated GBM there is a correlation between *MGMT* promoter methylation and hypermutator phenotype consequent to mismatch repair deficiency (Cancer Genome Atlas Research Network, 2008a; McCord et al., 2020).

1.3.3.1.3 Indirect DNA repair: Base excision repair

Base excision repair (BER) is described as the primary pathway of DNA repair mechanism involved in repairing DNA damage induced by a variety of ionizing radiation and alkylating agent before replication (Almeida & Sobol, 2007; Alexander et al., 2012). N7-meG and N3-meA, which represent more than 90% of methyl-DNA adducts resulting from TMZ action, are the substrates for the BER system. Recently, Liu et al. (2017) reported that these substrates are identified by N-methylpurine DNA glycosylase (MPG) which will break the N-

glycosidic that links the target base with its sugar in the sugar backbone. Subsequently, single strand breaks are created by the split of the phosphodiester bond linking nucleotide subunits at the 5' end of the apurinic/apyrimidinic site by an enzyme called Apurinic/apyrimidinic endonuclease (APE-1). These DNA single strand breaks will activate Poly (ADP-ribose) polymerase (PARP) which will synthesise Poly (ADP-ribose) chains from cytosolic ADP-ribose units obtained from the degradation of NAD+. Thus, a complex of BER-involved proteins will be recruited to carry out the strand repair process.

It has been demonstrated that the reduced genotoxicity of TMZ-induced N7-meG and N3-meA DNA lesions is the result of the prompt and enhanced efficiency of the BER system repair (Alexander et al., 2012; Ferri et al., 2020). Accordingly, N3-meA is shown to be the commonest purine adduct if the BER system is repressed and results in an accumulation of non-repaired double strand DNA breaks and then apoptosis (Zhang, Wei et al., 2012; Woo et al., 2019). In a group of GBM patients where the *MGMT* promotor was methylated, Agnihotri and colleagues reported a negative correlation between high MPG protein expression and patient survival. Similarly, in an orthotopic xenograft model mouse as well as in patient-derived glioma cells, chemoresistance to TMZ was induced as a result of MPG over-expression in otherwise sensitive glioblastoma cells (Agnihotri et al., 2013; Serrano-Heras et al., 2020). Earlier, Bobola et al. (2014) had shown the contribution of the BER system in TMZ chemoresistance, as they reported a positive correlation between high APE-1 activity levels and tumour progression after alkylating therapy in high grade GBM. By suppressing APE-1 activity, TMZ cytotoxicity could be restored in human chemo-resistant glioblastoma cell lines (Silber, et al., 2002; Montaldi et al., 2015).

1.3.3.2 Epigenetic alterations

1.3.3.2.1 Post-transcriptional mechanisms: MicroRNA

Low et al. (2014) and Banelli et al. (2017) have reported another molecular mechanism involved in the chemoresistance to TMZ. This mechanism is the post-transcriptional epigenetic regulation of gene expression by microRNA. The expression of more than one third of human genes is regulated through MicroRNAs. As a short endogenous noncoding single strand RNA (19-25 nucleotides), MicroRNAs inhibit the translation of genes by complementary pairing to target mRNA. Interestingly, MicroRNA acts in a complex regulatory network where multiple mRNAs can be the target of the same microRNA, and multiple microRNA can target the same mRNA (Krol et al., 2010). Two subclasses of microRNA were described in relation to tumour genesis “oncomirs” and “anti-oncomirs”.

Oncomirs include microRNAs involved in apoptosis, proliferation, and tumour invasion processes, whilst anti-oncomirs function as tumour suppressors or are involved in anti-apoptotic process. MicroRNA-21 (miR-21) is reported to be the most studied oncomir in cancer research, and described to be upregulated in human GBM cells (Chan et al., 2005; Aloizou et al., 2020). Over expression of miR-21 induce chemoresistance to TMZ, by decreasing Bax/Bcl-2 ratio and caspase-3 activity. Bax and caspase-3 have pro-apoptotic activity while Bcl-2 has an anti-apoptotic action (Shi et al., 2010). It was reported that overexpression of miR-21 is also associated with the chemoresistance of GBM cells to doxorubicin, sunitinib, and taxol (Costa et al., 2013). Other ''oncomirs'' were also reported to be overexpressed in TMZ-resistant glioblastoma cells, such as: miR-16, miR-125b, miR-138, miR-195, miR-455-3p, and miR-10a (Ujifuku et al., 2010; Han & Chen, 2015; Haemmig et al., 2014; Stojcheva et al., 2016; Li et al., 2017).

Anti-oncomirs are microRNAs for which their downregulation in GBM cells induce a TMZ chemoresistant phenotype. Different mechanisms of induced TMZ resistance have been reported for different anti-oncomirs. miR-128-1 is reported to be the most downregulated anti-oncomir in GBM cells, whereby its downregulation induces a positive regulation of cell proliferation, migration, invasion, and glioma stem-like cells self-renewal (Shan et al., 2016). Other mechanisms associated with downregulation after TMZ exposure were demonstrated such as increase in drug efflux membrane transporter (ABCC1) upregulation (miR-1268a) (Li et al., 2018), repression of MGMT via promoter methylation (miR-101) (Tian et al., 2016) and enhancement of Protein reversion-less 3-like (REV3L)-mediated DNA repair and mutagenesis in GBM involving the c-Myc-miR-29c-REV3L Signalling Pathway (miR-29c) (Luo et al., 2015).

The clinical significance of different microRNAs as prognostic markers has received increasing attention over the last decade. Recent studies have demonstrated an association between reduced expression of anti-oncomirs such as (miR-137, miR-497, and miR-125b) and shorter OS among GBM patients, suggesting their possible role in tumour monitoring (Li et al., 2016; Regazzo et al., 2016). Additionally, it was reported that TMZ inhibits miR-181d (which was already demonstrated to inhibit MGMT expression) resulting in acquired TMZ resistance (Zhang et al., 2012; Ramakrishnan et al., 2018). The cross-interaction described in many studies between microRNAs and transcription factors (TFs) in regulating the same mRNA, suggest that microRNA induced TMZ resistance is a result of a protein network instead of an individual one-to-one mechanism (Sun et al., 2012; Ahir et al., 2017).

1.3.3.2.2 Post-translational: Histone modification

Kitange et al., (2012) were the first to describe a new epigenetic change that affects TMZ sensitivity of GBM cells which involves chromatin remodelling and histone modification. In an *in vivo* paired GBM (parental and TMZ-resistant) tumour xenograft animal model, they demonstrated that increased acetylation of lysine 9 of histone H3 (H3K9-ac) and decreased demethylation (H3K9-me2) were associated with *MGMT* upregulation in TMZ-resistant specimens, while no significant change was detected in *MGMT* promoter methylation. Later, others reported similar mechanisms involving a histone modification TMZ resistance induced phenotype (Xi et al., 2016; Banelli et al., 2017). It was demonstrated that compared to parental cells, TMZ-resistant cells show an increase in the expression of histone lysine demethylase genes (KDMs) with slower growth and exhibiting a partially differentiated phenotype. Interestingly these cells were desensitised to TMZ by inhibiting *KDM5A* by short hairpin RNA (shRNA) (Banelli et al., 2015).

Recently, Abe et al. (2018) reported that histone mutations such as K27M and G34V/R in histone-3 (H3) induce DNA hypomethylation leading to an increase in MGMT expression and consequently TMZ resistance. Nevertheless, GBM patients carrying H3K27M mutation are shown to have shorter OS and a worse prognosis than those with H3G34V/R mutation independent of tumour location (Sturm et al., 2012), suggesting a resistance-induced epigenetic mechanism independent of known DNA repair axes. Abe et al., (2020) demonstrated that mutations in histone gene induces epigenetic changes including DNA hypomethylation, frequently for *MGMT* gene leading to an increase in MGMT expression and TMZ resistant phenotype.

1.3.3.2.3 Drug efflux

Another mechanism involved in the chemoresistance to TMZ, is the efflux of the drug across the tumour cell membrane by the ATP-dependent Transporters (Gottesman et al., 2002). The multiple drug resistance-1 (MDR) gene functions in a general way mediating resistance for multiple drugs in cancer cells through a cassette of about 48 proteins known as ABC (for ATP-Binding Cassette) transporter proteins (Gottesman et al., 2002; Da Ros et al., 2018). The 3 major proteins of the ABC family are: P-glycoprotein (P-gp), the breast cancer resistance protein (BCRP also known as ABCG2) and the multidrug resistance-associated protein (MRP). As a 12-transmembrane ATP-dependent drug efflux pump, P-gp has been shown to be over-expressed in TMZ resistant GBM cell lines and patient tissue samples (Schaich et al., 2009; Munoz et al., 2015; Bouzinab et al., 2020).

In an earlier study, Tivnan and colleagues demonstrated that ABC transporters (especially MRP1) are substrate specific, and that inhibition of MRP1 has effect only on vincristine and etoposide drug response and not TMZ in GBM cell lines (Tivnan et al., 2015). The study also showed that the concomitant inhibition of MRP1 and P-gp restored the cytotoxicity of all three drugs. Studies on xenograft animal model, showed that P-gp and BCRP-mediated efflux restricts the passage of erlotinib, and their concomitant inhibition increases the delivery of the drug to the tumour (Agarwal et al., 2013; Munoz et al., 2015). Accordingly, in a clinical study, a shorter OS was associated with a relatively high level of BCRP protein in GBM patient specimens (Emery et al., 2017). Recent studies have also demonstrated that ABCG2 and ABCB1 are clinically important ATP-dependent transporters which are over expressed at the BBB and contribute effectively to the limitation of drug entry to brain tumour tissues (Bauer et al., 2019; Traxl et al., 2019).

1.3.3.2.4 Autophagy

A new mechanism of acquired TMZ resistance in GBM related to tumour cell autophagy was recently introduced (Hombach-Klonisch et al., 2018). Autophagy is described as a cytoprotective process in which the lysosomes contribute to the degradation of damaged cytoplasmic organelles and dysfunctional proteins (Codogno & Meijer, 2005). Early *in vitro* functional studies showed that TMZ cytotoxicity is enhanced following the inhibition of the autophagy process (Knizhnik et al., 2013) which was stimulated in human GBM cells while exposed to an increased TMZ doses (100 – 500 µM) (Carmo et al., 2011). Recent studies demonstrated that the autophagy process could be regulated using specific microRNAs (Stojcheva et al., 2016; Wang et al., 2017) or through histones modifications mechanisms (Wang et al., 2016). The molecular mechanisms and the paradoxical roles of autophagy in gliomagenesis have been recently extensively reviewed (Batara et al., 2021).

1.3.3.2.5 Receptor tyrosine kinase signal transduction pathway activation

Receptor tyrosine kinase (RTK) are high-affinity transmembrane receptors which are responsible for different natural cellular process through the initiation of signalling pathways. Dysregulation of their expression is reported as critical in the genesis and the development of tumours (Zwick et al., 2001). Epidermal growth factor receptor (EGFR) is one of the most studied RTK in GBM, and its gene amplification has been reported in about 65% of such primary malignancies (An et al., 2018). The constitutively active variant is EGFR variant III is mostly found in astrocytic tumour cells in the brain (Kim et al., 2021).

EGFR signalling has been reported to interfere in the mechanism of TMZ resistance by enhancing the expression of Bcl-xL, which is an anti-apoptotic protein, and consequently reducing TMZ action (Messaoudi et al., 2015). Liffers et al. (2015) demonstrated that EGFR is amplified and over expressed on the stem-like phenotype of GBM-derived GS-cells suggesting its role in inducing TMZ resistance. Interestingly, this protein was not expressed in most normal adult brain cells (Denduluri et al., 2015).

Additionally, Maki and colleagues, described a new RTK member which is the Insulin-like growth factor (IGF) as being implicated in the development of chemoresistance in glioblastoma and other tumours such as breast, prostate, colon, and ovarian cancer (Denduluri et al., 2015; Maki, 2010). Over expression of IGF-1 receptor in 25% of GBM patients and the presence of crosstalk in the signalling pathways (PI3K/AKT/mTOR pathway) between this receptor and EGFR receptor could explain the failure of anti-EGFR therapy in GBM, suggesting an important role of IGF receptors in acquired TMZ chemoresistance (Maki, 2010; Westphal et al., 2017).

1.3.3.3 Tumour microenvironment

1.3.3.3.1 Hypoxia

Uncontrolled cell proliferation at the tumour site results in a hypoxic environment which can be as low as 1% of levels in arterial blood in the tumour core in the case of GBM. Thus, hypoxia is regarded as a hallmark of glioblastoma which creates a selective pressure leading to adaptive responses (Jawhari et al., 2016). Interestingly, hypoxia-inducible factor 1 (HIF-1) showed an increased tumour cell nuclear availability, a well-studied mechanism in relation to hypoxia induced glioblastoma growth (Pandya et al., 2017). The two subunits α and β of HIF-1 factor dimerize and become active in response to hypoxia and will target more than 100 genes.

In GBM, studies showed that the downstream pathways activated by chronic hypoxia are involved in cellular mechanisms such as cell survival (gene target: IGF-2) (Feldser et al., 1999), enhanced glycolysis (gene target: glucose transporter-1, 3), tumour invasion (gene target: MMP) (Jensen, 2009), enhancement of autophagy (Jawhari et al., 2016), and the proliferation of GSC (Soeda et al., 2009; Kolenda et al., 2011). Reardon et al. (2008) reported that vascular endothelial growth factor (VEGF-A) which is an important angiogenic mediator in malignant gliomas, gives promising clinical effects if inhibited at the same time as chemotherapy treatment in many cancers and thus could be a relevant therapeutic target for GBM. Unfortunately, in two randomized phase III clinical trials, bevacizumab, a recombinant

humanized monoclonal antibody inhibiting VEGF-A did not show any improvement in OS with newly diagnosed glioblastoma patients who received IR plus TMZ treatment (Gilbert et al., 2014; Chinot et al., 2014). In their studies they included 612 and 458 GBM patients, respectively.

Recently, Dico and colleagues suggested that HIF-1 could have a crucial role in TMZ resistance by modulation of apoptosis related genes (Fabbri et al., 2010). The study demonstrated that the downregulation of HIF-1α gene improved sensitivity of TMZ-resistant cells, whilst blocking chaperone-mediated autophagy (CMA)-mediated HIF-1α degradation induced resistance in TMZ-sensitive cells. Earlier studies demonstrated that expression of anti-apoptotic proteins such as Bcl-2 and Livin as well as drug efflux ABC transporters could be enhanced as a result of repetitive cycles of hypoxia and reoxygenation leading to acquired TMZ resistance in human GBM xenografts (Chou et al., 2012; Chen et al., 2015; Hsieh et al., 2015).

1.3.3.3.2 Connexin gap junction activity

In glioblastoma tissue, it was demonstrated that cells exchange cell wall molecules, second messengers, ions, and microRNA through channels made by gap junctions (Grek et al., 2018). This study also showed that the most abundant plasma membrane protein is Connexin 43 (Cx43) also named gap junction protein A1 (GJA1). This protein was reported to be associated with MGMT-induced mechanisms of TMZ resistance. Many studies have reported the negative association between the level of expression of Cx43 and TMZ-sensitivity (Gielen et al., 2013; Munoz et al., 2015; Murphy et al., 2016; Lai et al., 2018). Katakowski et al., (2010) and Gielen et al., (2013) have suggested that the induced TMZ-resistant phenotype of human glioma cells driven by Cx43, is the result of inhibition of apoptotic process by increased Bcl2 expression (anti-apoptotic protein) following the transfer between tumour cells of micro-RNA such as miR-67.

Chen et al. (2015) reported another mechanism of induced TMZ-chemoresistance involving calcium, glutathione, and inositol 1, 4, 5-triphosphate (IP3), (all three regarded as second messengers of the apoptosis process; Decrock et al., (2013)) which were found in excess in the cytoplasm of GBM cells (Chen et al., 2015). In the same study, they demonstrated that TMZ-cytotoxicity is attenuated in normal astrocytes when cocultured with Cx43-knockdown GBM cells. In a targeted therapy of the cell line, studies demonstrated a promising result to restore TMZ sensitivity using Cx43-knockdown cells and specific inhibitors (Murphy et al., 2016).

1.3.3.3.3 Glioma stem cells

A stem cell phenotype is characterised by the ability of self-renewal, capacity to proliferate and multipotency. The presence of glioma cell populations possessing a stem cell phenotype is receiving more attention during the last decade, as evidence grows for their existence (Sundar et al., 2014). Many research studies support the hypothesis of a glioblastoma stem cells (GSC) population identifiable by their specific expression of typical stem cell molecular biomarkers such as CD133, SOX2, and NOTCH1.

In xenograft animal models, human cells were able to form neurospheres in serum-free conditions and exhibited tumour growth mimicking stem cell behaviour (Singh et al., 2004; Ogden et al., 2008; Gangemi et al., 2009). More recent studies showed that following TMZ chemotherapy, GBM cells could dedifferentiate and acquire a stem cell phenotype suggesting a bidirectional growth process and giving a new explanation of TMZ chemoresistance and tumour recurrence (Cheng et al., 2017) which was further investigated in clinical studies (Alves et al., 2021).

The suggested mechanisms of induced GSC chemoresistance involve most of the aforementioned mechanisms including anti-apoptotic proteins (Bcl2), drug efflux pumps, DNA damage checkpoints, enhanced EGFR activity and overexpression of MGMT (Bao et al., 2006; Liu et al., 2006; Murat et al., 2008; Schmalz et al., 2011; Shi et al., 2012; Sundar et al., 2014). Furthermore, (Kim et al., 2014) demonstrated in paired patient tumour tissue, the presence of a GBM stem cell-like phenotype, characterised by the expression of *HOX* gene responsible for self-renewal of the TMZ-resistant cell population. It was also demonstrated that MGMT expression is 32-fold higher among CD133+ GSCs compared to CD133- tumour cells, supporting the involvement of DNA repair mechanism (Liu et al., 2006; Oldrini et al., 2020).

Although there is growing evidence of the key role of GSC in the mechanism of resistance to TMZ, the absence of specific biomarker leaves an enigma about their identification. As it was previously described by (Beier et al., 2011; Alves et al., 2021), stem cell-induced GBM chemoresistance is much more complex than expected. However, GSC are still regarded as the primary contributor to tumour recurrence.

1.4 Molecular Genetics of GBM

The histopathological classification of grade-III and grade-IV astrocytomas has been acknowledged to be insufficient to guide therapy alone for many years (Phillips et al., 2006). The integration of molecular characterisation is now indispensable, and biopsies are routinely screened for mutations in the *IDH1* or *IDH2* genes and *MGMT* promotor methylation status (Cancer Genome Atlas Research Network, 2008; Verhaak et al., 2010). The first aberration marks the milder type of astrocytoma, while the second helps to predict the tumour response to alkylating agents, specifically TMZ, which in combination with radiotherapy is considered as the gold-standard chemotherapeutic agent for GBM (Nam & de Groot, 2017).

1.4.1 Genetic Alterations in primary GBM

Three major genetic aberrations characterise primary GBM. The first is the amplification and/or a high rate of *EGFR* mutation at chromosome 7p. The second is the homozygous deletion of the Cyclin Dependent Kinase Inhibitor gene (*CDKN2A-p16INK4a*) on chromosome 9p (with absence of one or both isoform transcripts *CDKN2A alpha* (*p16INK4A*) and *beta* (*p14ARF*). The third is the deletion of the phosphatase and tensin homolog (*PTEN*) gene typically in association with chromosome 10 monosomy (also called monosomy 10). These mutations have been confirmed by high-density single nucleotide polymorphism arrays technique (Vital et al., 2010; Crespo, Inês et al., 2012; Appin & Brat, 2014).

Additionally, in nearly 15% of primary GBM that lack tumour protein p53 (*TP53*) mutations and telomerase reverse transcriptase (*TERT*) promoter mutations, an amplification of the Mouse double minute 2 homolog (*MDM2*) oncogene was reported (Nonoguchi et al., 2013; Arita et al., 2013). Epidermal growth factor receptor variant III ($EGFR^{vIII}$) characterised by an 801-bp in-frame deletion of exons 2 to 7, is the most common EGFR mutant type leading to an enhanced proliferation and survival of mutated cells (Hatanpaa et al., 2010). Gan and colleagues have reported that in most GBM tumours overexpression of $EGFR^{vIII}$ variant is associated with an amplification of the *EGFR* gene, and in more than 70% of primary *GBM* cases overexpression of *EGFR* gene is associated with *EGFR* gene amplification (Gan et al., 2013; Saadeh et al., 2018).

Homozygous deletion of *CDKN2A-p16INK4a* was described to be more frequent in primary GBM than secondary malignancies (Nomura et al., 2001). It was reported also that the homozygous deletion of chromosome 9p involving *CDKN2A-p16INK4a* gene typically

target surrounding genes like methylthioadenosine phosphorylase (*MTAP*) (Crespo et al., 2012).

Loss of heterozygosity (LOH) of chromosome 10 is described in more than 70% of primary GBM cases with the three most commonly deleted regions being: 10p14-15, 10q23-24 (involving *PTEN* gene), and 10q25-pter (Carico et al., 2012). Interestingly, the *PTEN* gene is mutated in about a quarter of all GBM, with more than 50% of these mutations being an insertion of a stop codon that leads to a truncated peptide (Ohgaki & Kleihues, 2007). *PTEN* gene alteration reported in most of advanced glioblastoma stages and the association of LOH 10 with *EGFR* gene amplification in most primary GBM suggest that the aggressive phenotype of GBM is the result of the inactivation of suppressor genes on chromosome 10 (Liu et al., 2016).

Additionally, in primary GBM a number of other genetic alterations were commonly reported, such as Neurofibromatosis Type 1 (*NF1*) mutation / homozygous deletion (18%) and regulatory subunit 1 of phosphatidylinositol 3-kinase (*PIK3R1*) mutations (10%) (Cancer Genome Atlas Research Network, 2008b; Crespo et al., 2015).

1.4.2 Genetic Alterations in secondary GBM

The most frequent mutations seen in secondary GBM are on chromosome 17p. *TP53* gene mutations are the most frequent and are characterised by mutations at codons 248 and 273 with G/C to A/T mutations at cytosine-phospho-guanine (CpG) sites (Ohgaki et al., 2004). These alterations are detectable at the early stages of GBM formation and are considered as early events associated with malignant transformation to aggressive secondary GBM. Interestingly, *TP53* alterations especially G/C to A/T mutations are frequently associated with methylation of the promotor of *MGMT* (Nomura et al., 2001; Yu et al., 2018).

Gliomas with mutated IDH1 and IDH2 have been reported to have a better prognosis than those with wild-type IDH (Zou et al., 2013; Molenaar et al., 2018). IDH1 and IDH2 mutations have been described as an early event in the progression of secondary GBM in most low-grade malignancies. Accordingly, the presence of these mutations in primary GBM is rare (Deng et al., 2018). These mutations were reported in association with an increase in DNA methylation status, which suggest their involvement in oncogenesis process by deactivation of tumour suppressor genes through hypermethylation mechanism (Yan et al., 2009; Hwang et al., 2019).

Compared to primary GBM, secondary tumours are characterised by a high frequency of specific genetic alterations including LOH of chromosome 10q (Fujisawa et al., 2000), 13q (including retinoblastoma (*RB*) gene locus), 19q (including 19q13.3 region commonly deleted) (Nakamura, et al., 2000) and 22q (including the Metalloproteinase inhibitor 3 (*TIMP-3*) putative tumour-suppressor gene at 22q12.3) (Nakamura, et al., 2005). **Table 1.3** is a comparison between primary and secondary GBM involving genetic and epigenetic alterations and differences in gene expression profiles.

Table 0.3 Epigenetic and genetic alterations found typically in primary versus secondary GBM.

Variable	Primary glioblastoma, % (95%)	Secondary glioblastoma, % (5%)
Promoter methylation		
MGMT	*36*	*75*
TIMP-3	*28*	*71*
RB	*14*	*43*
CDKN2A-p14^{ARF}	6	31
CDKN2A-p16^{INK4a}	3	19
Genetic alterations		
IDH1 mutation	5	67–85
IDH2 mutation	0	0
EGFR amplification	36–60	8
TERT mutation	58	28
CDKN2A-p16^{INK4a} deletion	31–78	19
TP53 mutation	28	65
PTEN mutation	25	4
LOH 10p	47	8
LOH 10q	47; 70	54; 63
LOH 22q	41	82
LOH 1p	12	15
LOH 13q	12	38
LOH 19q	6	54
Gene/protein expression profiles		
Fas (APO-1; CD95)	100	21
Survivin	83	46
MMP-9	69	14
EGFR	63	10
EGFR	High	Low
MDM2	31	0
VEGF	High	Low
VEGF fms-related tyrosine kinase 1	High	Low
IGFBP2	High	Low
Tenascin-X-precursor	High	Low
Enolase 1	High	Low
Centrosome-associated protein 350	High	Low
TP53	37	97
ASCL1	33	88
Loss of TIMP-3	17	64
PDGFRA/PDGFRB	Low	High
ERCC6	Low	High
DUOX2	Low	High
HNRPA3	Low	High
WNT-11 protein precursor	Low	High
Cadherin-related tumour-suppressor homolog precursor	Low	High
ADAMTS-19	Low	High

Abbreviations

ADAMTS-19, ADAM metallopeptidase with thrombospondin type 1 motif, 19.
APO-1, apoptosis-mediating cell membrane protein.
ASCL1, achaete-scute complex-like 1.
DUOX2, dual oxidase 2.
EGFR, epidermal growth factor receptor.
ERCC6, excision repair cross-complementation group 6.
HNRPA3, heterogeneous nuclear ribonucleoproteinn A3.
IGFBP, insulin-like growth factor binding protein.
LOH, loss of heterozygosity.
MDM, mouse double minute.
MMP, matrix metalloproteinases.
PDGFR, platelet-derived growth factor receptor.

Table Modified from (Crespo et al., 2015).

1.4.3 Key molecular effectors in GBM development

In a previous study 365 genes were described as differentially expressed in GBM patients among 2365 genes identified using gene expression profiling (Long et al., 2017). Most of these genes were enriched in 10 different pathways. *MMP9*, *FN1*, *FGF13*, and *COL4A2* have been identified as important genes in the pathways associated with cancer while *COL3A1*, *COL6A3*, *COL1A2*, *FN1*, and *TNC* are significant genes in the focal adhesion pathway. *CAMK2A*, *HTR2A*, and *GRIN2A* are found to be significant genes in the calcium signalling pathway and finally *COL3A1*, *CD44*, *SV2B*, and *COL6A3* represent important genes involved in ECM-receptor interactions.

Overexpression of CD44 (cell surface adhesion receptor) was associated with the growth and survival of GBM (Yoshida et al., 2012). *COL3A1* (Collagen, Type III, Alpha 1) which encodes fibrillar collagen (principal component of ECM), plays a crucial role in cancer cell apoptosis, proliferation, and anti-tumour drug resistance (Skog et al., 2008; Gao et al., 2016). Yu & Stamenković, (2004) described a functional relationship between *CD44*, *MMP9*, and *TGF* beta in the control of tumour-associated tissue remodelling. Interestingly, it was reported that extracellular localization of Matrix metalloproteinase 9 *(MMP9)* is required to affect cancer cell motility, invasion, and metastasis (Yu & Stamenković, 2004; Prud'homme, 2007; Jacob & Prekeris, 2015). *MMP9* is involved in the pathophysiology of malignant GBM by ECM remodelling associated with neovascularisation (Forsyth et al., 1999; Sun et al., 2019) and, in contrast to normal tissue, *MMP9* is only detected in GBM patients.

Finally, *FN1* (fibronectin 1) gene, is upregulated in GBM patient and found to have a great importance in the maintenance of integrin b1 fibronectin receptors in glioma cells (Wang, et al., 2011). Overexpression of *FN1* in GBM is correlated with poor patient survival (Yang et al., 2019).

1.4.4 Clinical relevance of differentially expressed genes in glioblastomas

Molecular mechanisms in the origin of complex diseases such as GBM can be depicted by identification of a robust and reliable study of differentially expressed genes (DEGs). In a large, combined cohort of GBM and normal samples, Jing Tang and colleagues have identified 100 unique genes connected to GBM among 147 robust gene signatures (median overlap value > 0.9) (Tang et al., 2018). Among the 100 genes associated with GBM, 80 were differentially expressed in GBM samples (60 upregulated, 12 downregulated and 8 with unknown status).

The **table 1.4** shows the top 10 most significant down or up-regulated DEGs, and **Table 1.5** shows the relationship between these genes and GBM. These genes were associated with the different evolutionary status of GBM such as survival, growth, invasive and proliferation.

Table 0.4 Top 10 most significantly up- or down-regulated DEGs expressed in GBM tissues compared to normal samples

Gene symbol	Gene description	Fold Change
(1) Upregulated in GBMs		
COL3A1	collagen, type III, alpha 1	5.628
TOP2A	topoisomerase (DNA) II alpha 170 kDa	8.713
CRISPLD1	cysteine-rich secretory protein LCCL domain containing 1	4.072
RRM2	ribonucleotide reductase M2	9.195
COL1A2	collagen, type I, alpha 2	3.750
FCGBP	Fc fragment of IgG binding protein	4.004
CDCA7L	cell division cycle associated 7-like	4.539
SMC4	structural maintenance of chromosomes 4	5.165
TMEM45A	transmembrane protein 45 A	4.857
PTX3	pentraxin 3, long	8.298
(2) Downregulated in GBM		
MAL2	mal, T-cell differentiation protein 2 (gene/pseudogene)	0.252
GJB6	gap junction protein, beta 6, 30 kDa	0.285
NEFM	neurofilament, medium polypeptide	0.419
SYNPR	Synaptoporin	0.407
TMEM130	transmembrane protein 130	0.334
GABRA1	gamma-aminobutyric acid (GABA) A receptor, alpha 1	0.335
RBFOX1	RNA binding protein, fox-1 homolog (C. elegans) 1	0.399
SLC12A5	solute carrier family 12 (potassium/chloride transporter), member 5	0.440
NEFH	neurofilament, heavy polypeptide	0.406
AK5	adenylate kinase 5	0.398

Table taken from Tang et al., (2018)

Table 0.5 Gene functions associated with the top 10 most significantly up- or down-regulated DEGs between GBMs and normal samples.

Gene symbol	Descriptions of genes associated with GBM	UP/Down
COL3A1	COL3A1 may be suitable biomarkers for diagnostic or therapeutic strategies for GBM	Down
TOP2A	Over-expression of TOP2A as a prognostic biomarker in patients with GBM	UP
CRISPLD1	UN	UN
RRM2	BRCA1-mediated RRM2 expression protects GBM cells from endogenous replication stress	UP
COL1A2	COL1A2 is highly expressed genes in GBM spheroids as compared with normal brain	UP
FCGBP	Primary glioblastomas exhibited higher expression of extracellular response-associated gene FCGBP	UP
CDCA7L	It has been reported that CDCA7L is correlation to GBM patient survival time	UP
SMC4	Overexpression of SMC4 activates TGFβ/Smad signaling and promotes aggressive phenotype in GBM cells	UN
TMEM45A	Suppressing of TMEM45A expression in glioma cells remarkably suppressed cell migration and cell invasion	UN
PTX3	Knockdown of PTX3 significantly decreases GBM8401 cell migration and invasion	UN
MAL2	UN	UN
GJB6	GJB6 (Cx30) has the potential to influence growth, proliferation and migration of GBM cells.	UN
NEFM	KLF6 inhibits the malignant phenotype of GBM *in vitro* and upregulates neuronal marker NEFM.	UP
SYNPR	SYNPR is downregulated differently expressed genes (DEGs) in GBM tissue samples.	Down
TMEM130	UN	UN
GABRA1	Upregulation of miR-155 in GBM could may downregulate GABRA1 which renders tumor cells unresponsive to GABA signaling.	Down
RBFOX1	Downregulated RBFOX1 is identified in GBMs compared with normal brain.	Down
SLC12A5	UN	UN
NEFH	miR-25 promotes GBMs cell proliferation and invasion by directly targeting NEFL.	UN

UP indicated that the gene was identified as up-regulated in GBMs; **Down** indicated that the gene was reported as down-regulated. **UN** suggested the gene has not been reported in current GBM-associated studies. Table taken from Tang et al., (2018).

1.4.5 Functional significance of DEGs

In order to understand the biological functions of different DEGs, a functional analysis for the top 10 up and down- regulated genes in GBM is required. This analysis gives an understanding of the pathology of the disease and potentially opens new therapeutic options. Functional analysis is a gene set enrichment analysis (GSEA) carried on two levels, first the gene ontology (GO) term enrichment and second the Kyoto Encyclopedia of Genes and Genomes (KEGG) pathways enrichment analysis (Liu et al., 2017).

In terms of biological processes, the upregulated genes in GBM are found mainly to be involved in the cell cycle and immune response, whilst the downregulated genes are involved in anion and neurotransmitter transport. In terms of cellular components, upregulated genes are mainly associated with the extracellular space and extracellular matrix, e.g., collagen, as well as the Golgi apparatus, whilst down regulated ones are associated with neuron and cell projections, intermediate filament, and the synapse. In terms of molecular functions, upregulated genes are associated with cell receptors and enzyme binding sites, whereas the downregulated genes are predominantly associated with transporter, receptor, and structural molecule activity (Bo et al., 2017).

KEGG pathways analysis, demonstrate that the upregulated genes are associated with extracellular matrix / receptor interactions, complement and coagulation cascades, p53 signalling pathway, focal adhesion, and immune network, whereas downregulated genes are associated with neuroactive ligand receptor interaction and amyotrophic lateral sclerosis (ALS) (Bo et al., 2017).

More recently, Yin et al. (2019) used the same strategy as Bo et al., (2017) on 292 survival-related genes selected from the overlapping DEGs. In this study the authors reported the presence of five genes which could predict overall survival namely *PTPRN* (protein tyrosine phosphatase, receptor type N), *RGS14* (Regulator of G Protein Signalling 14), *G6PC3* (glucose-6-phosphatase catalytic subunit 3), *IGFBP2* (Insulin Like Growth Factor Binding Protein 2), and *TIMP4* (TIMP Metallopeptidase Inhibitor 4). The results are summarised in **Table 1.6**.

Table 0.6 Genes which could predict overall survival of GBM patients

Gene	*Biological function*	*Expression in GBM patient*	*High expression Associated prognosis*
PTPRN	Secretion of hormones and neurotransmitters	Downregulated	Poor
RGS14	Centrosome function, transcriptional regulation, and stress-induced cellular responses	Downregulated	Poor
G6PC3	key enzyme that regulates glucose homeostasis and glycogenolysis regulating proliferation and invasiveness in several tumours	Upregulated	Poor
IGFBP2	modulates cell growth, differentiation, migration, and invasion in neoplasms	Upregulated	Poor
TIMP4	involved in several processes of tumorigenesis including proliferation, migration, and invasion	Upregulated	Good

Taken from Yin et al. (2019).

1.5 Microfluidic system applied to glioblastoma model

1.5.1 Tumour structure and different culture system of tumour cells

Tumours represent a complex 3-dimensional structure with dynamic crosstalk established between adjacent tissues through a complex signalling set of chemicals. Mechanisms underlying the formation, pathology and drug development of tumour tissues were made possible due to the use of cell culture systems and animal models. Since the first use of cell culture by Harrison 1907 on nerve cells (Vertrees et al., 2009), this technique has been improved to study the growth and differentiation of cells outside the body. Currently, the most commonly used method of cell culture is the 2-dimensional (2D) model (Białkowska et al., 2020a).

1.5.1.1 2D culture model

In 2D models, cell culture is carried out under adherent conditions, where immortalised cells are grown as a monolayer attached to a plastic surface in a flask or in a flat petri dish (Breslin & O'Driscoll, 2013). This monolayer system have been proven very effective in majority of research dealing with *in vitro* evaluations by providing a convenient means of treating and analysing cells (Ryan et al., 2016). This model is used as the first step when testing pharmaceutical ingredients prior to going further to animal testing and clinical trials for many reasons. First because this technology is less expensive than any other culture system (e.g., 3D or microfluidic system). Second, the 2D culture system is a well-established

technique and most known in research as it gained widespread acceptance in the 1940s, and finally, it is typically easier to perform cell observations and measurements than in other culture systems (Ryan et al., 2016; Białkowska et al., 2020a).

The advantages of the 2D model are summarised as simplicity, relatively low cost, and the possibility of performing functional tests. However, in 2D culture, the cell-cell and cell-ECM environment interactions do not mimic the real interactions existing between tumour cells and their environment. The lack of these interactions represents the major disadvantage of 2D model. These interactions are responsible for a continuous flow of signals for cell differentiation, proliferation, vitality, gene expression, responsiveness to stimuli, drug metabolism and other cellular functions (Baker & Chen, 2012).

Interestingly, many recent studies still use 2D culture model to validate their research before going further to 3D and other tumour models. In their study, Gerigk et al. have used conventional 2D model to assess RNA purity and cell viability, differentiation and proliferation of U87 cell line prior to using 3D and flow enabled cultures (Gerigk et al., 2021). There was no significant difference in purity of RNA extracted under 2D and 3D model while 2D cell culture shows a significant decrease in the stemness markers of U87 cells (CD44, CD133, nestin, olig2 and sox2) measured at day 3. Other studies focused on U87 cells morphology and structure, reported that after seven days in culture, U87 were fusiform (spindle-like shape), flat and epithelioid in 2D culture and small, round and formed a multi-layer structure with cilia or microvilli on their surface in 3D collagen scaffolds (Lv et al., 2016).

Additionally, in 2D culture, cells lose diverse phenotypes such as morphology and polarity which results in changes in cell division rate, function, inside organisation and structure, secretion and cell signalling (Meyers et al., 2006; Kapałczyńska et al., 2018). In 2D monolayer cell culture, cells have a continuous supply of nutrients, oxygen and signalling molecules in contrast to the natural conditions where the availability of these elements is variable among the cells of the multilayers tumour mass (Pampaloni et al., 2007; Langhans, 2018).

Finally, it is conventional that adherent monolayer cultures allow for the study of only one cell type in contrast to cells in the tumour niche where cancer cells interact with other cells in their microenvironment such as vascular cells and nonneoplastic glial cell types (Fischbach et al., 2007). With the establishment of cell-cell interactions during the formation

of spheroids, the 3D static system has been reported to mimic the physiological properties of the tumour better than the traditional 2D monolayer system (Kapałczyńska et al., 2018).

1.5.1.2 3D spheroid formation models

In order to better mimic the tumour cell environment inside the body, it was necessary to create new models of cell culture that would overcome the disadvantages of the 2D cell culture model described above. The 3D culture system has proven in many cancer studies to be a good solution. Since its first use by Hamburg and Salmon in 1970 (Hamburger & Salmon, 1977), many studies have reported a striking similarity of cell morphology and behaviour between cells in the tumour mass and those cultured under 3D conditions (Mazzoleni et al., 2009). Three types of 3D culture model are common in cancer research: (1) suspension cultures on non-adherent plates; (2) cultures in concentrated medium or in gel-like substances and (3) cultures on a scaffold (Kapałczyńska et al., 2016; Hoarau-Véchot et al., 2018).

In the first model, single cells are cultured with a medium in ultra-low adherent plates (**Figure 1.13a**) or in suspension (**Figure 1.13b**) and develop 3D structure in 3-4 days. This method is characterised by its simplicity and ease in culturing cells for further experiments (Weiswald et al., 2015a). While the use of petri dishes is common in this model, for some cell lines the cost of this experiment would rise because of the need for expensive plates coated with specific materials.

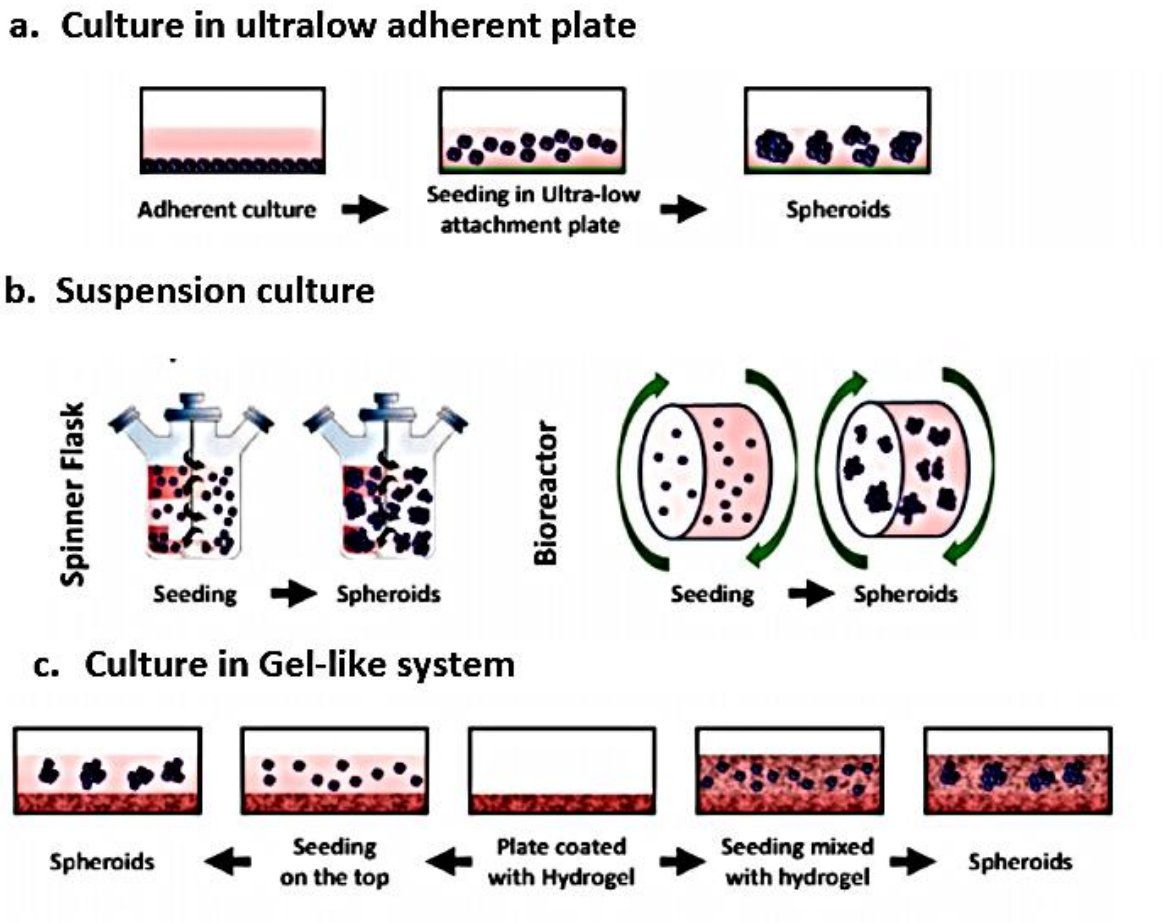

Figure 0.13 Common 3D models for creation of spheroids
a) Cells are seeded in an ultra-low attachment plate preventing them from adhering. b) cells are put under gravitational forces in a spinner flask or bioreactor. C) Cells are seeded on top of hydrogel with the medium or embedded in the gel also called scaffold-based model. Adapted from Hoarau-Véchot et al., (2018).

Another drawback of culture in suspension is the movement of cells in the medium which could result in the formation of aggregates of cells. In aggregated cells, individual cells can be seen attached to each other while in spheroid cells appear fused together and individual cells cannot be seen easily (**Figure 1.14**). Spheroid formation is induced when these aggregated cells are coated with Matrigel which will not be achieved when agarose is used alone (Li et al., 2011). Matrigel is an extracellular matrix consisting of natural polymers secreted by Engelbreth-Holm-Swarm (EHS) mouse sarcoma cells. In cell culture, Matrigel is commonly used as a basement membrane as it is enriched with laminin, collagen type IV, perlecan, and entactin (Funaki & Janmey, 2017).

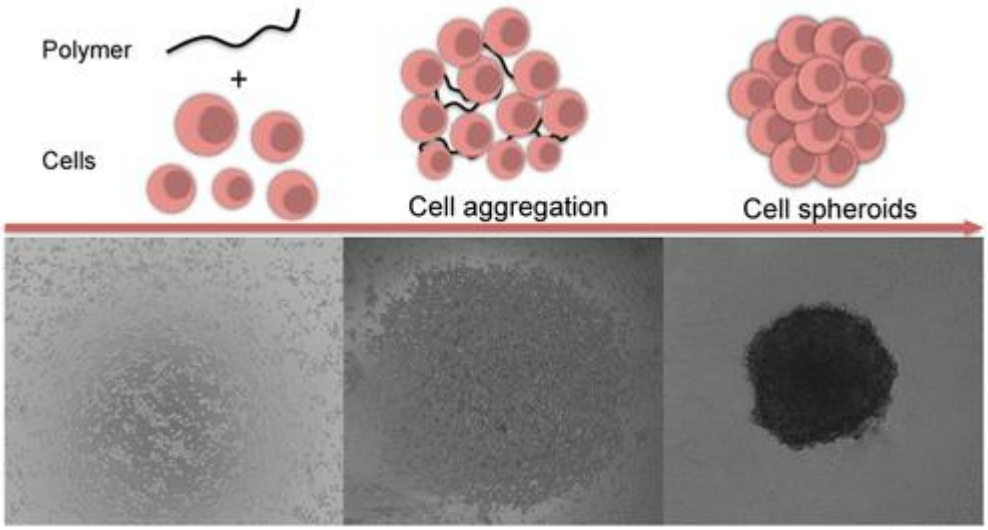

Figure 0.14 Spheroid formation process from cells then aggregate then spheroid
Taken from (Amaral & Pasparakis, 2016).

The second model consist of the culture of cells in a medium with gelling properties (**Figure 1.13c**). In this model, a low layer is obtained after solidifying in a plate a mixture of low-melting agarose with cell medium. The upper layer consists of agarose and the medium with single cells being added then flooded in Matrigel (Sodunke et al., 2007a; Li et al., 2011) . In this cell culture model, 3D structures can be seen after 7 days, and this model is usually used to test the potential of tumour cells to progress toward metastasis.

Interestingly, the use of soft agar allows for the growth of single cell with no attachment and anoikis induced cell death (Weiswald et al., 2015b). In this case cells grow without adhering which facilitates cell aggregation and spheroid formation. Also, the use of Matrigel make both the culture and the extraction of cells which can form a tissue like structure with 3D interactions (Sodunke et al., 2007b; Zoetemelk et al., 2019). The major drawbacks of this model include the non-spherical shape for some cell lines, the time needed for the preparation of agar layers, low reproducibility and the difficulty of extracting cell for immune-staining assays (reviewed in (Weiswald et al., 2015b; Lv et al., 2017).

The third model consists of culturing cells in a scaffold of biodegradable fibres such as silk (**Figure 1.15**) (Jastrzebska et al., 2014), collagen (Nocera et al., 2018), laminin (Yamada et al., 2020) or alginate (Li et al., 2020). Compared to the gel like system, in this model cells are easily prepared for immunohistochemical analysis. Additionally, this system is more convenient for commercial functional tests and extraction kits (DNA, RNA and proteins).

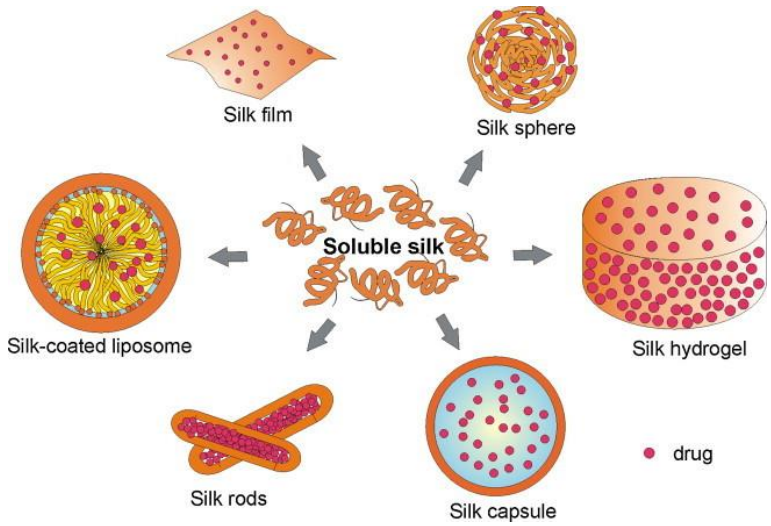

Figure 0.15 Different biomaterials made of silk used for chemotherapeutic assays (Jastrzebska et al., 2014).

Surprisingly, in addition to the difficulty of observation and extraction of cells for some analysis cells grown in scaffold of biodegradable fibres, are incapable of forming spheroid shapes and grow flattened like in adherent conditions. These features influence aggregation process toward spheroid formation, which will induce a big difference between the behaviour and characteristics of cells cultered in a scaffold and those in real tumour mass (Aggarwal et al., 2009; Jastrzebska et al., 2014; Bassi et al., 2020).

1.5.1.2.1 Biological characteristics of Spheroids

Spheroids are created as a result of division of cells under non adherent conditions, where cells display reduced cell-cell and cell-matrix interactions and escape from anoikis phenomena (Chen et al., 2012). According to the architecture of the spheroid shape, three kinds can be grown i) tight spheroids, ii) compact aggregates and iii) loose aggregates (Vinci et al., 2012; Vinci et al., 2015). In his study Weissenrieder has excluded loose aggregates from counting spheroids formed using GBM U87 cell line. Spheroids considered in this study should be “rounded aggregates” of cells with a smooth surface and poor cell-to-cell definition’’ (Weissenrieder et al., 2020).

Hirschhaeuser et al. (2010) and Weiswald et al. (2015) suggested that spheroids should only be compact aggregates with spherical shape and not loose aggregates. The compactness of spheroids with multilayer structure can be checked under microscope to evaluate intercellular spacing and differentiate it from loose aggregate. This feature allows them to exhibit features most similar to *in-vivo* tumour tissues and make them a more suitable

tool to drug testing assays comparing to 2D monolayer cell cultures (Edmondson et al., 2014).

In general, in a spheroid system three distinct layers can be formed according to their proliferation rate **Figure 1.16A**. The outer 4-5 cell layers form the proliferating layer (Ziółkowska et al., 2013). These layers mimic the angiogenesis-induced sites when cancer cells are cocultured with endothelial cells. An intermediate layer made with inactive cells forming the inactive layer, and a necrotic core recapitulating the hypoxic necrotic tumour core which normally appear in spheroids with a diameter >500 μm (Santo et al., 2016).

In contrast to 2D monolayer systems, where cells are continuously exposed to nutrients, oxygen, and drugs, multilayer spheroid system generate physiologically relevant gradients and reduced intake of nutrients, oxygen, and drugs as you move further into the mass; **Figure 1.16B** (Curcio et al., 2007; Ruppen et al., 2014). Additionally, in 3D spheroid model cells make cell-cell and cell-ECM attachments as well as interactions between cells of different layers strongly affecting the cytotoxicity assays. Cells in the outer layer have an exponential growth rate (Kelm et al., 2003) which slows as cell move towards the core of the spheroid because only cells near the outer spheroid layer are replicating (Engelberg et al., 2008) which is consistent with *in vivo* data (Sutherland & Durand, 1984; Kunz-Schughart et al., 1998).

Many other *in vivo* tumour tissue features, can be seen in 3D spheroid model, such as: chemotaxis-driven cell movements, low pH at the core due to the production of lactic acid under the low oxygen conditions **Figure 1.16C** (Alvarez-Pérez et al., 2005) and, in some cases, can lead to the formation of lumen as a result of cell apoptosis in the central part of the spheroids (e.g. acinar-like spheroids; Kapałczyńska et al., (2018). Finally, an advantage for cancer research and regenerative medicine is that 3D spheroids can form co-cultures and recapitulate the complexity of natural tumour tissues (Hsiao et al., 2012; Lee et al., 2013; Ruppen et al., 2015) **Figure 1.16D**.

In conclusion, despite spheroids recapitulating the anatomy of a tumour mass in the body with its multi-layered structure, the use of 2D culture model is crucial to validate studies before moving forward to other culture systems which are often more expensive and time consuming.

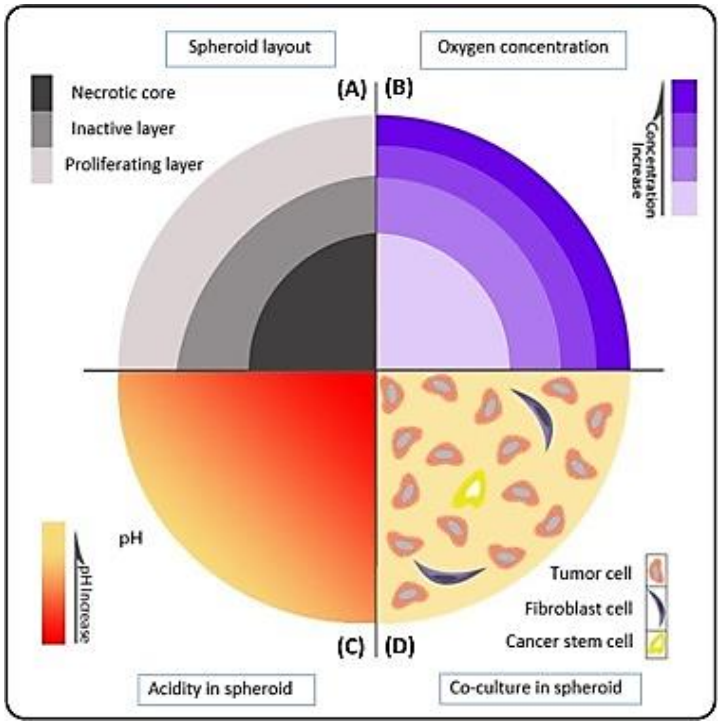

Figure 0.16 Physical characteristics of a spheroid
(A) Three layers with different proliferation rates; (B) Oxygen concentration gradient with hypoxic environment at the core of the tumour spheroid; (C) pH gradient and creation of an acidic environment in the core as a result of anaerobic activities; (D) Co-cultured cells in a tumour spheroid Moshksayan et al., (2018).

1.5.1.3 Culture in microfluidic system

1.5.1.3.1 Materials used in microfluidic devices

The history of microfluidics started in the 1950s, with the invention of tiny tubes that transport the ink in computer printers (Perestrelo et al., 2015). This technology has massively improved over time and in the 1990s was first applied to biology which allowed researchers the control of liquids in microchannels (reviewed by Convery & Gadegaard, (2019)).

Later, in the 2000s, thanks to the improvements in cost and production time of these devices, many laboratories were able to conduct microfluidic research based on moulding micro-channels in different polymers. These polymers include poly-di-methyl-siloxane (PDMS) (Hattersley et al., 2008; Hattersley et al., 2011; van Midwoud et al., 2011; Bower et al., 2017; Zhu et al., 2019) and thermoplastic-based materials (Bale et al., 2019) .

PDMS is a widely used material to make microfluidic chips in biology systems. This material possesses many advantages such as being transparent at optical frequencies (240 nM – 1100 nM), having a low autofluorescence, it is bio-compatible, deformable, inexpensive, and easy to mould (Mata et al., 2005; van Poll et al., 2007; Zhou et al., 2010; Zhu et al., 2019). However, because PDMS is made of a silicone rubber, it is very hydrophobic and

hence can adsorb small hydrophobic molecules like drugs and their metabolites (Duffy et al., 1998; Toepke & Beebe, 2006). Additionally, two other drawbacks were reported, first, PDMS can leach un-cross-linked toxic oligomers into solution (Regehr et al., 2009) and secondly this polymer is shown to be sensitive to the exposure to some chemicals and it sometime, return to its hydrophobic state after surface treatment (Kim et al., 2000; Bunge et al., 2017).

Because of the disadvantages cited above, more desirable materials for microfluidic cell cultures are being increasingly used instead of PDMS (Meyvantsson & Beebe, 2008). These are the thermoplastic materials (Young et al., 2011a; Jeon et al., 2011). Thermoplastic-based materials are highly crosslinked polymers with two benefits in addition to the low electrical conductivity. First, the physical characteristics making them more stable than PDMS and secondly, hydrophilicity can be retained for years after oxygen plasma treatment or UV/ozone exposure (Nge et al., 2013).

Thermoplastic materials include commonly used ones in microfluidics like Polystyrene (PS), Polycarbonate (PC), Poly(methyl methacrylate) PMMA, and Cyclic Olefin Copolymer (COC). Less commonly used thermoplastics include, Poly(ethylene glycol) diacrylate (PEGDA), and Teflons: perfluorinated compounds (FEP/ PFA/PFPE/PTFE) (Liu & Fan, 2011; McMillan et al., 2020). Interestingly, these polymers, after being cured by reaching glass transition temperature (Tg), can be remoulded many times (Ren et al., 2013). Some other less used thermoplastics are listed in the table below (**Table 1.7**). **Table 1.8** summarises important properties, advantages, and drawbacks of commonly used thermoplastics in microfluidics.

In their work, Midwoud & Sturla (2013) have compared the adsorption properties and biocompatibility of microfluidic devices made from different thermoplastic materials (PMMA, PS, PC and COC) as alternatives for PDMS. They found that only UV-ozone-treated PC and COC devices satisfied both criteria when culturing human hepatoma (HepG2) cells. Early studies on PMMA use in microfluidic devices showed that this material as well as PC, PS and COC polymers are more resistant to solvents both acids and bases than PDMS (Liu et al., 2009; Tsao, 2016). In his review about the use of thermoplastic material in microfluidic system, (Gencturk et al., 2017) report that PMMA material offers good thermal stability and insulation properties. He showed also that PMMA present some advantageous characteristics over other thermoplastic materials which include high mechanical strength, hardness, and rigidity. Accordingly, Sözmen & Yildiz, (2021) have developed a PMMA

microfluidic chip using simple and rapid fabrication methodology which provides high bonding strength while protecting microchannel integrity in a less than one hour process.

Table 0.7 Properties of different thermoplastics used to fabricate chips

Thermoplastics	CTE [m/(m K)] 10^{-6}	Young's modulus (GPa)	Tg (°C)	Tm (°C)	Solubility parameter δ $(MPa)^{1/2}$	Water absorption (%)	O2 permeability (x10^{-13} cm^3. cm cm^{-2} s^{-1} Pa^{-1})	Biocompatibility	Transparency	Auto-fluorescence
Cyclo olefin (co) polymer (COC/COP)	60–70	1.7–3.2	70–180	190–320	17.7	0.01	NA	Biocompatible	Transparent	Low
Polymethyl methacrylate (PMMA)	7077	2.4–3.4	105	250–260	20.1	0.1–0.4	0.1	Biocompatible	Transparent	Low
Polyethylene terephthalate (PET)	59.4	2–2.7	70	255	20.5	0.16	0.03	Biocompatible	Transparent	Medium
Polyethylene-low density (LDPE)	100–200	0.11–0.45	−125	105–115	17.6	0.005–0.015	2	Biocompatible	Both opaque and transparent	Medium
Polyethylene-high density (HDPE)	120	0.8	−80	120–180	18.2	0.005–0.01	0.4	Biocompatible	Both opaque and transparent	Medium
Polypropylene (PP)	72–90	1.5–2	−20	160	16.3	0.01–0.1	1.7	Biocompatible	Both opaque and transparent	Medium
Polystyrene (PS)	70	3–3.5	95	240	18.7	0.02–0.15	2	Biocompatible	Transparent	High
Polycarbonate (PC)	65–70	2.6	145	260–270	19.4	0.23	1	Biocompatible	Transparent	High
Polyvinyl chloride (PVC)	54–110	2.4–4.1	80	100–260	19.4	0.04–0.4	0.04	Biocompatible	Transparent	High
Polyamide (Nylon)	110	2.5	47–60	190–350	28	1.6–1.9	0.03	Biocompatible	Transparent	High
Polysulfone(PSU)	55–60	2.48	185	180–190	18.7	0.2–0.8	NA	Biocompatible	Translucent	High
Polylactic acid (PLA)	740	3.5	60–65	150–160		0.68	NA	Biocompatible (problematic)	Transparent	High
Polytetrafluoroethylene (PTFE)	112–135	0.4	115	326	12.6	0.005–0.01	3	Biocompatible	Translucent	High
Polyetheretherketone (PEEK)	26	4–24	143	343	21.9	0.1–0.5	0.1	Biocompatible	Opaque	NA
Acrylonitrile butadiene styrene (ABS)	72–108	1.4–3.1	105	Amorphous	18.8	0.05–1.8	0.5	Not suitable	Both opaque and transparent	High

Tg: glass transition temperature; Tm: melting temperature; CTE: coefficient of temperature expansion (Gencturk et al., 2017)

Table 0.8 Advantages, drawbacks, applications, moulding and bonding methods, and glass transition temperature of most used thermoplastics in microfluidic devices

	Advantages	Drawbacks	Common applications	Moulding methods	Bonding methods	Tg (°C)
Polystyrene (PS) (Chen et al., 2008; Young et al., 2011b)	- Optically transparent - Biocompatible. - Adapted for the use in manufacturing porposes - Possiblity of rapid bonding.	- Expensive equipment -Thermal bonding difficult - Channels collaps when width-to-height aspect ratios are too high.	- Cell culture on microfluidic chip - Organ-on-chip system	-Injection moulding -Hot embossing.	-Thermal bonding, with plasma treatment	92-107
Polycarbonate (PC) (Ogończyk et al., 2010; Wang et al., 2010)	-Durable material - Transparency in the visible - Low cost - High resistance - Low moisture absorption	- Poor resistance to certain organic solvents - Absorbance in UV - Thermal bonding only - Channels geometry could be altered due to bonding temperature.	- DNA thermal cycling - Design of multilayer devices - Enzymatic amplification - Nucleic acid extraction - Pathogen detection		- Thermal bonding	145-155
Poly (methyl methacrylate) PMMA (Zhang et al., 2009; Zhang et al., 2014; Matellan et al., 2018)	- Low price - Least hydrophobic polymer - Rigid - Excellent optical transparency - Ease of fabrication - Re-usable	-Temperature resistance - Moisture absorption properties	- Ecological microchips - DNA sequencing machines - Electrophoresis	-CO2-laser micromachining - Injection moulding - Hot embossin - Compression moulding	-Hot-press bonding - Microwave bonding - Thermal fusion bonding - Adhesive bonding	85-165
Cyclic Olefin Copolymer (COC) (Jena & Yue, 2012)	- Good resistance to: (Hydrolysis, Acids, Bases) - Low autofluorescence - High heat resistance	-Expensive equipment - Surface treatment needed to minimize cell adhesion	- Packaging films - Lenses and vials - Medical devices. - Lab-on-a-chip	- Injection moulding - Injection and stretch blow moulding - Compression moulding	- Solvent bonding - Adhesives - Thermal fusion bonding	70-177

1.5.1.3.2 Continuous flow microfluidics applied to cancer research

A microfluidic chip is a pattern of hollow microchannels with dimensions ranging from ten to hundreds of micrometres (Wei et al., 2014), creating a microenvironment with holes of different size through which liquids are injected and evacuated. The microchannel network is designed in a manner to achieve desired features of different applications such as lab-on-a-chip, organ on a chip, detection of pathogens, electrophoresis, digital microfluidics, DNA analysis and continuous flow microfluidics (Ng et al., 2019).

In continuous flow systems, the microfluidic device allows a continuous flow of fluids, and especially in biological systems it allows a continuous feed of nutrients (and pharmaceutical compounds) with removal of waste products, in order to recreate key features of human tissue physiology. Recently, this system emerged as a powerful tool in the study of cancer biology and treatment commonly termed tumour-on-a-chip (Hachey & Hughes, 2018; Wan et al., 2020).

1.5.1.3.3 Microfluidics for the study of cancer tissues (tumour-on-a-chip model)

Tumour-on-a-chip models, provide microscale fluid handling components that allows a continuous flow of programmable nutrient supply and waste removal to the microenvironment of tumour tissues (sliced or mico-dissected) extracted from patients, emulating *in vivo*-like properties of these tissues in the body (Reviewed by Liu et al., (2021)).

This approach was first used by Blake et al. (2007) and Choi et al. (2007) using rat brain tissues in hollow SU-8 microneedle system (**Figure 1.17A)** or PDMS system respectively (**Figure 1.17B**). Even though, both studies reported that cell viability could not be maintained over 4hr, the results opened prospects in the use of microfluidic system in studying tissue cancer biology.

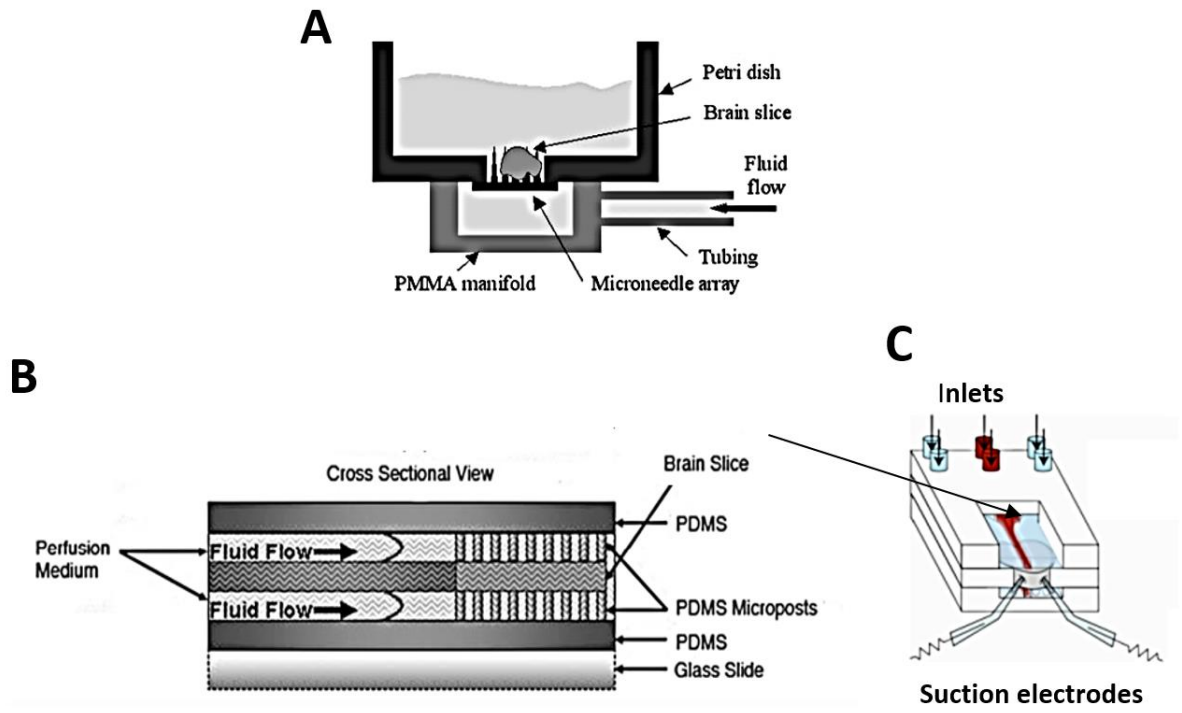

Figure 0.17 Schematic view of A) SU-8 microneedle array system and (B-C) 3 layers PDMS system
B) Cross section displaying the side view of the device. The brain slice fits into the middle layer. C) Graph of the PDMS device showing the suction electrodes attached to nerve roots to record spontaneous respiratory motor output. (Blake et al., 2007).

Additionally, (Khong et al., 2007) developed an intra-tissue perfusion (ITP) system in which thick liver slices (>>300µm) were maintained for about 3 days. Later on, (Hattersley et al., 2008) developed a new microfluidic device in which liver tissue explants were kept viable and functional over 4 days (**Figure 1.18**). Later, different microfluidic devices were used to study effect of chemotherapeutic drugs (Sylvester et al., 2012), radiation (Carr et al., 2014), or in combination (Cheah et al., 2017) **(Figure 1.19)** on head and neck squamous cell carcinoma (HNSCC) tissue biopsies.

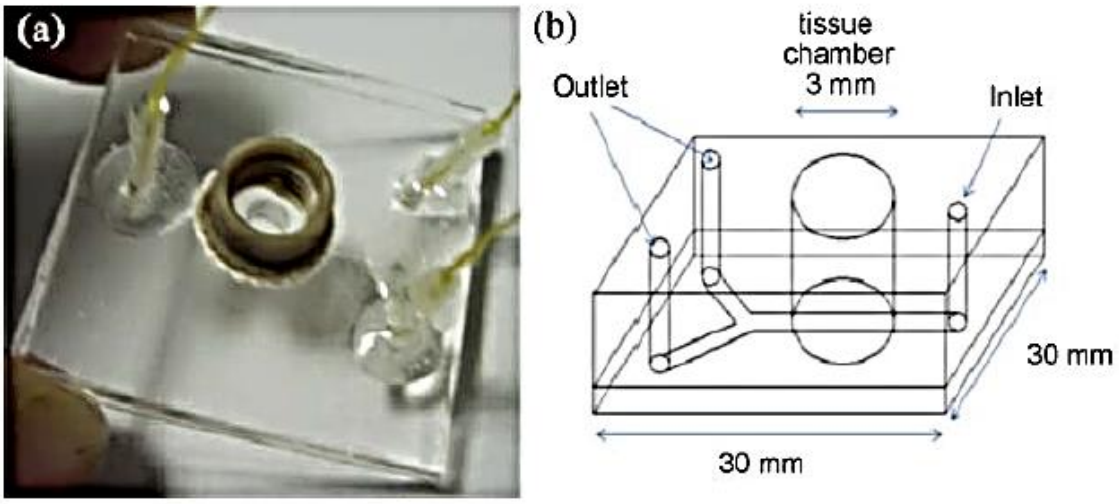

Figure 0.18 Photograph (a) and schematic (b) of the device used for maintaining and probing tissue sample *(Hattersley et al., 2008).*

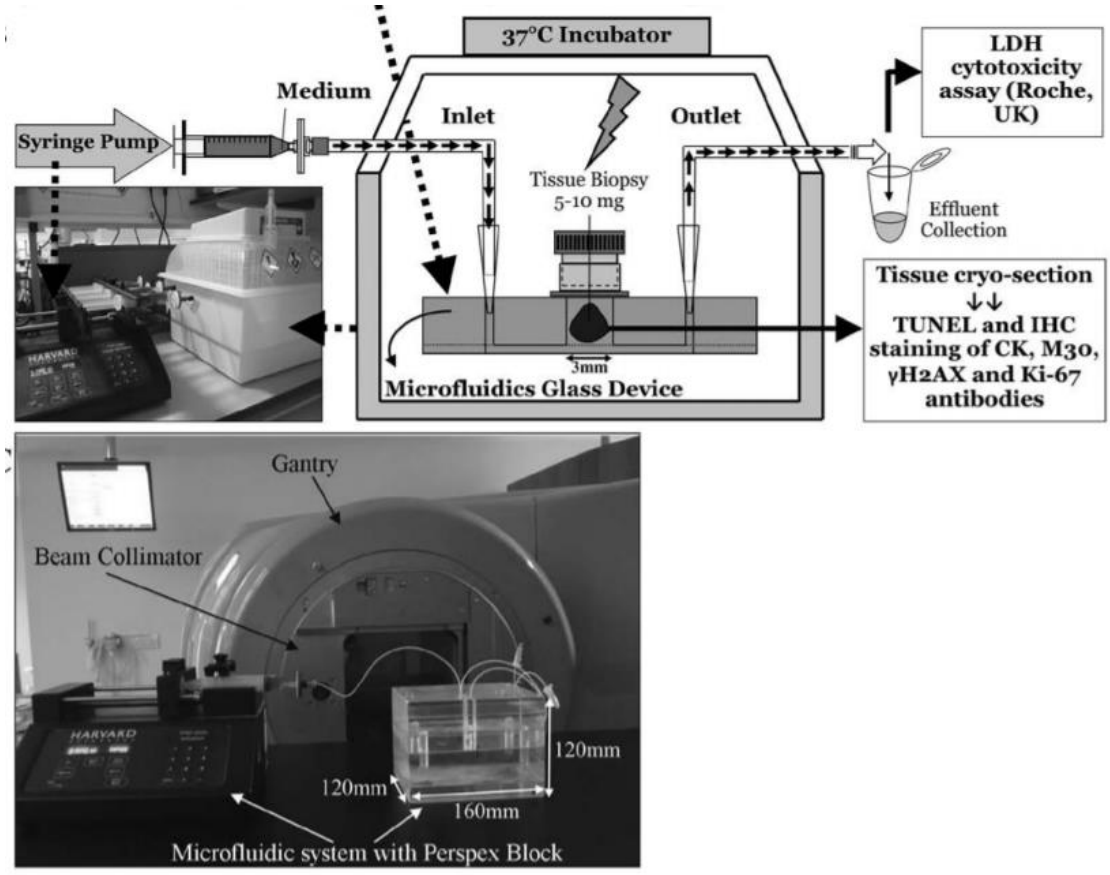

Figure 0.19 Microfluidic device used to test irradiation on incubated tumour tissue
Top – a schematic diagram of the entire microfluidic device. Bottom - photograph of the microfluidic device used to test irradiation on incubated tumour tissue. Taken from (Cheah et al., 2017).

Currently, tissues derived from different types of cancers have been constructed on microfluidic chips, including ovarian cancer (Astolfi et al., 2016), breast cancer (Gioiella et al., 2016), lung cancer (Hassell et al., 2017; Yang et al., 2018), rectal cancer (Rodriguez et al., 2020) and many other healthy and diseased tissues and organs (Liu et al., 2021).

Brain tissue based microfluidic studies started earlier than the liver slices with (Murry et al., 2006) studying metastasis on a brain slice model. Later on many studies were carried on brain tumour sliced or microdissected from mouse (Chang et al., 2014) or human model (Frimat & Luttge, 2019; Cho et al., 2021).

It was only in recent studies where glioblastoma was used for tissue-based study in a microfluidic platform. In a large study Olubajo et al., (2020) studied 128 glioblastoma biopsies (2 mm^3) derived from 33 different patients and introduced into a Y-shaped microfluidic device. They showed that the GBM tissue could be preserved in this microfluidic device **(Figure 1.20)** for over 72 hours while different viability and immunohistochemical tests conducted on-chip were comparable to those conducted on freshly harvested tissues (Olubajo et al., 2020).

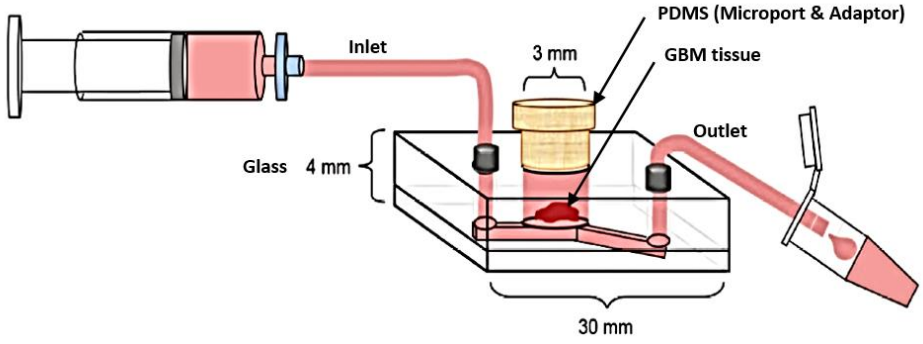

Figure 0.20 Schematic of the microfluidic setup
showing a syringe attached to the inlet and collection tube attached to the outlet of the device enabling a constant media influx and simultaneous removal of waste products. The tissue sample is in the device chamber. Scheme adapted from Olubajo et al., (2020), and Dawson et al., (2016).

In parallel, Xin Cui and colleagues have reported the possibility of developing patient specific immunotherapeutic approach for GBM cases by culturing immune cells as well as tumour tissue from the same patient in a microfluidic GBM-on-a-Chip platform (**Figure 1.21**) (Cui et al., 2021). In their patient-specific GBM-on-a-Chip, they successfully studied the immunosuppressive mechanism as well as optimizing anti-PD-1 immunotherapeutic approach for unrelated GBM subtypes. Equally, many other studies have successfully co-

cultured GBM cell with other cells like tumour-associated macrophages (Cui et al., 2020), micro-glial cells (Leite et al., 2020) and more recently with HUVECs cells (Amemiya et al., 2021).

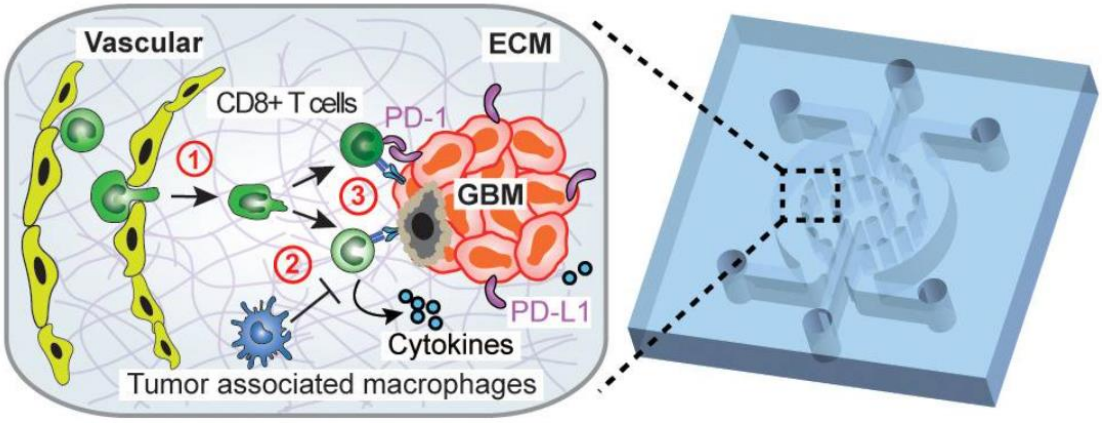

Figure 0.21 A schematic diagram of GBM-on-a-chip device
(on the right). On the left, interactions of immune cell (CD8+ T-cells) ① with brain microvessels, ② tumour-associated macrophages (TAMs) and ③ GBM tumour cells in an engineered 3D brain-mimicking ECM (Cui et al., 2021).

1.5.1.4 GBM spheroids in microfluidic system

Another model which is widely used for the research of new effective therapeutic approach for GBM, is the use of spheroid system coupled with microfluidic device. In this model spheroids are either formed in the microfluidic device called spheroid formation chip or formed outside then introduced in the microfluidic device.

1.5.1.4.1 Microfluidic spheroid formation chip (μSFC)

Many recent studies have focussed on developing chips that produce size-controllable GBM spheroids on which high-throughput drug screening can be conducted. (Ayuso et al., 2015) reported the first application of a microfluidic device to observe the migratory aptitude of GBM U87 multicellular spheroids. In their study, spheroids were embedded in collagen then introduced in a chip, demonstrating that in contrast to oral squamous carcinoma OSC–19 spheroids which invade collectively as a whole, U87-MG multicellular spheroids migrate as individual cells. Fan et al. (2016) have developed a three-dimensional (3D) brain cancer chip composed of photo-polymerizable poly(ethylene) glycol diacrylate (PEGDA) hydrogel with microfluidic dimension of 2.7 cm × 4 cm (**Figure 1.22A**). On this chip GBM U87 spheroids were formed then a successful combinatorial treatment was conducted using Pitavastatin and Irinotecan and demonstrated that on day 4, the respective cell viabilities levels for the

untreated, Pitavastatin treated, and Irinotecan treated spheroids showed a significant decreased to 95%, 85% and 50% (Fan et al., 2016).

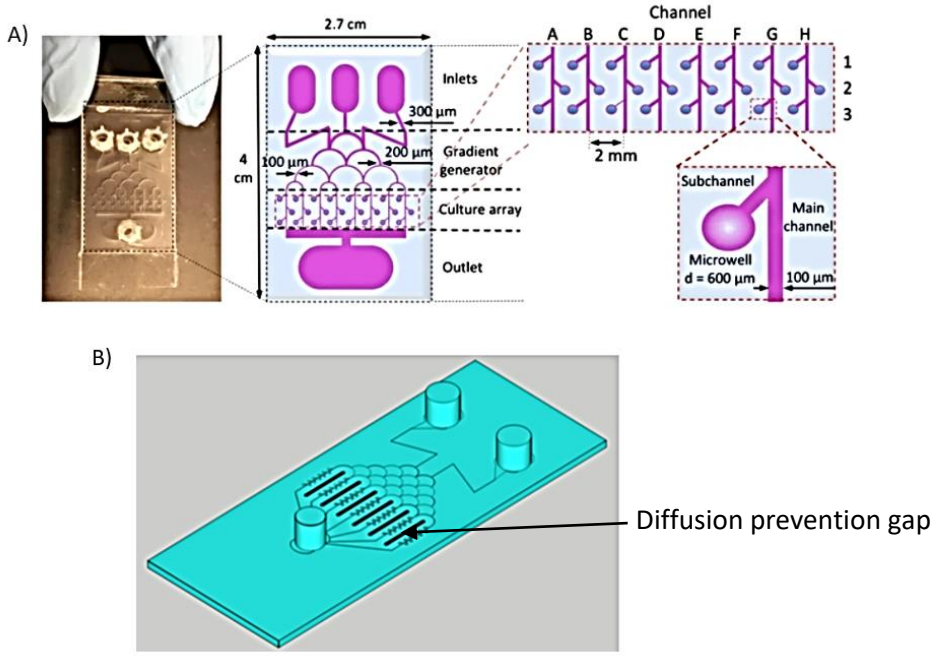

Figure 0.22 A) photo and scheme of the devices used by Metin Akay group
B) scheme of the modified device with two inlets and a single outlet, connected by 7 microfluidic channels with 9–11 microwells per channel. They added a 600 µm wide diffusion-prevention gap between each microfluidic channel to prevent diffusion of drug molecules through the porous hydrogel matrix from one channel to another. Photo modified from (Fan et al., 2016) and (Akay et al. 2018).

Later on, in order to be able to generate relatively large number of uniformly-sized spheroids a Korean group have used a microfluidic device with pillars (diameter: 40 µm, height: 70 µm, centre-to-centre distance: 140 µm), called a microfluidic pillar array (µFPA) device (**Figure 1.23**). About three hundred spheroids were formed within 3 days using U87, U251 GBM and triple negative breast cancer (TNBC) primary cells. A respective drug screening as well as expression of cancer stem cell markers (CD133, HIF-1α) were performed on the same device (Lim et al., 2018).

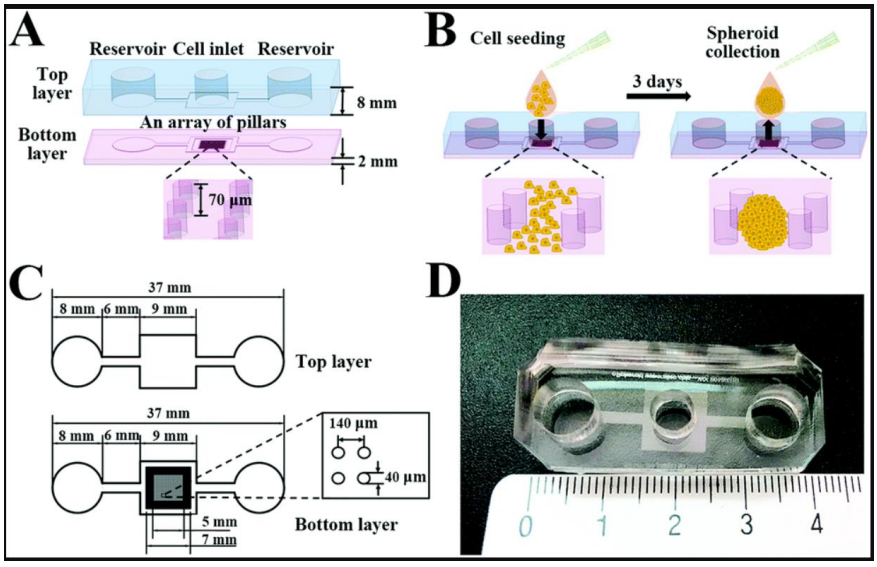

Figure 0.23 Microfluidic pillar array device
(A) Scheme of the µFPA device showing different layers. (B)cells seeding and spheroid harvesting. The dimensions (C) and image (D) of the µFPA device. (Lim et al., 2018).

More recently, Metin Akay's group has introduced some modification on previous microfluidc device (Fan et al., 2016) allowing to overcome the the diffusion across channels of drug molecules through the porous hydrogel matrix. On this new device (**Figure 1.22B**), the action of TMZ associated with bevacizumab over a range of concentrations, was tested on 3D spheroids formed using GBM patient derived cells, demonstrating that TMZ works more effectively when it is combined with bevasisamub than when administered alone (Akay et al., 2018). In another study, using a very similar device (**Figure 1.24**) it was demonstrated that GBM spheroid formation is inhibited using TMZ in combination with an NF-κB inhibitor (Xia et al., 2020).

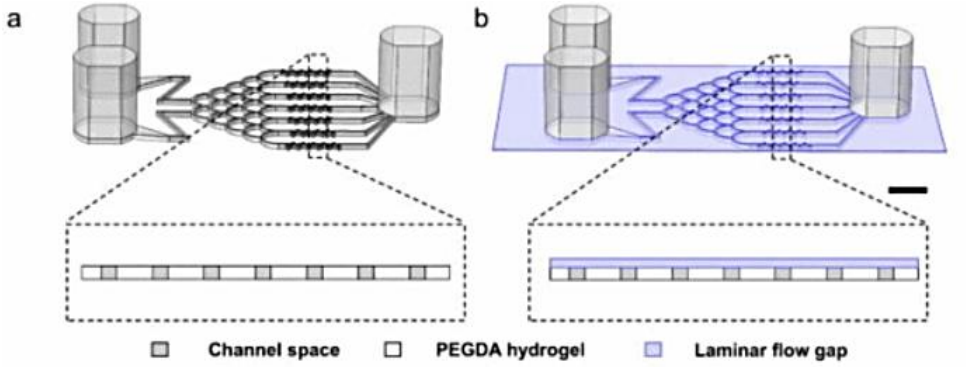

Figure 0.24 Brain cancer chip
(a) Schematic of the original microfluidic device design, without the laminar flow layer, and a cross section over the microwell array reported in Akay et al. (2018). (b) Schematic of the new microfluidic device design with the additional laminar flow layer, and a cross section over the microwell array. Scale bar is 5 mm. Figure adapted from (Xia et al., 2020).

1.5.1.4.2 Spheroid formed off the chip then introduced to the microfluidic device

The second model of using spheroids in a microfluidic platform is to form the spheroids then introduce them in a chip where cancer metastasis studies and testing of new therapeutic approaches can be performed. This model was previously applied to spheroids formed using breast ductal carcinoma *in situ* (DCIS) cells (Choi et al., 2015) and cardiac spheroids formed using human induced pluripotent stem cell lines (hiPSC) (Christoffersson et al., 2018). Choi and colleagues formed the spheroids in ULA plates then introduced them after 3 days to a Matrigel and fibronectin coated PDMS multi-layered microfluidic device Choi et al., (2015), while Christoffersson et al. (2018) formed the spheroids within 48 hr in Statarrays© MCA96-16.224-PSLA Low Attachment Surface plates then introduced them to microfluidic channel slides with dimensions 17 × 3.8 × 0.4 mm (length × width × height) coated with laminin (100 µg/mL) to each channel to facilitate spheroids attachment (Christoffersson et al., 2018).

Only few data were published using GBM spheroids off-chip then introduced in a chip. In the university of Hull two research studies have been conducted using spheroid off-chip model. In the first study (Collins et al., 2021a) used different cell lines to form spheroids including adenocarcinoma metastatic cell lines (MDA-MB231 and MCF7), GBM; astrocytoma primary cell line U87 and colorectal adenocarcinoma primary cell lines (HT29 and HCT116). Spheroids were formed in ULA plates at cell densities (2.5×10^4 or 3.5×10^4 cells per well) then transferred to a microfluidic device as 1 spheroid per device. The spheroid is entrapped in a specific zone whilst the media is continually perfusing over it with a syringe attached to the inlet and a collector tube to the outlet of the device. The device was made of Schott B270 glass, and the tube connectors were made of PTFE (polytetrafluoroethylene), and all the set was placed in an incubator at 37ºC with a flow rate set to 3µl/min. To increase performance and utility, the device underwent 3 iterations (**Figure 1.25**). The study showed that the designed device allowed a direct imaging of the spheroid on the chip. In addition, U87 spheroids showed no significant differences in cell invasion in Matrigel between on and off the chip while IL-6 and VEGF levels and the migration on chip in collagen were increased in the on-chip models within hydrogel conditions compared to the off-chip counterparts.

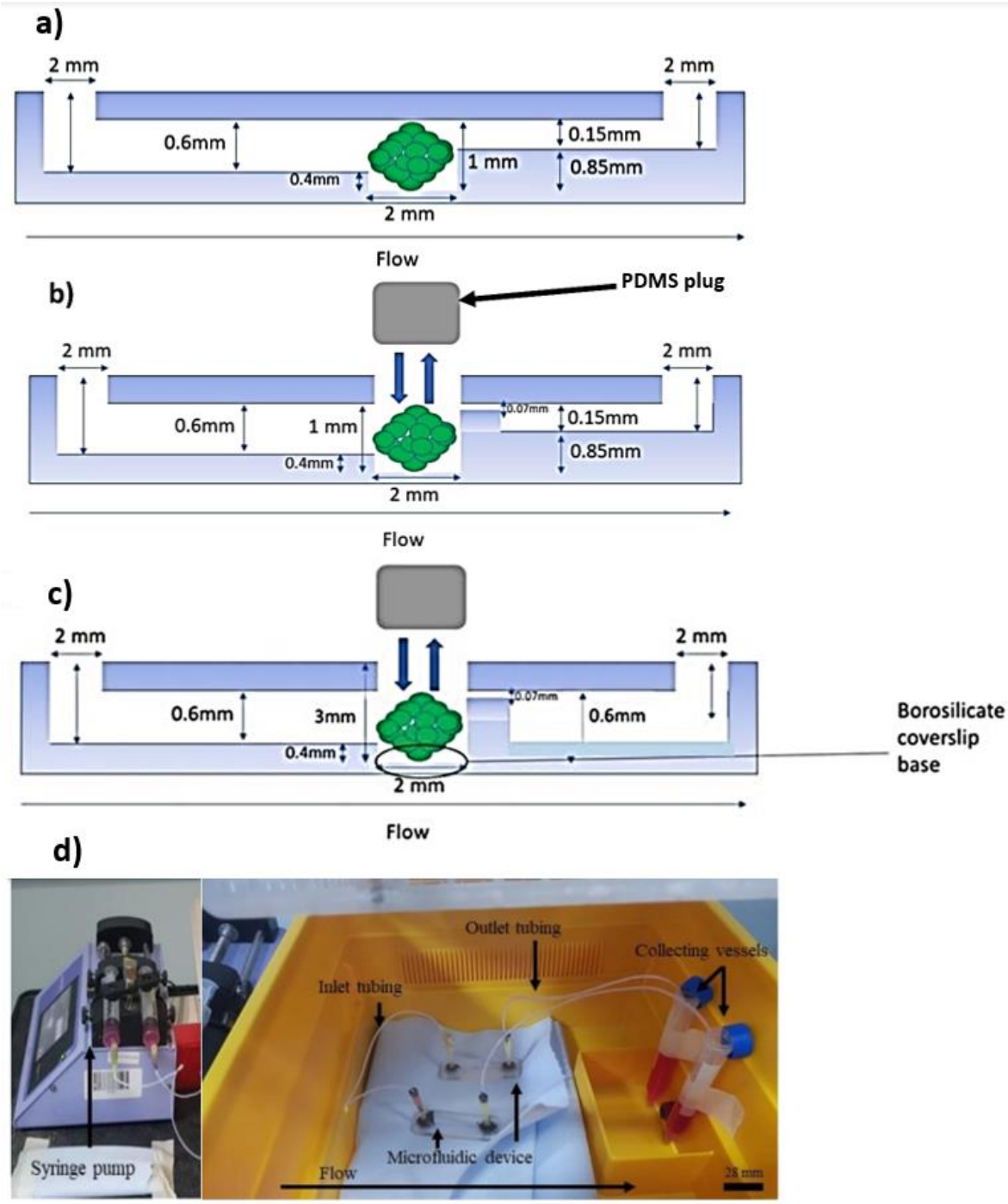

Figure 0.25 Scheme and photo of the microfluidic device used by (Collins, PhD thesis 2019)
a, b and c) Schematic view of the device setup with an example spheroid (green) entrapped in the micro-well. a) The generation 1 of the device. b) The generation 2 showing an access port (2 mm wide and 3 mm deep) was added directly above the micro-well (with a removable transparent PDMS plug) enabling ease access of the spheroid to the microwell preventing channel blockage when usin g the inlet port and direct imaging of a spheroid within the microwell. A 70 µm weir was milled at the entrance of the shallow channel after the microwell to prevent any through flow of spheroids out of the microwell. C) The generation 3 of the device with a borosilicate coverslip added at the base of the microwell preventing light reflection and enabling clearer images. D) Photo of the device setup showing the device inside the egg incubator. Adapted from (Collins et al., 2021a).

In a second study Michael Jeffrey used the human U87 MG primary cell line to assess spheroid viability and to investigate the effect of drug therapy (Doxorubicin and TMZ, alone and in combination) on spheroids in a microfluidic platform. Spheroids were formed in agarose gel in a 96-well round-bottomed plate. Experiments were done on two microfluidic chips, an "old style" (discussed above see **Figure 1.18**) and compared to a "new style" design (**Figure 1.26)**. The "new style" device is made of three separate pieces of poly (methyl methacrylate) (PMMA).

In his thesis Michael Jeffrey reported that the "old style" had many leakage issues and therefore was unsuitable for long term study of spheroids or tissue. Using the "new style" device he demonstrated that Doxorubicin or TMZ alone and in combination inhibit LDH release from GBM spheroids which could be kept alive on a chip for at least two weeks.

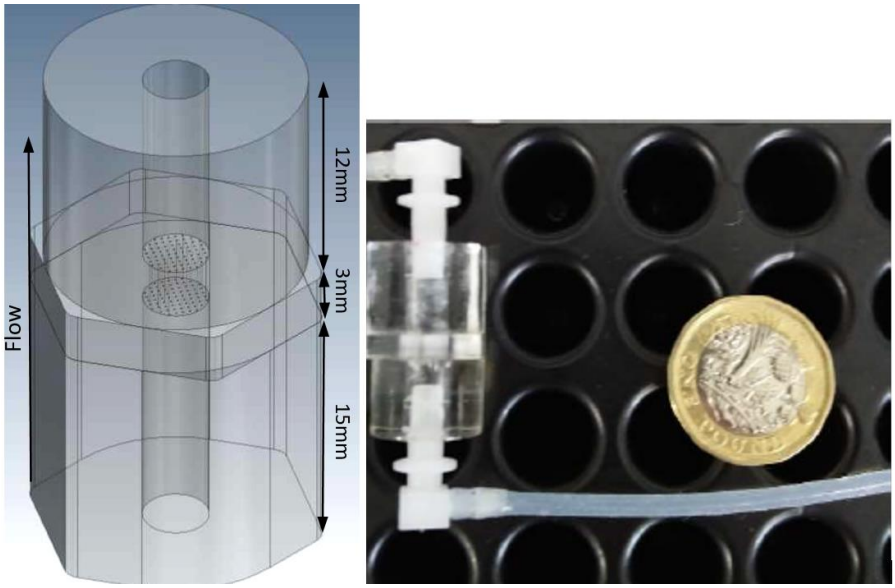

Figure 0.26 Microfluidic device used by Michael Jeffrey
To the left schematic view and dimensions of the device. The central piece is equipped with 0.05mm holes drilled to the centre of it to right a photo of the chip. Adapted from (Michael Jeffrey Viswanath Chidambara, 2019).

In cancer on-a-chip technology a huge number of targeted therapeutic approaches can be tested rather than using animal models or human subjects with saving of time and costs. Obviously, this technology will help in reducing the use of animals in pharmacodynamic and pharmacokinetic investigations, as well as toxicology studies. Microfluidic tumour in-a-chip devices could lead in a time manner to imminent advances in the prevention and treatment of different cancer types. The device used in this current study is made of PMMA, on which gene knockdown using GBM primary cell lines will be conducted. Compared to the device

(**Figure 1.26**), for the well set of spheroids and to facilitate spheroid manipulation, the inlet part (15mm) was split in two pieces (10mm + 6mm). Additionally, the central piece was equipped with 0.1mm holes (instead of 0.05mm in the device presented in **Figure 1. 26**) drilled to the centre of it, to decrease the flow velocity and by the way decreasing the shear rate in this region and so that to prevent a possible spheroid damage or aggregate dissociation as described previously with (Qiu et al., 2018).

1.6 RNA interference use in glioblastoma

1.6.1 Definition and different kind of RNA interfering molecules

Originally described in Caenorhabditis elegans (Fire et al., 1998), the RNA interference (RNAi) phenomenon was reported in plants, animals, Neurospora crassa, nematodes, fungi, trypanosomes and even viruses (Bass, 2000; Cogoni & Macino, 2000; Waterhouse et al., 2001). RNAi is a mechanism by which gene expression is partially or totally inhibited (posttranscriptional gene-silencing) using small molecules of RNAs which could be either microRNA (miRNA), small interfering RNA (siRNA), or short hairpin RNA or small hairpin RNA (shRNA, Wang et al., (2011)).

1.6.1.1 miRNAs

miRNAs are small noncoding endogenous RNA molecules, playing an important role in regulating cellular functions (reviewed by Ha & Kim, (2014)). First, in the nucleus, a primary miRNA transcript (pri-miRNAs) is synthesized from genome-encoded hairpins by RNA polymerase II or III (Lee et al., 2004; Borchert et al., 2006). Then, pri-miRNAs, are processed within the nucleus into 60–70 bp hairpins by the microprocessor complex, consisting of RNase-III enzyme (Drosha) and RNA-binding protein DGCR8 (Saini et al., 2007; Finnegan & Pasquinelli, 2013). The released small RNA hairpin (about 60 nt) has a two-nucleotide overhang at its 3′ and is termed as a pre-miRNA (Denli et al., 2004; Han et al., 2004; Lee et al., 2004).

Subsequently, pre-miRNA is exported to the cytoplasm via the Ran-GTP dependent nuclear exporter Exportin-5 (Bohnsack et al., 2004) where the loop of the pre-miRNA is cleaved by an RNAase III enzyme (Dicer-1) generating an RNA heteroduplex with two-nucleotide overhangs at both 3’ ends containing approximately 22 nucleotides (mature miRNA) (Hutvágner et al., 2001). Subsequently, one of the two strands of mature miRNA is loaded into argonaute-1 protein containing miRNA induced silencing complex (miRISC; Khvorova et al., 2003). The miRISC partially hybridise to the 3’ untranslated regions (UTR)

of target mRNAs resulting in translational repression followed by mRNA degradation (Schwarz et al., 2003; Bartel, 2009).

1.6.1.2 siRNAs and shRNAs

siRNA are double stranded RNA molecules consisting of 19–23 base pairs with 3′ two-nucleotide overhangs. SiRNA can be chemically synthesised and introduced to mammalian cells to induce specific gene silencing by the degradation of mRNA target (Elbashir et al., 2001). Inside the cells, siRNA direct destruction of the target mRNA and gene silencing using the same pathway effectors of miRNA pathway previously explained (Setten et al., 2019). Alternatively, siRNA gene silencing can be endogenously induced by transfection of cells with plasmids or viral/bacterial vectors expressing short hairpin RNA (shRNA). Expressed shRNA are transformed to siRNA molecule by the Dicer resulting in long-term gene silencing in mammals.

With more than 60 % of human mRNAs regulated by miRNA, this RNAi pathway is reported to be dominant in mammals over other mRNAs regulation pathways (Friedman et al., 2009). In contrast, the siRNA pathway is rudimentary in mammals, and it is thought to primarily be involved in the defensive action against viruses and repetitive elements (a patterns of DNA or RNA small repeats occurring all over the genome in multiple copies), reported in plants and invertebrates (Obbard et al., 2009), has been taken over by other molecular mechanisms during evolution, such as immune system in mammals (Svoboda, 2014). A striking exception in mammals, siRNA mechanism was experimentally demonstrated in mouse oocytes (Svoboda et al., 2000; Wianny & Zernicka-Goetz, 2000).

In contrast to miRNA where one miRNA controls the expression of thousands of RNAs, siRNAs are designed to target single genes and, when used in cancer studies, they generally target over-expressed genes for a more efficient and less toxic therapeutic approach (Mahmoodi et al., 2019). Once introduced to the cell, siRNA binds to its specific sequence of mRNA inducing a short-term silencing for 2-3 days. For stable transfection in cell lines and animal models, a DNA construct is administered, encoding a hairpin loop dsRNA (shRNA; **Figure 1.27**) offering the possibility to study the chronic effect of the treatment (Brummelkamp et al., 2002).

Actually, microfluidic system was used for siRNA gene knockdown using different human cells such as mesenchymal stem cells (Yoshikawa et al., 2004), T lymphocyte Jurkat cells (Toriello et al., 2008) and recently human primary lymphocytes and hematopoietic stem

and progenitor cells (Loo et al., 2021). No published studies undergo siRNA gene knockdown using GBM model in a microfluidic settlement.

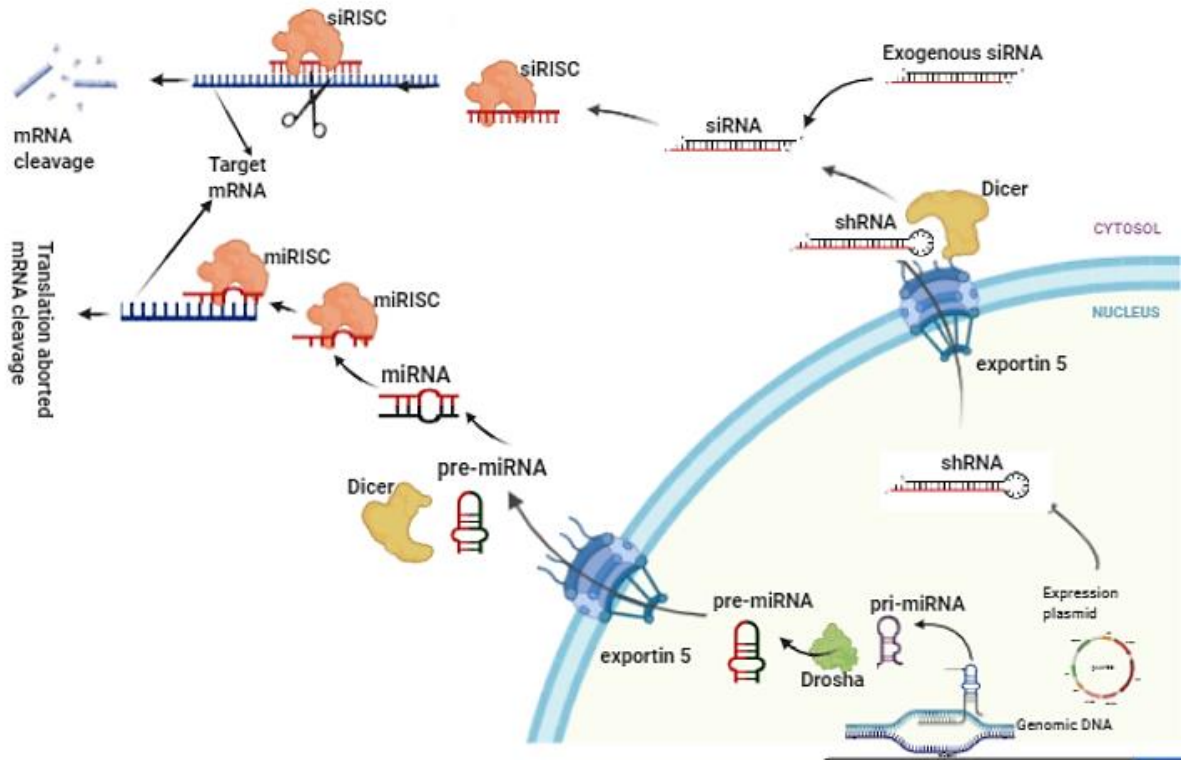

Figure 0.27 Gene silencing mechanism of miRNA, siRNA and shRNA
miRNA gene is transcribed by RNA polymerase II in the nucleus and give pri-miRNA, which next will be cleaved by Drosha to form pre-miRNA. pre-miRNA is transported to the cytoplasm via exportin 5 where it will be processed by the dicer into miRNA. MiRNA is loaded to the RISC forming miRISC complex, where the passenger strand (in black) will be discarded, and the remaining guide strand will guide the miRISK to the target mRNA through imperfect base pair complementarity binding. This will result in the mRNA inhibition of translation, degradation, or inhibition. Exogenous siRNA is directly processed by the RISC once introduced to the cytoplasm, where the passenger strand (in black) will be discarded, and the remaining strand will guide the siRISK to the target mRNA through complementary binding leading to the mRNA leads to the cleavage of mRNA. For a more stable siRNA silencing an expression vector is introduced to the nucleus where it will continuously express molecules of shRNA. These molecules are exported to the cytoplasm through exportin 5 then processed by the Dicer to produce small RNA molecules siRNA. The figure is created using Biorender website following information reported by Maduri, (2015).

1.6.2 siRNA applied to GBM mouse models

Using cell lines and mouse models, siRNA-based targeted therapy, has demonstrated a great potential over other therapies that are currently in the clinic, when targeting oncogenic and cell survival pathways. Currently mouse models are the most used strategy to test new

RNAi experiments for GBM treatment including transgenic, xenograft, orthotopic, syngeneic, and chemically induced models.

One of the most used mouse models is the subcutaneous xenograft model. In this model, GBM cells are injected under the skin in one flank of a mouse (Carlson et al., 2011). This technique was used to test siRNA anti-tumour effect on GBM, for its low technical complexity with no specialised equipment required for tumour implantation, the simplicity of intra-tumoural injection and tumour monitoring (Wanget al., 2016; He et al., 2017). These studies used siRNA technology to knockdown Histone deacetylase 6 (HDAC6) and the EGFR gene respectively, which were administered by intravenous injection in the tail. However, this model fails to recapitulate the original behaviour of tumour mass inside its organ of origin. In this model the tumour cells are surrounded by non-neoplastic cells instead of the real surrounding tumour microenvironment cells (Dendritic cells, macrophages, and neurons) which have been demonstrated to release factors essential for tumour growth and invasion (Quail & Joyce, 2013; Kamińska et al., 2015; Venkatesh et al., 2015). Even though this model offers an *in vivo* microenvironment to grow tumours, in this model the BBB is non-existent which make this technique inappropriate as a clinically translatable model for GBM targeted therapy especially for siRNA (Zou et al., 2020).

For more reliable platforms to mimic the real environment of brain tumours, another model was used which is the orthotopic xenograft mouse model (Teplyuk et al., 2016; Fareh et al., 2017). In this model the human GBM cells are directly implanted in the mouse brain. Even though the tumour mass will grow in its organ of origin (brain) with the high clinical relevance for initial drug screening experiments, this model presents many inconveniences. First, the mice used in this technique should be immunocompromised (nude) or severe combined immunodeficient (SCID) which eliminates the important role of the immune system in the tumour progression and drug response (Chen & Hambardzumyan, 2018). Second, the exogenous implantation of tumour mass may affect the microenvironment because of the lack of spontaneous tumour formation which reduces the possibility to study tumorigenesis using this model. Additionally, even though the use of patient-derived primary GBM cells in this model, could increase the clinical relevance of drug discovery experiments, the culturing process still represent a limit as it induces DNA methylation which might affect tumour progression and response to therapy (Varley et al., 2013). Recently, Wang et al., (2021) used an orthotopic GBM xenograft mouse model to study the effect of siRNA

knockdown of MGMT gene using iron oxide nanoparticle (NP) system. The simultaneous administration in mice of these NP and TMZ compared to TMZ alone, induces an increase in cell death by apoptosis of GBM stem-like cells, reduces tumour growth, and significantly-improve the survival rate.

For a more clinically relevant model, a new mouse model has been described which allows cancer drugs to be tested in an immunocompetent environment called a syngeneic or allograft model (Passaro et al., 2019). This model consists of the implantation of mouse GBM cells of the same genetic profile as the host (Wu et al., 2018). Some studies have used this model to validate previously targeted therapy studies on GBM conducted using the orthotopic mouse model (Priester et al., 2013; Teplyuk et al., 2016). Recently, Yang et al., (2021) have used syngeneic GBM models to study a new approach of T-cell-based immunotherapy by the knockdown of two genes IL-6 and CD40. They found that this dual-targetting treatment could be used as an adjuvant after surgery and radio-chemotherapy which will induce an immunogenic cell death of GBM cells. This study successfully improves sensitivity of glioblastoma checkpoint inhibitors and overcome immunosuppression mediated by macrophages. To better recapitulate GBM tumorigenesis, a new mouse model was created, in which spontaneous mouse models have been generated. The need to study tumorogenesis (Jijiwa et al., 2011) have created previously a mouse model with spontaneous intracranial malignant tumours enriched with multipotent brain tumour stem cells. This mouse model is the progeny of breeding a spontaneous tumour mouse model of non-obese diabetic/severe combined immunodeficiency (NOD/SCID) mice heterozygous for a mutation in the Sonic hedgehog receptor patched 1 (Ptc) with NOD/SCID mice heterozygous for the P53 gene (Ptc +/−, p53 +/−) (Jijiwa et al., 2011). Using this mouse model, and siRNA gene knockdown, they demonstrated that CD44v6 (the variant form 6 of CD44 which is a marker of TMZ resistance) could be a potential candidate for GBM stem-like cell therapy. Recently, (Qin et al., 2020) have used this induced spontaneous glioma mouse model and demonstrated that the siRNA inhibition of p53 gene combined with the over expression of the HGF/MET axis could lead to the transformation of neural stem cells into GSCs.

Even though the two latter models seem promising in providing clinically relevant results, they are still time consuming and involve moderate/severe pain to the animals, thus there is a need for further investigations on utilising human samples.

1.7 Accell siRNA

Since the first use of siRNA in mammalian cells for mediating sequence specific gene silencing in 2001 (Elbashir et al., 2001), these molecules along with shRNA have shown their high efficiency in gene knockdown in both human cell lines and primary cells (Berezhna et al., 2006; Shtam et al., 2013; Sioud, 2020; Furukawa et al., 2020). siRNA has been reported as a powerful tool to study gene functions by observing phenotypic changes (Fellmann & Lowe, 2014). It was also used for therapeutic purposes to disrupt disease-related genes (Jiménez Calvente et al., 2015; Singh et al., 2018).

1.7.1 Limitations related to the use of siRNA technology

Despite their extensive use in gene silencing approaches and therapeutic strategies, siRNA technology use is hampered due to its physicochemical and poor pharmacokinetic properties associated with limited delivery and low overall efficiency of siRNA molecules. These properties include the size, metabolic instability, stiff structure, high negative charge (poly-anionic molecule) and the vulnerability of phosphodiester bonds to nuclease cleavage and phosphatases. The limitations of the use of siRNA technology for therapeutic and gene silencing in human cells are a direct consequence of its inherent poor pharmacokinetic properties already mentioned above. With a small size ranging from 7 to 10 nm and a small molecular weight (approximately13KDa), Kim et al., (2009); Jackson & Linsley, (2010); Zahir-Jouzdani et al., (2018) reported that siRNAs molecules are subjected to renal clearance resulting in short half-life of siRNA molecules in the human body (5 to 10 min). (Shu et al., 2011) demonstrated that in the control group siRNA molecules could not be detected in the serum of mice beyond 5 min of post-injection upon systemic administration. Additionally, (Soutschek et al., 2004) have demonstrated that after 1hr of incubation in human serum at 37°C, only 5% of initially administered intact apolipoprotein B (apoB) siRNA was found, demonstrating the low metabolic instability of this molecule which was improved to reach 50% when it is conjugated to cholesterol.

It was reported that the stiff backbone structure of siRNA presented by the stable phosphodiester and torsion angles conformation of the RNA duplex, rendered the molecule less amenable to attack by unwinding molecules (Hoerter et al., 2011) and contribute to the poor binding ability to lipids carriers (Liu et al., 2014). On the other hand (Ruigrok et al.,

2017) stated that because of the high negative charge imbued by the phosphate group, siRNA does not cross easily the cell membrane hence requiring to be encapsulated in cationic nanocomplexes which also appeared have limited penetration into cells (Merz et al., 2017). It was also demonstrated that siRNA negative charges should be shielded with positively charged molecules to promote epithelial cell membranes uptake and increase siRNA corneal bioavailability (Schiroli et al., 2019). Recently, Sajid et al., (2020) discussed the intravascular instability of siRNA molecules which was a direct result of the degradation of these molecules by ribonuclease in the serum.

Finally, siRNA technology use in human cells showed other limitations not directly related to the pharmacokinetic properties. First, despite its small size siRNA when inside the human body triggers the immune system leading to its degradation and reduces its efficiency in target cells. The immune system was stimulated by the siRNA molecules and/or the delivery system (Meng & Lu, 2017). Second, it has been demonstrated that some cell lines are shown to be refractory to siRNA silencing strategy, and they are hard to be transfected by conventional methods such as lipid-based transfection. This was previously demonstrated for primary T cells (Freeley et al., 2015a), keratinocytes (Hickerson et al., 2011) and many other cell lines including the U87 GBM cell line are listed by Dharmacon company (Zaklina & Yamada, 2018).

1.7.2 Accell siRNA a new approach for gene knockdown

In order to try and mitigate some of the limitations associated with siRNAs, the introduction of chemical modification on siRNA molecules was shown to dramatically improve gene silencing efficiency, stability and specificity of these entities. The new modified siRNA is known as self-deliverable siRNA or Accell siRNA which enhances delivery of siRNA without the need of viral vectors or lipid-based transfection reagents (Ruigrok et al., 2017). Since the identification of major contributors of siRNA-specific features that may bias its overall silencing efficiency (Reynolds et al., 2004), a panel of chemical modifications have been established and tested on the siRNA structure involving the ribose, the base or the phosphate group. These modifications are grouped in the database published by (Dar et al., 2016). The use of Accell siRNA technology present a promising approach to carry gene silencing experiment especially in cells described as refractory to siRna transfection using traditional methods such as viral and lipid based.

1.8 Aims of study

Glioblastoma is the most aggressive and deadly brain tumour (Kanderi & Gupta, 2022). Despite intensive research to find new therapeutic approaches, further investigation to discover effective ones is still required to improve the survival outcomes for patients with glioblastoma. Microfluidic system is the most developed in vitro model that allow a real-time monitoring of the interactions between cancer cells and their microenvironment compared to monolayer and 3D static culture systems. In the current study glioblastoma spheroid model was used to perform gene silencing in a microfluidic platform. siRNAs have emerged as a powerful tool to perform specific single gene knockdown. It is described as a promising therapeutic modality, where any disease-related genes can be silenced (Hu et al., 2020). In cancer biology researchers use siRNA to target genes that are expressed in cancer cells compared to normal cells (Bahreyni & Luo, 2020). In traditional 2D culture, siRNA is a well-established and routinely used tool for high-throughput screening because it is simple, convenient, and economical. In 3D culture siRNA gene knockdown was shown to be successful using different delivery systems (Iles & Bartholomeusz, 2016; Morgan et al., 2018).

The overarching goal was to establish a flow-based system for repressing genes in a microfluidic device using a glioblastoma spheroid model. The first aim was to confirm the expression of predefined genes in the GBM cell line (U87) used in this study. Based on published literature four genes were chosen among the highly expressed genes in U87 cells (*AKT2*, *AHR*, *PRMT2* and *RAB21*). To do so, the number of spheroids required for sufficient mRNA isolation was first determined followed by a comparison of expression of the selected genes in GBM spheroids cultured in static and flow system.

Once the expression of the designated genes was proven in the Hull GBM cell line, the aim was to do siRNA gene silencing experiments in three culture systems 2D, 3D static and 3D flow system. The optimisation of parameters for delivery of siRNA to knockdown specific genes was carried out in U87 cells cultured in 2D monolayer, 3D static and flow systems. For this, qPCR and western blot techniques were used to assess the effect of lipid-based siRNA transfection on the gene and protein expression respectively, and MTS proliferation assay and phenotypic tests were used to study the effect of gene silencing on the metabolic activity of spheroids. To improve the delivery of siRNA to cells within spheroids,

the optimisation of gene knockdown using Accell siRNA strategy (without transfection reagent) was done.

Finally, the aim was to identify the biological processes and pathways activated and repressed when spheroids were cultured in the flow system and compare it to those cultured in static conditions. To do so, and to validate the suitability of the currently used microfluidic chip for culturing other GBM cell lines, the gene expression profile of three independent GBM cell lines was studied using whole transcriptome analysis. For this, U87 and two other GBM patient derived cell lines were cultured in 3D static and flow system followed by RNA extraction, identification of differentially expressed genes (DEGs) using Next-generation sequencing (NGS; RNA sequencing), Correlation analysis, and enrichment analysis (GO and KEGG pathways) of DEGs.

Hopefully, the successful development of a gene knockdown system using microfluidic platform will allow more accurate and translationally-relevant therapeutic target identification and validation in glioblastoma.

Chapter 2
Material and methods

2.1 Cell culture

Human glioblastoma cell lines U87 and SNB19 were purchased from European Collection of Authenticated Cell Cultures (ECACC). Cell Line Authentication test was carried out by short tandem repeat "fingerprinting" where the DNA Profile generated from the provided samples were compared to a profile located on the Cellosaurus Database (NorthGene UK); a 100% match was achieved. The cell lines tested negative for any mycoplasma contamination and were regularly retested every 6 months.

2.1.1 General Reagents and consumables

General plastics used in the study were purchased from BD Bioscience (Oxford, UK), Sarstedt (Leicester, UK), Fisher Scientific (Loughborough, UK), or Starlab (Milton Keynes, UK), unless otherwise noted. General chemicals were purchased from Sigma (Gillingham, UK), or Fisher Scientific (Loughborough, UK), unless otherwise noted.

2.1.2 Culture of GBM cell lines (U87 and SNB19)

GBM cell lines (U87 and SNB19) cells already stored in cryo-vials were taken from liquid nitrogen and defrosted in bead bath at 37°C. When fully defrosted, the vial was sprayed with 70% ethanol and placed inside a Class II safety cabinet. Cells were cultured in full medium containing 500 mL of Dulbecco's Modified Eagle Medium (DMEM, Lonza, UK) with 10% (v/v) foetal bovine serum (FBS, Gibco, Life Technologies, Loughborough, UK), penicillin/streptomycin for a final concentration of 100U/ml (Lonza, Castleford, UK). Cells were seeded from frozen in T25 flasks (Sarstedt) and placed in an incubator (Nuaire, UK) at 37°C, with a humidified atmosphere with 5% CO2, then transferred after 3 days to T75 flask (Sarstedt). Cells were passaged at specific ratio (1:5) to maintain exponential growth reaching 70 to 90% confluency in three days.

For the SNB19 cells, 5 mL of sodium pyruvate (Lonza) is added to medium, and the passage was done at specific ratio 2:5 to reach the confluency of 60 to 80% in three days.

2.1.3 Patients derived cell (PDC) line culture

2.1.3.1 Coating flasks

In 1.5 ml Eppendorf tubes, a stock of 10 mg/ml poly-L-ornithine (Merck Life Science, Dorset, UK) was prepared in sterile water (ddH_2O). From this stock solution a dilution of 1:2000 in sterile ddH_2O was prepared in a 50ml polypropylene tube, then filtered into a new tube through a 0.22 μm syringe filter (Gelman Sciences Ltd., Northampton, UK) Then 10ml of the diluted poly-L-ornithine solution was added to T75 flasks (or 4 ml to a T25 flask) and

incubated flat for 1hr at room temperature. The flasks were then washed with approximately 3ml of sterile ddH_2O. Ten ml of laminin (Merck Life Science; 1:500 dilution in sterile Phosphate buffered saline (PBS)) were then added to T75 flasks (or 4 ml to T25 flasks) and again flasks were incubated flat overnight at room temperature. These were either used immediately or stored for up to 6 months at -20˚C.

2.1.3.2 Media Preparation

The media was prepared by adding 5 ml of B27 supplement (for a final concentration of 0.5x), 2.5 ml of N-2 supplement (for a final concentration of 0.5x), 1 ml of recombinant human basic fibroblast growth factor (BFGF; final concentration of 40µg/ml), and 1ml of epidermal growth factor (EGF; final concentration of 0.5x), to 500 ml of Neurobasal medium. The media then was filtered using a 0.22µm syringe filter, stored as aliquots of 50ml and warmed to 37˚C when needed. All components of prepared media (except EGF) were purchased from Thermo Fisher Scientific (Paisley, UK). EGF was purchased from R&D Systems (Abingdon, UK).

2.1.3.3 Thawing Cells

Cells were removed from the freezer, and first warmed slowly in the hands. Prewarmed media (5 ml) was added slowly to the thawed vial. To remove the DMSO the vial was centrifuged at 300x g for 5min. The pellet was resuspended in 2ml of appropriate fresh media and added to the pre-coated T25 flasks along with an extra 2ml of fresh media. The flasks were then incubated at 37˚C and 5% CO2.

2.1.3.4 Seeding Cells

First the media was aspirated from the T25 flask which was further washed with warm sterile PBS. The T25 flask was then incubated for 2 to 3 min at 37˚C after adding 1ml of trypsin (Gibco, 0.25% Trypsin-EDTA 1x) (5 ml to T75 flask). Following this, cells were collected by adding 4 ml of medium to a T25 flask (or 10ml to a T75 flask) then transferred to a 50ml polypropylene tube and centrifuged at 300x g for 5min. The media was aspirated, and cells were resuspended in 5ml of fresh media and counted for new seeding or use in experiments.

2.1.3.5 Freezing Cells

The media was removed from confluent T75 flasks, and trypsinisation was performed as described above. The pellet was resuspended in 3 ml of neurobasal medium with 10 % (v/v) DMSO. An aliquot (1ml) was transferred to cryovials, placed in an isopropanol freezing

container, and incubated at -80°C overnight before being transferred to liquid nitrogen for long term storage.

2.2 Spheroid formation

Spheroids were generated in round-bottomed 96 well plate Ultra-Low Attachment (ULA) (Corning Costar, UK) (Wang et al., 2016; Collins et al., 2021). Suspensions of U87 and SNB19 cells were seeded (2 x 10^4 or 3 x 10^4 cell/well) in 100µl of medium/well. Cells were counted in a Neubauer Improved Haemocytometer (Hawksley, Sussex, UK). After cell seeding, the ULA plate was stored in an incubator at 37°C and 5% CO_2 concentration for 3 days, without changing of the culture medium. For GBM58 and GBM63 spheroids these were formed using an initial cell density of 3 x 10^4 cell/well and were cultured in ULA plates for 10 days.

2.3 Gel count

The spheroid size was measured using the GelCount (Oxford Optronix Ltd) device. Images were analysed using ImageJ software to determine the spheroid diameter. Two measures were taken each time, one horizontal and one vertical, and the average was considered as the "real diameter" of spheroid. All spheroid experiments were done in triplicate.

2.4 Cells and spheroids transfection

2.4.1 Selection of target genes for the knockdown experiments

Based on a literature search for highly expressed genes in the U87 cell line, four were selected: Aryl Hydrocarbon Receptor (*AHR*) (Jin et al., 2019), *RAB21*, Member RAS Oncogene Family (*RAB21*) (Ge et al., 2017a), *AKT* Serine/Threonine Kinase 2 (*AKT2*) (Cui et al., 2012) and Protein Arginine Methyltransferase 2 (*PRMT2*) (Oh et al., 2014). While silencing of *RAB21* (Ge et al., 2017) and *PRMT2* (Dong et al., 2018) were reported to inhibit cell growth and proliferation respectively in glioma and GBM cells, no association with brain cancer development or progression has been reported fo *AHR* (Perepechaeva & Grishanova, 2020) or *AKT2* (Liu al., 2020).

2.4.2 SiRNA transfection

Gene silencing experiments were done using lipid based transfection (DharmaFECT Transfection Reagent) mediated siRNA (ON-TARGETplus Human siRNA) transfection of cells cultured in a monolayer system, or spheroids cultured in static and flow systems

(Borawski et al., 2007; Oner et al., 2021). Anti-PRMT2 and anti-RAB21 siRNA (ON-TARGETplus Human siRNA, catalogue number L-004033-00-0010 and L-009450-00-0010 respectively) as well as scrambled siRNA (ON-TARGETplus Non-targeting Control siRNA, catalogue number D-001810-01-20) and transfection reagent were purchased from Horizon Discovery LTD (Cambridge, UK). The siRNA solution used were a "SMARTpool" which is a mixture of 4 siRNAs targeting the same gene provided as a single reagent for improved potency and specificity (Duivenvoorden et al., 2021). The transfection mixture was prepared according to DharmaFECT siRNA transfection protocol and calculations were made to get the desired siRNA concentration needed for each experiment. Example of calculation of amounts needed for transfection experiment in the microfluidic device in the **Figure 2.1**. For monolayer culture U87 cells were transfected after 24hr of seeding in 6 or 96 well plates while in 3D system, spheroids were first formed in ULA plates then transfected with siRNA either in static or in a flow system.

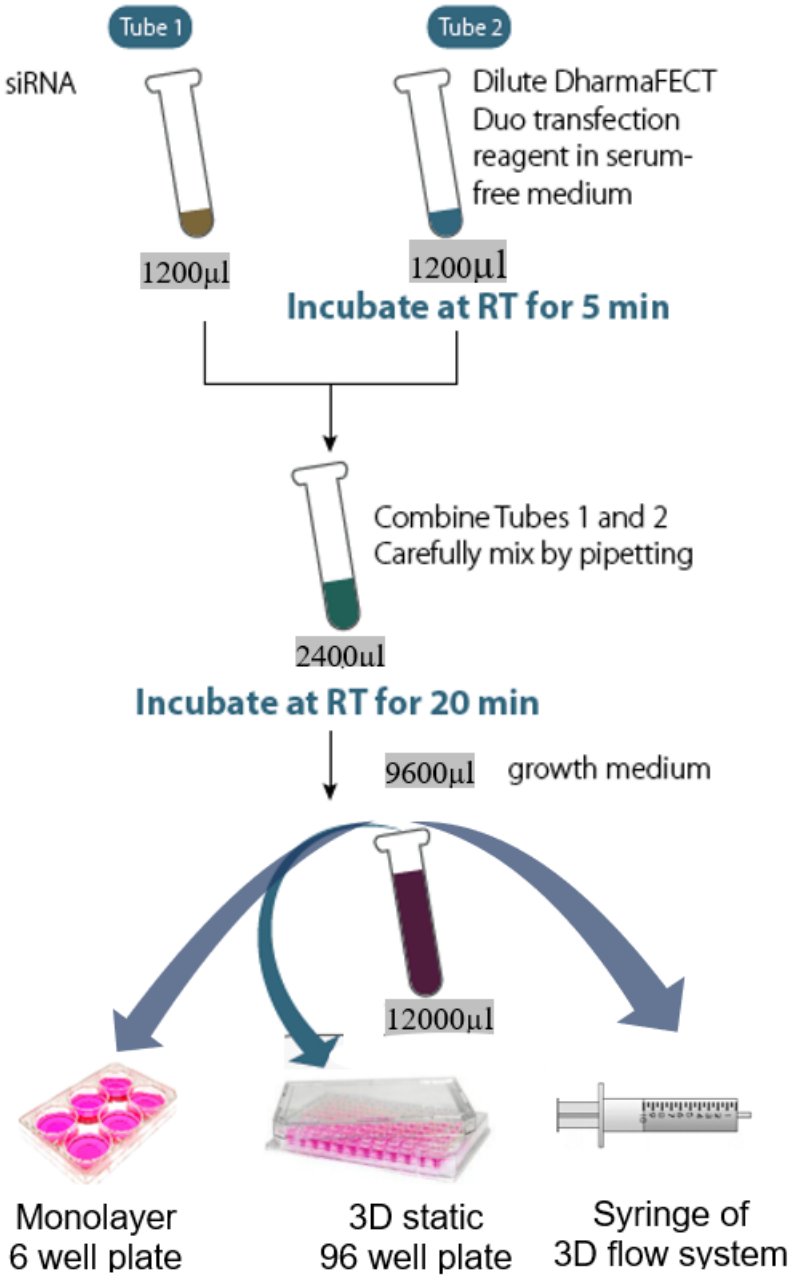

Figure 2.1 Protocol for transfection with siRNA
Amounts calculated for 1 syringe/1 device for transfection with 5nM siRNA for 100 hours in a flow of 2 µl/mn (from DharmaFECT transfection protocol). For monolayer and 3D static culture systems amounts were calculated in the same way as shown in the figure according to specific experimental conditions. Tube1 contains 12µl of siRNA(5µM) added to 1188µl of serum free medium for each siRNA. Tube2 contains 12 µl of DharmaFECT reagent added to 1188µl of serum free medium.

2.4.3 Accell siRNA transfection

Accell siRNA is a chemically modified siRNA (patented technology) used for gene silencing without the use of a lipid transfection reagent. Accell siRNA anti-FUS (Accell

Human FUS RNA binding protein) and the Accell siRNA control (Accell Non-targeting Control Pool) were purchased from Horizon Discovery Biosciences (Cambridge, UK). After dissolving the Accell siRNA in 5x siRNA Buffer (Horizon Discovery Biosciences Cambridge, UK) to get the solution stock of 100µM, the amount of Accell siRNA delivery media was added to get the concentration needed depending on the experiments. Transfection was done according to Dharmacon™ Accell™ siRNA delivery protocol (horizondiscovery.com, 2021), on spheroids cultured in static and flow system, after spheroid formation using U87 cells cultured in ULA plates for 3 days.

2.5 Microfluidic system setup

2.5.1 The microfluidic chip

The microfluidic chip was made of polymethylmethacrylate (PMMA). It is the combination of four separate pieces, the inlet piece (hexagonally shaped), sample chamber, tissue retaining piece and outlet piece (circular; **Figure 2.2**). Pieces were provided by Dr Alex Iles (Hull University Microfabrication Facility) and then assembled using chloroform as described previously (Zhang, He et al., 2014; Matellan et al., 2018). The hollow microchannel from the inlet and the outlet has a diameter of 4mm, which allows easy manipulation (inserting and retrieving) of spheroids. The chamber capacity which has been used previously with 3 and 4 spheroids, had an internal diameter of 0.6 mm (Collins et al., 2021c).

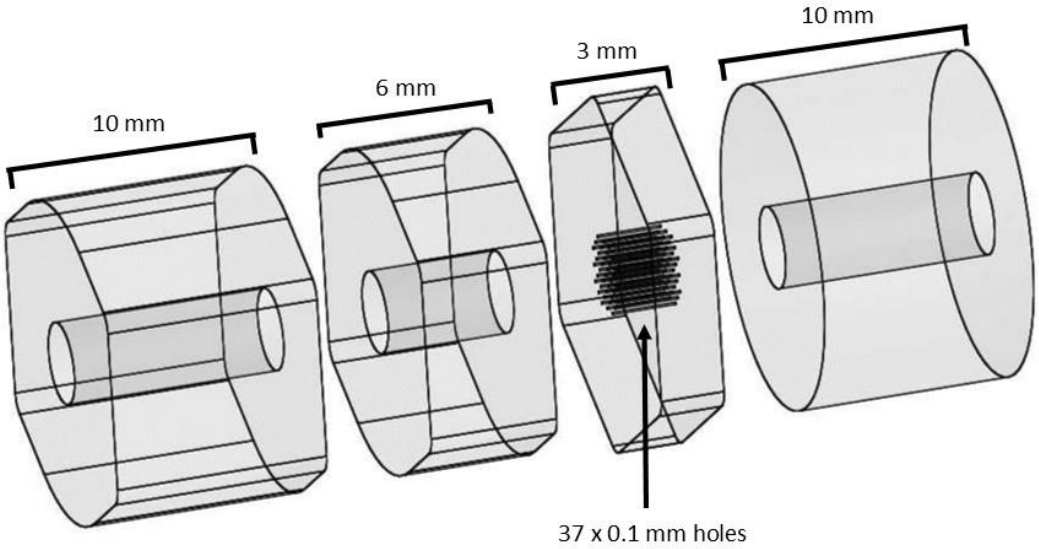

Figure 2.2 3D schematic of the microfluidic chip
The hexagonal inlet layer was 10 mm thick; the sample chamber was 6 mm thick, tissue retaining layer was 3 mm with 37 x 0.1 mm holes drilled to allow fluid flow through the device and the outlet layer was 10 mm thick. Designed by Dr Alex Iles.

2.5.2 The microfluidic flow system setup

The medium was prepared to be used for the microfluidic system by adding (to the medium prepared at **section 2.1.2**) 12.5ml of 4-(2-hydroxyethyl) piperazine-1-ethanesulfonic acid (Hepes 1M, Fisher Scientific) to the full medium. After that the chip was sterilised using 70% (v/v) ethanol and primed using sterile medium. The syringes were filled with medium (volume depending on the experiment) and the spheroids, collected from ULA plates, were transferred to the device in a Class II biological safety cabinet before being placed in an egg incubator at 37°C (Chapter 3, **Figure 3.1**). A 0.22 µm syringe filter connected the syringe to the inlet of the chip, and an effluent collector (50 mL polypropylene tube) was connected to the outlet. The syringes were placed in the electronic syringe pump (Harvard apparatus) which was set to a flow rate of (2µl/min) (Olubajo et al., 2020).

2.6 RNA extraction

RNA extraction from cells was done using TRIzol (Fisher Scientific, Loughborough, UK) as described by manufacturer. The extraction of RNA from spheroids was done using the same protocol with some modifications. Before starting the RNA precipitation, spheroids were retrieved from the ULA plate or chip and transferred to RNAse free Eppendorf tubes (Fisher Scientific, Loughborough, UK). Then 500µl of TRIzol™ Reagent was added per sample without washing the spheroids with PBS to avoid mRNA degradation. Then samples were stored at -80°C overnight. Extracted RNA from spheroids and cells was checked for concentration and purity using nanodrop (Fisher Scientific, Loughborough, UK).

2.7 Reverse transcription

Reverse transcription is the process that transform RNA template into complementary DNA (cDNA) which will be used for qPCR experiments to assess gene expression. For this, to the RNA solution containing (1000ng of RNA), nuclease free water was added until a volume of 12.7µl. These samples were heated at 55°C for 5min, and then incubated at room temperature for 5min. For each sample a master mix containing 4µl of buffer, 2µl of dNTPs 4mM (Fisher Scientific), 1µl of oligo dT (20µM; Fisher Scientific) and 0.3µl Reverse transcriptase (Promega, Hampshire, UK)) was added. Oligo dT primers bind specifically to mRNAs containing a poly(A) tail and promote the reverse transcription reaction (Kuang et al., 2018). The mixture was then incubated at 37°C for 1 hour, then pulsed in a microfuge. The samples were pulsed again after incubation at 100°C, and finally diluted with the addition of 180µl PCR-grade water (Fisher Scientific).

2.8 Real Time quantitative PCR

First the master mix for one reaction (all components from Sigma-Aldrich) was prepared using, 5µl of SYBR® Green JumpStart™ Taq ReadyMix™, 0.1µl of Rox Dye, 0.4µl of primers (1:20 dilution of 1µg/µl primer's stock solution) and 2.1µl of molecular grade water. Primers used in this study are listed in **Table 2.1**. The master mix was vortexed briefly, then placed in the wells on a 96 well PCR plate (8µl/well), finally adding 2µl of sample post-reverse transcription (**Section 2.7**) to each well. The plate was sealed using a MicroAmp™ Optical Adhesive Film (Fisher Scientific). The mixture was vortexed then pulsed in a microfuge. The plate was then placed into a quantitative real-time PCR machine, and the desired protocol was run. Real time PCR reactions were performed in a 96-well PCR plate using a StepOnePlus system (Applied Biosystems) The reaction of each sample was done in triplicate wells. For each experiment, Ribosomal Protein Lateral Stalk Subunit P0 (RPLP0) was used as a control (housekeeping gene) as expression levels were stable under the different test conditions. Depending on the intended experiment two methods were used to analyse qPCR data, first the ΔΔCt analysis and second the relative standard curve method (Larionov et al., 2005). For the ΔΔCt method, the ΔCT values were calculated for the experimental and control conditions CTs (generated automatically) normalised against the housekeeping gene RPLP0). Then the ΔΔCt was further calculated. ΔΔCt is the variance between the ΔCT values for the experimental and the control conditions. To get the expression fold change, $2^{-\Delta\Delta Ct}$ was calculated. The standard curve method is based on graphical representation as a semi-log regression line plot of CT value against log of input nucleic acid. This method is used to estimate the efficiency of amplification of a real-time PCR reaction. A slope of –3.32 indicates a 100% efficiency of a PCR reaction (Larionov et al., 2005).

Table 2.1 Primers used for quantitative real-time PCR.

Gene symbol	Full name of gene	Strand	Primer sequence (5′–3′)	Gene accession number
AHR	Aryl hydrocarbon receptor	F	ATGGATCAATACTTCCACCTC	NM_001621
		R	TTTGGCATCACAACCAATAG	
AKT2(1)	AKT serine/threonine kinase 2	F	GAAACACAAGGAAAGGGAAC	NM_001243027
		R	AGGTCTTGATGTATTCACCTC	
AKT2(2)		F	CACCATGAATGAGGTGAATAC	
		R	CTACGGAGAAGTTGTTTAAGG	
AKT2(3)		F	CACCATGAAAACCTTCTGTG	
		R	ACATCATCTCGTACATGACC	
PRMT2	protein arginine methyltransferase 2	F	CCCCACATCTCAAAAAGTTG	NM_206962
		R	AAGATATGCACACTGCTTTC	
RAB21	RAB21, member RAS oncogene family	F	AAGGATGATAGAAACAGCAC	MN_309579
		R	CATCAATAATCTGTACACCTCG	
FUS(1)	FUS RNA binding protein	F	AAGACAAACAAGAAAACGGG	NM_004960
		R	GCAAATGAGACCTTGATAGG	
FUS(2)		F	CCGAACAGGATAATTCAGAC	
		R	GCCACAGACTCAATTGTAAC	
FUS(3)		F	ATTCAGACAACAACACCATC	
		R	GTCATCAAAAGAGACCGTTG	
RPLP0	ribosomal protein lateral stalk subunit P0	F	GGAGAAACTGCTGCCTCATCATA	NM_001002
		R	GGAAAAAGGAGGTCTTCTCG	

2.9 Western blot analysis

Whole protein was extracted either from cells in monolayer culture or spheroids cultured in 3D static conditions (Xu et al., 2016; Lagies et al., 2020).

2.9.1 Preparation of lysates

To prepare lysate from cells, cells were seeded in 6 well plate as 75 x 10^3cell/well in 2ml of antibiotic-free complete medium to achieve the appropriate plating density (**Figure 2.3A)**. After 24 hours cells were transfected with 5nM siRNA, as stated above (**section 2.5.1**), and were collected at 96hr post-transfection. The medium was discarded from the 6 well plate then the cells were washed with cold PBS and then 50µl of RIPA buffer was added (Abcam, Cambridge, UK) (with protease inhibitor cocktail (Sigma) at the ratio of 1:10).

To prepare lysate from spheroids, cells were seeded in 100µl of complete medium for 3 days to form spheroids (**section 2.2**). The spheroids were formed and maintained in 96 ULA plates at the density of 2 x 10^4 cells/well. Then, spheroids were transfected with 0.5µM of Accell siRNA and retrieved at 96hr post-transfection in an Eppendorf tube and washed with cold PBS. After that 100µl of RIPA buffer was added to the spheroids and samples were re-

suspended by pipetting up and down followed by a 10min incubation on ice. The lysate was then centrifuged at 10,000rpm for 15min at 4˚C in a cooled microfuge (Eppendorf). Samples were kept in ice and the supernatant was aliquoted into 1.5ml tubes; the pellet was retained and both phases were stored at -20˚C.

2.9.2 Protein evaluation using BCA assay

The total concentration of protein in samples was determined using BCA Protein Assay following the manufacturer's guidelines (Fisher Scientific). It is a common colorimetric method to detect and quantify the total protein in a solution. It is usually performed before western blot to know the amount of protein needed to be loaded onto a polyacrylamide gel (Cortés-Ríos et al., 2020). The absorbance was measured at 595nm, and the analysis was done using BioTek Gen5 software.

2.9.3 Gel electrophoresis

Using the BCA assay each loaded sample contained 50µg of total protein. The reducing buffer was made by the combination of 4xLaemmli Sample Buffer (Bio-Rad, Watford, UK) with 10µl of β-mercaptoethanol (Catalogue number M7154-100ML, Fisher Scientific). The reducing buffer was added to the sample to make a total volume of 36µl. The samples were heated for three minutes at 95°C, then incubated on ice for one minute. After that, the samples were centrifugated at 13,000rpm for 15 seconds in a microfuge and maintained on ice. In the meantime, a polyacrylamide 10% Mini-PROTEAN® TGX™ Precast Protein Gels (Bio-Rad) was transferred to an electrophoresis plate holding rack, then placed in the electrophoresis tank. The tank was filled with 10x Tris/Glycine/SDS buffer (Bio-Rad), and the comb was removed. Then the total volume of sample (36µl) was added into each well, and the electrophoresis was run at 100V for 2hr (**Figure 2.3B)**.

2.9.4 Protein transfer

The proteins were transferred from the gel to the membrane using Trans-Blot Turbo RTA Mini 0.2 µm PVDF Transfer Kit (Bio-Rad). The Polyvinylidene difluoride (PVDF) membrane was activated by placing in methanol for 30 seconds, before moving to transfer buffer. The filter paper and foam pads were also soaked in the transfer buffer. The transfer sandwich is assembled in a cassette as follows, foam pad, filter, the gel, PVDF membrane, filter paper and lastly the foam pad (**Figure 2.3C**). The cassette was placed into the inner chamber of the transfer apparatus filled with transfer buffer and ice block, then run at constant voltage of 100V for 1hr.

2.9.5 Antibody incubation

The membrane was transferred to a plastic tray filled with a solution of skimmed milk (10g powder in 200ml of 1x Tris buffered saline with Tween (TBS/T)) to allow any free membrane sites to be blocked with milk protein, this was incubated on a gyro rocker for 1 hour at room temperature. 10X TBS is prepared by mixing 24.2g of Tris base (final concentration 200mM), 80g of NaCl (final concentration 1500mM) dissolved in 900ml of distilled water with pH adjusted to 7.6. A solution of 1x TBS/T is prepared by mixing 100ml of 10x TBS with 1ml of 0.1% Tween-20 (Abcam, Cambridge, UK) and 900ml of distilled water. The membrane was then transferred to a 50ml polypropylene tube with the transferred proteins "facing inwards", and further incubated overnight on a roller at 4˚C with the primary antibody at the recommended dilution (1:1000). Details of antibodies used in western blot are shown in **Table 2.2**. After that the membrane was washed three times with 1x TBS/T for 5min each. The membrane was incubated with the recommended dilution (1:2000) of the appropriate horse radish peroxidase (HRP) conjugated polyclonal secondary antibody (Agilent Technologies, Cheshire, UK) using 5% skimmed milk at for 45min on a shaker at room temperature. The membrane was further washed for 3x for 5min with TBS/T then once with PBS for 5 min and incubated in Clarity Max Western ECL Substrate (Bio-Rad) for 2min (**Figure 2.3D)**. The membrane was imaged on a ChemiDoc XRS+ with Image Lab software (Bio-Rad). For re-probing, the membrane was washed briefly in TBS/T followed by PBS, then the stripping buffer (Abcam) was applied for 30min, and then washed briefly in PBS, followed by TBS/T and another PBS wash. At this point the membrane can be frozen for future re-probing.

Table 2.2 List of antibodies used in western blot

Target	Manufacturer	Origin	Dilution	Band size kDa	Clonality	Catalogue number
PRMT2	Abcam	Rabbit	1:1000	49	Mono	ab154154
FUS	Proteintech	Mouse	1:1000	53	Mono	60160-1-Ig
GAPDH	Abcam	Rabbit	1:1000	36	Mono	ab181602

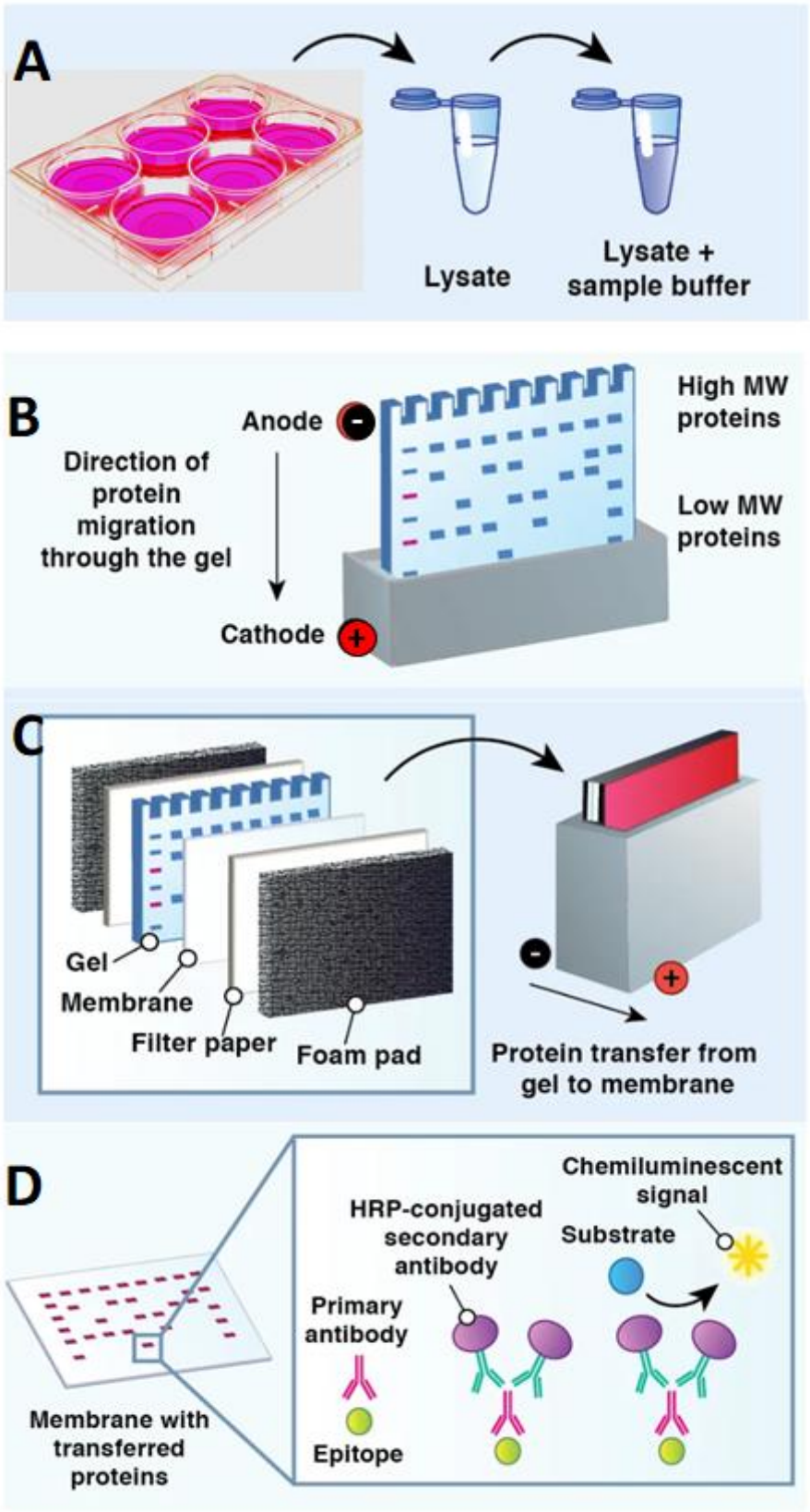

Figure 2.3 overview of n=2 procedures

A) preparation of cell lysate. B) Gel electrophoresis. C) Membrane transfer. D) Protein immunodetection. Modified from https://www.antibodies.com/es/western-blotting.

2.10 Proliferation assays

2.10.1 MTS assay

Cells were placed in 96-well plates at a density depending on the experiment in 100µl of growth medium. After 24hr from seeding, cells were transfected siRNA and then incubated for different times depending on the experiments. For the measurement of optical density cells were incubated in dark with 20µl of MTS reagent (Fisher Scientific) at 37℃ for 2hr. The absorbance was measured at 490nm, and the analysis was done by BioTek Gen5 software. Assays were performed in three repeatss of six wells/condition and statistical analysis was done using GraphPad Prism9 (California, USA).

2.10.2 Phenotypic assay

Cells were placed in 6-well plates at a density of 75 x 10^3 cells/well in 2ml of medium, and incubated at 37°C, with a humidified atmosphere with 5% CO_2 for 96hr and 120hr. after that, the media was removed, and the wells were washed twice with 1ml of PBS. About 400µl of trypsin was added to the well and during the incubation, cells were checked under the microscope every 2min to detect the detachment of all the cells. Once the cells were detached 1.1ml of media was added and the suspension was transferred to a 1.5ml Eppendorf tube. The tube was centrifuged at 400x *g* for 3min, the media was then removed, and the pellet was resuspended in 750µl of fresh medium. Cells were then counted on haemocytometer using trypan blue (1:1 ratio) and 3 independent counts per well should be taken and average of them was calculated.

2.10.3 Cell Counting

Cell suspension (10µL) was first transferred to a sterile 1.5 mL tube. Then, for staining, an equal volume (10µL) of Trypan blue is added to the cell suspension and mixed by pipetting up and down. A glass coverslip is placed on the counting chambers of an improved Neubauer haemocytometer, and the mixture is loaded onto 1 chamber of each side (**Figure 2.4**) so that the mixture exactly fills the chamber. The central counting area (**Figure 2.4**) of each chamber is observed under a light microscope, and the viable/live (clear) or non-viable/dead (blue) cells are recorded for each square. The formula used to calculate the number of cells per ml of original sample (Piccinini et al., 2017), is as follows (number of live cells in both central counting area /2 × dilution factor (2) × 10^4 cells/ml). The volume of the central counting area is 0.1µl, thus, to find the number of cells per ml, the number of cells counted in the central counting area was multiplied by 10^4.

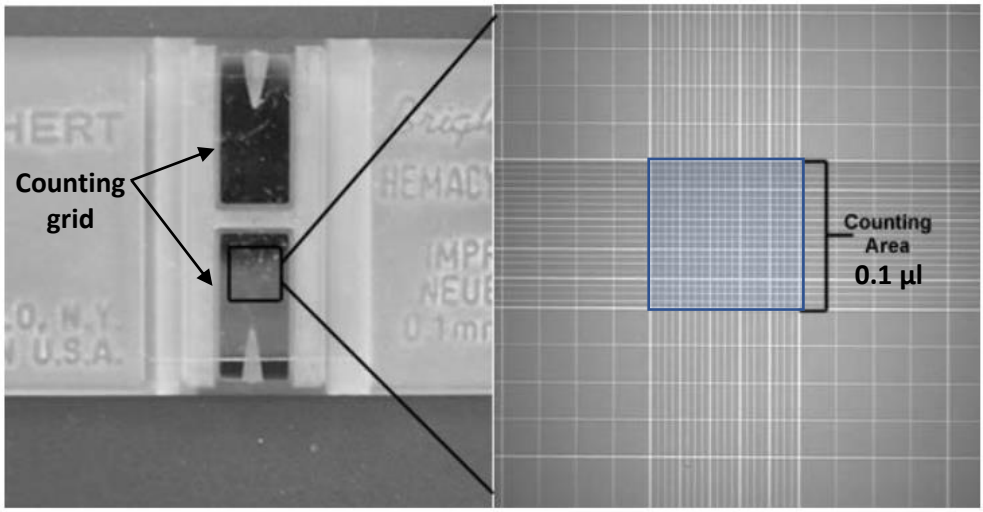

Figure 2.4 Photo (left) and diagram (right) of a haemocytometer
On the left the counting grid of each side where sample are being loaded. On the left the counting area used to count cells observed under a light microscope. Modified from http://www.vivo.colostate.edu/hbooks/pathphys/reprod/semeneval/hemacytometer.html

2.10.4 Statistical analysis

All experiments were done in three repeats unless otherwise noted in the figure legend. The means of data values were calculated with standard error of the mean (SEM). The normality distribution of the data was investigated using D'Agostino & Pearson and Shapiro-Wilks normality tests to select the appropriate statistics that could be used. For normally distributed data, parametric tests were used (one way ANOVA or unpaired T test) whilst for non-normally distributed data, non-parametric tests were used (KruskalWallis or Mann-Whitney U-test). Statistical analysis was done using GraphPad Prism 9 and significance was considered for p values<0.05. p values denote values being less than * 0.05, ** 0.01 ***0.005 ****0.0001, or ns for not significant (p values>0.05).

2.11 Whole transcriptome analysis

Whole RNA was extracted from GBM cell lines (U87, GBM58 and GBM63) cultured in 3D static and a flow system. RNA concentration and purity were first checked using Nanodrop. Each experiment was done in three repeats and RNA samples were sent to Novogene (Cambridge, UK) for sequencing. Methods for whole transcriptome analysis were provided by Novogene.

2.11.1 Sample Quality Control (QC)

RNA samples had to pass a preliminary QC test using agarose gel electrophoresis and Nanodrop, then sample Quantitation and purity were further tested using Nanodrop and sample Integrity was done using Agilent 2100 or ATTI (Riedmaier et al., 2010).

2.11.2 Library Construction, Quality Control and Sequencing

First mRNA was purified from the total RNA using chromatography where poly-T oligo-attached magnetic beads will complementarily fix the poly-A mRNA sequences. Then double strand cDNA library was constructed. The first and the second strands of cDNA were synthesised using random hexamer primers. Respectively, either dUTP or dTTP were used for synthesis of the second cDNA strand, for directional or non-directional library (Townsley et al., 2015).

The workflow of non-directional and directional libraries is shown in **Figure 2.5** and **Figure 2.6** respectively. Following this, libraries check include the detection of the size distribution using bioanalyzer and the quantification using Qubit and real-time PCR. Quantified libraries were then sequenced on Illumina platforms (Robin et al., 2016).

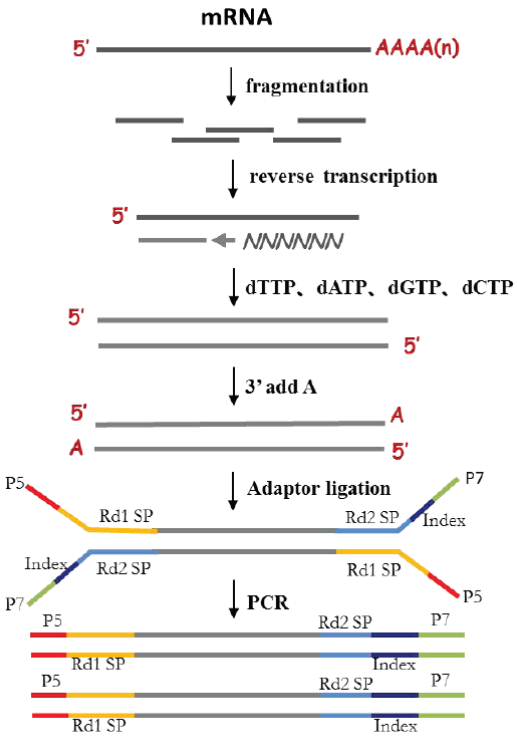

Figure 2.5 Workflow of non-directional library construction
Scheme provided by Novogene

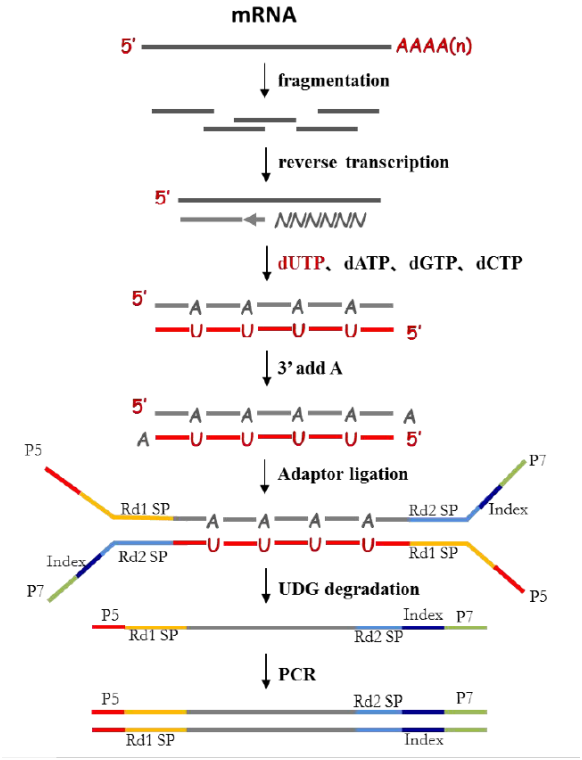

Figure 2.6 Workflow of directional library construction
Scheme provided by Novogene.

2.11.3 Analysis

2.11.3.1 Quality control

Fastq sequences format generated by sequencing project (raw reads) were firstly analysed through perlscripts (Novogene). In this step, reads containing adapter as well as reads containing poly-N and low-quality reads were eliminated to select only clean reads. Following this, error rate GC content the clean data were calculated before starting the downstream analyses based on high quality clean data.

2.11.3.2 Reads mapping to the reference genome

Clean reads were mapped to a reference genome (hg38) downloaded from genome website directly: (https://ftp.ncbi.nlm.nih.gov/genomes/all/GCF/000/001/405/GCF_000001405.39_GRCh38.p13/GCF_000001405.39_GRCh38.p13_genomic.gtf.gz). It also contains gene model annotations. Alignment was done using Hisat2 v2.0.5, also generating database of splice junctions (Dehghannasiri et al., 2021).

2.11.3.3 Quantification of gene expression level

FeatureCounts v1.5.0-p3 was used to count the reads numbers mapped to each gene. Then Fragments Per Kilobase of transcript sequence per Millions base pairs sequenced (FPKM) was calculated of each gene based on the length of the gene and reads count mapped to this gene. FPKM, reflects the sequencing depth and gene length for the read counts at the same time, and is currently the most commonly used method for estimating gene expression levels (Zhao et al., 2020).

2.11.4 Differential expression analysis

Differential expression analysis of samples was performed using the DESeq2 R package (1.20.0). DESeq2 provide statistical analysis of differentially expressed genes between samples maintained under different conditions. The high number of genes studied, can lead to the accumulation of false positives so that, obtained p values were adjusted using the Benjamini and Hochberg's approach (Jafari & Ansari-Pour, 2019). Genes with an adjusted P-value ≤0.05 were considered as differentially expressed.

The resulting P-values were adjusted using for controlling the false discovery rate. Genes with an adjusted P-value≤0.05 found by DESeq2 were assigned as differentially expressed.

2.11.5 Enrichment analysis of differentially expressed genes

Enrichment analysis of differentially expressed genes (DEGs) include Gene Ontology (GO) and Kyoto Encyclopaedia of Genes and Genomes (KEGG) enrichment analysis. Both were done using the clusterProfiler R package (Wu et al., 2021). GO terms with padj value < 0.05 were considered significantly enriched by differential expressed genes. GO terms include biological processes (BPs), cellular components (CCs) and molecular functions (MFs). KEGG enrichment analysis uses online database resources (http://www.genome.jp/kegg/) to identify different biological pathways and cellular mechanisms in which DEGs were most probably involved in. Again, KEGG terms with padj value < 0.05 were considered significantly enriched by differential expressed genes.

2.11.6 Gene Set Enrichment Analysis

Gene Set Enrichment Analysis (GSEA) is a computational method to determine the correlation of gene expression pattern of predefined set of genes between two biological states. The degree of differential expression in the two samples is used to rank the genes and where they were clustered depending on the expression level determined by the FPKM values. GSEA analysis was done using GSEA analysis tool found online at http://www.broadinstitute.org/gsea/index.jsp.

Chapter 3.

siRNA knockdown in glioblastoma cell lines cultured under 2D, static 3D, and 3D in a flow system

3.1 Spheroid generation and microfluidic setup

In the last decade microfluidic systems have been more widely used in cancer research and show great potential in studies of cancer metastasis and drug discovery (Ma et al., 2018a). The ability to control the cellular, physical, and biochemical microenvironment precisely gives the microfluidic approach more physiological relevance than many, if not all, *in vitro* models. Previous studies demonstrated that multicellular 3D spheroids generated from tumour cells are more physiologically relevant and predictive of the *in vivo* system than monolayer 2D culture system in studying cancer biology (Jensen & Teng, 2020). Recent studies have demonstrated that when put in a flow system, spheroids better mimic the real tumour physiology than a 3D static system (Petreus et al., 2021). The aim of the work in this chapter was to optimise conditions for maintaining pre-cultured spheroids in a microfluidic device.

Spheroids were formed in ultra-low attachment (ULA) plates (**Figure 3.1A**), then transferred to the microfluidic device **(Figure 3.1B)**. The chip is made of 4 parts of PMMA with an inlet (hexagonally shaped) and outlet (circular). The hollow tube was of 4 mm diameter with a central filter piece (3 mm thick) with 0.1 mm holes drilled into the centre **(Figure 3.1C)** where the spheroids will be trapped and not drained to the outlet. This chip was an upgrade of the one described previously in (**Figure 1.26**) made of 3 parts with 0.05 mm holes drilled in the central piece. The microfluidic chip was put inside a heated egg-incubator set at 37^{o}C. It was connected from the inlet to a syringe pump to control the flow of the medium through a 0.2-micron filter **(Figure 3.1D)** and from the outlet to a tube collecting the effluent.

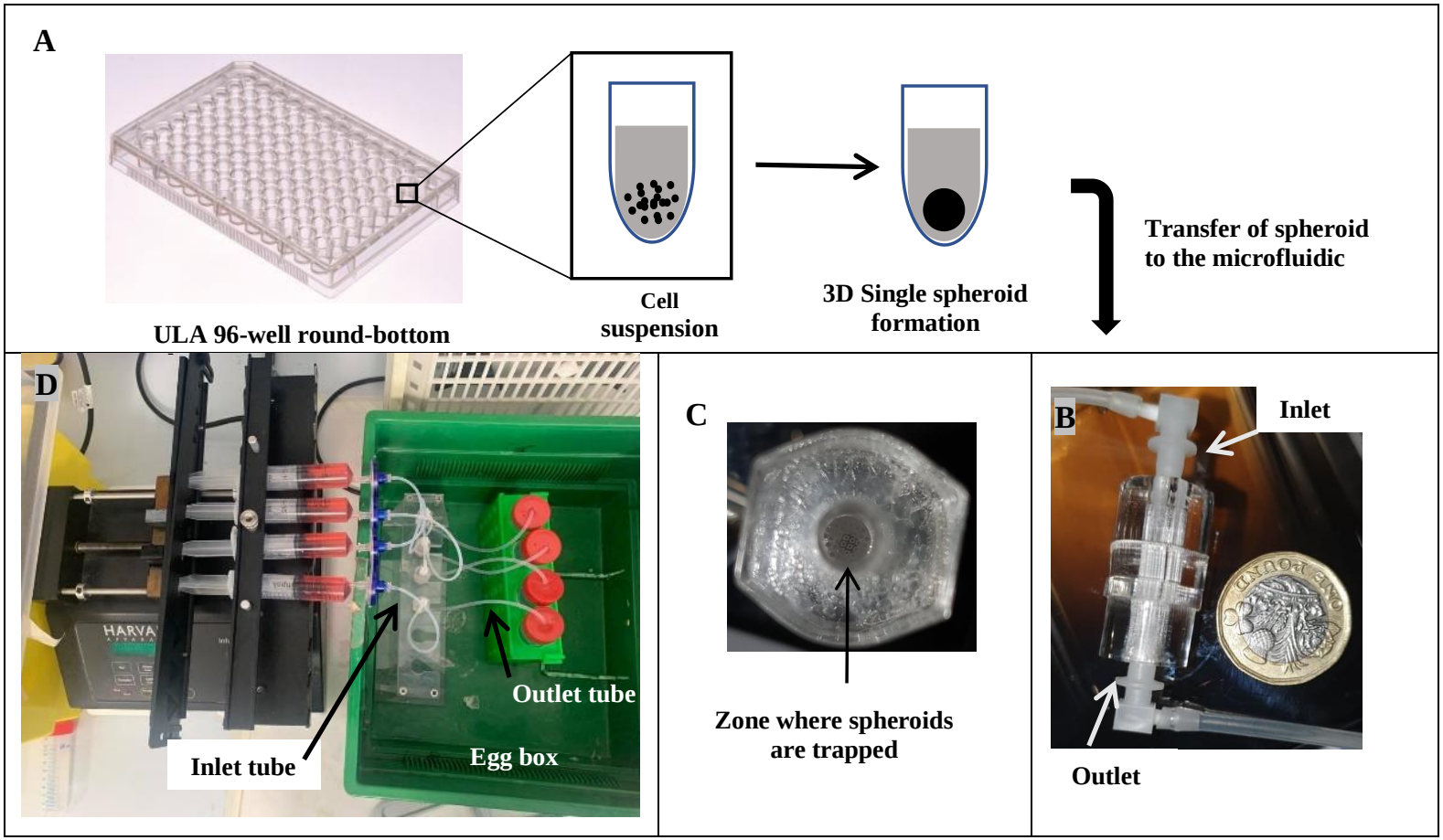

Figure 3.1 Spheroid generation and microfluidic system setup
A) Ultra-low attachment (ULA) 96-well round-bottomed plates were used to culture reproducibly sized, single, spheroids in each well. B) Photo of the microfluidic device with a one-pound coin alongside to show scale. C) Photo from the inlet hole showing the zone where spheroids are going to be trapped. D) The microfluidic setup is made of 4 syringes in parallel with each syringe connected to the inlet of the chip, with an in line 0.3 micron filter, collecting in the a 50ml tube connected to the outlet of the device. The chip and the tube collector are put in an egg box ensuring a temperature of 37°C.

3.2 Comparison of spheroid morphology between 3D static and flow system.

Spheroid diameter and shape are among the key parameters that will affect uptake of substances. Spheroids are formed following the seeding of a known concentration of cells, i.e., 2 x 10^4 cells/well, and cell-cell interactions are established forming a compact, multi-layered structure. These are either left statically in culture medium in a 96 well plate or placed in a microfluidic device and subjected to fluid flow. Spheroids are defined as compact and spherical in shape, distinct from loose and easily fragmented cell aggregates (Hirschhaeuser et al., 2010; Weiswald et al., 2015a).

Previous studies have demonstrated that U-shaped wells are the most appropriate geometry for generating compact and uniformly-sized spheroids (Lee et al., 2013; Fu et al., 2014; Ruppen et al., 2015). It was demonstrated that after 2 days of culture, round-bottomed microwells generate one spheroid whilst flat-bottomed ones often contained 2 or three structures of varying sizes.

Most studies on tumour spheroids in a flowing system are done using the microfluidic formation chips (μSFCs) model, where spheroids are formed and tested in the same chip. This model possesses some limitations, however. The major drawback of the use of μSFCs to study spheroid biology are, first, the time needed in adjustment of flow rate (Choi et al., 2016) and the width of microwells and channels (Chen et al., 2015) to limit the loss of cells and spheroids to the outlet driven by the laminar flow forces, and second its limited use for high throughput screening (Santo et al., 2016; Moshksayan et al., 2018). Because of the limitations that are present when forming spheroids *in situ* it was decided to form spheroids in ULA plates then transfer them to a microfluidic device where they will be used under flowing conditions.

Spheroid imaging using light microscopy is a powerful tool to assess the morphology and shape of the spheroids when using different culture models. It is important prior to conducting experiments on spheroids on a microfluidic device, to understand whether maintenance on the device itself will induce any major changes to the morphology of the spheroids. Any loss of the spheroid or disaggregation of it into the outlet tubing is very likely to alter the results. The first aim therefore was to ensure that there were no major changes of the morphology of spheroids when transferred from 3D static to a flow system.

A comparison of the shape of U87 spheroids cultured in 3D system and in the microfluidic setup (n=2) shows a uniform well rounded shape with compact structure when spheroids were cultured in the 3D system (**Figure 3.2A**). On the other hand, after 72hr in the microfluidic setup the spheroids appear to lose their round shape and become slightly more oval-shaped which could be due to the forces of the liquid flow (flow rate of 2µl/min) and/or due to the handling of the spheroids during the extraction from the device and imaging process (**Figure 3.2B**). **Figure 3.2C** shows that, spheroids tended to clump together when more than one spheroid was put in the device over 72 hours.

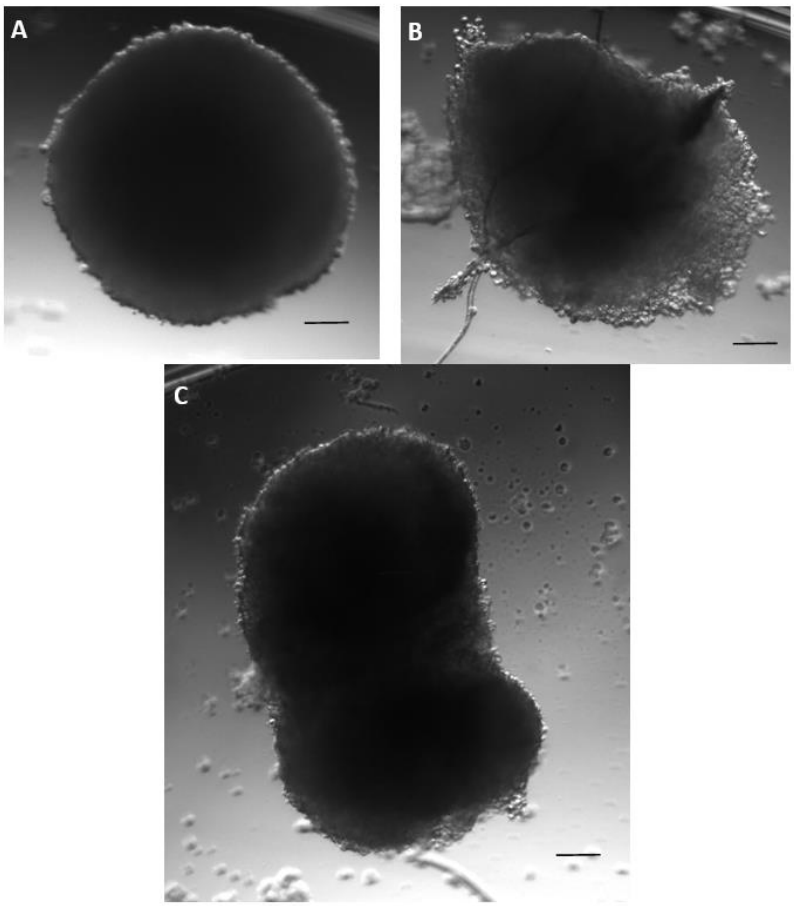

Figure 3.2 Images under ZEISS microscopy of U87 spheroids
Spheroids were cultured for 72hr in 3D static with a diameter of about 600 µm (A) and in microfluidic device (1 spheroid /device (B), 2 spheroids / device (C)). Spheroids in 3D culture system (A) are well round shaped with compact structure while after 72hr in the microfluidic setup the shape of spheroid is slightly altered but still with compact structure (B). Clumping appeared when more than one spheroid was put together in the device for72hr (C). Photos were taken while spheroids were in the ULA plate which does not permit a side view to be taken. Scale bar: 100µm. This experiment was done twice.

Another GBM cell line (SNB19) was also used to generate spheroids and was tested in the microfluidic device. SNB19 cells like the U87 cells were cultured in three systems: 2D, static 3D, and as 3D in a microfluidic system. SNB19 spheroids were formed using two cell

densities (2 x 10^4 cells/well and 3 x 10^4 cells/well) and were compared to U87 spheroids formed using 2 x 10^4 cells/well. Statistical analysis of spheroid diameter, measured by the Gel Count, (**section 2.3**) showed no significant difference between SNB19 and U87 spheroids (**Figure 3.3A**). In 3D static system (ULA plate) SNB19 spheroids had a similar round shape with a uniform size in multiple independent experiments (2 experiment - 3 wells / experiment) (**Figure 3.3B**). SNB19 spheroids were made from an initial seeding of 3 x 10^4 cells/well (sodium pyruvate was added to the medium as a supplement to improve the cell survival), then transferred to the microfluidic device. Unfortunately, it was not possible to retrieve the spheroids at 48hr or 72hr, they had apparently disaggregated and were lost in the device effluent.

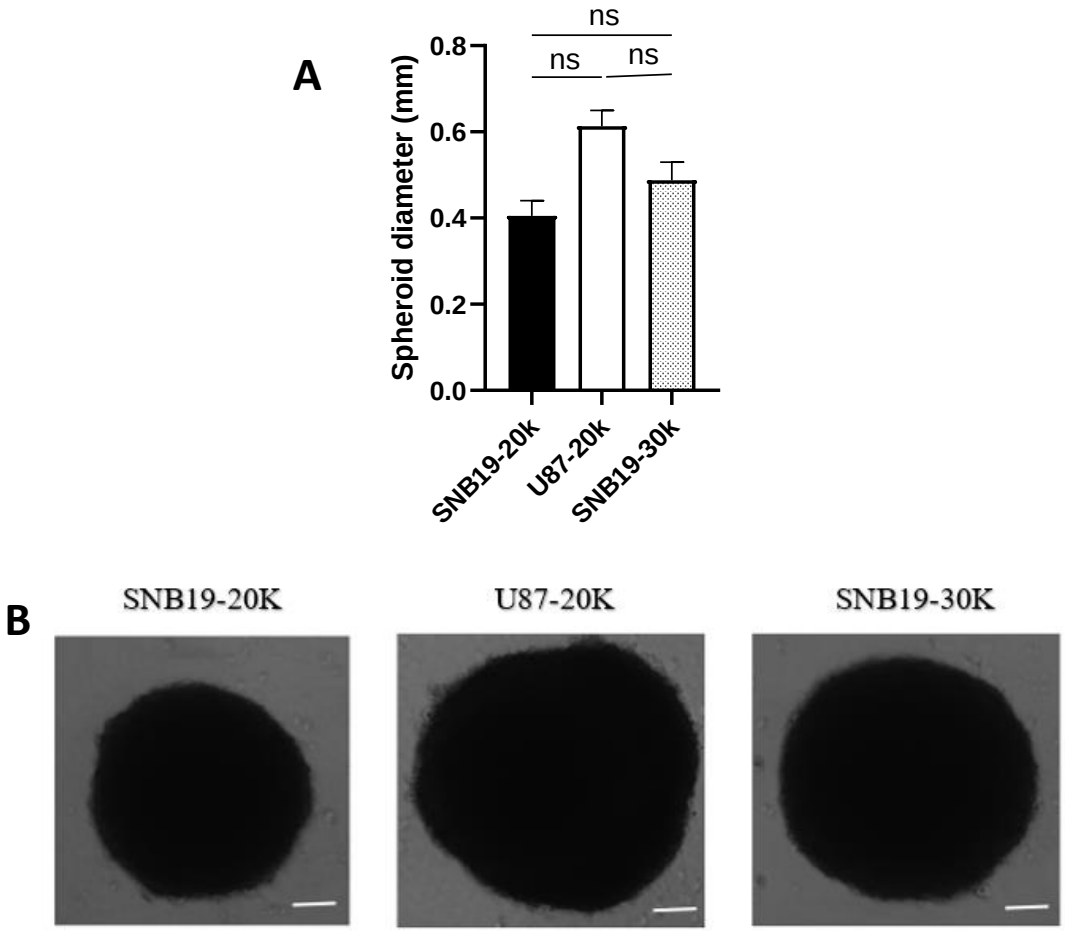

Figure 3.3 Comparison between SNB19 and U87 multicellular spheroids
Spheroids were formed in 96-well ULA round-bottomed plates after culturing for 72hr. A) Bar graph showing comparison of the spheroid diameter measured by Gel Count, between SNB19 spheroids formed using different cell densities 2 x 10^4 and 3 x 10^4 cells per well vs U87 spheroids formed using 2 x 10^4 cells/well. Values shown are the mean ±SEM of n=2. B) Light microscopy photos showing morphology of different spheroids. Data were not normally distributed according to Shapiro-wilk test and statistical significance was assessed using Kruskal-Wallis test. ns: not significant. Scale bar=100µm.

3.3 Optimisation of number and culturing time of spheroids that give the best yield of RNA

It was important to first optimize the number of spheroids that gave a sufficient yield of RNA for future analysis. In this study extracted RNA was used to run qPCR which needs good quality RNA with no phenol contamination. Phenol contamination in the extracted RNA solution will inhibit the reverse transcription reaction and lead to the wrong estimation of RNA concentration by UV spectrophotometry (Unger et al., 2019). RNA quality was always checked using UV spectrophotometry aiming to achieve absorbance values (A_{260}/A_{280}) > 1.8 and (A_{260}/A_{230}) > 2.0) (Udvardi et al., 2008). The aim was to ensure that the microfluidic devices used were able to maintain spheroids suitable for conducting further experiments.

ULA plates have been shown to be optimal for generating reproducible spheroids from many cell types including glioblastoma lines (Vinci et al., 2012; Gudbergsson et al., 2019). Cells in ULA plates aggregate into a compact structure that shows an increase in spheroid size over the time just as described previously (Gudbergsson et al., 2019). These plates were used to generate single U87 spheroids by adding 2 x 10^4 cells/well. The average diameter of spheroids was 612.80 ± 52.40 µm determined using the Gelcount.

The optimization of the spheroid number was done to get a sufficient yield of RNA, which is about 1000ng, as recommended for reverse transcription reaction (Kuang et al., 2018). The experiment was performed with 6, 9 and 12 spheroids cultured for 3 days in a 3D static system (**Figure 3.3.4**). Results showed that there were no statistically significant differences in RNA yield between the 3 conditions. Thus, to get sufficient RNA yield while using less reagent in the microfluidic system it was decided to use 9 spheroids consistently.

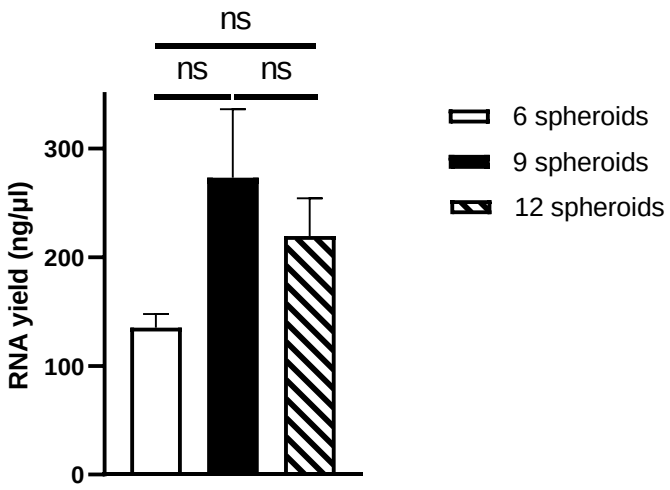

Figure 3.4 Comparison of RNA yield (ng/µl) between U87 spheroids cultured in 3D static conditions for 3 days using 6, 9 and 12 spheroids

Values shown are the mean ±SEM of n=3, ns: not significant. Data was not normally distributed (Shapiro-Wilk normality test) and Kruskal-Wallis test was used to test for significance.

The next step was to optimise the culturing time that gave sufficient RNA yield for future qPCR experiments. For this, 12 spheroids were cultured in both systems (static and flowing) and the RNA was extracted at 3 and 7 days after spheroid formation (n=3). The results of RNA yield in this experiment are shown in **Figure 3.5.**

The results in **Figure 3.5** show that the RNA yield of spheroids cultured in the flow system is significantly higher after 7 days (2.90±1.80 fold change $p \leq 0.05$) than after 3 days (1.50±0.30 fold change $p \geq 0.05$) compared to RNA yield of spheroids cultured statically.

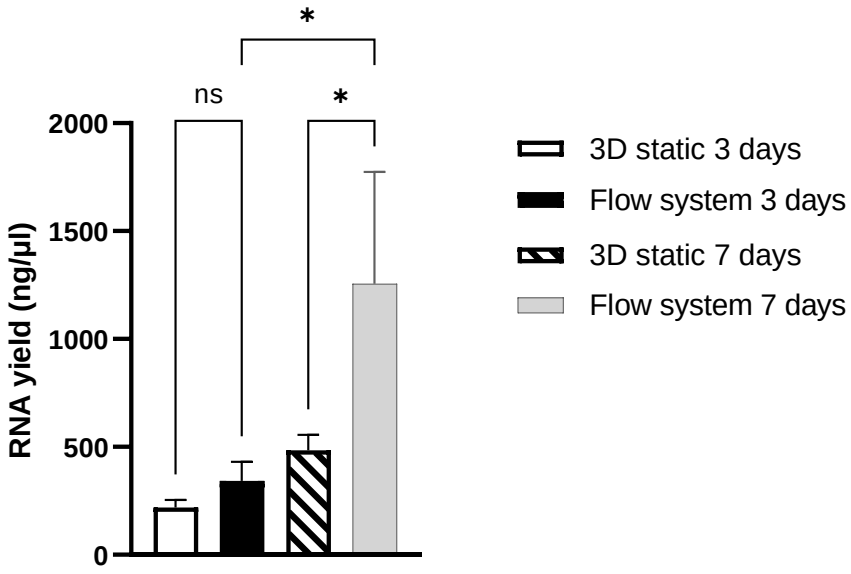

Figure 3.5 Comparison of RNA yield (in ng/µl) between U87 spheroids cultured in 3D static and 3D flow systems (12 spheroids in each experiment) for 3 and 7 days
*Values shown are the mean ±SEM of n = 3 repeats. Data is normally distributed (Shapiro-Wilk normality test) and one-way ANOVA test was used for statistical analysis ns: not significant *P ≤ 0.05.*

3.4 Selection of genes expressed in human primary glioblastoma cell line

To demonstrate specific gene knock-down appropriate targets had to be selected. An important characteristic of these target genes was that they are highly expressed in the cell line(s) of choice. U87 is a human primary cell line derived from a glioblastoma (Diao et al., 2019) that is frequently used in brain cancer research (more than 1489 published papers used U87 cell line in the last three years).

Based on a literature search for highly expressed genes in the U87 cell line, which play key roles in oncogenic processes the following were identified as potential targets: *AHR*, *RAB21*, *AKT2* and *PRMT2*. The expression of these genes in U87 cells was tested by qPCR (**Figure 3.6)**. The amplification plots in **Figure 3.6** show that in Hull's U87 cells *AHR* is not expressed, *AKT2* expression was very low, while *PRMT2* and *RAB21* are both well expressed. Two other pairs of primers were used for *AKT2* (**Table 2.1**) to verify that it was not expressed in U87 cells, and the same result as in **Figure 3.6** was given. Therefore, *PRMT2* and *RAB21* were selected as suitable target genes for future experiments.

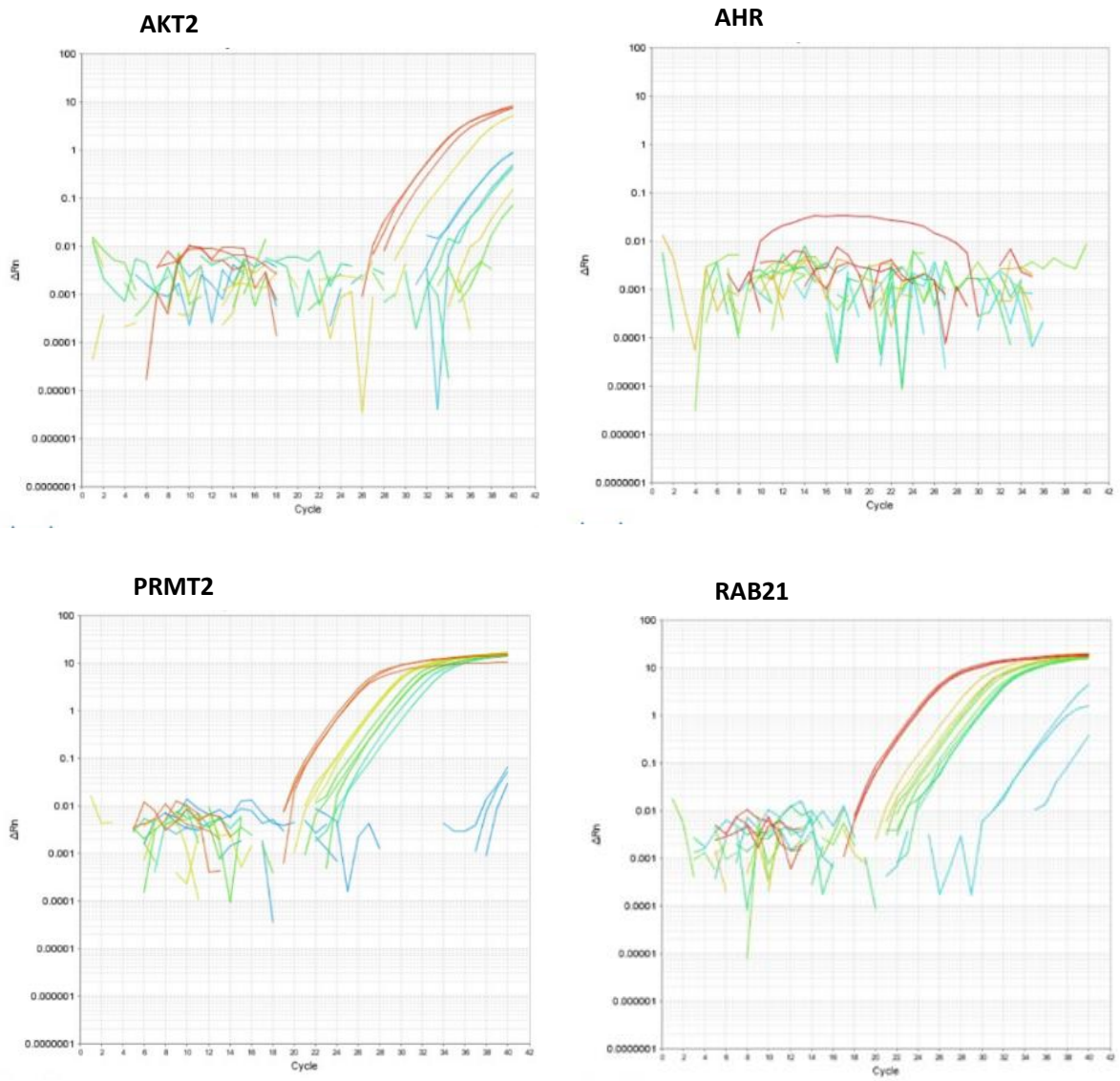

Figure 3.6 Amplification plot of the qPCR data of AKT2, AHR, PRMT2 and RAB21 gene expression in U87 cell line

Y-axis is for the ΔRn (delta Rn): fluorescence signal while x-axis is for the cycle number. Colours in the plot correspond to different dilutions of the sample: red: not diluted, yellow 1:50, green 1:20, blue 1:10.

3.5 Selection of housekeeping gene

Data normalisation is an important process in gene quantification analysis. Errors in sample quantification and sample-to-sample variation in qPCR efficiency can be corrected by including an invariant endogenous control in the assay (Dheda et al., 2004). A number of housekeeping genes are commonly used as a reference because they are present in all nucleated cell types and their mRNA synthesis is relatively stable in various tissues, even under experimental treatments, e.g. Glyceraldehyde-3-Phosphate Dehydrogenase (*GAPDH),*

albumin, actin, tubulin, cyclophilin, microglobulin, *18S* rRNA or *28S* rRNA, (Tichopad et al., 2004). For qPCR the perfect endogenous control should be expressed at roughly the same crossing points (CP) level as the target gene (Bustin, 2000).

Four housekeeping genes were initially assessed: Ribosomal Protein Lateral Stalk Subunit P0 (*RPLP0*), *GAPDH*, 18S ribosomal RNA (*18S*) and Ribosomal Protein L13a (*RPL13A*). U87 spheroids (n=12) were cultured in the 3D flow system for 7 days and the expression of *PRMT2* and *RAB21* was assessed by qPCR (relative standard curve) and the amplification plot results are shown in **Figure 3.7**. These plots show a standard qPCR amplification curve with three distinct phases, a base line, an exponential region, and a plateau suggesting that the genes are expressed in U87 cells.

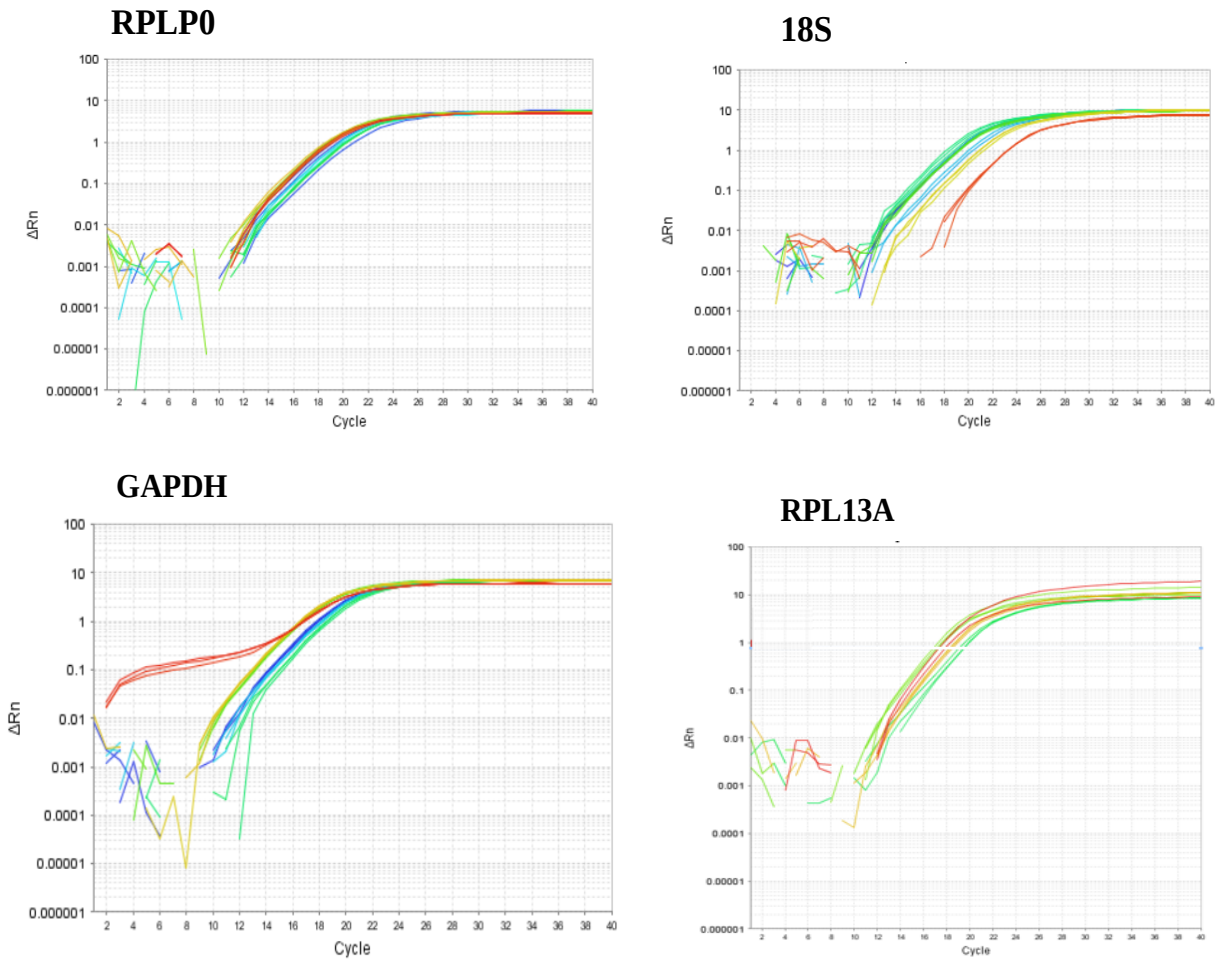

Figure 3.7 Amplification plot of the qPCR data of RPLP0, 18S, GAPDH and RPL13A gene expression in U87 cell line
Y-axis is for the ΔRn (delta Rn): fluorescence signal while x-axis is for the cycle number.

To choose the best control, each of the four potential housekeeping genes were used as a control to evaluate the gene expression level of *PRMT2* and *RAB21* genes in U87 spheroids. The fold change between flow system compared to static of gene expression of *PRMT2* and *RAB21* was normalised to the housekeeping gene and the results are presented in **Figure 3.8**. The bar graphs show that when using *GAPDH* as control, *PRMT2* and *RAB21* seem to be highly expressed in U87 cell line cultured in 3D flow system compared to the static one, with an increase of 1.90±3.32 fold change for both genes. In contrast the expression of both genes, using 18S as a control for qPCR, are shown to have a decrease of expression in the 3D flow system of *PRMT2* and *RAB21* by 0.48±0.12 and 0.54±0.21 fold change respectively. Using *RPL13A* as a control, the expression of the two genes in the flow system increased by 1.73±0.98 and 2.08±0.92 fold change for *PRMT2* and *RAB21* respectively. Finally, the increase, using *RPLP0*, was respectively 1.31±0.54 and 1.63±0.41 fold change.

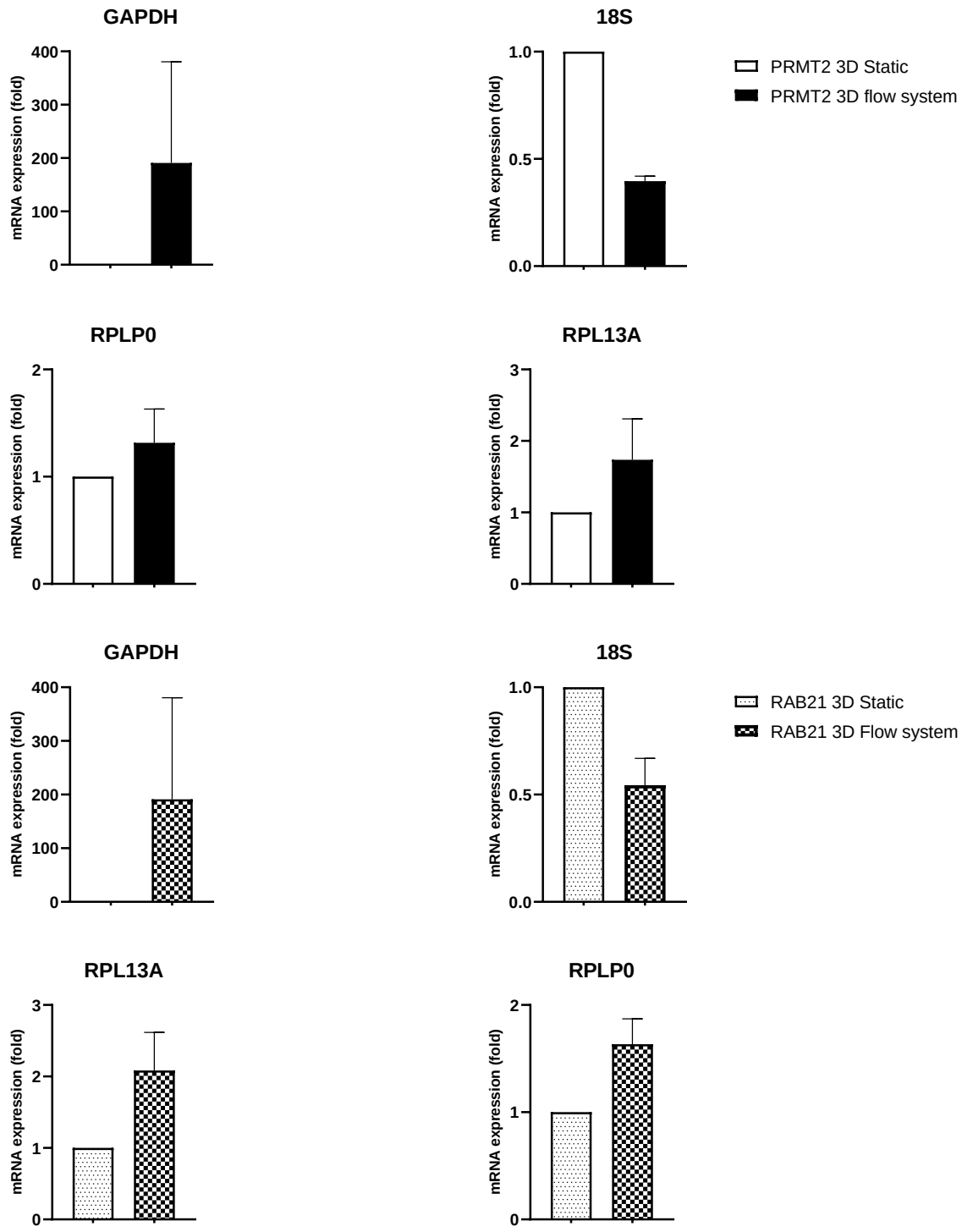

Figure 3.8 Fold change of mRNA expression of PRMT2 and RAB21
Expression was normalised to different housekeeping genes (GAPDH, 18S, RPLP0 and RPL13A). Values shown are the mean fold change of relative gene expression ±SEM of n=3(12 spheroids at 7 days) in 3D flow system compared to 3D static. Y axis scales were according to the level of mRNA expression in each experiment and GAPDH expression is relatively too low compared to the microfluidic setup and can't be seen in the graph.

Based on these data both *GAPDH* and *18S* genes are the least useful controls. First, because *GAPDH* shows a wide range from the standard deviation compared to the median. Second, it was demonstrated in the previous section that both *PRMT2* and *RAB21* are over expressed in U87 cells which is in contrast with the results obtained when using *18S* as control, suggesting that the latter gene is also being altered during growth. Therefore, *RPLP0* and *RPL13A* were chosen for further testing as to being the optimal housekeeping gene.

To select one of these two genes (*RPLP0* and *RPL13A*), a comparison between experimental and control CT (threshold cycle) values for both genes was done using U87 spheroids (n=12) cultured in flow vs static systems (**Figure 3.9**). The bar graph shows that there is no significant difference between experimental and control CT values for *RPLP0* ($p>0.999$) while the difference was significant for *RPL13A* ($p<0.05$). Thus, the *RPLP0* gene was selected for use as a control for future experiments.

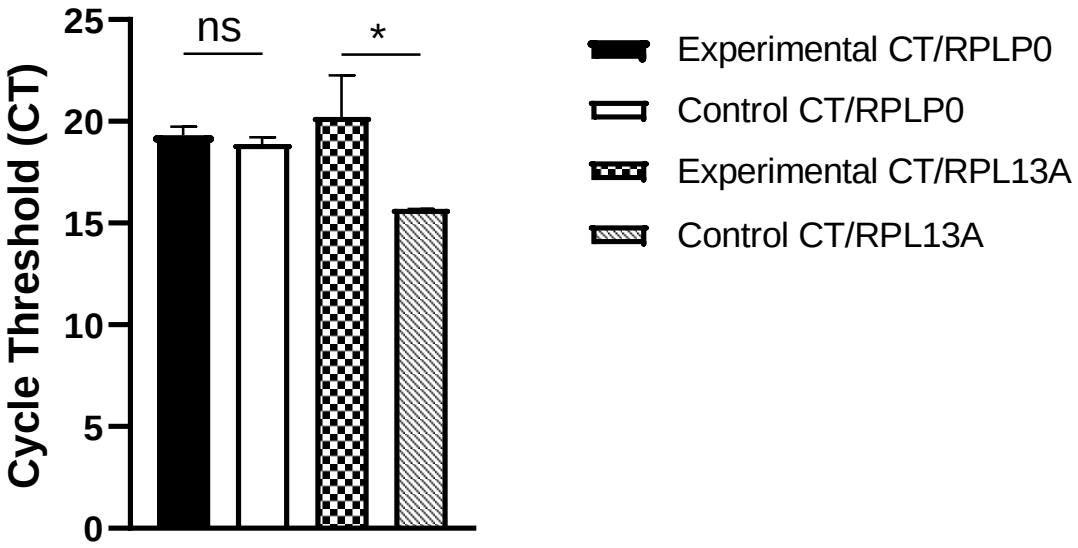

Figure 3.9 Experimental and control CT (Cycle Threshold) for RPLP0 and RPL13A genes

*U87 spheroids cultured in 3D static and 3D flow system for 7 days using 12 spheroids Values shown are the mean ±SEM of n=3; ns: not significant; *P≤ 0.05 vs. expression of corresponding gene in 3D culture model. Data are presented as a mean of CT values. mRNA expression in the flow system was normalised to that of (RPLP0 or RPL13A) and then standardised to the mRNA expression in 3D culture model. Data were not normally distributed and so the Kruskal-Wallis test was used to statistically analyse the data.*

3.6 Gene expression of PRMT2 and RAB21 in U87 spheroids cultured in a microfluidic system compared to those cultured in static phase

The use of microfluidic devices for culturing spheroids is well documented. As was mentioned previously, the microfluidic set-up better mimics the real microenvironment of a tumour mass than a 3D static culture. Recently, Wan & Lu, (2020) demonstrated that microfluidic technologies have enabled high-density and high-quality gene expression studies to be undertaken. To do gene knockdown experiments it is essential to ensure that the target genes are well expressed in spheroids under the appropriate culture conditions. The aim was to study the *PRMT2* and *RAB21* gene expression variability between spheroids cultured in static and flow system.

PRMT2 and *RAB21* gene expression were revealed by qPCR analysis on U87 spheroids (12 spheroids) cultured for 3 and 7 days in both set-ups. **Figure 3.10** shows a significant difference of expression of both genes in the two different environments with an increase of *PRMT2* and *RAB21* by 2.41±0.63 ($P \leq 0.001$) and 2.72±0.51 ($P \leq 0.0001$) fold respectively in spheroids maintained for 7 days in the microfluidic system compared to those in the static state. The fold change in gene expression of both genes was not significant after 3 days of culture in the flow system (0.70±0.04 and 1.22±0.14 fold change respectively). As described previously, gene silencing experiments are easily visualised when targeting over expressed genes (Ding et al., 2015). Importantly, the expression of both genes was maintained after culture under flow conditions. Gene expression analysis was done as it was described previously (**section 2.8**) and results are shown in **Figure 3.10**.

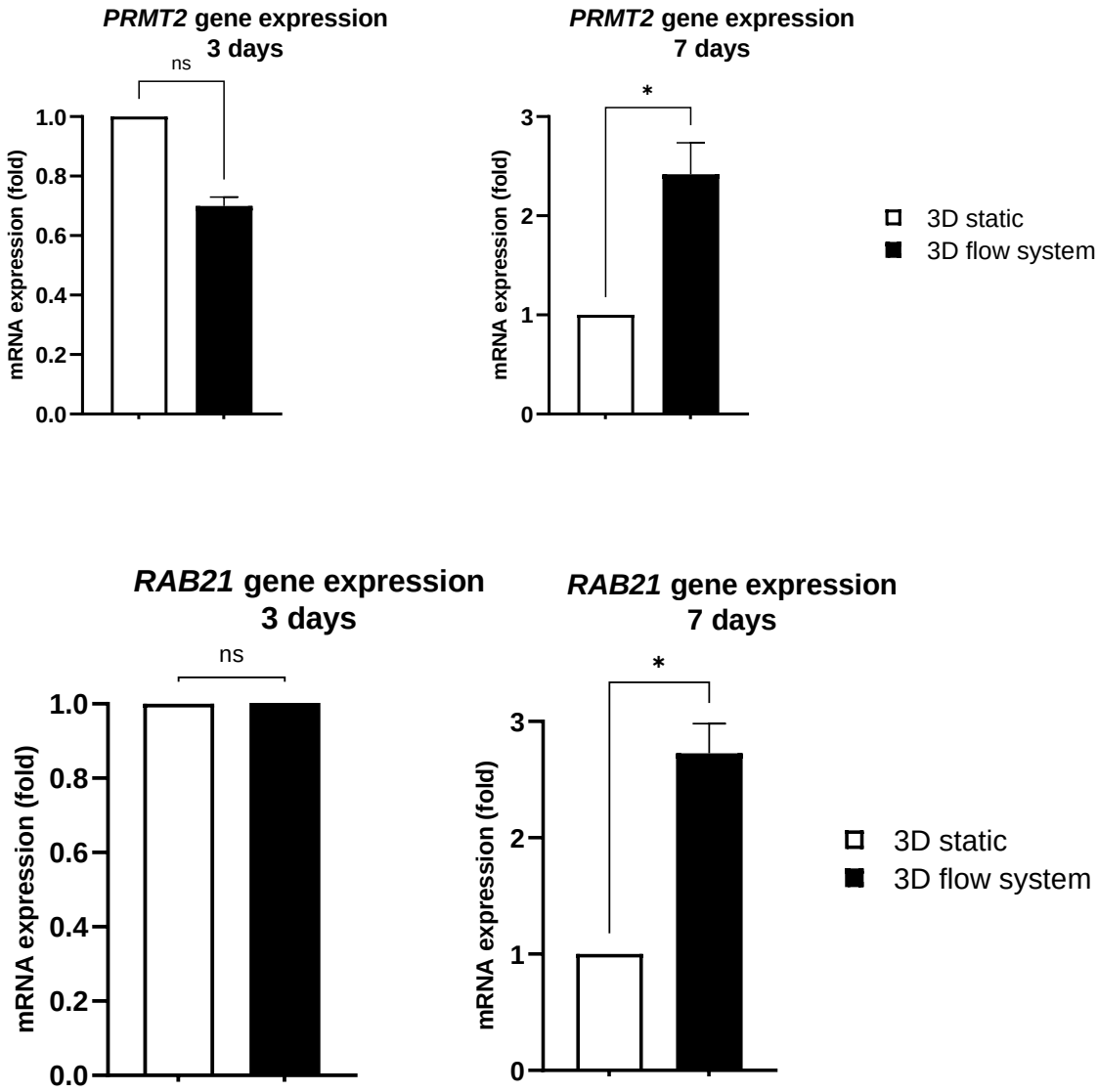

Figure 3.10 The gene expression of PRMT2 and RAB21 in U87 cells in static and a flowing microfluidic system

*Spheroids (n=12) were cultured for 3 and 7 days. Data are presented as a mean fold change of relative gene expression compared to control. mRNA expression was normalised to RPLP0 and then standardised to the mRNA expression in 3D culture model. Values shown are the mean ±SEM of n=4, ns: not significant, *P≤ 0.05vs. expression of corresponding gene in 3D culture model (as analysed by one way ANOVA test).*

3.7 Optimisation of siRNA concentration needed for the knockdown of PRMT2 and RAB21 in U87 cells cultured in 2D

After ensuring that the *PRMT2* and *RAB21* genes were well expressed in the microfluidic device, siRNA gene silencing experiments were carried out. Before doing gene knockdown on the flowing microfluidic device, it was decided to validate and optimise the silencing experiments in 2D and 3D static culture systems.

U87 cells were first cultured in ULA plates and transfected with different siRNA concentrations for both genes to determine the optimal concentration that effectively induced inhibition of gene expression. Three concentrations of siRNA were used: 5nM, 12.5nM and 25nM based on a literature review (Haiyong, 2018). The gene expression was tested by qPCR in three repeats (**Table 3.1 and Figure 3.11**). For both genes knockdown was statistically significant at all concentrations tested.

Table 3.1 Gene knockdown results on U87 cells cultured in 2D conditions

siRNA concentration (nM)	Knockdown level of PRMT2	*P* value	Knockdown level of RAB21	*P* value
5	75.66±5.13%	≤0.0001	86.33±9.01%	≤0.0001
12.5	75.66±10.69%	≤0.001	88.53±5.77	≤0.0001
25	56.0±25.94%	≤0.05	89.33±5.13%	≤0.0001

Percentages presented in the table are the mean ±SD of n=3 repeats

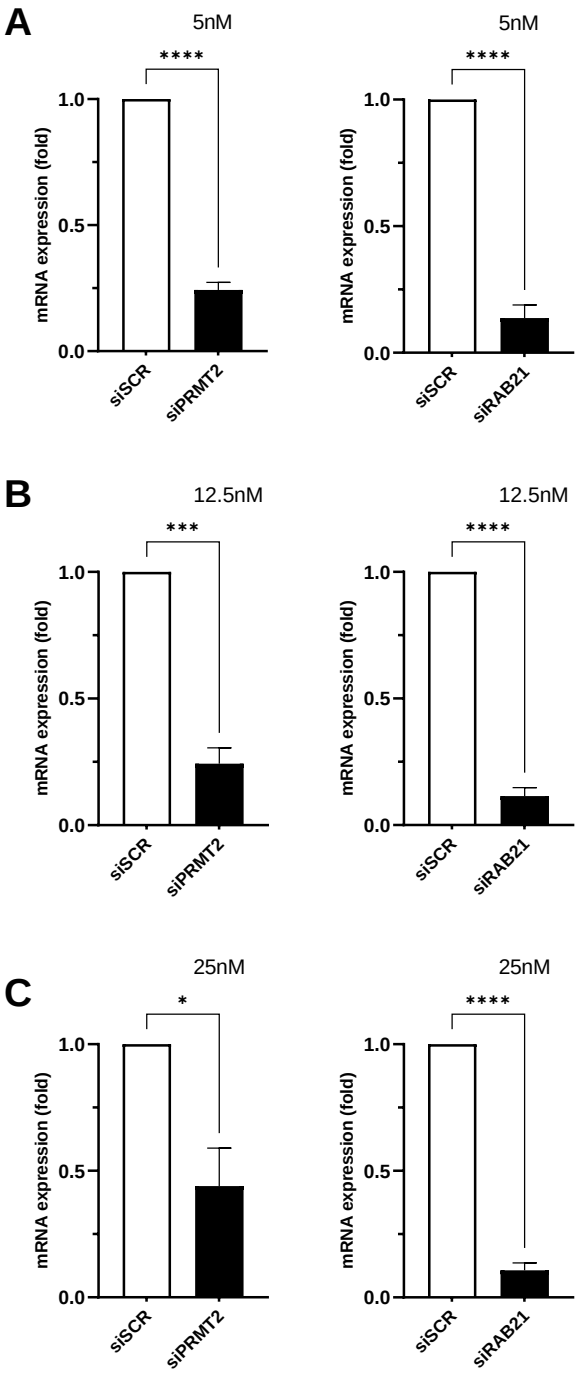

Figure 3.11 Real-time PCR analysis of gene expression level of PRMT2 and RAB21 genes in U87 cells cultured in 2D model and transfected with different concentrations of siRNA at 48 hours post-transfection

*Cells were transfected with 5nM (A), 12.5nM (B) & 25nM (C) of siRNA. Data are presented as the mean fold change of relative mRNA expression compared to control. Values shown are the mean ±SEM of n = 3, *≤0.05; ***P ≤0.001 and **** P≤ 0.0001 vs. expression of corresponding gene in U87 cells treated with scrambled siRNA (siSCR). Statistical significance was evaluated using an unpaired t test.*

3.8 Effect of siRNA knockdown on proliferation of U87 cells cultured in 2D

Recent studies described *PRMT2* as a transcriptional activator of oncogenes and it has been implicated in the pathogenesis of GBM and other cancer types (Cura & Cavarelli, 2021). It was reported also that the knockdown of *RAB21* inhibited cell growth and induced cell apoptosis in GBM cells including the U87 cell line (Ge et al., 2017b). The aim was to study the effect of *PRMT2* and *RAB21* gene knockdown on the proliferation of U87 cells cultured under 2D conditions. For this a series of MTS assays (**section 2.10.1**) were done using different siRNA concentrations and different cell concentrations.

3.8.1 MTS assay using 3.5 x 10^3 cells/well treated with 5nM of siRNA

U87 cells were grown on a 96 well plate; for 3.5 x 10^3 cell/well, and a 5nM solution of siRNA (siPRMT2 and siRAB21) was added to the medium. The effect of siRNA knockdown was measured using MTS assay at different times (0hr, 24hr, 48hr and 72hr). The results are presented in **Figure 3.12** and showed that there is no effect on cell proliferation when *PRMT2* (**Figure 3.12A**) or *RAB21* (**Figure 3.12B**) are knocked down (which was confirmed by q-PCR). Experiments were done in 3 replicates and statistical significance was evaluated using one-way ANOVA test.

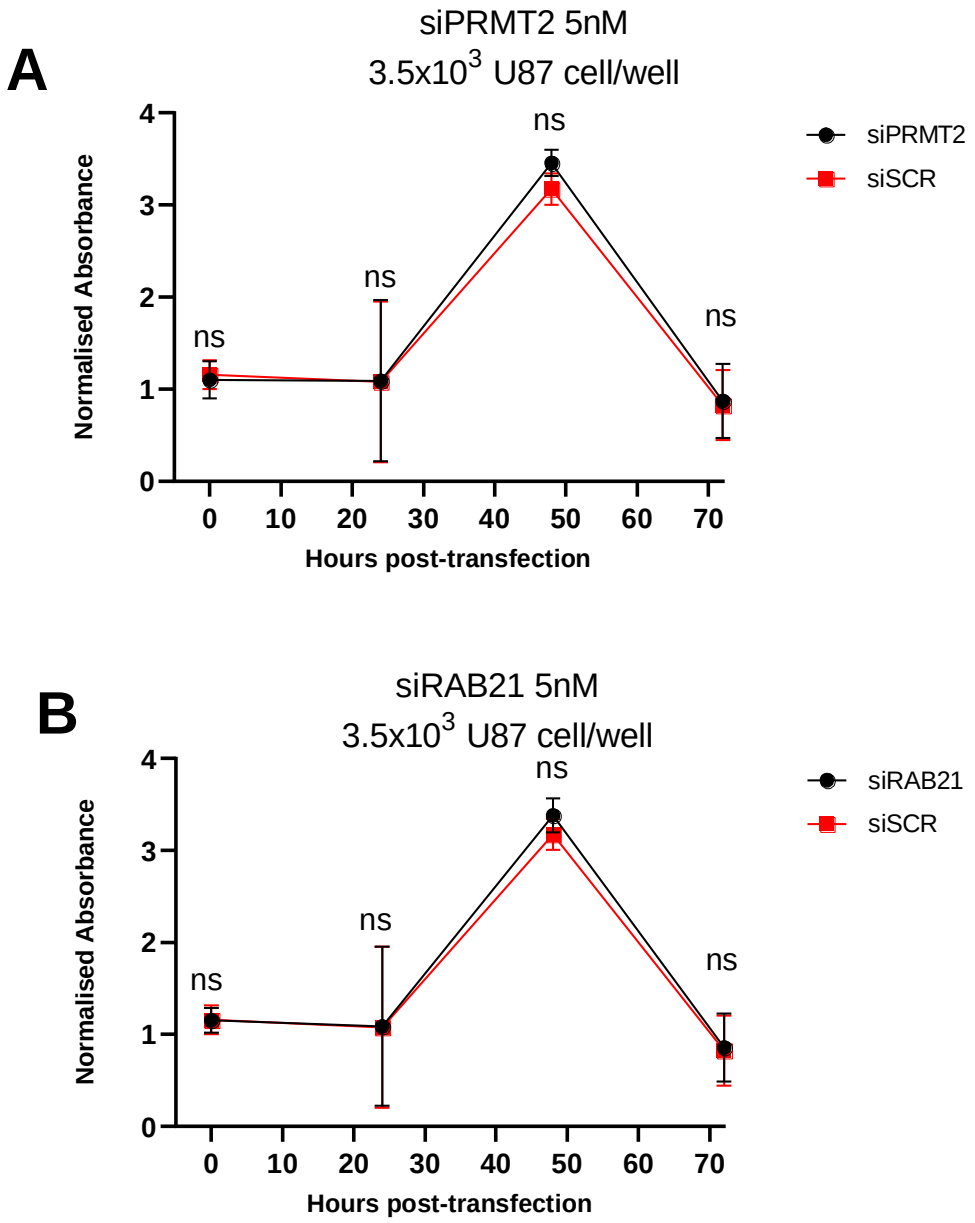

Figure 3.12 Effect of siRNA knockdown on proliferation of U87 cells cultured on a 96 well plate

U87 cells cultured in 96 well plates (3.5 x 10^3cells/well) were treated with either 5nM of siRNA (siPRMT2 (A), siRAB21(B)) or scrambled siRNA control (siSCR). MTS values were determined at 0, 24, 48 and 72 hours post-transfection. Y axis: optical density of samples normalised to that of 0hr. Standard error of the mean is indicated as bars in the figure. Normal distribution was investigated using D'Agostino & Pearson and Shapiro-Wilk normality tests. Difference significance was determined using one-way ANOVA test. ns: not significant.

3.8.2 MTS assay using 2.5 x 10^3 cells/well treated with 5nM of siRNA

During the previous experiment using 3.5 x 10^3 cell/well a clump of cells was observed over the incubation period. To reduce cell clumping the MTS assay experiments were repeated using 2.5 x 10^3 cells/well. Results of three replicates are shown in **Figure 3.13**. Again, it was shown that cell proliferation was unaffected by siRNA knockdown of either *PRMT2* or *RAB21*. It was interesting to notice that cell clumping was reduced compared to the previous experiment and the absorbance was lower than for the higher cell concentration, as would be expected.

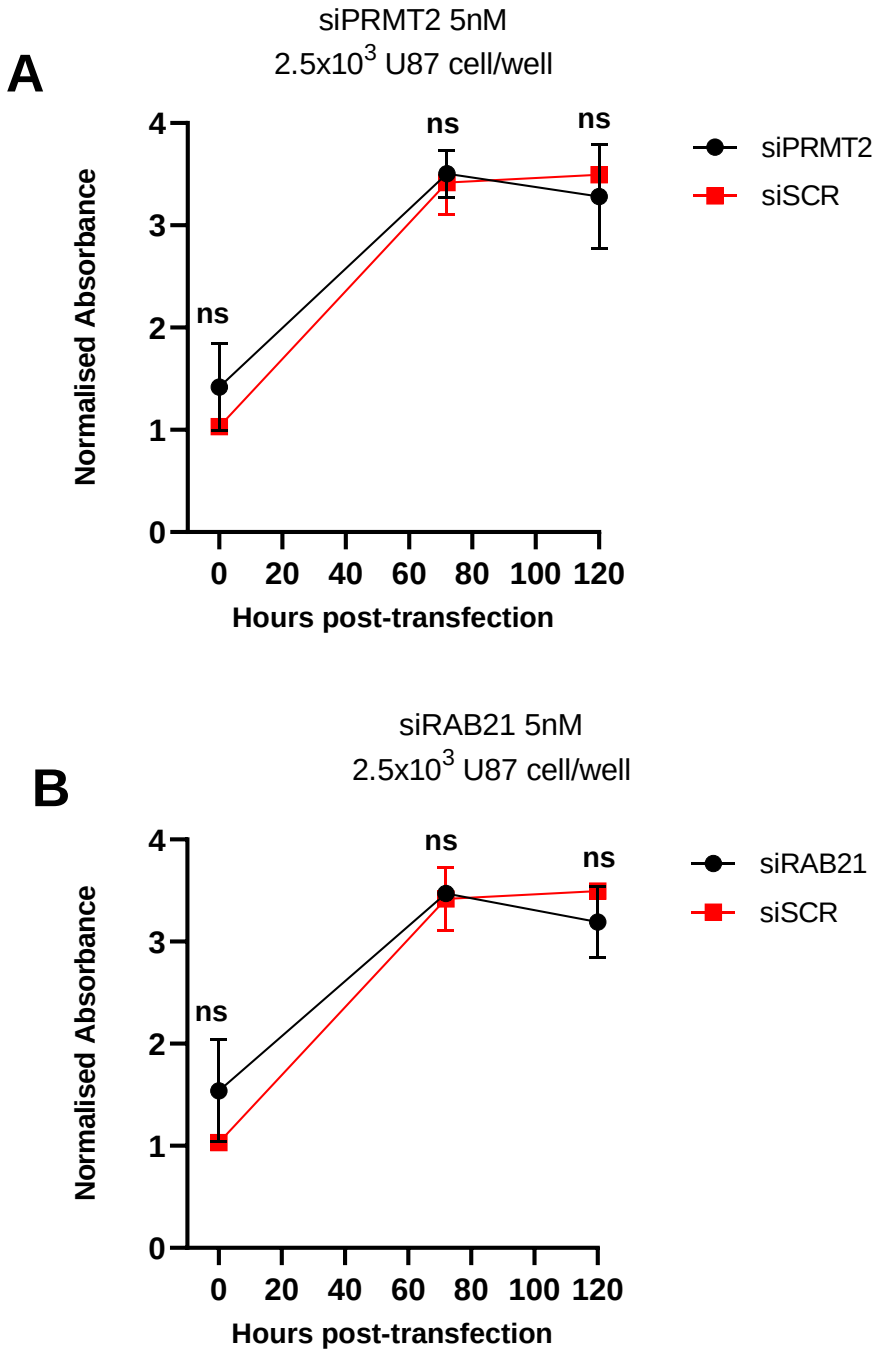

Figure 3.13 Effect of siRNA knockdown on proliferation of U87 cells cultured on a 96 well plate

U87 cells cultured on 96 well plates (2.5 x 10^3 cells/well) were treated with either 5nM of siRNA (siPRMT2 (A), siRAB21(B)) or scrambled siRNA control (siSCR). MTS values were determined at 0, 72 and 96 hours post-transfection. Y axis: optical density of samples normalised to that of 0hr. Standard error of the mean is indicated as bars in the figure. Normal distribution was investigated using D'Agostino & Pearson and Shapiro-Wilk normality tests. Difference significance was determined using one-way ANOVA test. ns: not significant.

3.8.3 MTS assay using 2.5 x 10^3 cell/well double transfected with 5nM of siRNA

Previous studies reported that the intracellular half-life of siRNA ranges from 24hr to 72hr (Bartlett & Davis, 2006; Brown et al., 2020). It was thought that perhaps *PRMT2* and *RAB21* gene knockdown did not affect U87 cell proliferation in the previous experiments (**section 3.8.2**) due to the short half-life of these siRNA molecules. To avoid this possibility MTS assays were done on U87 cells (2.5 x 10^3 cells/well) treated with 5nM of siRNA as usual, which was renewed at 48hr post transfection for the final incubation period (double transfection). MTS assays were done in three repeats and results are shown in **Figure 3.14**. It is clear that the cell proliferation was not affected by siRNA knockdown for both genes, even when additional siRNA was added during the incubation period.

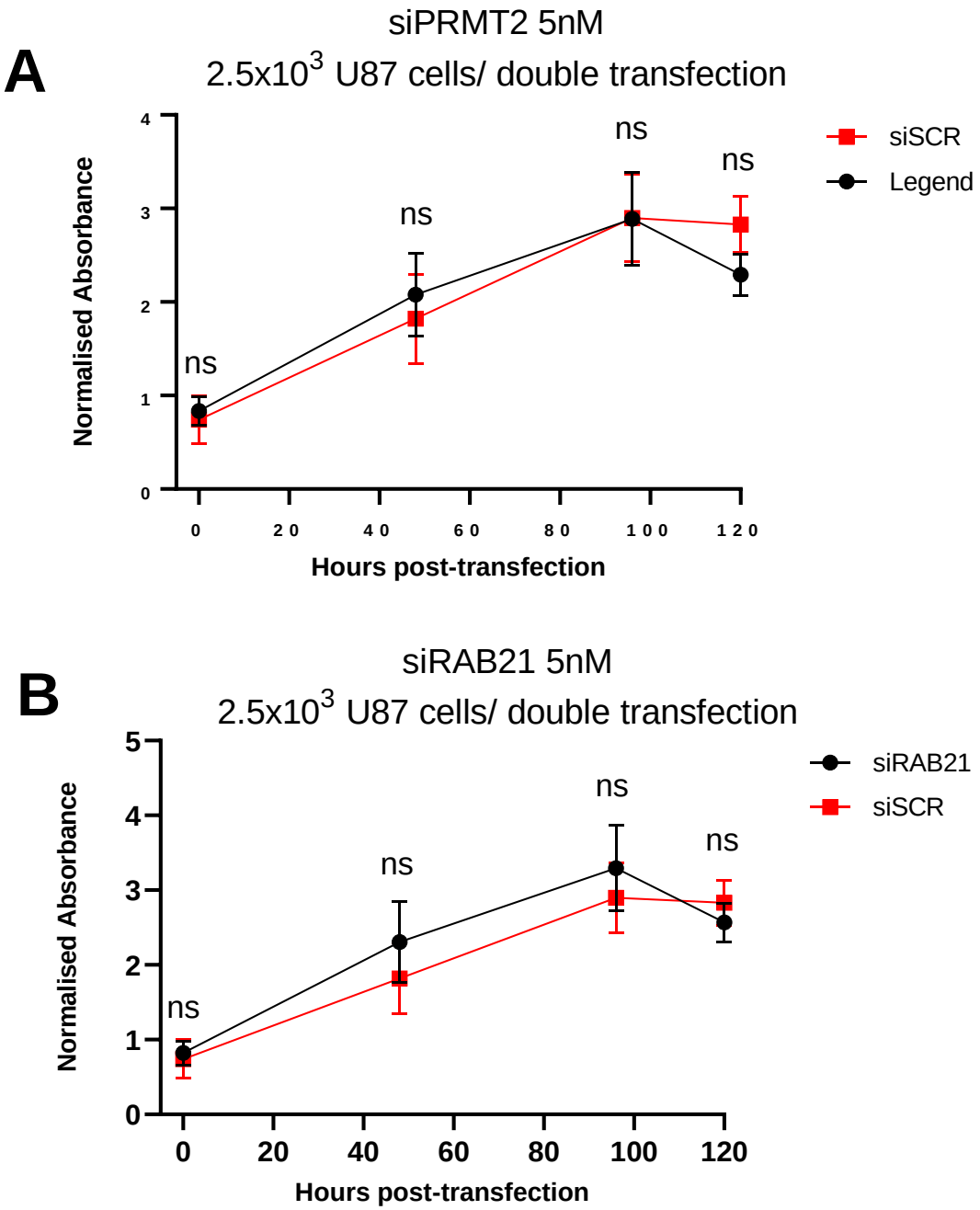

Figure 3.14 Effect of siRNA knockdown on proliferation of U87 cells cultured on a 96 well plate

U87 cells were cultured in 96 well plates (2.5 x 10^3 cell/well) were treated with either 5nM of siRNA (siPRMT2 (A), siRAB21(B)) or scrambled siRNA control (siSCR). Cells were transfected again with fresh siRNA solution at 48hr post-transfection. MTS values were determined at 0, 48, 96 and 120hr post-transfection. Y axis: optical density of samples normalised to that of 0hr.Standard error of the mean is indicated as bars in the figure. Normal distribution was investigated using D'Agostino & Pearson and Shapiro-Wilk normality tests. Differences were analysed using one-way ANOVA test. ns: not significant.

3.8.4 MTS assay using 2.5 x 10^3 cell/well treated with 25nM of siRNA

As experiments (**section 3.8.2**) showed that 5nM of siRNA did not affect cell proliferation rate it was decided to increase the concentration of siRNA to 25nM, as it is possible that these genes were relatively abundant and that the level of knockdown is low. As before MTS assays were done at 0hr, 72hr, 96hr and 120hr, with an increased concentration of 25nM siRNA added to U87 cells (2.5 x 10^3 cells/well) added at the start of the experiment. Again, the results showed no difference in proliferation rate between cells treated with specific siRNA and those treated with the scrambled control (**Figure 3.15**). The experiment was only done once as there was no hint of any effect.

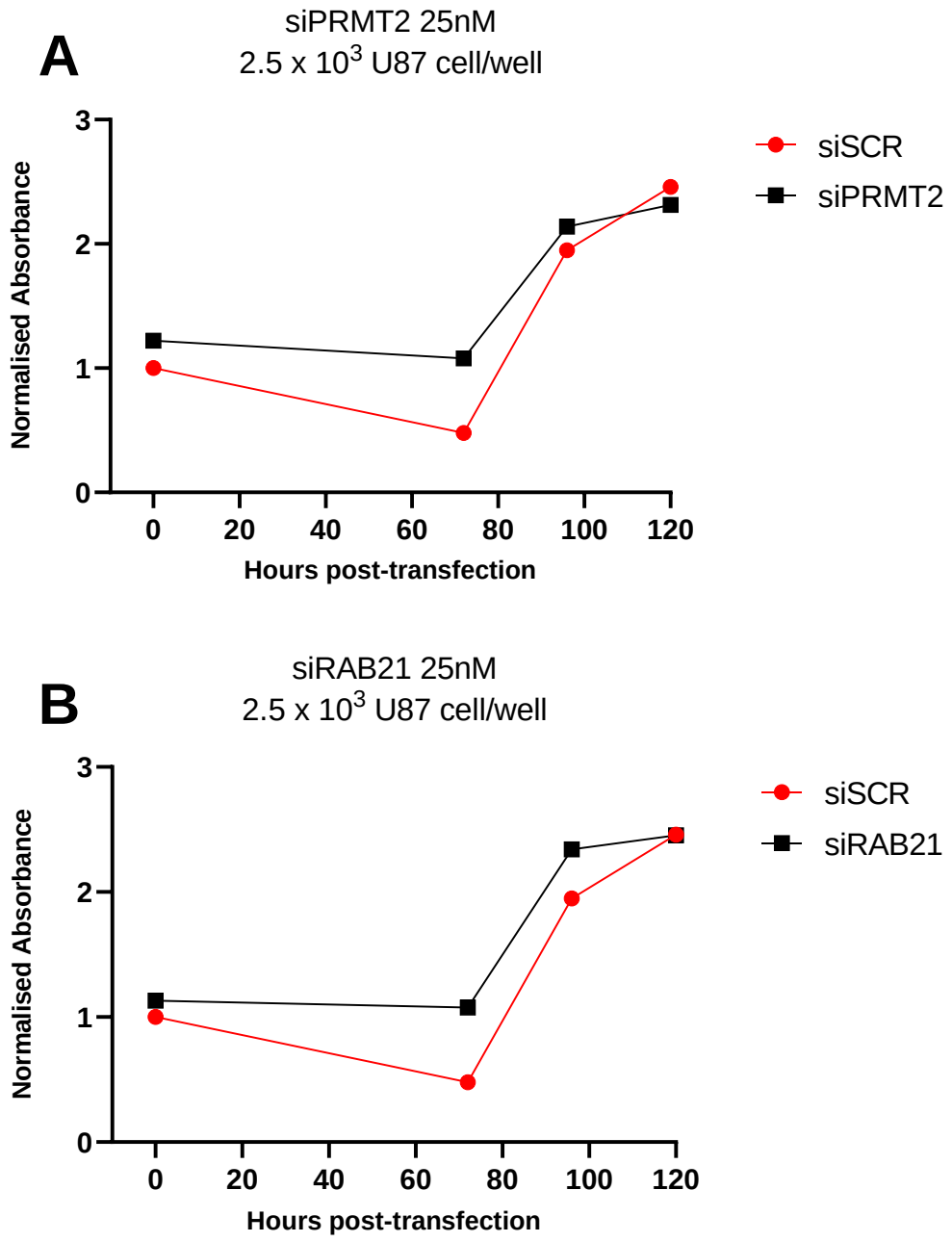

Figure 3.15 Effect of siRNA knockdown on proliferation of U87 cells cultured on a 96 well plate

U87 cells were cultured in 96 well plates (2.5 x 10^3 cell/well) were treated with either 25nM of siRNA (siPRMT2 (A), siRAB21(B)) or scrambled control siRNA (siSCR). MTS values were determined at 0, 72, 96 and 120hr post-transfection. Y axis: optical density of samples normalised to that of 0hr. The experiment was done once so no statistical analysis was done.

3.8.5 MTS assay using 2 x 10^3 cells/well double transfected with 5nM of siRNA compared to positive control

As previous experiments had not shown any effect of siRNA knockdown on cell proliferation it was decided to compare the effect with a chemical known to inhibit cell proliferation. The U87 cells were treated with 200mM of sodium azide (NaN_3) which induces cell apoptosis by inhibiting the function of cytochrome oxidase in the mitochondrial electron transport chain (Shan et al., 2017). MTS assays were done again at 0hr, 24hr, 48hr and 96hr post-transfection of 2 x 10^3 cell/well treated with 5nM of siRNA solution, which was renewed 48 hours post-transfection (double transfection) to maximise the chance of specific knock-down **Figure 3.16**. As before no obvious difference was noticed between cells treated with siRNA and those treated with the scrambled control, however the NaN_3 almost completely removed MTS metabolism by 96 hours.

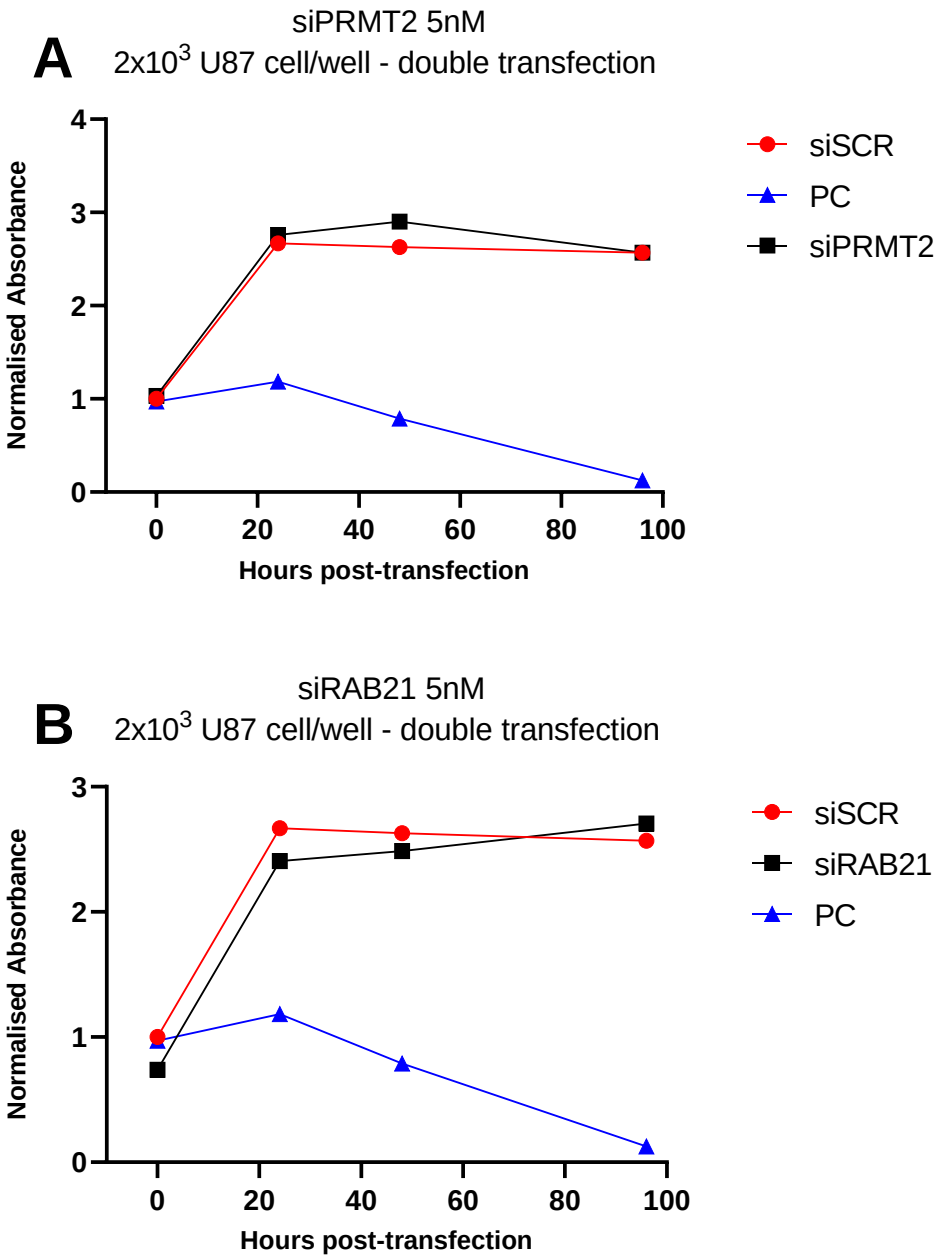

Figure 3.16 Effect of siRNA knockdown on proliferation of U87 cells cultured on a 96 well plate

U87 cells were cultured on a 96 well plate (2 x 10^3 cells/well) were treated with either 5nM of siRNA (siPRMT2 (A), siRAB21(B)) or scrambled control siRNA (siSCR). Cells were transfected again with fresh siRNA solution at 48hr post-transfection. A positive control (PC) was added to the experiment consisting of cells treated with a final concentration of 200mM of NaN_3. MTS values were determined at 0, 48, 96 and 120hr post-transfection. Y axis: optical density of samples normalised to that of 0hr. The experiment was done once so no statistical analysis was possible.

3.8.6 PRMT2 and RAB21 knockdown effect on U87 cell proliferation measured by cell counts

Previous MTS experiments showed that there was no effect of siRNA knockdown of *PRMT2* and *RAB21* on U87 cell proliferation/metabolism grown in 2D. Therefore, it was decided to assess proliferation using the trypan blue cell count. U87 cells were grown in 6 well plates using cell densities of 15 x 10^4, 1 x 10^5 or 75 x 10^3 cells/well. The optimal number that allows the cells to grow without clumping during 120hr post-transfection was 75 x 10^3 cells/well. Using this number U87 cells were seeded and transfected by 5nM (**Figure 3.17A**) and 25nM (**Figure 3.17B**) of siRNA solution. Results showed again that there were no significant differences of cell number change at 120hr post-transfection between U87 cells treated with specific *PRMT2* and *RAB21* siRNA (5nM and 25nM) and those treated with the scrambled control siSCR.

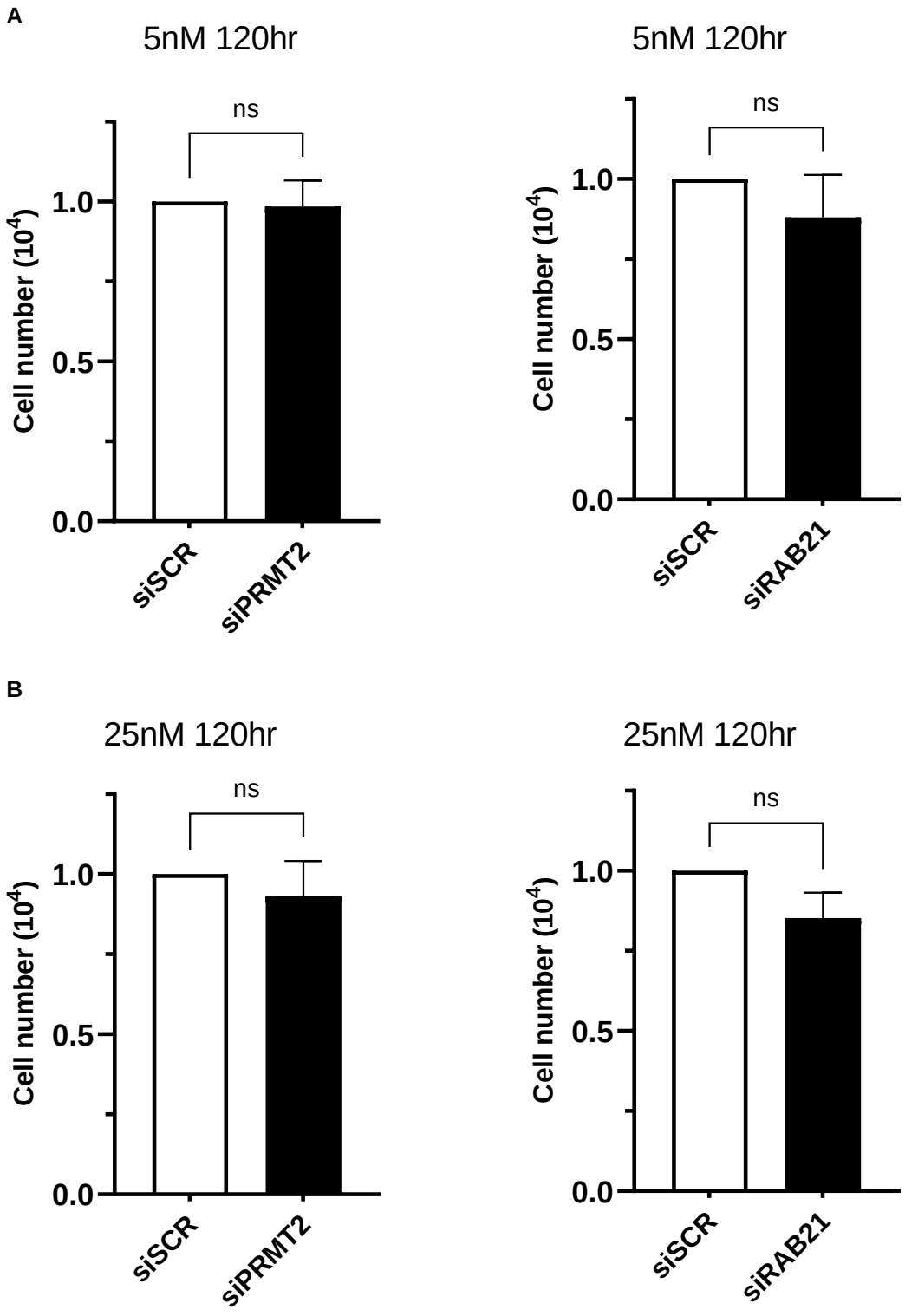

Figure 3.17 Phenotypic test of U87 spheroids treated with siRNA
U87 cells were cultured in 6 well plate and treated with different concentrations 5nM (A) and 25nM (B) of siRNA (siPRMT2 and siRAB21). Proliferation test was done using trypan blue cell count at 120hr post-transfection. The results of cell proliferation were normalised to the cell number in cells treated with scrambled siRNA. Statistical significance was determined using unpaired t test. ns not significant. Values shown are the mean ±SEM of n = 3.

3.8.7 Western blot analysis

Western blotting is used for protein detection and characterization. This technique is widely used for evaluating efficiency of gene knockdown on protein levels (Wu et al., 2004; Ruigrok et al., 2018). The aim was to investigate the effects of gene silencing seen at mRNA level by studying the levels of the specific protein in U87 cells cultured in 2D. The samples were collected after 96hr post-transfection, and cell lysate were prepared (**section 2.9.1**). The BCA assay was used to measure the concentration of all the cell lysates and determine the volume of solution needed to be loaded into each well of a polyacrylamide gel (**section 2.9.3**).

The BCA is a colorimetric method using the reactivity between Bicinchoninic acid (BCA), copper (Cu2+) sulphate, and proteins. The reduction reaction of copper ions under alkaline conditions is proportional to the protein concentration which is calculated using the light absorption of the solution at 595nm. A triplicate samples of unmodified and reductively methylated bovine serum albumin (BSA) standard solution are used to produce a calibration curve of absorbance versus protein concentration (µg/ml, **Figure 3.18**). The unknown protein concentration in a solution can be determined assuming that the analyte-proteins will react in the same manner as the BSA standard by plotting the normalized absorbance values against the protein concentration on the standard curve. Example of calculation of protein concentration is represented in the **Table 3.2**.

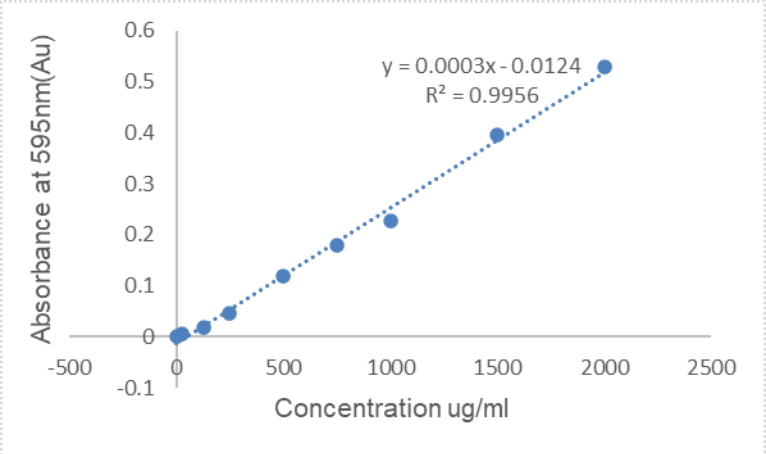

Figure 3.18 BCA standard curve. *Results of the BCA assay plotted as the normalised absorbance values (A595nm) versus the protein concentration determined for triplicate samples of BSA. X axis: protein concentration (µg/ml). Y axis: absorbance values at 595nm normalised to that at 0µg/ml (0.09).*

Table 3.2 values of absorbance at 595nm and calculated concentrations in samples of U87 cells cultured under 3D static conditions

SAMPLE	1	2	Average absorbance	normalised average absorbance	Concentration (ug/ml)	Concentration (ug/ml) with dilution factor	Concentration (ug/ul)	vol (ul) needed for 10ug of protein
U87 /3D static	0.32	0.32	0.32	0.23	826.33	6886.11	6.88611	1.45

Sample : U87 cultured in 3D static conditions
1 and 2: Absorbance values at 595nm in each replicate
Average absorbance: Average between 1 and 2
Normalised average absorbance: Average absorbance normalised to the absorbance at o cg/ml of BSA (0.09)
Concentration (µg/ml): Determined by plotting the normalised average absorbance value against the protein concentration on the standard curve
Concentration (µg/ml) with dilution factor: [25/volume of the sample (3ml)]x Concentration (µg/ml)
Concentration (µg/µl): Concentration (µg/ml)/1000
volume (µl) needed for 10µg of protein: 10/ Concentration (µg/µl)

Protein samples (50µg) were loaded into all wells of the gel. SiRNA knockdown efficiency was measured at the protein level on western blots at 96hr post-transfection of U87 cells cultured in 2D and treated with siPRMT2. The Figure below shows that there was no significant difference in *PRMT2* protein level between cells treated with siPRMT2 (5nM) and those treated with the scrambled control siSCR (**Figure 3.19)**. For *RAB21* no western blot analysis was done due to no anti-RAB21 antibody being available, but the potentially knocked down sample was included on the gel as another control lane for any effect on *PRMT2*.

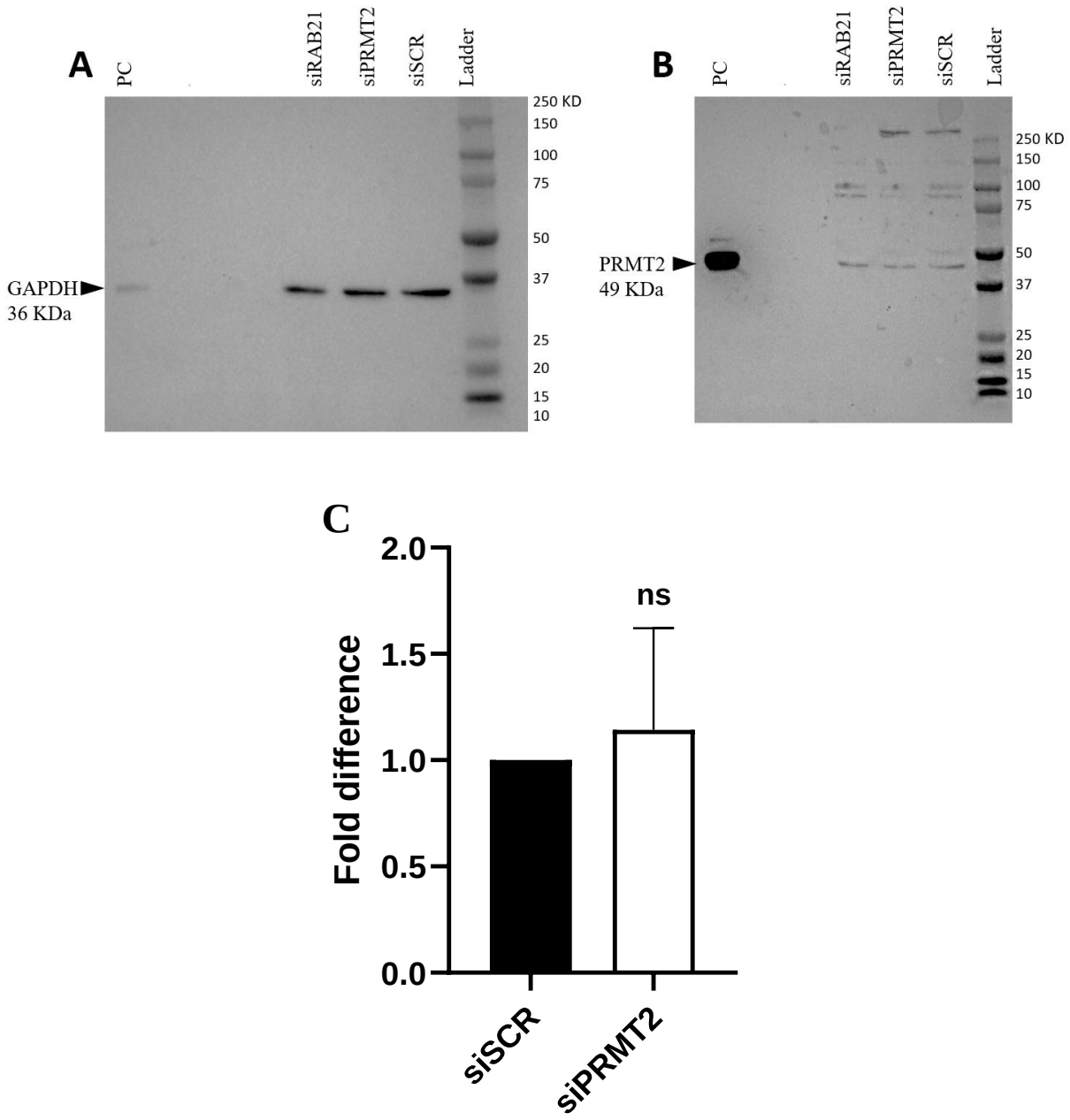

Figure 3.19 Western blot analysis and PRMT2 protein quantification after siRNA knockdown in U87 cells cultured in 2D

The protein level of PRMT2 after transfections with siPRMT2 and siRAB21 was compared with the expression in cells treated with scrambled (siSCR) by normalising to the expression of GAPDH. A and B: western blot analysis using anti-GAPDH (A) and anti-PRMT2 (B). ***PC****: is the positive control (10µg of cardiac lysate). High-molecular weight bands denote protein-protein interactions and antibody cross-reactivity generating dimers and multimers which could be due to samples not being fully denatured. C) statistical analysis and values shown are the mean ±SEM of n=3. Data were not normally distributed according to D'Agostino & Pearson and Shapiro-Wilk normality tests. Statistical significance was assessed using Mann-Whitney test. ns: not significant.*

3.9 Attempt at siRNA mediated knockdown of *PRMT2* and *RAB21* genes in U87 cells cultured in a static 3D culture model

After successful mRNA knockdown experiments in the 2D culture system, U87 cells were cultured in a static 3D model and then transfected with anti-PRMT2 and anti-RAB21 siRNA. U87 spheroids created in ULA plates were transfected with different siRNA concentrations for both genes to determine what concentration induced the highest inhibition of gene expression. The transfection experiments were done with different siRNA concentrations, based on the 2D work (5nM and 25 nM) and gene expression level was assessed at 48hr and 72hr post-transfection. Results are shown in the **Figure 3.20**, and gene knockdown levels are summarised in the **Table 3.3**. Results showed a statistically significant decrease in *PRMT2* and *RAB21* gene expression in U87 spheroids, after siRNA transfection compared to the control using scrambled siRNA, for both genes. The maximum significant knockdown was seen at 48hr post-transfection using 5nM of siRNA at 72hr by 43.00±24.75% and 59.00±4.58% for *PRMT2* and *RAB21* respectively.

Table 3.3 *PRMT2* and *RAB21* gene knockdown levels in U87 spheroids measured at 48hr and 72hr post-transfection using different siRNA concentrations (5 and 25nM)

	5nM-48h (%)	***P* value**	**5nM-72h (%)**	**pvalue**	**25nM -72h (%)**	***P value***
PRMT2	38.2±1.05	≤0.0001	43.00±24.75	≤0.05	14±26.51	ns
RAB21	-14.33±65.60	ns	59.00±4.58	≤0.0001	32.33±7.76	P ≤ 0.01

Percentages presented in the table are the mean ±SD of n=3 repeats. ns: not significant

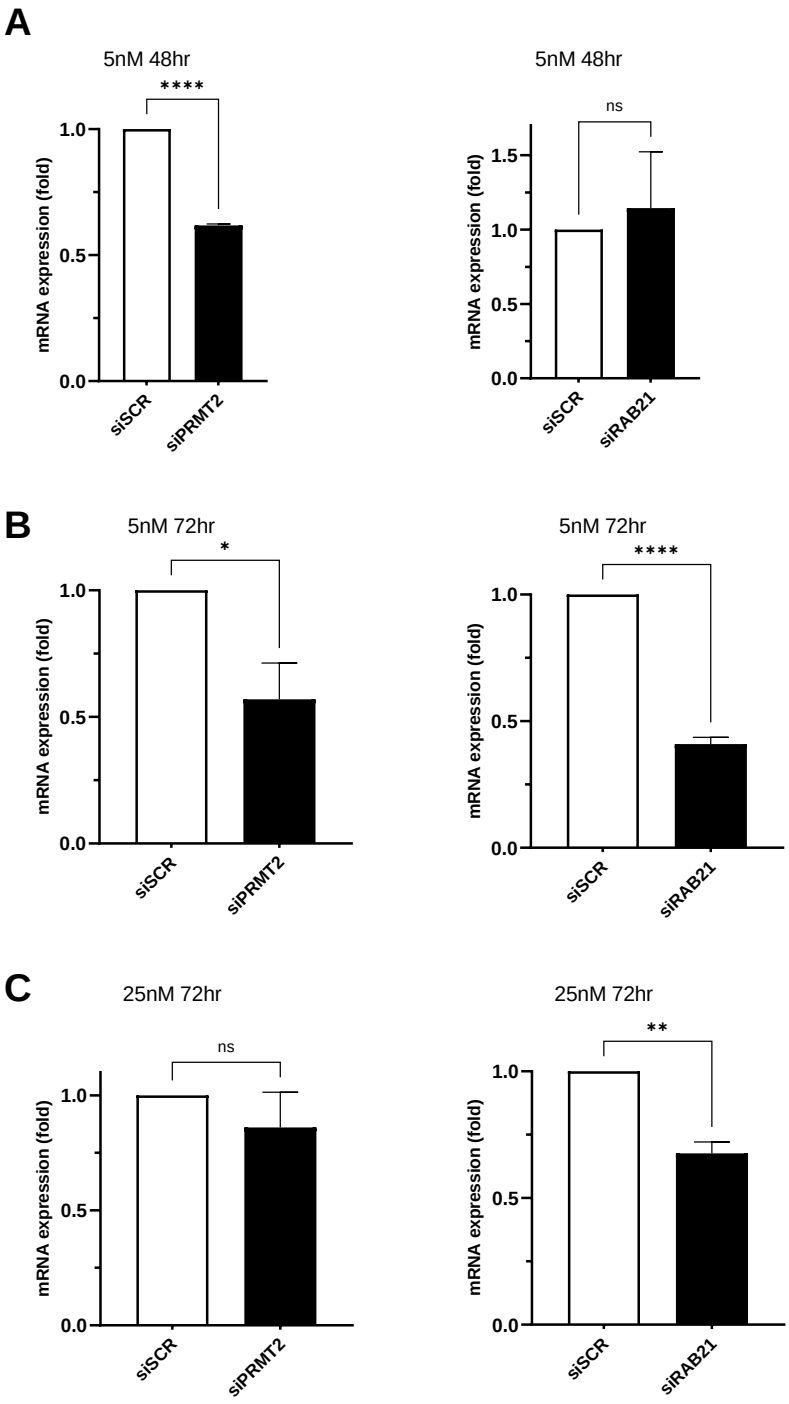

Figure 3.20 qPCR analysis of gene expression level of PRMT2 and RAB21 genes in U87 cells cultured in 3D spheroid system and treated with different concentrations of siRNA at 48/72 hours post-transfection

*A) Spheroids were transfected with 5nM of siRNA at 48hr post-transfection. B) Spheroids were transfected with 5nM of siRNA at 72hr post-transfection. C) Spheroids were transfected with 25nM of siRNA at 72hr post-transfection. Data are presented as the mean fold change of relative mRNA expression compared to control. Values shown are the mean ±SEM of n = 3, ns: not significant; *P ≤0.05; **P ≤ 0.01 and **** P≤ 0.0001 vs. expression of corresponding gene in U87spheroids treated with scrambled siRNA (siSCR). Statistical significance was evaluated using an unpaired t test.*

3.10 Knockdown in a microfluidic system

3.10.1 Knockdown using 5nM siPRMT2 or siRAB21 for 96 hours

After successful gene silencing in 2D and 3D static system the aim was to optimise gene knockdown in U87 spheroids maintained in a flow system. For that U87 spheroids were prepared and formed in ULA plates (**Section 2.2**), then transferred to the microfluidic device. Three spheroids were introduced to the chip and subjected to a 2µl/min flow rate of medium containing 5nM of siRNAs. Because a large amount of siRNA would be needed to perform the experiments over three time periods (48hr, 72hr and 96hr) and three repeats for each condition, it was decided to renew the medium (containing siRNAs) every 24hr. The purpose was to do a comparison between continuous and single dose perfusion of siRNA in a flow system. Therefore, spheroids were collected after 96hr from the microfluidic device in both conditions, and gene expression was analysed using qPCR in three repeats. Results are shown in the **Figure 3.21** and gene knockdown levels are summarised in **Table 3.4.** Results revealed that for both genes there was a statistically significant knockdown with continuous perfusion (**Figure 3.21A)**. In contrast, with a single dose perfusion, only *RAB21* showed significant gene silencing (37% p≤0.05) (**Figure 3.21B)**.

Table 3.4 *PRMT2* and *RAB21* gene knockdown levels in U87 spheroids measured at 96hr post-transfection using 5nM of siRNA. One trial with continuous transfection every 24hr and the other with a single transfection at 0hr.

	Continuous transfection (%)	pvalue	single transfection at 0h (%)	*P* value
PRMT2	26.33±2.51	≤0.0001	14.5±9.19	ns
RAB21	19.67±8.02	≤0.05	37.00±16.82	≤0.05

Percentages presented in the table are the mean ±SD of n=3 repeats. ns: not significant

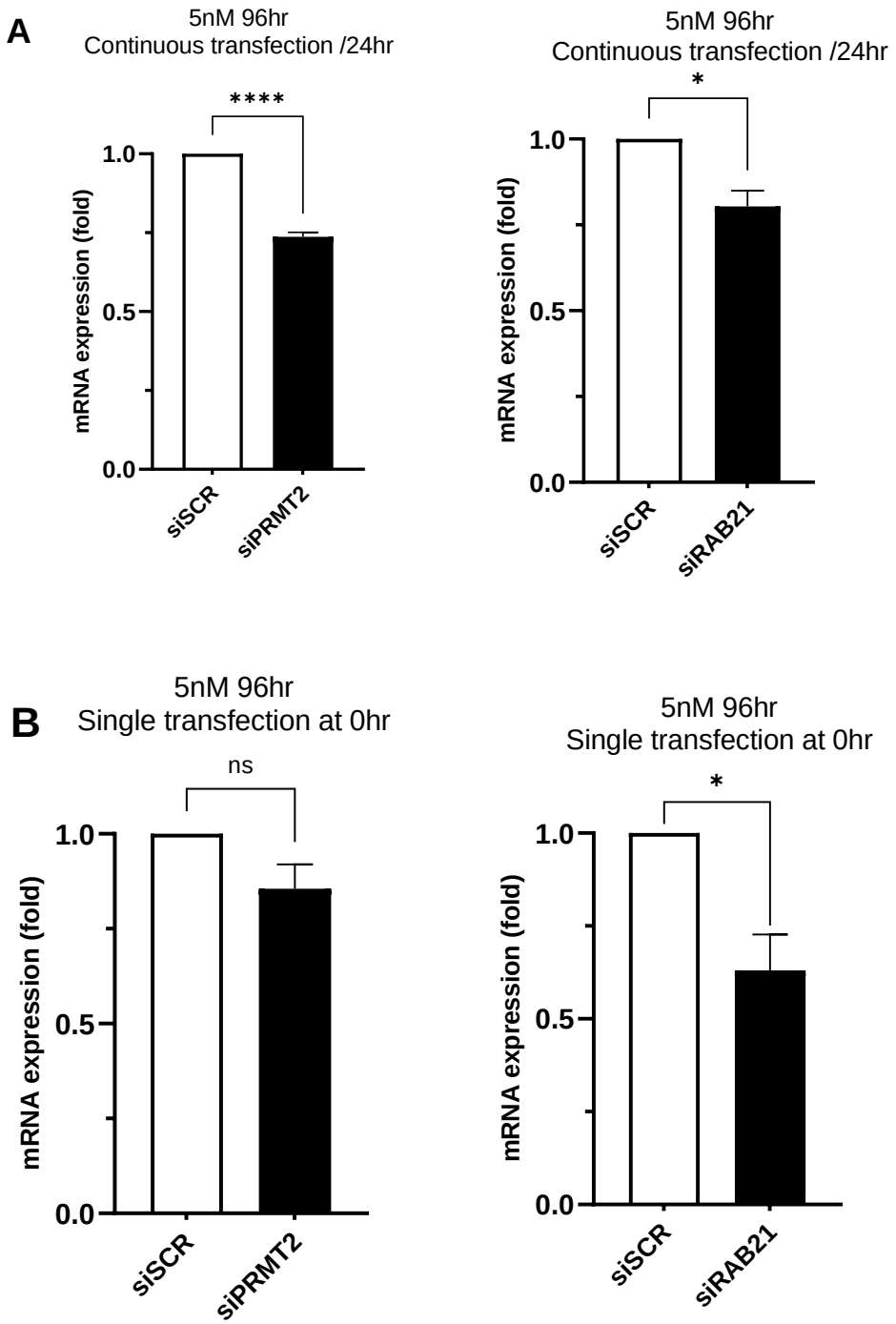

Figure 3.21 qPCR analysis of gene expression level of PRMT2 and RAB21 genes in U87 spheroids cultured in microfluidic system and treated with 5nM siRNA at 96 hours post-transfection

*A) The solution containing the medium and the siRNAs is recharged every 24hr. B) The solution containing the medium and the siRNAs is supplied 0hr post- transfection without renewal. Values shown are the mean ±SEM of n = 3, ns: not significant, **** P≤ 0.0001 and *P ≤0.05 vs. expression of corresponding gene in U87 cells treated with scrambled siRNA (siSCR). Statistical significance was evaluated using an unpaired t test.*

3.10.2 Knockdown in microfluidic system with 10nM siRNA (siPRMT2 & siRAB21) at 72 hours

To try and improve the gene knockdown level, it was decided to double the concentration of siRNA to 10nM. Spheroids were collected after 72hr post-transfection, and no reagent was left to do another trial for 96hr. Experiment was done in three repeats. No significant gene silencing was observed for both genes (**Figure 3.22**).

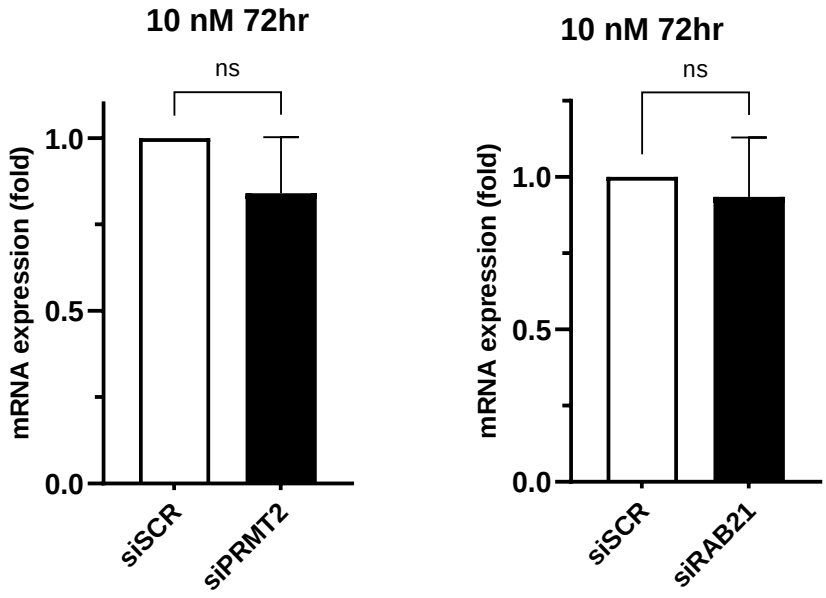

Figure 3.22 qPCR analysis of gene expression level of PRMT2 and RAB21 genes in U87 spheroids cultured in microfluidic system and treated with 10nM siRNA at 72 hours post-transfection

The solution containing the medium and the siRNAs is supplied in one time without renewal. Values shown are the mean ±SEM of n = 3, ns: not significant, vs. expression of corresponding gene in U87 cells treated with scrambled siRNA control (siSCR). Statistical significance was evaluated using unpaired t test.

3.11 Discussion

GBM is defined as grade VI astrocytoma (Stoyanov et al., 2022). It is regarded as is the most aggressive, invasive, and undifferentiated type of tumour (Hara et al., 2019). The tumour is characterised by a poor prognosis with a 5-year survival rate of 5.1% (Ostrom et al., 2015) and the signs and symptoms produced by this malignancy are closely related to the affected region of the brain. Surgical resection, followed by concurrent radiotherapy with TMZ as the main chemotherapeutic adjuvant, is the standard of care for patients diagnosed with GBM (Tan et al., 2020). The use of this chemotherapeutic agent in GBM has some significant limitations. First, the presence of the blood brain barrier (BBB), as it prevents the passage of small molecules and most of macromolecules (**section 1.2**). Second, acquired resistance after sustained use, with the main mechanism involved in this process is referred to the DNA repair mechanisms (**section 1.3.3.1**). Therefore, recurrence after resection is commonly reported within 10 months in approximately 80% of GBM patients due to the acquired TMZ resistance. Thus, most research about new therapeutic approaches for GBM are looking to improve the transfer across the BBB and/or limiting the resistance to TMZ (Banerjee et al., 2021). Despite huge efforts, new therapeutic targets are still urgently required, and translationally relevant models are needed to reliably identify and validate potential targets.

The aim of this study was to establish a flow-based system for performing siRNA gene knockdown using GBM spheroid model. To the author's knowledge this is the first study that deals with the siRNA gene silencing using GBM spheroid model cultured in a flowing system where spheroids were prepared then transferred in a microfluidic chip.

3.11.1 Spheroid formation and microfluidic device setup

Since their first use in cancer research, microfluidic systems have led to innovative advances in cancer development and drug discovery as these models has shown to mimic more the real tumour microenvironment than 2D and 3D culture models (Ma et al., 2018a; Niculescu et al., 2021; Akgönüllü et al., 2021a). Most of previous studies on tumour spheroids in a flow system used microfluidic spheroid formation chips (µSFCs), where spheroids were formed and tested in the same chip. As was mentioned before (**section 1.5.1.5**) the use of µSFCs present some limitations. For µSFCs, beside the increased time related to the setup of the device, new spheroids will be formed in different devices if new parameters were set for the study (Santo et al., 2016; Moshksayan et al., 2018). The newly

formed spheroids may have different characteristics (size and shape). The non-homogenous diameter of generated spheroids will affect the diffusion distance of molecules/drugs through the viable rim resulting in different drug responses leading to non-accurate results (Lim et al., 2018). Therefore, to obtain a uniform-sized spheroid and with the time saving using a pre-characterised microfluidic device it was decided to grow the spheroids in ULA plates then introduce them into the chip.

The microfluidic device used in this study was fabricated of poly (methyl methacrylate) (PMMA). PMMA is a commonly used thermoplastic material in the fabrication of microfluidic chips. Its advantages over other thermoplastic materials (PS, PC, and COC) and PDMS include its physiochemical properties such as transparency, chemical resistance, biocompatibility, and cost-effective molding (Matellan et al., 2018; Sözmen & Yildiz, 2021). The designed microfluidic device ensures a controlled flow of the medium from the inlet permitting continuous perfusion of the trapped spheroids, and the removal of waste products to the outlet. Alongside the collection of effluent, the device enables the investigation of the effect of different biochemical components on the physiochemical properties and biological activities of the spheroids.

3.11.2 Spheroids in the microfluidic device

Previous studies emphasised the importance of the shape and size of the spheroid in generating reliable results (Hirschhaeuser et al., 2010; Weiswald et al., 2015a). Results from these studies showed a uniform rounded shape, with compact structure, when U87 spheroids were cultured in round-bottomed ULA plates. These results are in line with what was published in earlier studies by (Lee et al., 2013; Fu et al., 2014; Ruppen et al., 2015; Han & Kim, 2021). Similar results were obtained with SNB19 spheroids. However, results showed that U87 spheroids became slightly oval-shaped when put under a flow of medium (flow rate of 2µl/min) within 72hr in the microfluidic device.

In an earlier study, (Gheibi et al., 2017) showed that patient-derived xenografts (PDXs) grew as ellipsoids in a 75µm deep microfluidic chambers. Additionally, they demonstrated that elliptical PDX-derived spheroids formed in microchambers retained the pattern of drug responsiveness and resistance observed in mice and display the same heterogeneity as in the *in vivo* tumour response. Despite the fact that tumour spheroids do not attain generally perfect circularity but rather have elliptical shape, studies demonstrated that these ellipsoids present similar distribution of oxygen and nutrients as regular spheroids (Grimes & Currell, 2018;

Mark et al., 2020). This demonstrates that the small change in shape does not appear to significantly alter the functionality and the physiological characters of U87 spheroids, and that successful experiments could be carried on them.

Nevertheless, whether this observed shape originated due to the forces exerted by the fluidic flow in the device or because of the handling of the spheroid during the imaging procedure needs to be checked by lowering the flow rate of the medium and/or trying to take the pictures *in situ*. Alternatively, more gentle methods of retrieving the spheroids from the devices could be devised. An example of this would be to invert the microfluidic device containing spheroids over a petri dish so that the inlet is down and apply medium to the outlet which should flush the spheroid out without any need for contact with a pipette tip.

Despite the round shape in the ULA plate, SNB19 spheroids became disaggregated and were lost in the outlet of the microfluidic device. Unlike U87 spheroids, the flow of the medium (2µ/min) induced the destruction of SNB19 spheroids, which may be due to weaker cell-cell interactions established during spheroid formation of SNB19. However, preliminary experiments with increased time of formation did not result in more robust spheroids. A similar disaggregation phenomenon was reported when spheroids from breast cancer cell lines MCF-7 were studied (Ho et al., 2012).

In the current study, in the 3D static system (ULA plate), a density of 2 x 10^4 U87 cells/well was sufficient to form well-round-shaped spheroids (diameter 612.75±52.44 µm) with compact structure. Previous work in the laboratory had shown that U87 cells could generate spheroids of >200µm diameter using 10^3cells/well. Recent studies for generating U87 spheroids (600 µm of diameter) have reported similar numbers of starting cells, e.g. (Collins et al., 2021c) cultured either 2.5×10^4 or 3.5×10^4 cells per well for 4 days.

Spheroid clumping or fusion observed in this study is a well-known phenomenon when growing more than one spheroid per well. Numerous studies have reported homotypic and heterotypic fusion of spheroids (Kim et al., 2018) which could be explained by the inherent high anchorage capacity of tumour cells to form cell-cell or cell-substrate, (Jiménez-P et al., 2018). Recently, (Grosser et al., 2021) reported that spheroids formed from non-tumorigenic cell lines fuse slower than spheroids made from metastatic cells, most probably reflecting changes in cell adhesion molecule expression.

3.11.3 Optimisation of number and culturing time of spheroids that give the best yield of RNA

The results of this study indicate that enough amount of RNA could be extracted from 6, 9 or 12 spheroids cultured for 3 days in a 3D static system. Purity and concentration of RNA were determined using optical density as previously described (Biró et al., 2019). Thus, any number of spheroids >6 could yield sufficient amount of RNA for the reverse transcription.

The increasing fold change of the RNA yield of spheroids cultured for 7 days compared to 3 days in the microfluidic system could be explained by the enhanced proliferation rate, as well as the over expression of differentially expressed genes compared to spheroids cultured in the static conditions. The influence of the flow system to promote the proliferation rate of cells within the spheroids was demonstrated previously (Gilbert et al., 2019; Tsai et al., 2019) and can reach in some cases statistically similar rates observed in the frozen tissue and fresh samples (Sylvester et al., 2012; Trujillo-de Santiago et al., 2019). In their study Sylvester et al., (2012) investigated the response to anticancer drugs of fresh or cryogenically frozen head and neck squamous cell carcinoma (HNSCC) tumour biopsies cultured in a microfluidic device. They found that the frozen tissue showed statistical similarity with the matched fresh samples in terms of proliferation, LDH release and drug response in agreement with published clinical data, but at lower levels than matched fresh tissue.

3.11.4 siRNA knockdown experiments

3.11.4.1 Selection of target and control genes

Four genes were selected based on a literature review (*AHR*, *RAB21*, *AKT2*, and *PRMT2*). The study of the expression of these genes in U87 cells used in the current study revealed that *RAB21* and *PRMT2* could be suitable targets for gene knockdown experiments. Results also show that *RPLP0* could be the perfect gene to use as control for qPCR which was in line with many other studies (Eissa et al., 2017; Nakayama et al., 2018; Nazet et al., 2019).

3.11.4.2 Gene expression of targeted genes

Gene expression analysis is a powerful tool to reveal the gene response to environmental condition changes of cells and infer these data on organism biology, growth, and survival. Among the wide range of techniques that can decipher molecular changes of cells in response to stimuli, real time quantitative PCR (qPCR) is the most frequently used

technique to quantify gene expression changes due to its efficiency, simplicity, and relatively low cost (Freitas et al., 2019).

Results of this study showed that the expression of *PRMT2* and *RAB21* was increased in the flow system compared to the static by 2.41±0.63 ($P \leq 0.001$) and 2.72±0.51 ($P \leq 0.0001$) fold respectively. These findings are in line with previous studies reporting an increase in gene expression in U87 (Onchuru & Kaltenpoth, 2019; Collins et al., 2021c) and other ovarian cancer spheroids (Dadgar et al., 2020) and cells (Ma et al., 2018a) cultured on a microfluidic chip compared to those cultured in static conditions. In their study (Collins et al., 2021c), showed an increase in *VEGF* and *IL6* in GBM (U87) and breast adenocarcinoma (MCF7) spheroids when cultured in a microfluidic system at a flow rate of 3 µl/min during 72 hours compared to static conditions. Dadgar et al. (2020), used patient derived ovarian cancer spheroids, and demonstrated that the expression of *Ki-67* was significantly higher in the flow system (pressure at 30 Pounds per square inch (PSI)) compared to static in Matrigel. It was reported also that brain microvascular endothelial cells (BMECs) increase their expression of tight junction (ZO-1 and Claudin-5) and adhesion (VE-Cadherin) in the flow system at a flow rate of 1 $\mu l\, min^{-1}$ (0.1 dyne per cm^2 shear stress) compared to static (Xu et al., 2016; Ma et al., 2018).

The current study demonstrates that maintenance on the microfluidic devices enhanced the expression of targeted genes, and it should be possible to conduct further experiments of siRNA gene silencing for both genes, *PRMT2* and *RAB21*.

3.11.4.3 Gene knockdown in 2D model

Silencing experiments in 2D static system showed a statistically significant knockdown for both genes (*PRMT2* and *RAB21*). These data are in line with previous studies which demonstrated successful gene knockdown experiments using siRNA anti- *RAB21* (Ge et al., 2017), and sh-RNA anti-PRMT2 (Dong et al., 2018) in GBM cell lines (U87 and T98G) cultured in 2D monolayer system. Other studies reported a successful siRNA knockdown of *PRMT2* in MCF-7 cells, demonstrating that it plays a pivotal role in cell cycle regulation and carcinogenesis (Oh et al., 2014), and *RAB21* in colorectal cancer cells decreasing the autophagosome/lysosome fusion when cultured in monolayer model (Lauzier et al., 2019).

3.11.4.4 Effect of gene silencing in 2 D culture model on proliferation of U87 cells

In the literature, there is growing evidence of the implication of *PRMT2* gene in the development and pathogenicity of GBM and other cancer types (Raposo & Piller, 2018;

Dong et al., 2018). Additionally, Ge et al., (2017) reported that siRNA mediated downregulation of *RAB21* in GBM cell lines (T98G and U87) inhibits cell growth and induces apoptosis. To validate knockdown experiments, the effect of gene silencing on the proliferation of U87 cells was investigated.

The results of this study did not show any significant decrease in cell proliferation after siRNA knockdown for both genes (*PRMT2* and *RAB21*) compared to control. Experiments were done using different cell densities (3.5×10^3 and 2.5×10^3) to avoid cell clumping and different siRNA concentrations (5 and 25nM). These results differ from earlier studies demonstrating that knockdown of *PRMT2* (Dong, F. et al., 2018) and *RAB21* (Ge et al., 2017) inhibit the cell growth of glioma cell lines (T98G and U87) seeded in monolayer culture (96 well plate). Dong et al., (2018) used MTS proliferation assays to show that the depletion of *PRMT2*, using shRNA, significantly inhibited the cell growth of both GBM cell lines in either colony formation assays in soft agar or monolayer culture at the concentration of 1×10^3 cell/well. Whereas Ge et al., (2017) used a Cell Counting Kit-8 (CCK-8) proliferation assay and demonstrated that the siRNA silencing of *RAB21* significantly inhibited cell proliferation and promoted cell apoptosis in T98G and U87 cell lines in 96-well plates at a concentration of 1×10^4 cell/well. The apparent discrepancy between current and previous findings could be therefore related to technical limitations.

First, shRNA induces long term gene knockdown while siRNA is used for transient (short term) gene silencing which may not affect the protein expression especially for long half-life and stable proteins which keep most of the protein functionality during gene knockdown (in this case *PRMT2*) and correspondingly U87 cell growth would not be altered. On the other hand, the inhibition of cell growth observed after siRNA anti-RAB21 silencing of *RAB21* may be due to the use of CCK-8 assays which was shown to have a detection sensitivity higher than other proliferation assays using tetrazolium salts such as MTT, MTS or WST-1 (Cai et al., 2019). To eliminate the intervention of unknown variables related to reagents during MTS experiments, a positive control was added to MTS assays. In the positive control sample, U87 cells were treated with 200mM of sodium azide.

Therefore, to address the non-observed effect of siRNA silencing on U87 cell growth it would be recommended to either use long term gene silencing or to use proliferation assays more sensitive than ordinary MTS.

Results also showed that protein expression was not affected by the gene knockdown. Again, this finding is not in agreement with Dong et al., (2018) experiments where western blot analysis showed a significant decrease in the protein expression. This differences in results could be explained by the same reasons mentioned in the previous paragraph about MTS assays.

siRNA gene silencing experiments, carried out on U87 spheroids cultured in static conditions in ULA plates, demonstrate a successful gene knockdown. The expression of both genes (*PRMT2* and *RAB21*) was significantly reduced compared to the control. The gene knockdown on U87 spheroids cultured in static conditions, was previously documented in numerous studies targeting different genes (Heuser et al., 2020; Binder et al., 2021) including *PRMT2* (Dong et al., 2018). There is no published data on *RAB21* gene knockdown in tumour spheroids cultured in a static system.

The decrease of gene knockdown level for both genes in U87 cells cultured in 3D static compared to those cultured in 2D monolayer system can be explained by the physiological and biological differences of tumour cells in both settings. In a 2D system all cells are in continuous contact with the medium containing siRNA molecules providing them with unlimited access to the components of the medium including the siRNA molecules (Kapałczyńska et al., 2018). In contrast cells within the spheroid have a decreasing gradient of accessibility from cells around the outer layers to those of the inner layers of the spheroid, the latter being characterised by a necrotic core at the centre as a result of absence of oxygen and nutrient supply (Pinto et al., 2020a). In addition, cells in 3D structure are more reluctant and less permeable to molecules than cells in monolayer culture due to permeability barrier made of cell-cell and cell-matrix interaction (Sant & Johnston, 2017; Białkowska et al., 2020b).

3.11.4.5 siRNA knockdown in a 3D flow system

After validating gene knockdown experiments on U87 cells cultured in 2D monolayer and 3D static system, spheroids were put in the microfluidic device under a flow of medium containing siRNA. Due to study limitations (i.e. the high cost associated with using the amounts of siRNA needed for three trials in each condition in the flow system), only two experiments were carried out. In the first the medium was renewed over three times (48hr, 72hr and 96hr) and in the second there was single perfusion of medium. *PRMT2* and *RAB21* expression was significantly reduced in continuous perfusion conditions whereas only *RAB21* expression was significantly repressed with single perfusion.

Results showed that the siRNA silencing levels are reduced in spheroids cultured in the flow system compared to the 3D static conditions. This could be explained by a decrease in the uptake of siRNA molecules driven by the effect of shear forces in the flow system which may further induce possible intracellular changes that interfere with the action of siRNA on target mRNA molecule. These hypotheses are supported by the fact that spheroids in a flow perfusion system are in a dynamic microenvironment that better reflects the real tissue environment. Spheroids in the microfluidic device are subjected to a continuous mechanical stimulation, such as shear stress and pressure, that can influence cell activity (Ong et al., 2017). The value of Reynold number is low, showing that the medium in the devices is a laminar flow, and would also help explain the very low value of the shear stress (calculated below). This low Re value is a result of the small dimensions of the microfluidic channels as described by (Saliba et al., 2018) and low pump speed.

Calculation of Reynold number (Re)

Reynold number formula: $Re = \rho.u.d/\mu$ (non-dimensional, Freund et al., (2012)) where:

ρ = Density of the medium (kg/m^3) = 1007 kg/m^3 (Poon, 2022)

u = Velocity of the liquid in the channel (m/s) = Calculated below

d = Diameter of the microchannel of the chip (m) = 4 mm = 4×10^{-3} m

μ = Dynamic viscosity (Ns/m^2) = 9.4×10^{-4} Ns/m^2 (Fröhlich et al., 2013)

Calculation of the velocity (u):

Relation between fluid velocity and the flow rate: $Q = A.u$

Q = flow rate (m^3/s) = 2 µl/min = $3.33\ 10^{-11}$ m^3/s

A = Area (m^2) = $\pi\ (d/2)^2 = 1.25 \times 10^{-5}$ m^2

$Q = A.u \rightarrow u = Q / A = 2.6 \times 10^{-6}$ m/s

Reynold number numerical calculation

$Re = 0.5 \times 10^{-2}$

Compared to the physiological conditions where the values of shear stress vary from 10–20 dynes/cm^2 in arteries, and around 1–6 dynes/cm^2 in veins (Roux et al., 2020), the low value found could be due to the large diameter of the channel (4mm) used with a very low

flow rate. These conditions could provide a suitable microenvironment for the spheroids and prevent them of possible change in the shape or even dissociation as a result of higher shear stress as described previously by Qiu et al., (2018). Accordingly, Trevisan et al., (2021) demonstrated that human placental cells exhibited changes in shape when cultured in a flow system with a shear stress of 0.05 dyne/cm^2 for 24hr, and even changes in morphology with 0.5 dyne/cm^2.

Calculation of shear stress (τ)

$\tau = 32\ \mu\ Q/\ \pi\ d^3 = (32 \times 0.94 \times 10^{-3} \times 3.33 \times 10^{-11}\ m^3/s)/\ \pi \times (4x10^{-3}m)^3$

$= 4.9\ 10^{-6}\ N/m^2 = 4.9\ 10^{-5}$ dyne/cm^2

τ = Shear Stress (N/m^2)

μ = viscosity of the medium (DMEM with 10% FBS)

$= 0.94$ cP $= 9.4x10^{-4}$ N.s/m^2 (Fröhlich et al., 2013)

(1 cP = 0.001 Ns/m^2)

Q= flow rate = 2µl/min = $3.33\ 10^{-11}$ m^3/s

d= diameter of the microchannel of the chip = 4mm = $4.0\ x10^{-3}$m

Another hypothesis suggested that the decrease of the uptake of siRNA molecules by the spheroid in the microfluidic setup could be the result of an increase of siRNA chemoresistance induced by the shear stress in the same way as it was previously described for other molecules in similar conditions.

In support of the idea that the 3D flow environment enhances spheroid resistance, compared with static culture, (Ruppen et al., 2014) demonstrated an increase of chemoresistance of malignant pleural mesothelioma (MPM) spheroids to cisplatin when continuously perfused, compared to static conditions for 48 hours. This increase was explained by the continuous support of nutrients and oxygen to the perfused spheroids. Additionally, in their study (Ip et al., 2016a) demonstrated that ovarian cancer spheroids under fluid shear stress exhibited an increased resistance to clinically relevant doses of chemotherapeutic drugs cisplatin and paclitaxel compared to those grown in static conditions.

Interestingly, U87 cells were listed from Invitrogen to be among a list of cells refractory to siRNA knockdown using conventional methods such as lipid-based transfection. Thus, it was suggested to use Accell siRNA instead. This agent is a chemically-modified siRNA molecule that can better cross the plasma membrane without the use of delivery agent.

3.12 Conclusion

In conclusion, *PRMT2* and *RAB21* are relevant genes to carry out knockdown experiments as they play a key role in oncogenic processes in GBM and were expressed in the U87 Hull cell line. This study shows successful, but gradual gene silencing in 2D, 3D static and 3D flow systems. This could be related to a gradual decrease of the siRNA uptake from 2D to 3D and more in 3D flow system in a similar way of resistance of cells when cultured in different systems and *in vivo* tissues against different anti-tumour drugs.

The microfluidic device used in this study enables a constant supply of oxygen and nutrients and continuous waste removal from spheroids, providing maintenance conditions that resulted in an increase in gene expression of *PRMT2* and *RAB21* genes when compared with statically grown spheroids. In addition, the tested flow system enables a successful knockdown experiment of both targeted genes. However, the gene knockdown level was not complete and further work is required to improve the uptake of siRNA molecules by U87 cells. This could be done by increasing the permeability of the spheroid, so that cells within the mass were in contact with sufficient siRNA, and/or using another delivery system that penetrates the cells better than Dharmafect reagent such as electroporation which was shown to be 7 to 10-fold more efficient (Sharifi et al., 2015) or without the use of delivery system such as Accell siRNA technology (Taniguchi et al., 2020).

Chapter 4

Accell siRNA knockdown in U87 spheroids cultured in a flow system

4.1 Introduction

Accell siRNA is reported to be a unique solution for achieving robust silencing of a target gene in many neuronal and primary cell lines (including U87 cell line) as well as tissue, which have proven refractory to traditional methods of mediating siRNA gene silencing (lipid, viral or electroporation method, Zaklina & Yamada, (2018)). As a chemically modified siRNA, Accell siRNA has been demonstrated to significantly improve stability and efficiency of RNAi gene silencing. This technology allows a passive delivery of siRNA molecules without the need of a specific transfection reagent which limits any toxicity effects related to viral and lipid products. Since the first design of Accell siRNA (Reynolds et al., 2004), this technology has enabled successful, long-term, gene silencing in many organs, tissues and cells (Bonifazi et al., 2010; Nakajima et al., 2012; Freeley et al., 2015b). Recently, (Osborn et al., 2018) reported a successful mRNA mediated silencing of the cyclophilin B (*PPIB*) gene and protein in GBM8 spheroids *in vitro* and *in vivo* in established orthotopic brain tumours using Accell siRNA.

Despite the potential advantages of Accell siRNA to improve the efficiency of gene knockdown in these cell types one of the disadvantages is the significantly higher cost compared to traditional knockdown techniques. In addition, the Accell siRNA protocol states that cells need to be maintained in media containing the Accell siRNA for up to 72 hours. This property means a lot of Accell siRNA is needed for a microfluidic knockdown compared to static culture. Therefore, a number of small experiments were run to understand the optimal growth and knockdown conditions required for potential future larger scale use of the technology. Due to the cost of reagents and limited time constraints (in part a knock-on effect of the Covid pandemic) multiple repeats of experiments were not always possible. This work highlights a new and cutting-edge option in terms of transient gene knockdown, but the discussion of the data is acknowledged as being preliminary.

The aim was to determine if siRNA mediated knockdown could be enhanced using Accell siRNA technology in static and flow culture using U87 spheroids.

4.2 Accell siRNA knockdown

4.2.1 FUS gene expression in U87 spheroids

Different anti-PRMT2 and anti-RAB21 antibodies bought from 3 different companies were tested in western blot without showing any protein detection. In contrast anti-FUS antibodies positively detected the protein when used in western blots of U87 and U251 cell lines (Yang et al., 2020). The FUS protein interacts with BACH2 to promote cancer progression of glioma cells (Yang et al., 2020). Therefore, FUS was utilised as a target for Accell siRNA knockdown experiments using the Hull microfluidic platform.

Before starting knockdown experiments in 3D settings, it was necessary to check the expression of the *FUS* gene, in a similar way to that done previous for *PRMT2* and *RAB21* to confirm the work of Yang et al. (2020). Therefore, three pairs of primers (**section 2.8**) were tested in qPCR experiments, to study *FUS* expression in U87 spheroids cultured in static conditions (ULA plates) for 72 hours. The 3 pairs of primers showed similar results of *Fus* expression (**Figure 4.1**).

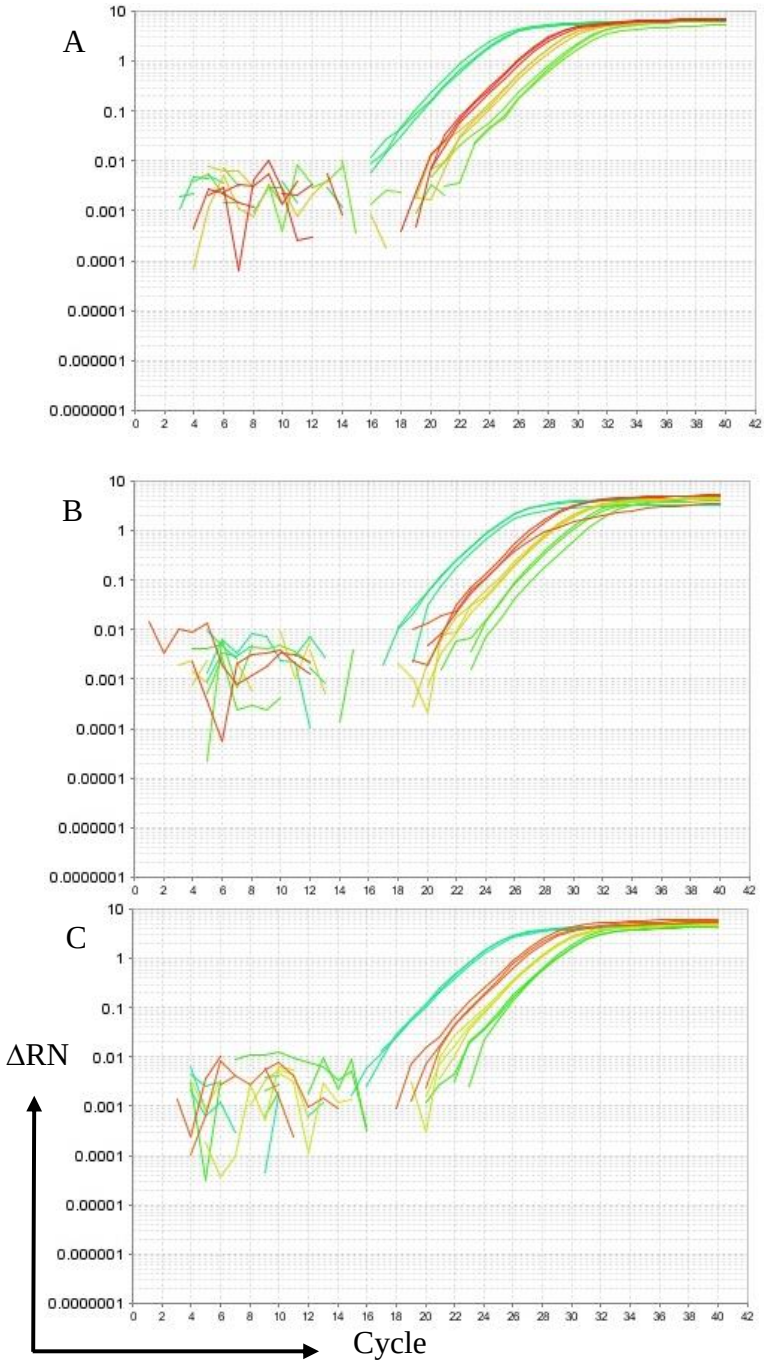

Figure 4.1 Amplification plot of the qPCR data of FUS gene expression in U87 cell line using three set of primers

Y-axis is for the ΔRn (delta Rn): fluorescence signal while x-axis is for the cycle number, A) primers set 1 B) primers set 2.C) primers set 3. Colours in the plot correspond to different dilutions of the sample: red 1:10, yellow 1:20, green 1:50, blue not diluted.

4.2.2 Comparison of *FUS* expression between U87 spheroids cultured under flow vs static conditions

Prior to silencing experiments in the flow system, it was also necessary to show the expression of *FUS* gene in spheroids cultured in the flow system. A comparison of *FUS* expression between U87 spheroids cultured for 3 and 7 days, in 3D static versus flow system, was performed. Results shown in **Figure 4.2**, indicate that the *FUS* gene expression cultured in the flow system was significantly higher after 3 days (2.6±0.48 fold change $p \leq 0.001$) than after 7 days (1.52±0.09 fold change $p \geq 0.05$), compared to the expression in statically-cultured spheroids. Subsequent knockdown experiments were done on spheroids cultured for 3 days in the flow system which is the time needed to see the silencing effect of Accell siRNA.

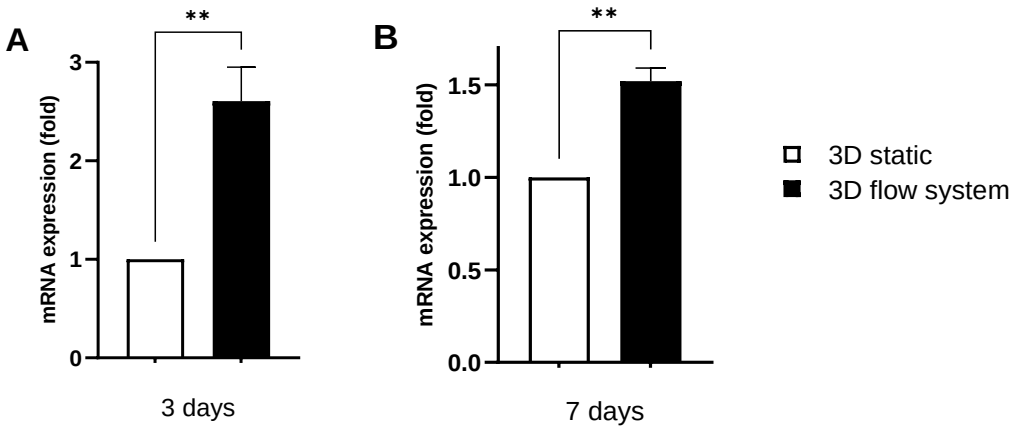

Figure 4.2 The FUS gene expression in U87 cells cultured in static and a flowing system

*Spheroids (n=12, 3/chip) were cultured for 3 days (A) and 7 days (B). Data are presented as a mean fold change of relative gene expression compared to control. mRNA expression was normalised to RPLP0 and then standardised to the mRNA expression in 3D static culture model. Values shown are the mean ±SEM of n=3, ns: not significant, **P≤0.01, and ***P ≤ 0.001 vs. expression of corresponding gene in 3D culture model (as analysed by one way ANOVA test).*

4.2.3 Accell siRNA gene knockdown in U87 spheroids cultured in static conditions

It was recommended from the manufacturer to use 1µM of Accell siRNA solution to achieve successful knockdown of target genes. After doing the calculation it was found that an unaffordable amount of Accell siRNA would be needed to do the experiments in the microfluidic system (the amount needed for 12hr in the microfluidic chip using only 2 syringes is 16µl/experiment of a solution of 100µM of Accell siFUS from the total amount of 50µl of a solution stock of 100 µM). For 2 trials in the flow system (72hr) using 2 syringes

the cost will be about £3200. Therefore, an optimisation experiment was performed to determine the minimal concentration of Accell siRNA that still caused effective gene knockdown. For this, Accell siFUS knockdown experiments were done on U87 spheroids in 3D static culture and *FUS* expression was compared to spheroids transfected with a non-silencing control (Accell siSCR).

As it was recommended less than 2.5% of FBS should be used in the culture medium for optimal knockdown. As it was described previously the internalisation of Accell siSRNA is done 6 hours after transfection (Healey et al., 2014). To check the effect of FBS on Accell siRNA activity FBS was added at 0hr and 6hr post-transfection of spheroids in 3D static system. Results (**Figure 4.3**) demonstrate that FBS added at 0hr post-transfection may inhibit the knockdown effect of Accell siFUS, as there was no silencing effect seen with this condition. In addition, a successful *FUS* gene knockdown was seen after adding FBS at 2.5% (**Figure 4.3).**

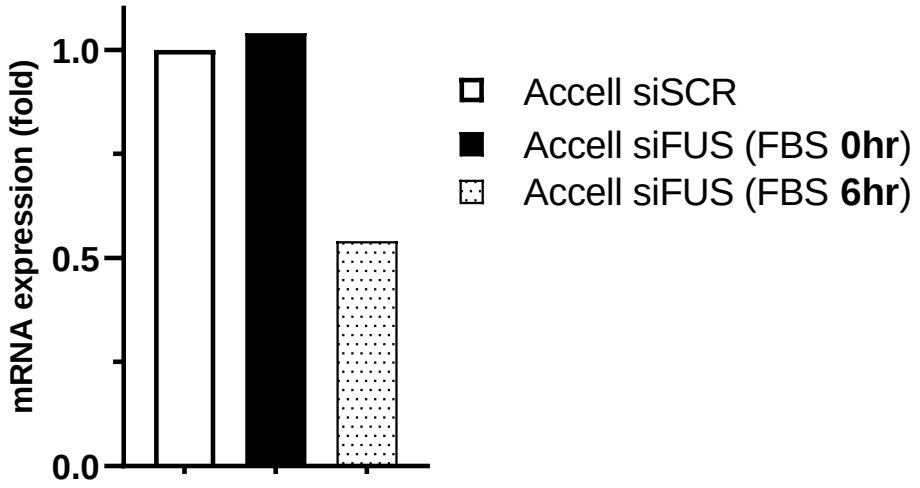

Figure 4.3 FUS gene expression fold change and knockdown levels in U87 spheroids
Spheroids (n=6) were cultured in 3D system with 2.5% FBS added at 0hr and 6hr post-transfection using 1µM of Accell siFUS. *Values shown for one trial. mRNA expression was normalised to RPLP0 and then standardised to the mRNA expression in cells treated with Accell siSCR in the same conditions in each experiment.*

To optimise the minimal concentration of Accell siRNA able to induce gene silencing, a series of concentrations (1, 0.5, 0.25, and 0.125µM) of Accell siFUS were tested, with 1% FBS added 6hr post-transfection of spheroids (n=6). The concentration of FBS was

reduced to 1% to minimise possible interference with the Accell siRNA. Results of the gene expression fold change compared to spheroids transfected with Accell siSCR (**Figure 4.4),** show that 1 and 0.5µM are equally effective concentrations for silencing experiments with Accell siFUS.

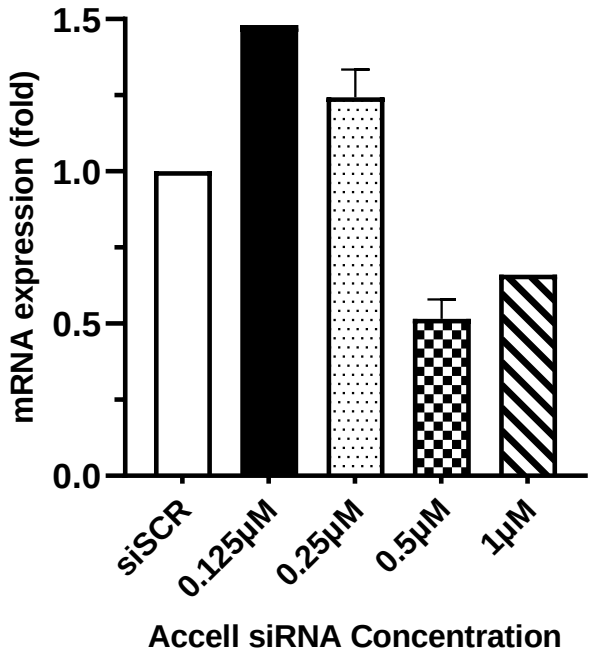

Figure 4.4 FUS gene expression fold change and knockdown levels in U87 spheroids
Spheroids (n=6) were cultured in 3D system with 1% FBS added at 6hr post-transfection with different concentrations of Accell siFUS. Values shown are the mean ±SEM of (n =1 for 0.125µM, n=3 for 0.25µM, n=2 for 0.5µM and n=1 for 1µM). mRNA expression was normalised to RPLP0 and then standardised to the mRNA expression in cells treated with Accell siSCR in the same conditions in each experiment.

4.2.4 Accell siFUS gene knockdown effect on FUS protein expression in static system

To validate the Accell siFUS gene knockdown results on the protein level, western blot analysis was done on lysates of U87 spheroids maintained in static system (with 1% of FBS added to the medium after 6hr of transfection) and transfected with 0.5µM of Accell siFUS. Western blot results (**Figure 4.5**) show that there appears to be FUS protein knockdown of 29.71±0.03% using the Accell siRNA. The expected band of FUS at 53KDa obtained with Accell siFUS, is less intense (**Figure 4.5**) compared to the one obtained with Accell siSCR. Other bands in the membrane seems to be non-specific.

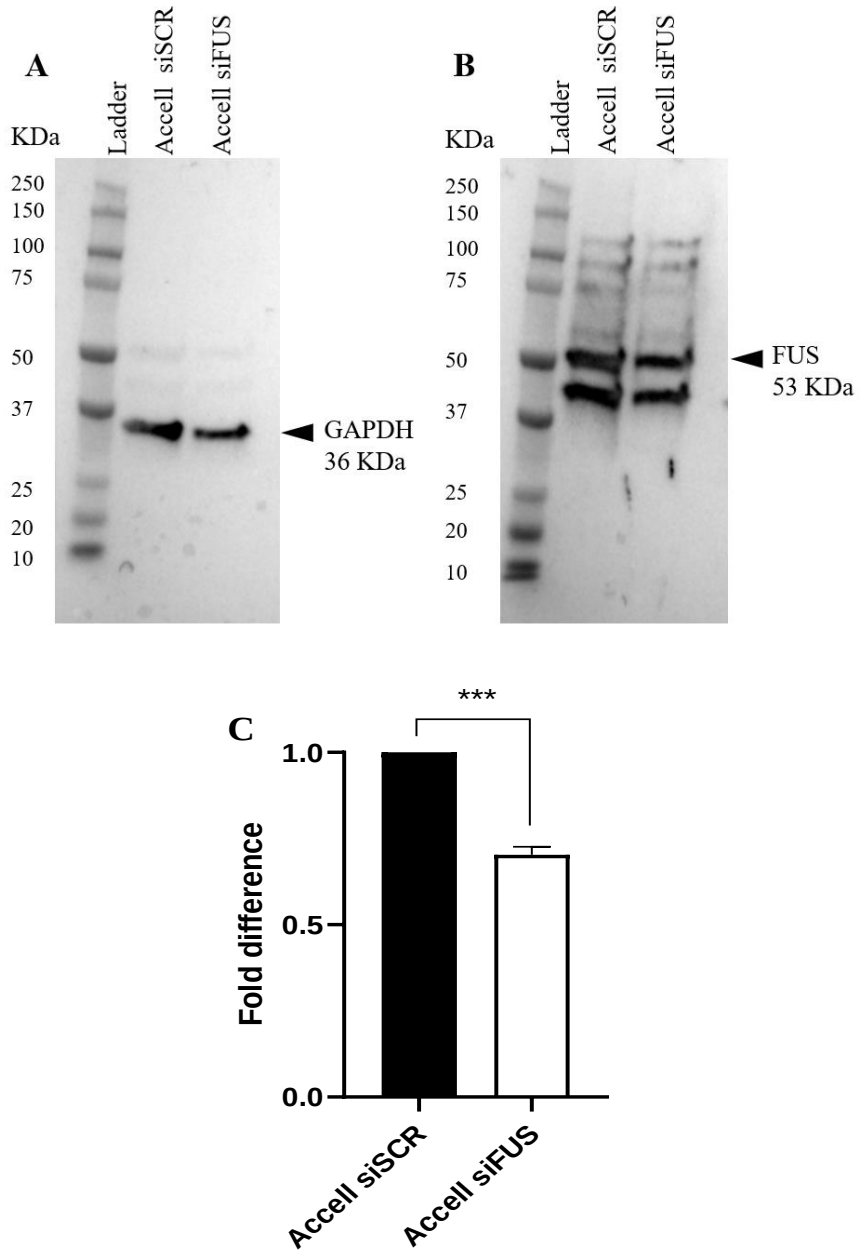

Figure 4.5 Western blot analysis and FUS protein quantification after Accell siRNA knockdown (0.5µM) in U87 cells cultured in 3D system with 1% of FBS added after 6hr post-transfection

The protein level of FUS after transfections with siFUS was compared with the expression in cells treated with scrambled (siSCR) by normalising to the expression of GAPDH. A and B: representative images of western blot analysis using anti-GAPDH (A) and anti-FUS (B) antibodies. The gel was incubated first with antibody anti-GAPDH, which could explain the faint FUS bands. C) Statistical analysis of densitometry analysis (n=2). Data were normally distributed according to D'Agostino & Pearson and Shapiro-Wilk normality tests. Statistical significance was assessed using unpaired T test. ns: not significant.

4.3 Accell siRNA knockdown in U87 spheroids cultured under starved conditions

4.3.1 Study of the spheroid size when cultured with starved conditions

From previous observations, it was noticed that FBS may inhibit the action of Accell siFUS. There was no effect with 2.5% of FBS added at 0hr post-transfection. In contrast a silencing effect was observed if FBS was added at 6hr post-transfection using the same concentration (2.5%) or even lesser (1%). Therefore, it was decided to try to do knockdown experiments in starved conditions, to see if FBS-free conditions would be more beneficial in enhancing gene knockdown.

To study the effect of starved conditions on the growth of U87 spheroids cultured in static system for 72 hours, a comparison was done between the size of spheroids grown under starved conditions and those with full medium (10% (v/v) FBS). The size of spheroids was determined using ImageJ Fiji software and results are shown in **Figure 4.6**. Results show that spheroids with full medium are larger than the spheroids cultured in starved conditions, but not statistically different. It was noticeable that the size of spheroids shrinks at 48hr then increases again at 72hr whichever media they are grown in. Therefore, future experiments were carried out on U87 spheroids cultured under starved conditions, as this provided the optimal conditions for Accell siRNA silencing.

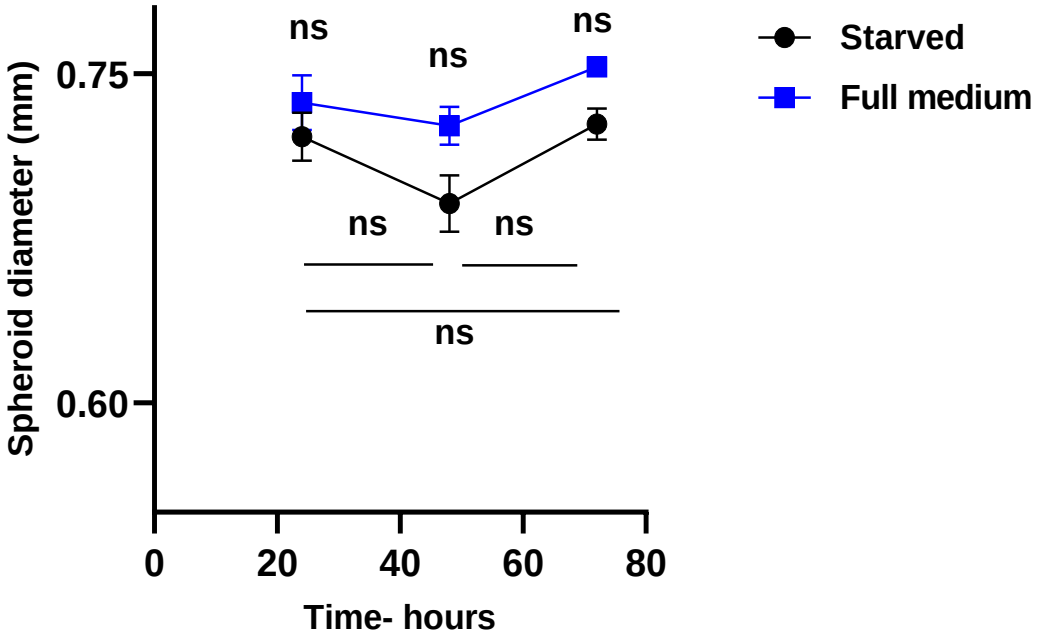

Figure 4.6 Effect of starved conditions on the growth of U87 spheroids cultured in static system for 72 hours (6 spheroids)

U87 cells were cultured in ULA plates (2 x 10^4cell/well) and grown in two different conditions. One without FBS (starved conditions) and the other with 10% (v/v) FBS added to the medium (full medium). Values were determined at 24, 48 and 72 hours (n=2 trials). The size was measured using GelCount machine and Imagej FIJI software. Standard error of the mean is indicated as bars in the figure. Normal distribution was investigated using D'Agostino & Pearson and Shapiro-Wilk normality tests. Difference significance was determined using one-way ANOVA test. ns: not significant.

4.3.2 FUS gene expression in spheroids cultured under starved conditions in static system

Before doing knockdown experiments, it was necessary to check *FUS* gene expression in spheroids cultured under starved conditions for 72 hours. For this, U87 spheroids were grown in a static system with starved conditions, and the *FUS* gene expression was assessed at 24, 48 and 72hr by qPCR and compared to the gene expression at 0hr (**Figure 4.7)**. Results show that *FUS* gene is highly expressed in starved conditions. It is interesting to notice that the gene expression in starved conditions is repressed at 48hr (compared to 24hr) then it increases to reach higher values than those at the start of the experiment.

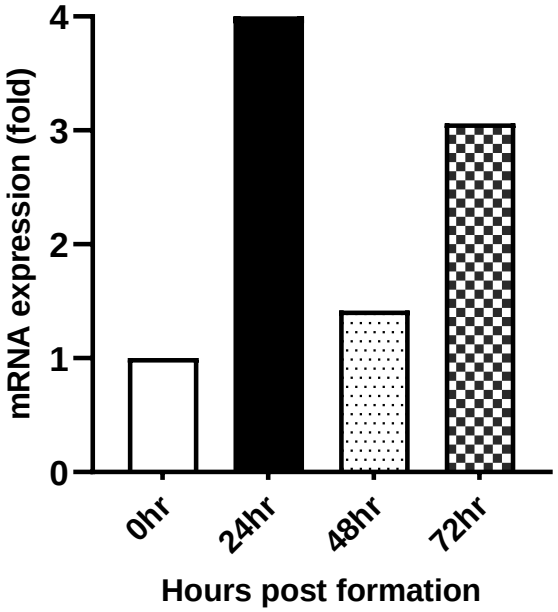

Figure 4.7 Fold change of FUS gene expression in U87 spheroids (n=6 spheroids) cultured in starved conditions compared to full medium
Values were normalised to the samples collected at 0hr. No statistics were done as there was only one trial for each experiment.

4.3.3 Accell siRNA knockdown in U87 spheroids cultured in static system with starved conditions

The next step was to validate the gene knockdown experiments in a static system, as static conditions are easily handled and consume less reagent. For this, U87 spheroids (n=6) were formed and maintained in ULA plates where they were transfected with Accell siFUS or Accell siSCR. Results of fold change in gene expression after gene knockdown using different concentrations of Accell siFUS (1 and 0.5µM) are summarised in **Figure 4.8**. These results show an efficient *FUS* gene knockdown for both concentrations of Accell siRNA in U87 spheroids cultured in static system with starved conditions.

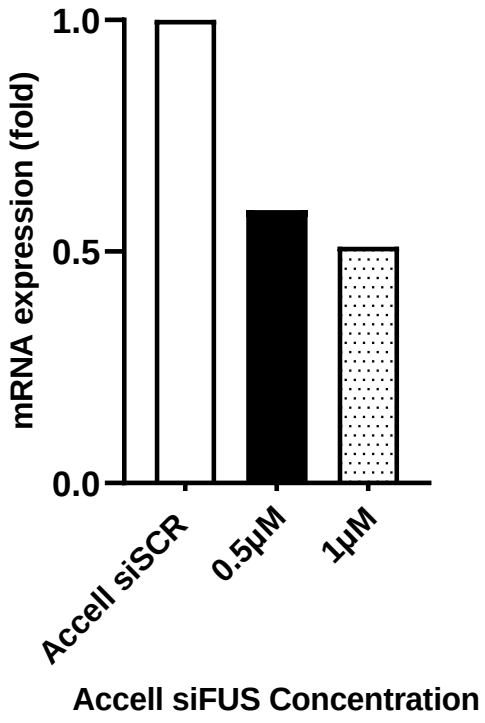

Figure 4.8 FUS gene expression fold change and knockdown levels in U87 spheroids
Spheroids (n=6) were cultured in FBS-free 3D system and transfected with different concentrations of Accell siFUS. Only one trial was done for each experiment. mRNA expression was normalised to RPLP0 and then standardised to the mRNA expression in cells treated with Accell siSCR in the same conditions in each experiment, hence no error bars could be added.

4.3.4 Accell siRNA knockdown in U87 spheroids cultured in flow system with starved conditions

During this experiment 4 syringes (2 for the Accell siSCR and 2 for Accell siFUS) were used for 4 chips. In this experiment 5 spheroids/device were used instead of 3 (in previous experiments with siRNA in **chapter 3**) to get a sufficient yield of RNA for the qPCR experiments. U87 spheroids were introduced to the chip then transfected with 0.5µM of Accell siRNA. The effluent was collected every 12 hours and reintroduced in the flow medium and gene expression was measured 72hr post transfection **Figure 4.9**. During the first experiment, one of the two syringes supplying Accell siFUS was blocked, and the flow stopped. The amount of extracted RNA was only 200ng. Then, during the second repeat, the same problem happened with the syringe supplying Accell siSCR. Therefore, it was not possible to compare against across the 2 experiments because the reverse transcription of Accell siSCR sample was not successful, the normalisation of the second sample transfected by Accell siFus was done versus the control of the first repeat.

Results showed that there was no knockdown effect of Accell siFUS on *FUS* gene in the flow system. In contrast, the gene expression increased by more than 2 fold (2.12±0.59 fold change) compared to the control.

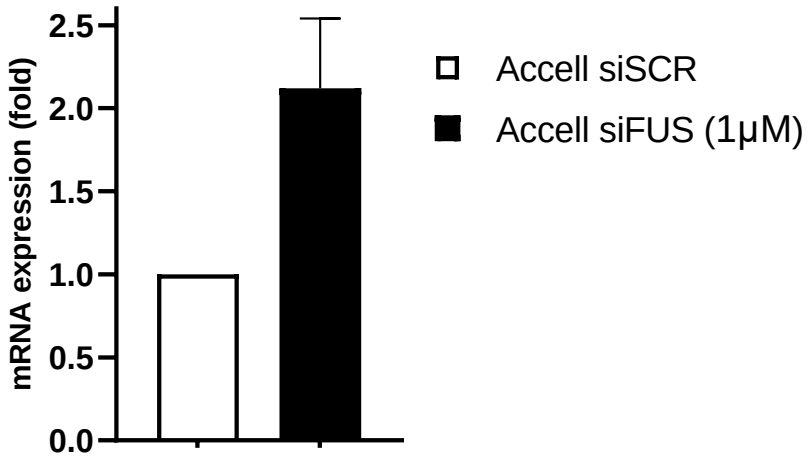

Figure 4.9 FUS gene expression fold change in U87 spheroids
Spheroids (n=6) were cultured in FBS-free 3D flow system and transfected with Accell siFUS (1µM). mRNA expression was normalised to RPLP0 and then standardised to the mRNA expression in cells treated with Accell siSCR in the same conditions in each experiment. Data are presented as the mean fold change of relative mRNA expression compared to control. Values shown are the mean ±SEM of n = 2.

4.4 Discussion

Despite the wide range and extensive use of siRNA technology in mediating specific gene silencing, it has some drawbacks that limit its effect of inducing RNA interference. These limitations can be grouped into two main categories. The first one involves the nature of transfected cells, as numerous cell lines are found to be refractory to traditional delivery methods of siRNA such as viral, lipid-mediated delivery or electroporation (Amarzguioui, 2004; Matsuda & Cepko, 2004; Kilroy et al., 2009; Wei et al., 2014; Zaklina & Yamada, 2018). The second reason is related to the siRNA molecule itself. Despite the improved uptake of siRNA in cells by different delivery methods, most of the internalised siRNA undergoes exocytosis (Sahay et al., 2013; Rietz et al., 2020; Malik et al., 2021). Additionally, it has been reported that naked siRNA molecules suffer from low stability and poor pharmacokinetic behaviour with possibility of degradation inside the cell by different nucleases or phosphatases.

Therefore, to improve knockdown efficiency in U87 cells it was decided to search for another delivery method of siRNA molecules independent of lipid-based transfection reagents. Accell siRNA technology has been shown to be effective in mediating gene silencing in cells that have been identified as difficult-to-transfect by traditional methods (Lopez-Castejon et al., 2013; Freeley et al., 2015a; Zaklina & Yamada, 2018). Accell siRNA is a proprietary formulation in which siRNAs have undergone chemical modification to facilitate cell uptake without the need of a transfection reagent (Freeley et al., 2015b).

4.4.1 FUS gene expression in U87 spheroids

FUS gene encodes for a protein that belongs to the family of RNA-binding proteins involved in gene expression and mRNA processing. Recently Yang et al., (2020) demonstrated that *FUS* is expressed in U87 and U251 cells and that it promotes malignant progression of glioma cells through the interaction with the BTB and CNC homolog 2 (*BACH2*) gene. Work in this thesis confirmed that the *FUS* gene was expressed in Hull's U87 cell population.

The current study showed that FUS gene expression varies under flow conditions. These observations could be explained by the effect of shear stress on the U87 spheroids in the microfluidic system, which induced an increase of *FUS* expression after 3 days. In contrast, after a prolonged exposure to shear stress of 7 days *FUS* expression is repressed significantly. Similar observations were reported previously, where endothelin-1 (*ET-1*)

expression was increased in human retinal microvascular endothelial cells (HRMECs) when exposed to low level of laminar shear stress (1.5 dyne/cm^2) and repressed at higher and prolonged shear stress (60 dyne/cm^2 for 6 hours or more) (Ishibazawa et al., 2011). Furthermore, human umbilical vein endothelial cells (HUVEC) exposed to shear stress in a flow system show that the gene expression profile of up and down-regulated genes is changing with the exposure time to shear stress in the microfluidic device Roman (Tsaryk et al., 2022). Also, it was shown from previous experiments in this thesis (**Figure 3.10**) that the microfluidic platform used induced a significant increase in the expression of *PRMT2* and *RAB21* in U87 spheroids maintained for 7 days compared to static conditions.

4.4.2 Accell siRNA knockdown experiments

Accell siFUS gene silencing experiments in spheroids cultured in static conditions (using 0.5µM of Accell siRNA and 1% FBS, added 6hr post-transfection) were successful at both, the gene (49±0.09%) and protein (49±11.34%) level. No previous studies have been reported utilising Accell siRNA gene silencing using U87 spheroid model. However, there are previous studies reporting successful Accell siRNA mediated gene knockdown on spheroid models using other cell lines, such as JAr cells (a trophoblast cell line (Montazeri et al., 2016); salivary gland-resident stem cells (Shin et al., 2018); colon cancer stem cells (Regan et al., 2017; Regan et al., 2021); and brain tissues (Taniguchi et al., 2020).

The absence of Accell siRNA knockdown effect when adding FBS at 0hr post transfection is most likely explained by the degradation of siRNA molecules by nucleases existing in the serum, as described previously by (Barnaby et al., 2014). Additionally, it was demonstrated that 6hr is the time needed for the internalisation of siRNA molecules into cells after transfection (Dong et al., 2020), which could explain the knockdown seen in experiments where FBS is added 6hr post-transfection, providing growth supplements to the U87 cells after Accell siRNA has been taken up.

Therefore, it was important to test knockdown experiments in starved (FBS-free) conditions to see if this further increased knockdown efficiency. Results of experiments in starved conditions showed a successful reduction of *FUS* expression in 3D static but not in the flowing system. The absence of silencing effect in the flow system could be the result of the increase in *FUS* expression in starved conditions coupled with further increase in expression in flow versus static culture. Therefore, in future work it is recommended to use higher concentrations of Accell siRNA to investigate any knockdown effect. Another hypothesis that may explain the absence of knockdown, is the possible influence of an

increase in shear stress when putting 5 spheroids/chip instead of 3 (in experiments with siRNA). It was demonstrated previously that the increase of shear stress in the flow system may induce changes in metabolism of cells within spheroids (Decarli et al., 2021).

In conclusion, Accell siRNA seems to be effective in inducing gene silencing in U87 spheroids maintained in static conditions in both low FBS (1%) and FBS-free medium. Accell siRNA knockdown effect on U87 spheroids in the flow system needs more investigation and more trials which could not be done in this study due to time and cost limitations. Despite the knockdown at the protein level in static conditions, further experiments are required to better assess the knockdown levels in 3D flow system compared to the use of lipid-based siRNA gene silencing. One suggestoipn is to use higher concentrations of Accell siRNA as the *FUS* gene expression was enhanced in the microfluidic system compared to the static one (2.6±0.48 fold change).

Chapter 5.

Whole transcriptome comparison of GBM spheroids cultured statically and in a flowing system

5.1 Introduction

Data from the previous chapter showed evidence of differences in biological characteristics and functions of spheroids cultured in a 3D flow system compared with those cultured as static spheroids. Previous results demonstrated that when spheroids were cultured in the flow system RNA yield was increased by 2.85±1.78-fold, and *PRMT2* and *RAB21* gene expression was augmented by 2.41±0.63 and 2.72±0.51-fold respectively. On the other hand, siRNA gene knockdown experiments showed significant differences between the two environments, which could be due to the mechanical forces (shear stress) in the flow system or to a specific reaction of U87 cells in the 3D flow system. These data demonstrate clearly that the microfluidic microenvironment influences the activity of U87 spheroids. To get a deeper insight into the changes in gene expression induced by the transfer of the spheroids to the flow system, a comparison of the whole transcriptome was carried out between U87 spheroids cultured for 7 days in 3D static (in the ULA plate) and 3D flowing systems (in the microfluidic device). To ensure that these findings were not an artefact specific to the U87 cell line, two additional GBM cell lines were also analysed (GBM58 termed G58, and GBM63 termed G63 cultured in both systems for 3 days). U87 are an established GBM cell line whereas GBM58 and 63 are primary, patient-derived, cell lines (PDCs) under 11 passages for G58 and 7 for G63. Repeats were generated for each cell line in each condition for analysis.

Total RNA was extracted and analysed using NGS to give the transcriptomic profile of the cells in the two different growth conditions. Data obtained were analysed using bioinformatic tools to identify differentially expressed genes (DEGs) comparing between different conditions and different cell lines. Gene Ontology (GO) annotation analysis, Gene Set Enrichment Analysis (GSEA) and Kyoto Encyclopaedia of Genes and Genomes (KEGG) pathway enrichment analysis were done to identify differences in expression of genes associated with different pathways and biological processes in the two culture systems. The aim of these experiments was to identify pathways/processes activated or repressed by microfluidic culture.

Acknowledgement: Library construction, sequencing experiments and bioinformatics analysis was done by Novogene.

5.2 RNA-sequencing workflow and analysis pipeline

5.2.1 RNA-sequencing workflow

RNA sequencing was carried out using the Illumina Illumina Novaseq 6000, based on the mechanism of sequencing by synthesis (SBS) for measuring RNA transcriptional activity (Wang et al., 2009). The different steps of the sequencing project are shown in **Figure 5.1**. After RNA extraction, samples underwent quality control (QC) to check RNA purity and suitability for the sequencing. High quality, contaminant-free, RNA is essential for obtaining accurate NGS data. For acceptable RNA purity the ratio A260/A280, as measured by Nanodrop, should be in the range of 1.8 to 2.0 and the concentration of RNA should be > 500 ng in a 20-100 µL for library preparation.

Library preparation for whole transcriptome analysis intended to study the gene expression, starts with mRNA enrichment or rRNA depletion from total RNA, where rRNA and potentially other non-coding RNAs were removed from the total RNA. In a second step to reduce rRNA, enriched mRNAs were eluted from magnetic beads containing poly T oligonucleotides which specifically binds to messenger RNAs. Eluted mRNAs underwent a reverse transcription reaction where RNA was converted to cDNA followed by the addition of adapters by ligation to be able to perform PCR amplification reactions.

Once ready, the libraries were loaded on to the Illumina sequencing instrument to undergo SBS. Every cDNA fragment was read in 2 steps, after reading the forward strand (read 1) the process was repeated for the reverse strand (read 2). After the sequencing process was finished, the instrument software automatically identified nucleotides in a process called “base calling” to control the quality and accuracy of reads. At the end, the bioinformatic analysis was carried out on all “clean reads” to study different aspects of gene expression profiling.

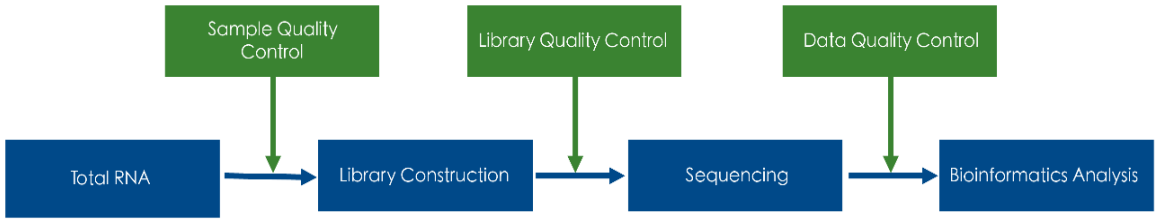

Figure 5.1 RNA sequencing projects were carried out as follows
After RNA extraction, a QC of purity and concentration of the RNA samples was done. cDNA produced by reverse transcription was used to construct a library by adding adapters making them ready for sequencing. The sequencing reads will undergo a further QC round and clean reads will be used for further bioinformatic analysis. Figure provided by Novogene.

5.2.2 Analysis Pipeline

Once the raw data of the RNA sequencing process was ready, they were automatically filtered through the QC analysis. Data QC included the sequencing error rate of each base and the GC content of reads where the sequences with error rate of a single base more than 1% are not considered for future analysis (Petrackova et al., 2019). The first step of the bioinformatic analysis was the alignment of the sequence reads to a human reference genome, version 38 (hg38), generating data including matches, mismatches, gaps and identification of a range of genetic alterations, including single nucleotide mutations, insertions and deletions (indels), and specific tumour genetic alterations (Roy et al., 2016). These metadata were then used for downstream bioinformatic analysis which involved gene expression quantification, and genome annotation through multiple online genomic databases to extract meaningful information concerning functional impact, correlation analysis and clinical significance (Roy et al., 2018; Joo et al., 2019). The workflow of the mRNA sequencing data and the standard bioinformatic analysis with a well-annotated reference genome are summarized as follows (**Figure 5.2**).

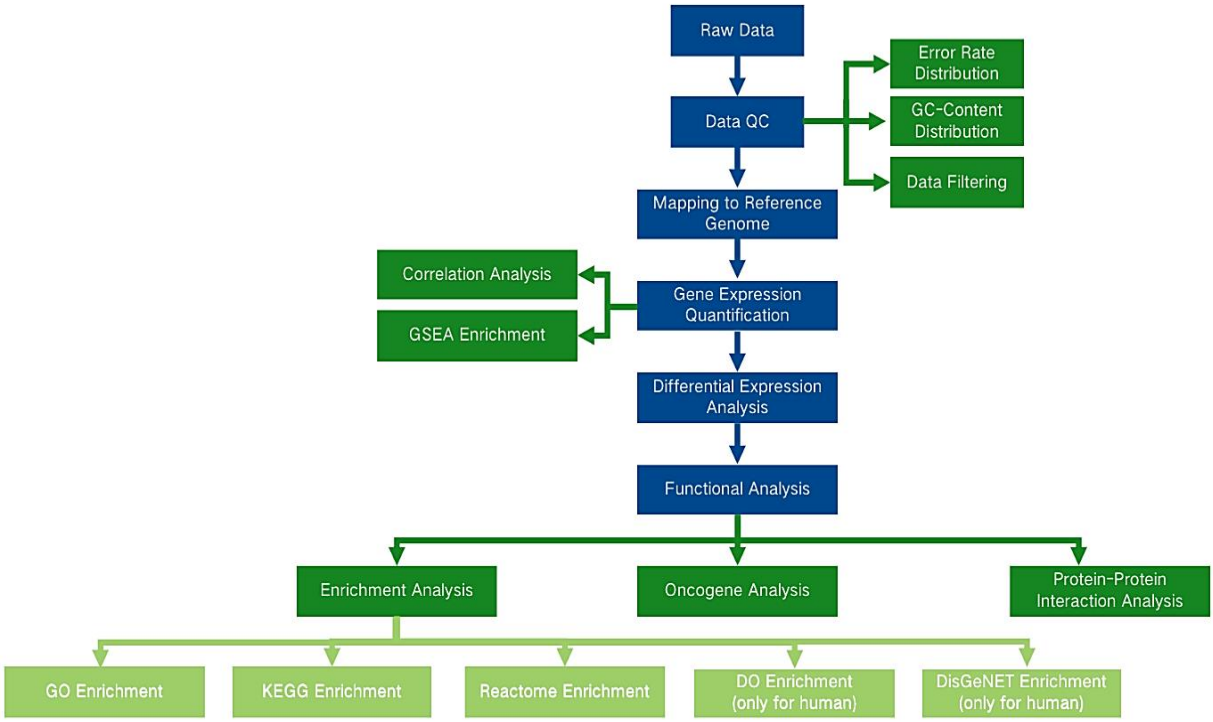

Figure 5.2 RNA-seq information analysis technology flow
The workflow starts with QC analysis to determine clean reads suitable for downstream bioinformatic analysis. cDNA sequences are mapped to human sequence of reference and data of correlation, gene function and integrated pathways involved are determined using online genomic data. Figure provided by Novogene.

5.3 Quality Control results

5.3.1 RNA QC

The transcriptome sequencing project started with the RNA extraction from cultured spheroids. As recommended in the previous section the RNA was of sufficient quality (1.8≤ A260/A280 ≤2) and the concentration was suitable for a successful sequencing project (> 500 ng in a 20-100 µL) for all samples (**Table 5.1**).

Table 5.1 RNA purity and concentration of samples from different GBM cell lines using the Nanodrop.

		3D static		3D flow system	
Cell line	**Sample**	**RNA concentration (ng/µl)**	**RNA purity (A260/A280)**	**RNA concentration (ng/µl)**	**RNA purity (A260/A280)**
U87	1	343	1.92	1645	2
	2	522	1.95	667	1.97
	3	586	1.92	1454	1.96
GBM 58	1	162	1.82	156	1.83
	2	297	1.79	71	1.74
	3	315	1.8	253	1.87
GBM 63	1	539	1.85	80.7	1.72
	2	202	1.86	60	1.77
	3	218	1.83	124	1.76

*For values of A260/A280 <1.8, samples were re-checked by Novogene and passed the quality control test (see **appendix 2**).*

5.3.2 Library QC

5.3.2.1 Sequencing data error rate distribution

Library QC check include error rate distribution along reads, GC content and reads quality filtering. Following sequencing, the error rate of all reads was approximately 0.029±0.002% (**Table 5.2)**. Sequencing error rate depends on sequencers, reagent residues, and different sample types. Error rate increases towards the end of the sequencing read, due to the accumulation of vestiges (scars) in Illumina sequencing. Scars are the result of remaining extra chemical molecules on purine and pyrimidine bases after the cleavage of the linker group that carries the fluorophore (Chen et al., 2013; Schirmer et al., 2016). Accumulation of scars during the sequencing process impairs the stability of the DNA double helix and consequently hampers substrate recognition and the extension of primers (Chen et al., 2013). Successfully sequenced reads should have a single base error rate lower than 1% (Erlich et al., 2008; Jiang et al., 2011). The error rate distribution profile along reads of all samples was similar, and an example of it is shown in **Figure 5.3.** Full sequencing data error rate distribution for all samples can be found in **Appendix 1**.

The name of samples appears as: Cell line name_culture system_number of the replicate. PR = a cell line cultured in a 3D static system and PO = a cell line cultured in a 3D flow system (in a microfluidic device). For example, (U87_pr_1) is for U87 cell line cultured in the 3D static system, replicate number 1, and (U87_po_1**)** is for U87 cell line cultured in 3D flow system (in a microfluidic device), replicate number 1.

Table 5.2: Profile of the transcriptome sequence data.

SAMPLE	RAW_ READS	RAW_ BASES	CLEAN_ READS	CLEAN_ BASES	ERROR_ RATE%	GC_PCT
U87_PR_1	52060968	7.81G	51378848	7.71G	0.02	43.99
U87_PO_1	45282602	6.79G	44675428	6.7G	0.03	49.73
U87_PR_2	42355694	6.35G	41923464	6.29G	0.03	50.35
U87_PO_2	47801606	7.17G	47217244	7.08G	0.03	50.35
U87_PR_3	50321446	7.55G	49690792	7.45G	0.03	50.59
U87_PO_3	41289022	6.19G	40786082	6.12G	0.03	50.07
G58_PR_1	40896306	6.13G	40384752	6.06G	0.03	49.37
G58_PO_1	49190084	7.38G	48449860	7.27G	0.03	46.05
G58_PR_2	55447300	8.32G	54801492	8.22G	0.03	49.7
G58_PO_2	49830820	7.47G	48881114	7.33G	0.03	49.64
G58_PR_3	46142996	6.92G	45490460	6.82G	0.03	49.8
G58_PO_3	51841792	7.78G	51003266	7.65G	0.03	49.87
G63_PR_1	54027998	8.1G	53329538	8.0G	0.03	49.52
G63_PO_1	51920788	7.79G	51216198	7.68G	0.03	49.48
G63_PR_2	61884678	9.28G	61244666	9.19G	0.03	49.46
G63_PO_2	44138206	6.62G	43659838	6.55G	0.03	49.25
G63_PR_3	49733810	7.46G	49147904	7.37G	0.03	49.52
G63_PO_3	41412794	6.21G	40880824	6.13G	0.03	49.57
AVERAGE	48643272		48008987			49.23

Sample*: SampleID*
Raw_reads*: Reads count from the raw data*
Raw_bases*: Base number of raw data. (number of raw reads) * (sequence length), converting unit to G*
Clean_reads*: Base number of raw data after filtering. (number of clean reads) * (sequence length), converting unit to G*
Clean_bases*: (clean base=clean reads*150bp) number multiply read length, saved in G unit*
Error_rate*: Average sequencing error rate*
GC_pct*: The percentage of G&C base numbers of total bases. (G&C base number) / (Total base number)*100*

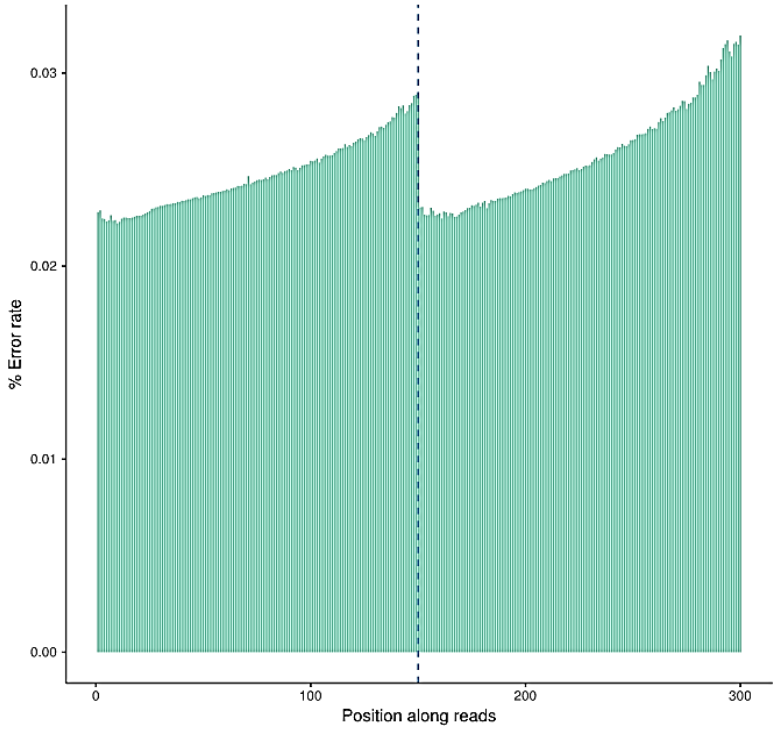

Figure 5.3 Sequencing data error rate distribution of sample G58-po-1 (G58 cultured in flow system (po), replicate 1)
The x-axis shows the base position along with each sequencing read and the y-axis shows the base error rate. The left side of the vertical dashed line is for read 1 (forward strand), the right side is for read 2 (reverse strand).

5.3.2.2 GC Content Distribution

Chen et al., (2013) and Browne et al., (2020) demonstrated that distribution of GC content may induce a bias to the genome sequencing process which may lower the accuracy of NGS data. They demonstrated also that gene expression quantification is affected directly by the coverage ratio of AT to GC which can be clearly seen through the GC content distribution of the coding sequence in double stranded DNA. For a successful sequencing experiment, G and C, A and T should be respectively equal, and the content should be stable throughout the entire sequencing process in double-stranded cDNA libraries. If the library is strand-specific (ssDNA), a deviation of A/T:G/C ratios may occur. Relatively large variations of sequencing error in the first 6-7 bases (**Figure 5.4**) are allowed considering the use of random primers in library construction, as a random hexamer of deoxynucleotides was used for the construction of cDNA library through the reverse transcription reaction. GC content analysis of the constructed cDNA libraries showed that for all samples G/C and A/T distributions are respectively equal, and the content was stable throughout the entire sequencing process. An example of this is shown in **Figure 5.4.** Full GC content distribution for all samples is shown in **Appendix 1**.

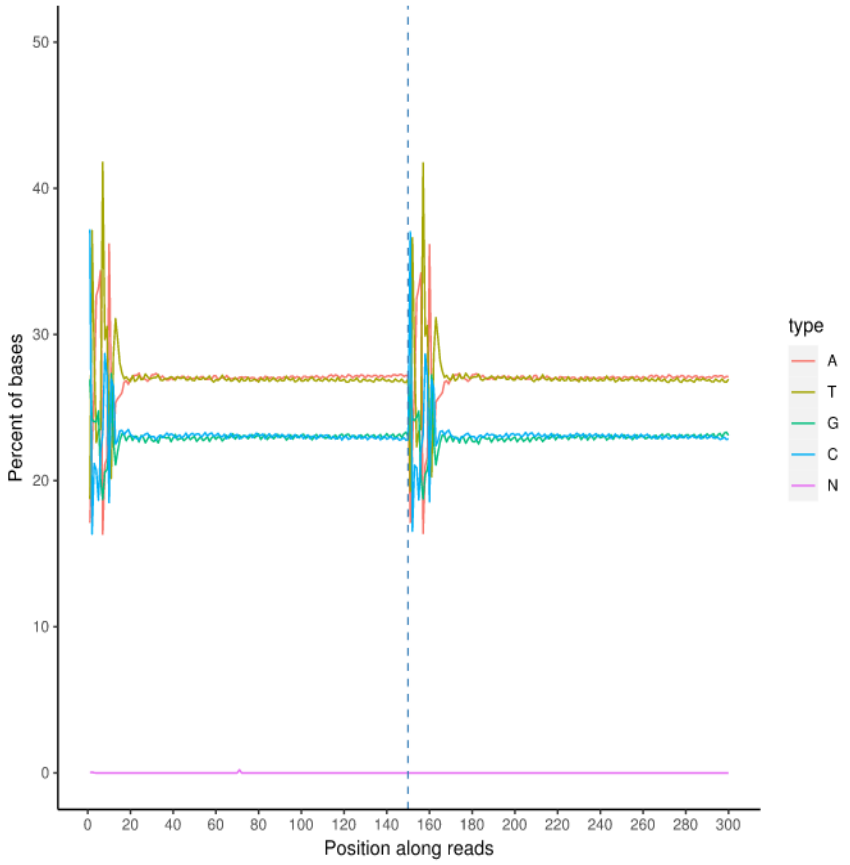

Figure 5.4 GC content distribution of the sample G58-po-1
The x-axis shows each base position within a read, and the y-axis shows the percentage of each base, with each base represented by a different colour. The left side of the vertical dashed line is the GC-content of read 1, the right side is the GC-content of read 2. N: no specific nucleotide could be assigned for this base.

5.3.2.3 Reads quality filtering results

The sequencing reads/raw reads often contain low-quality reads or reads with adapters, which will affect the quality of downstream analysis. To avoid this, it was necessary to filter the raw reads and obtain the "clean reads". Adapters are specific short DNA sequences added to cDNA library for higher accuracy of the sequencing process (see material and methods chapter). Raw reads filtering process is as follows:

The filtering process started with removing reads with adapter contamination then reads where uncertain nucleotides (N), constitute more than 10 per cent of either forward or reverse reads (N > 10%). Finally reads with low-quality nucleotides (Base Quality less than 5) that constitute more than 50 per cent of the read are filtered out.

The proportion of different components (clean reads, containing N, low quality, and adapter related) was analysed for all samples (an example is given in **Figure 5.5**). An average of 48,643,272 raw reads were obtained from each sample. After filtering by quality, the

average percentage of high-quality clean reads was 98.69±0.21 % (average number 48,008,987) with a GC content of 49.23±1.61 %. Clean reads were mapped to the reference genome. The profile of transcriptome sequence data is shown in **Table 5.2**. Full sample sequencing data filtering for all samples are shown in **Appendix 1**.

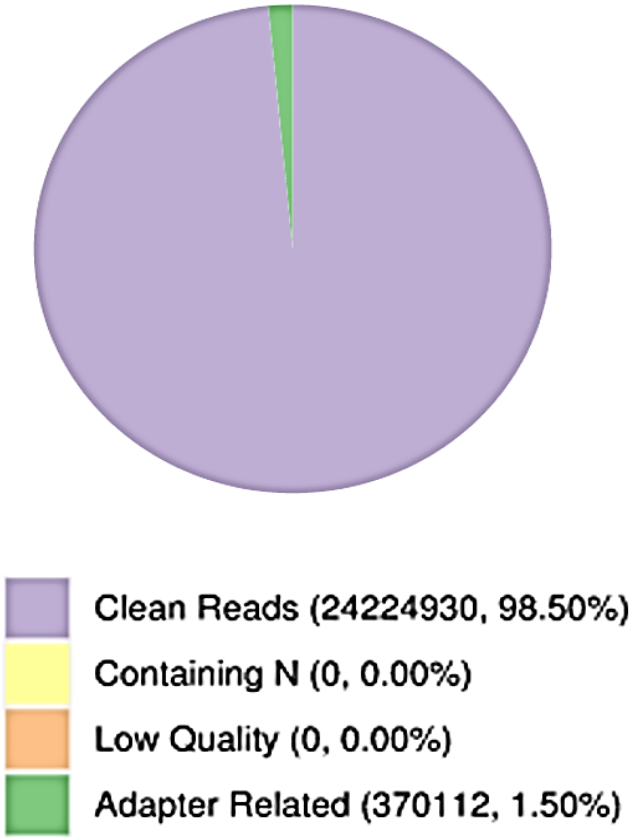

Figure 5.5 Sample Sequencing Data Filtering of the sample G58-po-1
Proportions of the different colours in the chart represent the proportion of different components. Adapter related: (reads containing adapter) / (total raw reads). Containing N: (reads with more than 10% N) / (total raw reads). Low quality: (reads of low quality) / (total raw reads). Clean reads: (clean reads) / (total raw reads).

5.3.2.4 Read Distribution in the Reference Genome

After undergoing the library quality control check, clean reads were mapped to the reference genome (hg38), using HISAT2 alignment program. For a successful read alignment, the total number of mapped reads should be higher than 70%. In this study the total number of mapping-reads for all three cell lines was higher than 95% (**Table 5.3)**. The accuracy of alignment is translated by the percentage of reads aligned to unique position of the reference genome which should be much higher than those aligned to multiple position of the reference genome. For all reads the percentage of unique mapping rate was more than 93% while the percentage of multiple mapping did not exceed 2.5% (**Table 5.3)** giving reassurance as to the

reliability of mapping results obtained from the reads from all three cell lines. Detailed mapping results are summarised in the A**ppendix 2**.

Table 5.3 Mapping results of reads from different cell lines

Sample	Total mapping rate (%)	Unique mapping rate (%)	Multiple mapping rate (%)
U87 static	96.51	94.30	2.20
U87 flow	95.45	93.32	2.13
G58 static	95.69	93.43	2.26
G58 flow	96.5	94.18	2.32
G63 static	96.32	93.97	2.35
G63 flow	95.46	93.19	2.27
Median	95.99±0.51	93.73±0.48	2.26±0.08

Total mapping rate: *Percentage of reads aligned to the genome ((mapped reads)/(total reads)*100).*
Unique mapping rate: *Percentage of reads aligned to the unique position of the reference genome ((uniquely mapped reads)/(total reads)*100).*
Multiple mapping rate: *Percentage of reads aligned to multiple locations in the reference genome ((multiple mapped reads)/(total reads)*100)*

Mapped regions can be classified as exons, introns, or intergenic regions. In an RNA sequencing project, exon-mapped reads should be the most abundant type of reads when the reference genome is well-annotated. Reads mapped to intronic regions may be the result of pre-mRNA contamination or intron-retention from alternative splicing. Finally, reads mapped to intergenic regions are mainly attributed to weak annotations of the reference genome (Kukurba & Montgomery, 2015). Mapping results showed that exon-mapped reads are the most abundant type of reads indicating that the reference genome was well-annotated with high degree of accuracy. Hence, the percentages of exon-mapped regions range from 83% to 88.40% for G58 and G63 samples and from 89.80% to 91.92% for U87 samples. An example of it is shown in **Figure 5.6**. Ratio of sequencing reads types in the genomic region for all samples is shown in **Appendix 1**.

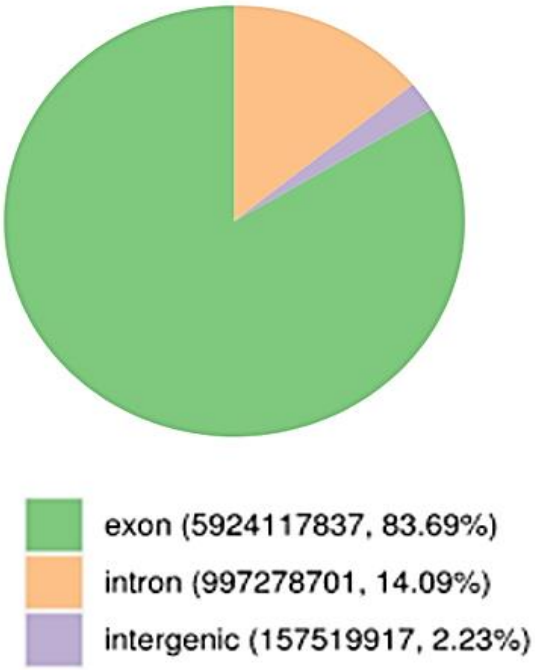

Figure 5.6 ratio of sequencing reads types in the genomic region of the sample G58-po-1
The ratios of the different colours in the chart represent the ratio of reads to different regions. Exon: The number of reads aligned to exon regions of the genome and its proportion in clean reads. Intron: The number of reads aligned to intron regions of the genome and its proportion in clean reads. Intergenic: The number of reads aligned to intergenic regions of the genome and its proportion in clean reads.

Once the QC was done, the analysis of differential gene expression profile between samples was carried out. This analysis was done with 2 aims in mind: the first was to study gene expression profile differences between the three cell lines cultured in static and flow conditions; the second aim was to perform enrichment analysis of the three cell lines cultured in the flow system and compare it to those cultured in the static system to identify genes and pathways differentially expressed in flow conditions compared to static culture.

5.4 Study of differentially expressed genes in three GBM cell lines

5.4.1 Distribution of gene expression levels between samples from different cell lines

Gene expression level was determined using the expected number of Fragments Per Kilobase of transcript sequence per Millions base pairs sequenced (FPKM) counting method, and results are shown in **Figure 5.7**. This figure shows box plots of gene expression with maximum, upper quartile, mid-value, lower quartile, and minimum of log2(FPKM+1) for each sample of the three cell lines. The box plot demonstrates that FPKM values (gene expression levels) from different samples are comparable and consistent, and sequence results

were reliable, since each sample yielded equivalent reads and coverage depths between repeats.

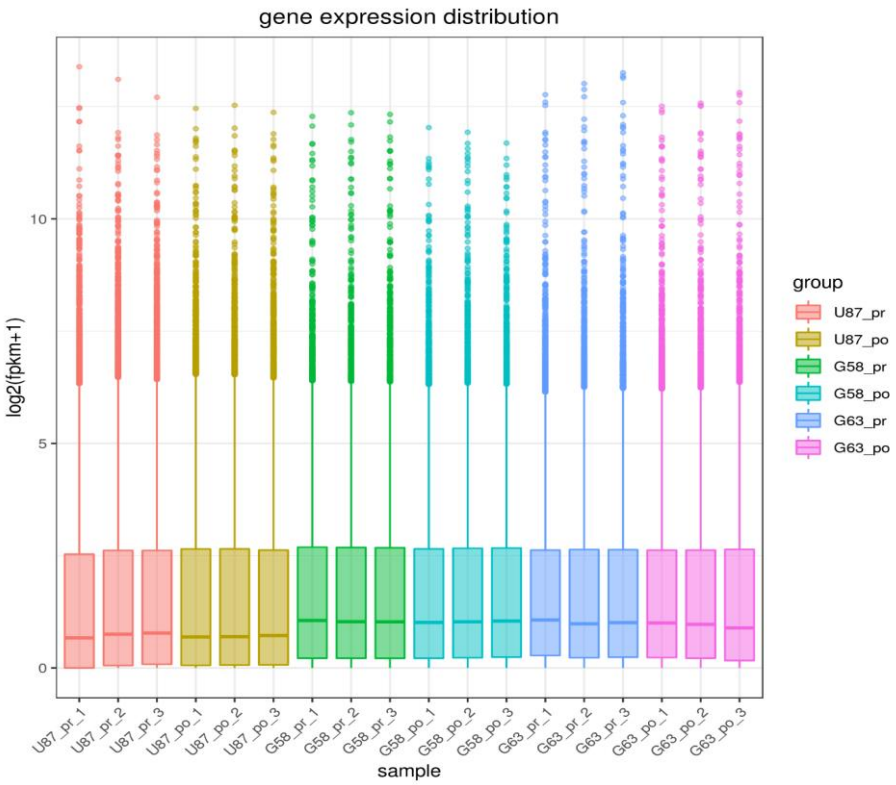

Figure 5.7 FPKM box plot of gene expression distribution of different samples
X axis represents the name of the sample. Y axis indicates gene expression as log2(FPKM+1). Parameters of box plots are indicated, including maximum, upper quartile, mid-value, lower quartile and minimum.

5.4.2 Correlation analysis of gene expression levels of different cell lines

Biological replicates reflect the repeatability of an experiment in different conditions. This is highly applicable to RNA-seq technology, where the study of the correlation of gene expression levels between samples of the same cell type treated identically can demonstrate the reproducibility of the experiment and will impact differential gene expression analysis. The more similar the samples are, the closer the correlation coefficient will be to 1 (LIU et al., 2016). In ideal experimental conditions the Pearson correlation coefficient should not be less than 0.92 and the R^2 should not be less than 0.8. A high correlation coefficient indicates high similarity in expression pattern between samples.

This can be graphically represented when the calculated correlation coefficients are drawn as heat maps (**Figure 5.8**). This heat map clearly shows the presence of three clusters of samples with R^2 values greater than 0.84 within each cluster. The clusters refer to the three different cell lines used in this study U87, G58 and G63. It is interesting to notice that the R^2

values between G58 and G63 cell lines are greater than 0.8 and higher than the R^2 values between either of these lines with the U87 cell line (R^2 between 0.5 and 0.7). This indicates that the expression pattern of both cell lines G58 and G63 cell lines are most similar to one another.

These results can be seen also in the Venn diagram (**Figure 5.9**) where there are about 4 times the number of genes co-expressed by G58 and G63 cells than those co-expressed by either of these 2 cell lines with U87 (~1900 genes vs~450) in the two culture conditions. Heat map results shows also that gene expression pattern is similar between spheroids cultured in static and flow system within each cell line (R^2>0.8).

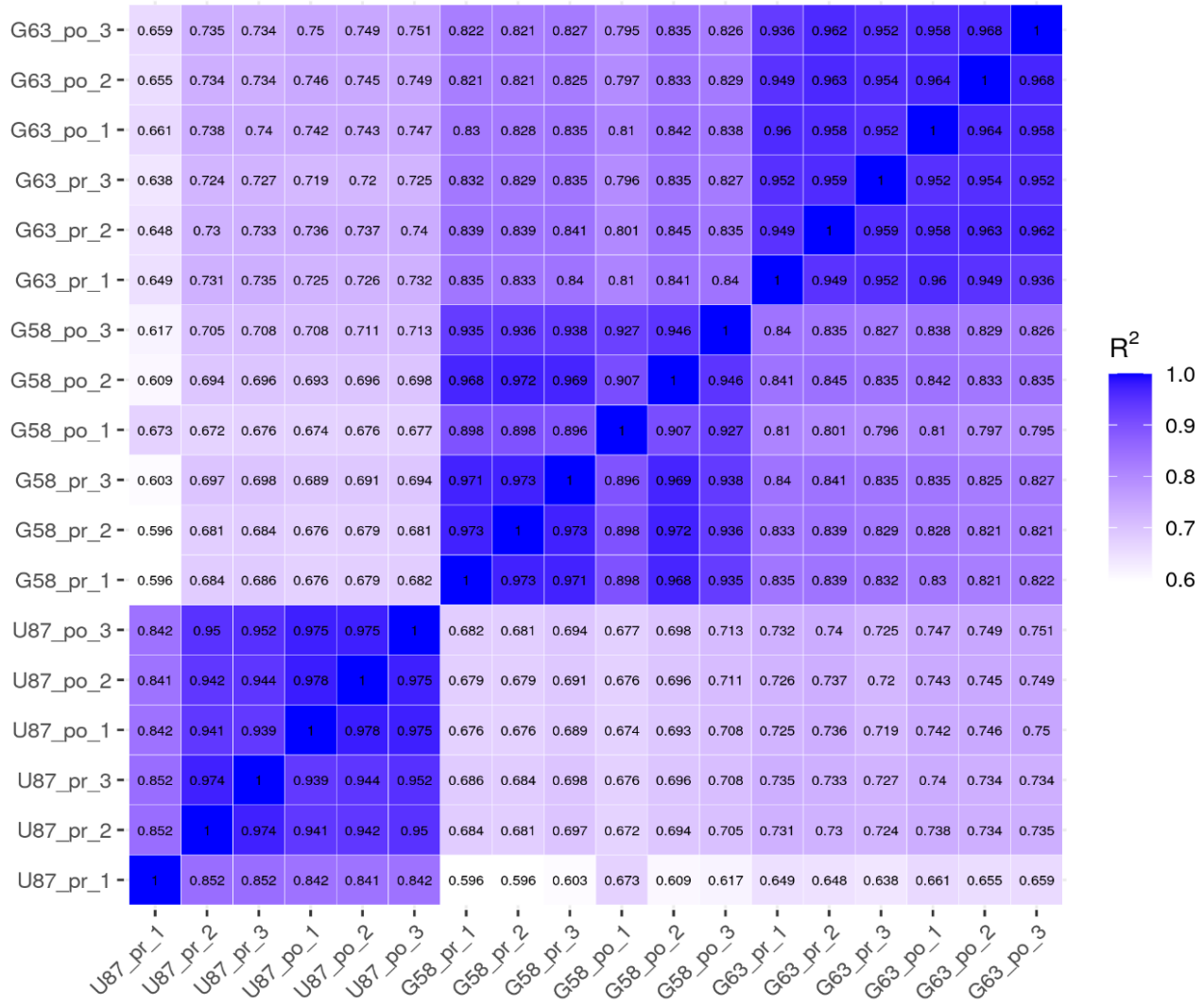

Figure 5.8 Correlation heatmap of samples using Pearson coefficient between different samples

The more intense the blue colour the higher the correlation coefficient with a maximum 1 in blue and the minimum in white (see gradient colour barcode). The more samples are highly similar to each other the closer the correlation value is to 1.

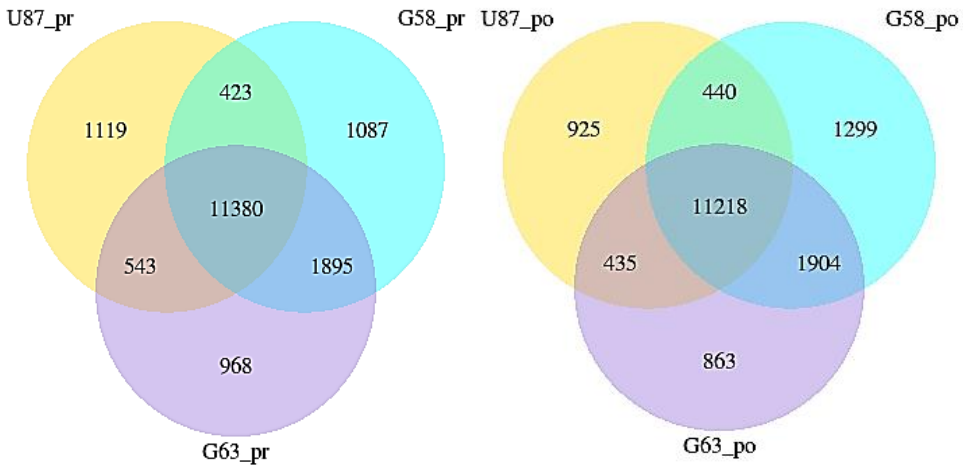

Figure 5.9 Venn chart of expressed genes
To the left, number of genes expressed by each cell line cultured in 3D static condition. To the right, number of genes expressed by each cell line cultured in microfluidic system.

5.5 Functional analysis of differentially expressed genes

Whole transcriptome analysis is a powerful tool that can provide a detailed insight into gene expression of cells or group of cells in a given time and under a given condition (Sá et al., 2018). The aim here was to study the gene expression profile of GBM spheroids cultured in a 3D flow system and compare it to those cultured in 3D static system for the same period of time.

5.5.1 Differential gene expression statistics

After gene expression quantification, statistical analysis of the expression level data was used to study the genes that are significantly differentially expressed for different cell lines cultured in different conditions. Due to the high number of genes studied, analysis can lead to the accumulation of false positives, a corrected value (padj for p adjusted value) of the hypothesis test p-value was therefore calculated to control the proportion of false positives (Young et al., 2010). The smaller the padj value the more statistically significant is the differentially expressed gene expression.

The number of DEGs for each cell line is shown in the table below (**Table 5.4 and Figure 5.8**). The threshold for screening is pvalue≤0.05 and log2FoldChange=0. A volcano plot showing the overall distribution of DEGs for the three cell lines (upregulated and downregulated genes) in each cell line cultured in the microfluidic system compared to those cultured in 3D static phase is shown in **Figure 5.10**. Results of top 10 up and down-regulated DEGs as defined by padj values, for all three cell lines are given in **Appendix 3**.

Table 5.4 Statistics of differentially expressed genes for three cell lines

Cell line	All DEGs	Up-regulated DEGs	Down-regulated DEGs
U87_	3708	1745	1963
G58_	3051	1781	1270
G63_	2222	1064	1158

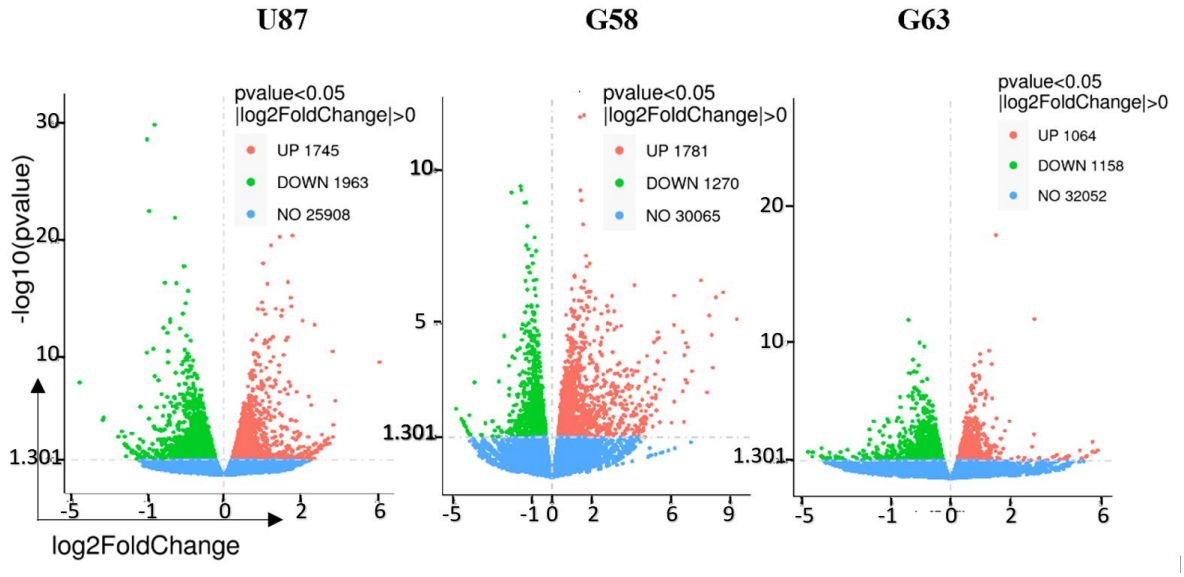

Figure 5.10 Volcano Map of differentially expressed genes of GBM spheroids cultured in 3D flow system (po) compared to those cultured in 3D static (pr)
The x-axis shows the fold change in gene expression between different samples (log2FoldChange), and the y-axis shows the statistical significance of the differences (-log10pvalue). Red dots represent up-regulated DEGs and green dots represent down-regulated DEGs. The blue dashed line indicates the threshold line for identifying differentially expressed genes.

To understand the relevance of the DEGs in relation to biological functions and associated pathways a functional gene ontology analysis was performed. This was done through the enrichment analysis using clusterProfiler software which includes GO and KEGG enrichment analyses (Yu et al., 2012).

5.5.2 GO enrichment analysis

Gene ontology (GO) is a major bioinformatic classification system, that unifies the presentation of gene properties across all species. It includes two main parts, first the ontology itself and second the GO annotation (Tomczak et al., 2018). The ontology is a tree-like hierarchical structure of relationships between different GO terms. GO annotation is a coding system that documents the evidence that led to the association of a given gene and the GO term. GO terms are categorised into a biological process (BP), cellular component (CC), or molecular function (MF) that have been associated with a particular set of genes.

GO analysis is a comparison between the actual (observed) number of genes (in a gene set of DEGs) associated to a given GO term, to the expected number of genes to be associated this category. The statistical significance of this association is called enrichment and is determined by calculating the probability (p-value or padj for multiple comparison) of appearing just by random chance of these observed values (Rhee et al., 2008; Huang et al., 2013; Reijnders & Waterhouse, 2021). It is considered significant enrichment when the padj of a GO term is < 0.05. GO terms of different upregulated DEGs expressed in spheroids cultured in the 3D flow system, are expressed as the ratio between the number of differentially expressed genes in each GO term and all genes concerning this GO term.

5.5.2.1 Biological Process enrichment analysis

This analysis calculates the significance of association between a given set of DEGs in each condition and identifies different biological processes (BPs) that these DEGs are most likely to be involved in. Results in **Table 5.5** show that significantly up-regulated BPs (padj<0.05) are related to mitotic cell cycle processes: "sister chromatid segregation"; "chromosome segregation" and "mitotic nuclear division" for U87 and GBM63. Specifically, for GBM63, BPs that trigger "intrinsic apoptotic signalling pathway" or stop the apoptosis ("negative regulation of apoptotic signalling pathway"), detoxification BPs and response to misfolded or unfolded proteins are among the top 10 upregulated BPs. In parallel for GBM58, all top 10 up-regulated BPs are those involved in the defence against infection by a virus or other organism such as ("defence response to virus", "type I interferon signalling pathway" and "defence response to other organism").

Results in **Table 5.6** indicate that there was similar down-regulated BPs between U87 and GBM58 spheroids which were not enriched in G63 spheroids cultured in the flow system. This includes BPs regulating the extracellular matrix structure and organisation ("extracellular matrix organization") and cell-adhesion related BPs ("cell-cell adhesion via plasma-membrane adhesion molecules", "cell-substrate adhesion", "homophilic cell adhesion via plasma membrane" and cell-substrate adhesion"). On the other hand, most of the top 10 (7/10) down-regulated BPs for GBM63 spheroids are those that regulate the movement of proteins to a specific location inside the cell (e.g., "protein targeting to ER") and their transport towards the cell membrane (e.g., "co-translational protein targeting to membrane"). In addition, BPs regulating the mRNA catabolic process (3/10) are found to be down-regulated in GBM63 spheroids (e.g., "nuclear-transcribed mRNA catabolic process").

Table 5.5 Top 10 significantly enriched up-regulated GO terms (padj<0.05) for the GO subclass of Biological Process for all three cell line.

U87			G58			G63		
Biological Process	**Gene Ratio**	**padj**	**Biological Process**	**Gene Ratio**	**padj**	**Biological Process**	**Gene Ratio**	**padj**
sister chromatid segregation	71/231	1.63E-15	defense response to virus	67/196	1E-19	intrinsic apoptotic signaling pathway	5/32	6.81E-06
nuclear chromosome segregation	78/293	1.59E-13	response to virus	81/276	1E-19	response to unfolded protein	16/89	1.28E-05
chromosome segregation	85/343	4.60E-13	type I interferon signaling pathway	36/73	3E-16	response to topologically incorrect protein	5/29	1.28E-05
DNA replication	72/283	1.57E-11	cellular response to type I interferon	36/73	3E-16	chromosome segregation	13/94	1.74E-05
mitotic sister chromatid segregation	48/147	1.57E-11	response to type I interferon	37/78	5E-16	phagosome maturation	14/41	3.10E-05
DNA-dependent DNA replication	47/149	1.06E-10	defense response to other organism	86/358	3E-15	mitotic nuclear division	7/47	3.10E-05
mitotic nuclear division	65/255	1.71E-10	response to interferon-gamma	53/168	4E-14	detoxification of inorganic compound	8/12	3.1E-05
sister chromatid cohesion	43/132	2.54E-10	negative regulation of viral process	35/86	1E-12	detoxification	22/101	3.1E-05
DNA replication initiation	23/43	4.01E-10	negative regulation of viral life cycle	32/73	1E-12	negative regulation of apoptotic signaling pathway	32/203	9.6E-05
negative regulation of cell cycle process	69/315	4.30E-08	negative regulation of viral genome replication	27/54	3E-12	sister chromatid segregation	35/234	9.6E-05

Table 5.6 Top 10 significantly enriched down-regulated GO terms (padj<0.05) for the GO subclass of Biological Process for all three cell lines

U87			G58			G63		
Biological Process	**Gene Ratio**	**padj**	**Biological Process**	**Gene Ratio**	**padj**	**Biological Process**	**Gene Ratio**	**padj**
extracellular matrix organization	74/302	1.37E-12	synapse organization	36/291	0.1096	SRP-dependent cotranslational protein targeting to membrane	29/92	9.72E-12
extracellular structure organization	78/345	1.29E-11	extracellular matrix organization	38/319	0.1096	cotranslational protein targeting to membrane	29/97	2.33E-11
homophilic cell adhesion via plasma membrane adhesion molecules	40/127	6.73E-10	synapse assembly	22/145	0.1096	protein targeting to ER	29/102	6.67E-11
cell-cell adhesion via plasma-membrane adhesion molecules	48/198	9.53E-08	skeletal system development	49/460	0.1243	establishment of protein localization to endoplasmic reticulum	29/106	1.50E-10
collagen fibril organization	18/41	2.93E-06	anterior/posterior pattern specification	25/183	0.1255	nuclear-transcribed mRNA catabolic process, nonsense-mediated decay	30/121	7.62E-10
SRP-dependent cotranslational protein targeting to membrane	27/91	9.44E-06	cardiac ventricle formation	5/10	0.1309	protein localization to endoplasmic reticulum	29/131	3.11E-08
angiogenesis	76/446	1.16E-05	glial cell differentiation	25/188	0.1378	protein targeting to membrane	34/184	1.09E-07
skeletal system development	73/422	1.16E-05	cardiac chamber formation	5/11	0.1669	nuclear-transcribed mRNA catabolic process	34/209	3.06E-06
glomerulus development	19/51	1.53E-05	homophilic cell adhesion via plasma membrane adhesion molecules	21/150	0.1669	translational initiation	31/193	1.74E-05
sensory organ development	74/435	1.53E-05	cell-substrate adhesion	34/300	0.1747	viral transcription	29/174	1.88E-05

5.5.2.2 Cellular component enrichment

CC enrichment analysis for U87 and GBM63 spheroids, shows that the most significantly enriched up-regulated CCs (10/10 for U87 and 4/10 for GBM63) (**Table 5.7**) are those involved in the initiation and regulation of DNA replication ("MCM complex", "chromosomal region", "condensed chromosome outer kinetochore", and "kinetochore"). On the other hand, GBM58 spheroids most enriched up-regulated CCs (**Table 5.8**) are involved in the endomembrane system including cell membranes and vesicles (e.g, "endoplasmic reticulum lumen", "external side of plasma membrane", "Golgi-associated vesicle membrane").

Interestingly, these results are in accordance with upregulated BPs where U87 and GBM63 showed an up-regulation of BPs regulating cell cycle process which mainly depend on DNA replication mechanism. Concerning GBM58 up-regulated CCs and BPs seems to be closely related. In fact, BPs related to viral life cycle and response to virus could be the result of upregulation of CCs involving the endomembrane system and vice versa. Accordingly, previous studies demonstrate that Endoplasmic reticulum (ER) ER-related proteins and Golgi are often essential for the replication of the viral genome(He et al., 2017; Hassan et al., 2021).

However, most down-regulated CCs were shown to be those involved in the structure of the extracellular matrix ("extracellular matrix component", "proteinaceous extracellular matrix"). Again, these findings are in line with previous observations of down-regulated BPs in U87 and G58 spheroids which were related to the extracellular matrix and organisation.

5.5.2.3 Molecular function enrichment

MF enrichment analysis demonstrates that in the flow system U87 spheroids over-expressed genes (**Table 5.9**) involved in MFs related to DNA replication activity (e.g., "chromatin binding" and "DNA replication origin binding") and the transport of amino acid through the membrane (e.g., "amino acid transmembrane transporter activity"). As indicated in **section 5.2.1** and **5.2.2** similar observations were reported previously with up-regulated BPs and CCs. While GBM58 spheroids share with those of U87 the up-regulation of MFs controlling the survival, growth, differentiation and effector function of tissues and cells ("cytokine activity"), they specifically over-express pro-inflammatory MFs such as ("chemokine activity", "CXCR chemokine receptor binding", and "tumour necrosis factor receptor superfamily binding"). In addition, GBM63 spheroids, showed an up-regulation of MFs related to the transport of protons and amino acids through the membrane (e.g., "proton-

transporting ATPase activity, rotational mechanism" and "neutral amino acid transmembrane transporter activity") and those involved in misfolded protein binding mechanism

Results in **Table 5.10** indicate that MFs associated to cell-adhesion (e.g., "cell adhesion molecule binding") and extracellular matrix organisation ("extracellular matrix structural constituent") are down-regulated in U87 spheroids in the flow system, while GBM58 and GBM63 spheroids showed that most of the top 10 down-regulated MFs are those controlling the ion channel ("ion channel activity") and the passive transmembrane transport activity ("passive transmembrane transporter activity").

Table 5.7 Top 10 significantly enriched up-regulated GO terms (padj<0.05) for the GO subclass of Cellular Component for all three cell lines

U87			G58			G63		
Cellular Component	**Gene Ratio**	**padj**	**Cellular Component**	**Gene Ratio**	**padj**	**Cellular Component**	**Gene Ratio**	**padj**
chromosomal region	75/332	4.64E-10	endoplasmic reticulum lumen	49/277	8.42E-04	melanosome	21/105	8.97E-05
chromosome, centromeric region	51/188	9.22E-10	endoplasmic reticulum-Golgi intermediate compartment	25/116	5.61E-03	pigment granule	21/105	8.97E-05
condensed chromosome, centromeric region	35/114	4.06E-08	external side of plasma membrane	36/204	6.95E-03	proton-transporting V-type ATPase complex	10/25	8.97E-05
MCM complex	10/11	9.59E-08	side of membrane	61/418	6.95E-03	chromosomal region	42/331	8.97E-05
condensed chromosome	48/204	3.17E-07	Golgi-associated vesicle membrane	22/105	7.82E-03	vacuolar membrane	48/404	8.97E-05
spindle	63/312	6.59E-07	melanosome	22/105	7.82E-03	condensed chromosome outer kinetochore	7/13	1.76E-04
condensed chromosome kinetochore	30/101	8.12E-07	pigment granule	22/105	7.82E-03	chromosome, centromeric region	28/189	1.76E-04
kinetochore	34/130	2.64E-06	coated vesicle membrane	29/160	9.28E-03	lysosomal membrane	42/349	1.76E-04
replication fork	21/69	6.74E-05	vesicle coat	14/54	1.11E-02	lytic vacuole membrane	42/349	1.76E-04
mitotic spindle	24/88	9.58E-05	Golgi-associated vesicle	29/164	1.13E-02	kinetochore	22/131	2.20E-04

Table 5.8 Top 10 significantly enriched down-regulated GO terms (padj<0.05) for the GO subclass of Cellular Component for all three cell lines

U87			G58			G63		
Cellular Component	**Gene Ratio**	**padj**	**Cellular Component**	**Gene Ratio**	**padj**	**Cellular Component**	**Gene Ratio**	**padj**
endoplasmic reticulum lumen	79/262	1.87E-20	extracellular matrix	62/425	9.03E-08	cytosolic ribosome	30/116	1.38E-10
extracellular matrix component	43/108	8.69E-16	proteinaceous extracellular matrix	52/339	2.33E-07	cytosolic large ribosomal subunit	19/65	1.73E-07
extracellular matrix	91/397	2.36E-15	collagen trimer	18/75	8.32E-05	extracellular matrix	54/441	1.69E-06
proteinaceous extracellular matrix	73/320	4.15E-12	extracellular matrix component	20/114	2.57E-03	transmembrane transporter complex	40/309	2.00E-05
basement membrane	32/85	4.55E-11	ionotropic glutamate receptor complex	12/48	2.64E-03	ribosomal subunit	29/186	2.00E-05
MHC protein complex	14/19	1.33E-09	neurotransmitter receptor complex	12/49	2.75E-03	transporter complex	40/317	3.27E-05
MHC class II protein complex	11/12	2.41E-09	postsynaptic density membrane	9/31	5.55E-03	cytosolic part	32/237	9.41E-05
ER to Golgi transport vesicle membrane	20/55	1.46E-06	AMPA glutamate receptor complex	8/26	7.39E-03	proteinaceous extracellular matrix	41/350	1.20E-04
focal adhesion	67/382	2.70E-06	postsynaptic specialization membrane	9/33	7.39E-03	polysomal ribosome	10/30	1.20E-04
complex of collagen trimers	11/18	2.70E-06	basement membrane	15/88	1.54E-02	postsynaptic density membrane	10/31	1.39E-04

Table 5.9 Top 10 significantly enriched up-regulated GO terms (padj<0.05) for the GO subclass of molecular function MF for all three cell lines

U87			G58			G63		
Molecular Function	**Gene Ratio**	**padj**	**Molecular Function**	**Gene Ratio**	**padj**	**Molecular Function**	**Gene Ratio**	**padj**
neutral amino acid transmembrane transporter activity	11/27	1.71E-02	cytokine receptor binding	53/208	8.19E-10	cell adhesion molecule binding	56/478	2.54E-04
catalytic activity, acting on DNA	9/46	1.71E-02	cytokine activity	44/161	2.81E-09	proton-transporting ATPase activity, rotational mechanism	9/21	2.84E-04
chromatin binding	9/59	1.71E-02	receptor ligand activity	67/353	4.41E-07	misfolded protein binding	10/27	2.84E-04
histone kinase activity	4/9	3.49E-02	receptor regulator activity	67/381	7.99E-06	cadherin binding	41/321	2.84E-04
amino acid transmembrane transporter activity	17/67	3.49E-02	chemokine receptor binding	16/40	1.68E-05	proton-exporting ATPase activity	10/28	3.31E-04
L-amino acid transmembrane transporter activity	13/46	5.29E-02	chemokine activity	14/31	1.68E-05	neutral amino acid transmembrane transporter activity	10/30	5.68E-04
helicase activity	7/37	6.52E-02	CXCR chemokine receptor binding	9/14	5.89E-05	ubiquitin-like protein ligase binding	38/313	1.31E-03
DNA helicase activity	13/49	7.76E-02	protein disulfide isomerase activity	8/19	1.22E-02	ubiquitin protein ligase binding	36/299	2.33E-03
DNA replication origin binding	6/14	1.29E-01	intramolecular oxidoreductase activity, transposing S-S bonds	8/15	1.22E-02	aminoacyl-tRNA ligase activity	11/44	2.47E-03
cytokine activity	26/143	1.29E-01	tumor necrosis factor receptor superfamily binding	12/41	1.46E-02	ligase activity, forming carbon-oxygen bonds	11/44	2.47E-03

Table 5.10 Top 10 significantly enriched down-regulated GO terms (padj<0.05) for the GO subclass of molecular function MF for all three cell lines

U87			G58			G63		
Molecular Function	**Gene Ratio**	**padj**	**Molecular Function**	**Gene Ratio**	**padj**	**Molecular Function**	**Gene Ratio**	**padj**
growth factor binding	28/119	4.80E-04	gated channel activity	35/308	6.69E-02	structural constituent of ribosome	28/156	7.71E-06
collagen binding	18/58	4.80E-04	monovalent inorganic cation transmembrane transporter activity	39/359	6.69E-02	ion channel activity	46/400	1.07E-04
extracellular matrix structural constituent	19/64	4.80E-04	ion gated channel activity	34/306	6.69E-02	ligand-gated ion channel activity	23/135	1.07E-04
heparin binding	28/129	1.49E-03	channel activity	43/422	6.69E-02	ligand-gated channel activity	23/135	1.07E-04
glycosaminoglycan binding	34/174	1.51E-03	passive transmembrane transporter activity	43/422	6.69E-02	ligand-gated cation channel activity	19/100	1.44E-04
exopeptidase activity	22/94	2.56E-03	substrate-specific channel activity	41/399	6.69E-02	substrate-specific channel activity	46/412	1.44E-04
carbohydrate binding	37/204	2.56E-03	ion channel activity	40/388	6.69E-02	channel activity	47/434	1.95E-04
cell adhesion molecule binding	66/460	6.28E-03	potassium channel activity	17/118	6.78E-02	passive transmembrane transporter activity	47/434	1.95E-04
metallopeptidase activity	30/160	6.28E-03	metal ion transmembrane transporter activity	43/432	6.78E-02	transmitter-gated ion channel activity	12/51	7.98E-04
metalloexopeptidase activity	14/50	6.94E-03	cation channel activity	32/295	6.78E-02	transmitter-gated channel activity	12/51	7.98E-04

5.5.2 KEGG Enrichment Analysis

Kyoto Encyclopedia of Genes and Genomes (KEGG) is a manually collected database containing resources on genomic, biological-pathway and disease information (Kanehisa et al., 2008). KEGG Enrichment Analysis deciphers the interaction of multiple genes that could be involved in certain biological functions. It identifies significantly enriched (padj<0.05) metabolic pathways or signal transduction pathways associated with DEGs, and they are expressed as the ratio between the number of DEGs in each pathway to all genes concerning this KEGG pathway.

KEGG enrichment analysis shows that most significantly enriched (padj≤0.05) up-regulated pathways in GBM spheroids cultured in the microfluidic device compared to the static system (**Table 5.11)**, are similar in all three cell lines belonging to three categories. The first category includes oncogenic pathways involved in cell cycle and proliferation e.g. “Cell cycle”, “Transcriptional misregulation in cancer”, “Pathways in cancer”, “DNA replication”. The second category include proinflammatory pathways e.g., “Rheumatoid arthritis”, “NOD-like receptor signaling pathway”, “Proteasome”, “Measles” and “Phagosome”. The third category includes pathways related to cellular senescence, cell aging and necrosis e.g., “Cellular senescence”, “Epstein-Barr virus infection”, “p53 signaling pathway”, “Ferroptosis”, and “Necroptosis”. Ferroptosis and necroptosis were among the top 30 enriched pathways (**appendix 2**).

Additionally, pathway enrichment analysis shows that the most enriched down-regulated pathways (**Table 5.12**) are those involved in the cell adhesion and the extracellular matrix organisation (“Focal adhesion”, “ECM-receptor interaction” and “Cell adhesion molecules (CAMs)”). It is interesting to notice that for U87 and GBM58 spheroids, some of the down-regulated pathways suggest the imbalance of the energy supply and demand under stressed conditions resulting in the inability to maintain normal ATP levels (“Hypertrophic cardiomyopathy (HCM)”, “Dilated cardiomyopathy (DCM)”). While in GBM63 spheroids specifically, carbohydrates and amino acid metabolism pathways are down-regulated (“Other glycan degradation”, “Starch and sucrose metabolism” and “Taurine and hypotaurine metabolism”).

Table 5.11 Top 10 most enriched up-regulated pathways for all three cell lines

U87			G58			G63		
Molecular Function	**Gene Ratio**	**padj**	**Molecular Function**	**Gene Ratio**	**padj**	**Molecular Function**	**Gene Ratio**	**padj**
Cell cycle	38/117	7.11E-08	TNF signaling pathway	42/102	2.33E-13	Vibrio cholerae infection	13/46	1.88E-03
DNA replication	16/35	3.10E-05	NOD-like receptor signaling pathway	44/146	6.94E-09	Phagosome	22/117	1.88E-03
Cellular senescence	31/139	7.74E-03	Influenza A	41/131	6.94E-09	Mineral absorption	12/46	4.49E-03
Rheumatoid arthritis	17/64	2.91E-02	NF-kappa B signaling pathway	29/82	1.15E-07	Protein processing in endoplasmic reticulum	24/153	8.46E-03
Human T-cell leukemia virus 1 infection	39/209	3.33E-02	Herpes simplex infection	40/140	1.15E-07	Collecting duct acid secretion	8/25	1.08E-02
p53 signaling pathway	17/68	3.68E-02	IL-17 signalling pathway	29/83	1.15E-07	Aminoacyl-tRNA biosynthesis	10/41	1.75E-02
Proteasome	12/40	3.68E-02	Measles	33/103	1.15E-07	Glutathione metabolism	11/50	2.02E-02
Selenocompound metabolism	7/17	5.11E-02	Epstein-Barr virus infection	41/155	6.99E-07	Cell cycle	19/121	2.12E-02
Epstein-Barr virus infection	28/151	1.17E-01	Protein processing in endoplasmic reticulum	40/154	1.62E-06	Epithelial cell signaling in Helicobacter pylori infection	12/62	3.01E-02
Oocyte meiosis	22/111	1.17E-01	Rheumatoid arthritis	21/64	4.15E-05	Rheumatoid arthritis	12/63	3.14E-02

Table 5.12 Top 10 most enriched down-regulated pathways for all three cell lines

U87			G58			G63		
Molecular Function	**Gene Ratio**	**padj**	**Molecular Function**	**Gene Ratio**	**padj**	**Molecular Function**	**Gene Ratio**	**padj**
ECM-receptor interaction	24/71	8.54E-07	Focal adhesion	23/189	0.23	Ribosome	29/128	1.2E-08
Focal adhesion	37/182	1.22E-04	ECM-receptor interaction	12/75	0.23	cAMP signaling pathway	21/182	1.59E-01
PI3K-Akt signaling pathway	50/295	3.20E-04	Cardiac muscle contraction	11/73	0.31	Complement and coagulation cascades	10/62	1.92E-01
Ribosome	27/126	6.94E-04	Dilated cardiomyopathy (DCM)	12/84	0.31	Nicotine addiction	7/37	2.68E-01
Amoebiasis	20/85	1.94E-03	Axon guidance	19/170	0.36	Other glycan degradation	4/15	4.46E-01
Cell adhesion molecules (CAMs)	22/103	3.26E-03	Hypertrophic cardiomyopathy (HCM)	11/79	0.36	ECM-receptor interaction	10/78	5.09E-01
Dilated cardiomyopathy (DCM)	16/71	1.43E-02	Arrhythmogenic right ventricular cardiomyopathy (ARVC)	10/70	0.36	Galactose metabolism	5/27	5.40E-01
Small cell lung cancer	18/87	1.67E-02	cAMP signaling pathway	19/180	0.43	Taurine and hypotaurine metabolism	3/10	5.40E-01
Hypertrophic cardiomyopathy (HCM)	15/67	1.78E-02	Adrenergic signaling in cardiomyocytes	15/134	0.46	Starch and sucrose metabolism	5/29	5.95E-01
Toxoplasmosis	18/89	1.78E-02	Oxidative phosphorylation	14/125	0.46	Arachidonic acid metabolism	7/51	5.95E-01

5.6 Discussion

To better understand the observed phenotypic differences between spheroids cultured under static conditions versus those cultured in the flow system within a microfluidic setup (**Figure 3.5, Figure 3.10**), their respective gene expression profiles were analysed using NGS technology. Total RNA was extracted from GBM spheroids cultured in static and flow system for 3 days (GBM58 and 63 cell lines) and for 7 days for U87 cell line, aiming to identify pathways/processes induced or repressed by the microfluidic system.

5.6.1 Correlation of the gene expression between GBM cell lines

RNA quality and library checks were done and successfully passed. The similarity in gene expression pattern and the high number of shared DEGs between G58 and G63 in comparison with U87 gene expression profile is most likely related to the origin and characteristics of each cell line, i.e. both being recently generated lines. The U87 cell line has been established for about 56 years (Allen et al., 2016) whereas G58 and G63 are primary PDCs which are much closer in passages to the original tumour than U87 will be. Long established cell lines (U87), lose some cell functions while acquiring an indefinite proliferative activity (Zhuang et al., 2021). Allen et al., (2016) demonstrated previously that the DNA profile of GBM cell line U87 was different from that of the original tumour cells and described U87 as a human GBM cell line of unknown origin. In contrast primary PDCs are isolated directly from human tissues and cultured with a low number of passages under defined serum-free conditions (Stringer et al., 2019). G58 and G63 as many other GBM PDCs present common histological features of high-grade glioma. Previous studies demonstrated that PDCs exhibit similar histological hallmarks of glioblastoma (Stringer et al., 2019) such as hypercellularity, nuclear atypia , pleomorphism which may include also angiogenesis activation (microvascular proliferation) and palisading necrosis (D'Alessio et al., 2019).

Accordingly, Feng et al., (2020) demonstrated that established gallbladder carcinoma (GBC) PDCs (JXQ-3D-902R4, JXQ-3D-4494R, and JXQ-3D-4786R) present histologic, phenotypic, and genotypic characteristics such as cell shape irregularity, chromosomal number variability and STR pattern similar to that of the original tissues of primary GBC. Although PDCs cell lines have a limited life span they are considered the gold standard for a better understanding of tumour biology and to discover more effective treatment strategies. These cells were shown to retain histological features, major somatic alterations and drug

response properties of the original tumour tissue preserving the donor variability and tissue complexity (Al-Mayhani et al., 2009; Ehrenberg et al., 2019; He et al., 2021).

These studies suggest that the strong correlation in gene expression pattern between G58 and G63 is related to the fact that they are both PDCs, in contrast to U87 which is a long-established cell line and showed lower correlation with both cell lines as seen in the heat map.

5.6.2 Functional analysis of DEGs

5.6.2.1 GO enrichment analysis

GO enrichment of up-regulated DEGs in GBM spheroids cultured in the microfluidic system compared to the static conditions, showed that the most enriched BPs, CCs and MFs for U87 cell line were related to the cell cycle and DNA replication process. For G58 up-regulated DEGs were those involved in BPs and CCs related to the defence mechanism of cells against viruses and MFs associated to the activity of pro-inflammatory cytokine and chemokine. For G63, in addition to BPs and CCs regulating mitotic cell cycle and DNA replication process, most enriched up-regulated DEGs were those implicated in MFs that regulate transport of proton and amino-acid through the membrane, detoxification, and response to misfolded protein.

GO enrichment of down-regulated DEGs showed that the most common BPs, CCs and MFs in U87 spheroids are those controlling the extracellular matrix and the cell adhesion mechanisms. The same results were found with G58 spheroids along with the enrichment of MFs related to ion channel and passive transport membrane activity. For G63, in addition to the down-regulation of BPs controlling the synthesis and the transport of the protein inside the cell and the mRNA catabolic process, GO analysis showed the down-regulation of CCs related to extracellular matrix and (CCs and MFs) regulating ion channel and passive transport membrane activity.

The enrichment of pro-proliferative GO terms controlling the cell cycle and DNA replication process over other mechanisms in a long established GBM spheroid line (U87) can be explained by the biological properties of this cell line as stated above (see **section 5.6.1**).

Additionally the proliferative activity of U87 and other GBM cell lines was previously reported in 3D static (Diao et al., 2019) and PDMS 2D flowing systems(Han et al., 2016). The enrichment of pro-proliferative GO terms could also be related to the structural properties of multicellular spheroid model characterised by the presence of cells with a higher

proliferation rate being present in the outer layers compared to others in the inner layers (Shen et al., 2021).

These results were in line with previously published studies about cancer tissues describing proliferation as an important feature of cancer development and progression (Feitelson et al., 2015) and more especially for GBM tissues (Liu et al., 2021). Moreover, Kim et al, (2013) reported specifically that rapid proliferation is a major characteristic of GBM tissues.

All this together, suggest that the microfluidic system, compared to static conditions, enhances the pro-proliferative gene activity of GBM cells which is consistent with cell's behaviour of *in vivo* GBM tumour tissue. But, at this point, whether this is caused by the culture on the device (i.e. is an artefact) or is the flow system allowing the spheroids to behave as the tumour mass *in vivo* is not yet clear. The enrichment of GO terms related to the activity of pro-inflammatory cytokines and chemokines observed in G58 spheroids ties well with previous studies which report the upregulation of cytokines and chemokines in both GBM cell lines as well as patient derived tissues (Yeung et al., 2013). Alt et al., (2018) demonstrated that the silencing of TRAF3 Interacting Protein 2 (TRAF3IP2) in GBM cell lines reduces both, the tumour size, and the expression of pro-inflammatory cytokines. TRAF3IP2 is an upstream regulator of transcription factors of proinflammatory mediators.

Interestingly, previous studies on tumour tissues demonstrated that pro-inflammatory responses promote all stages of cancer development (Greten & Grivennikov, 2019) and pro-inflammatory genes are biomarkers for oral squamous cell carcinoma (Rao et al., 2010). Recently, Das et al., (2021) report that the crosstalk between tumour cells secreting pro-inflammatory factors and immune cells contribute to the survival, growth, and progression of the tumour by maintaining a successful niche for it.

It was reported previously, that NF-κB-signalling pathways, involved in GBM tumour growth and development (Uddin et al., 2021), induces the production of pro-inflammatory-molecule including IL-6 (Olivier et al., 2020). Also, proinflammatory-gene expression was reported to be upregulated in GBM cells promoting migration and proliferation of cells close to the necrotic core which is characterised by a hypoxic environment (Zagzag et al., 2006; Torrisi et al., 2022a). Together these findings suggest that GBM spheroids in the microfluidic device may upregulate the expression of pro-inflammatory genes in response to the hypoxic microenvironment created at the necrotic centre of the spheroids, which may further enable the cells to acquire migratory ability.

The up-regulation of different GO terms in G63 could be explained as a cellular biological response to the down-regulated BPs and MFs. GO enrichment of G63 spheroids shows the down-regulation of terms controlling the synthesis and the transport of the protein inside the cell and through the membrane as well as the down-regulation of the mRNA catabolic process leading together, to the accumulation of toxic compounds in the cytoplasm which will induce the activation of biological detoxification processes. On the other hand, the down-regulation of the protein synthesis mechanisms will induce the activation of different processes that enable the cell to respond to misfolded or unfolded proteins (**Figure 5.11**). Recently, (Uchenunu et al., 2018) described dysregulation of protein synthesis and RNA catabolic process as a hallmark in cancer.

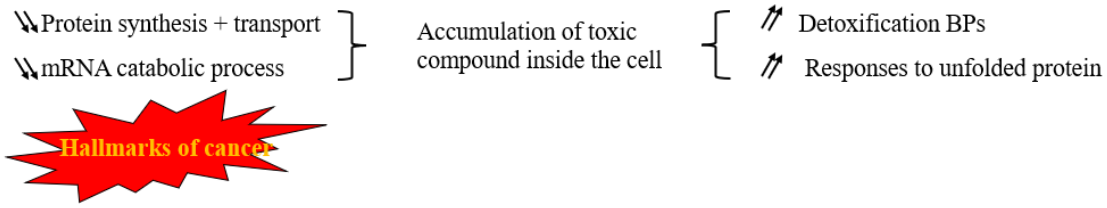

Figure 5.11 Scheme showing the pathways activation in G63 cells maintained in 3D flow system
Up arrow: up-regulation and down arrow down-regulation

The down-regulation of GO terms involving genes that control the cell adhesion and the extracellular matrix structure and organisation processes was reported in all three GBM cell lines cultured in a 3D flowing system. Previous studies demonstrated that ECM proteins play a pivotal role in cellular communication promoting migration and invasion of tumours, where ECM is usually remodelled inducing desmoplasia (Virga et al., 2019). In normal tissues cell-ECM adhesion enables the cell, principally via integrin family members, to respond in a coordinated manner to external stimuli. The dysregulation of the cell-adhesion process and ECM organisation are reported as a fundamental factor in acquiring invasiveness and metastasis state of a tumour (Gkretsi & Stylianopoulos, 2018). In the tumour mass, malignant cells from the outer layers start to dissociate as a result of the alteration of cell-ECM adhesion dynamics leading to the degradation of ECM and the migration of malignant cells to adjacent tissues (Wei & Yang, 2016; Winkler et al., 2020). The down regulation of cell-adhesion and ECM pathways may reflect the outer layers of the spheroids acquiring an invasive phenotype when cultured in the flow system mimicking the behaviour of cells in the tumour mass *in situ*.

This hypothesis is supported by the study demonstrating that U87 spheroids migrate as individual cells in contrast to oral squamous carcinoma cells (OSC–19) spheroids which invade collectively in the microfluidic chip. Thus, cells of the outer layers of the U87 spheroids maintained in the flow system, in contrast to static conditions, will show dysregulation of the ECM and reduced cell-cell interactions, preparing for the dissociation followed by the migration of individual cells (Ayuso et al., 2015).

5.6.2.2 KEGG enrichment analysis

KEGG enrichment analysis of DEGs expressed in GBM spheroids cultured in the flow system compared to the static conditions showed the enrichment of pathways controlling similar biological processes and molecular functions described already in GO enrichment analysis. However, KEGG analysis demonstrated that in addition to the up-regulation of pro-proliferative and pro-inflammatory pathways, the flow system was found to enhance the activation of genes involved in cellular senescence and necrosis.

It has been demonstrated previously that under different stresses, proliferating cells undergo cellular senescence process as a defence mechanism preventing them from acquiring unnecessary damage (Calcinotto et al., 2019). This process is closely related to cell aging and leads to permanent cell cycle arrest in which cells become resistant to cell death. Although the relation between aging and cancer is not clear yet, there is growing evidence that the accumulation of senescent cells contributes efficiently to the progression of cancer (Yang et al., 2021). Recent studies suggest the use of IL6 as a target for adjuvant chemotherapy for GBM patients, as IL6 is secreted by senescent GBM cells, and is thought to be a marker of poor prognosis (Gu et al., 2021).

Up-regulated DEGs involved in necrotic pathways could be associated directly with cells in the interior of the spheroid, analogous to the necrotic core of many tumour masses. This dying core is surrounded by multiple, increasingly proliferative, layers from the inside to the outer layers (Browning et al., 2021; Rocha et al., 2021). Han & Kim, (2021) reported that cells at the centre of the spheroid remain in a senescent or necrotic state due to the limited supply of oxygen and nutrients and the increase of CO2 and waste.

The high proliferation rate of cancer cells in the outer layers of the spheroid induces a limitation of supply of oxygen and nutrients for the cells in the inner layers resulting in creation of a hypoxic microenvironment (Riffle et al., 2017). This hypoxia will induce proteomic and genomic changes of tumour cells around the centre of the spheroid initiating

cell arrest and necrosis mechanisms (**Figure 5.12**) as described previously for solid tumours by (Al Tameemi et al., 2019; Ziółkowska-Suchanek, 2021).

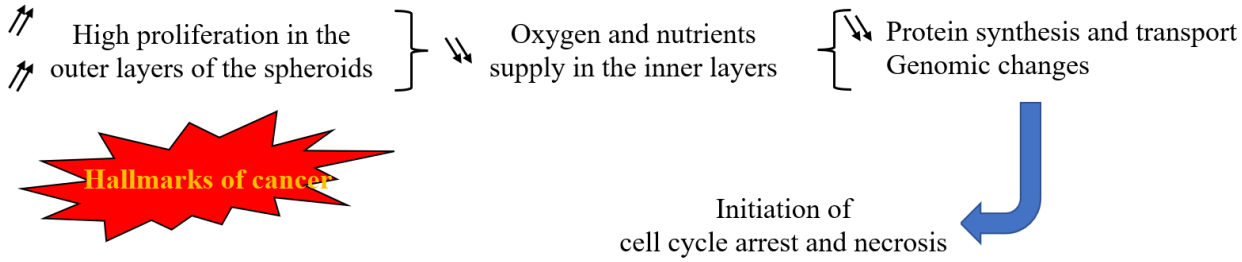

Figure 5.12 scheme showing the intervention of high proliferation rate in enhancing necrosis at the centre of the GBM spheroid maintained in flow system
Up arrow: up-regulation and down arrow down-regulation.

On the other hand, pathways enrichment of down-regulated DEGs demonstrated that in addition to pathways involved in cell adhesion and extracellular matrix (discussed above in GO analysis), the analysis showed the downregulation of pathways regulating the ATP, energy supply, and metabolism. This can be regarded as a response of GBM cells of the inner layers of the spheroids undergoing a limitation of supply of nutrient and oxygen. (Bertuzzi et al., 2010) demonstrated that the deficit of ATP and energy metabolism was associated with necrosis in the core of the tumour spheroid.

However, the dysregulation of metabolic process is described as a hallmark of GBM tumours known as “metabolic rewiring or alteration” (Torrisi et al., 2022a). The diminution of availability of oxygen and nutrient in the tumour mass creates a complex and hostile environment of hypoxic conditions where GBM cells are subjected to metabolic reshaping to provide energy needed for their survival (Li et al., 2016). Metabolic dysregulation includes glycolysis, lipid, amino-acid, and nucleotide metabolism reprogramming, creates an increased acidification rate which support invasiveness and stimulate migration in vitro and metastasis *in vivo* (Garcia et al., 2021).

KEGG enrichment of G63 cells shows the dysregulation of metabolism of different molecules, i.e. galactose, taurine, hypotaurine, and arachidonic acid which could be a response of the inner cells of the spheroids, to the hypoxic environment created by the scarcity of oxygen and nutrients. As it was reported previously, in addition to the dysregulation of ECM structure hypoxia trigger the escape of cancer cells and induces invasive phenotype and metastatic expansion.

5.7 Conclusion

In conclusion, this study demonstrates clearly that compared to the static conditions, spheroids in the flow system exhibit increased expression of many hallmarks of GBM: including metabolism dysregulation, activation of pro-proliferative, proinflammatory and necrotic pathways. Additionally, GBM spheroids in the flow system showed the downregulation of genes and pathways involved in cell adhesion and extracellular matrix allowing for an *in vivo*-like microenvironment of developing invasive phenotype and the progression to metastasis (**Figure 5.13**).

Whether these data are a response to the microfluidic system, or the fact that the fluid flow better mimic the *in vivo* scenario will require more study. However, these results suggest that the microfluidic device is a useful platform for culturing GBM spheroids and possibly other tumour models and for studying drug responsiveness and tumour evolution. In addition, primary PDC lines are shown to be equally well maintained on the device as spheroids from long-established lines, and it is likely they better reflect the pathophysiology and responses of the original tumour.

A future avenue of work that would help address the question of whether the static or microfluidic culture changes are artefact, or a better reflection of the *in vivo* environment would be to correlate gene expression changes in spheroids, with and without treatment, in static and flow conditions compared to gene expression data available from GBM patients.

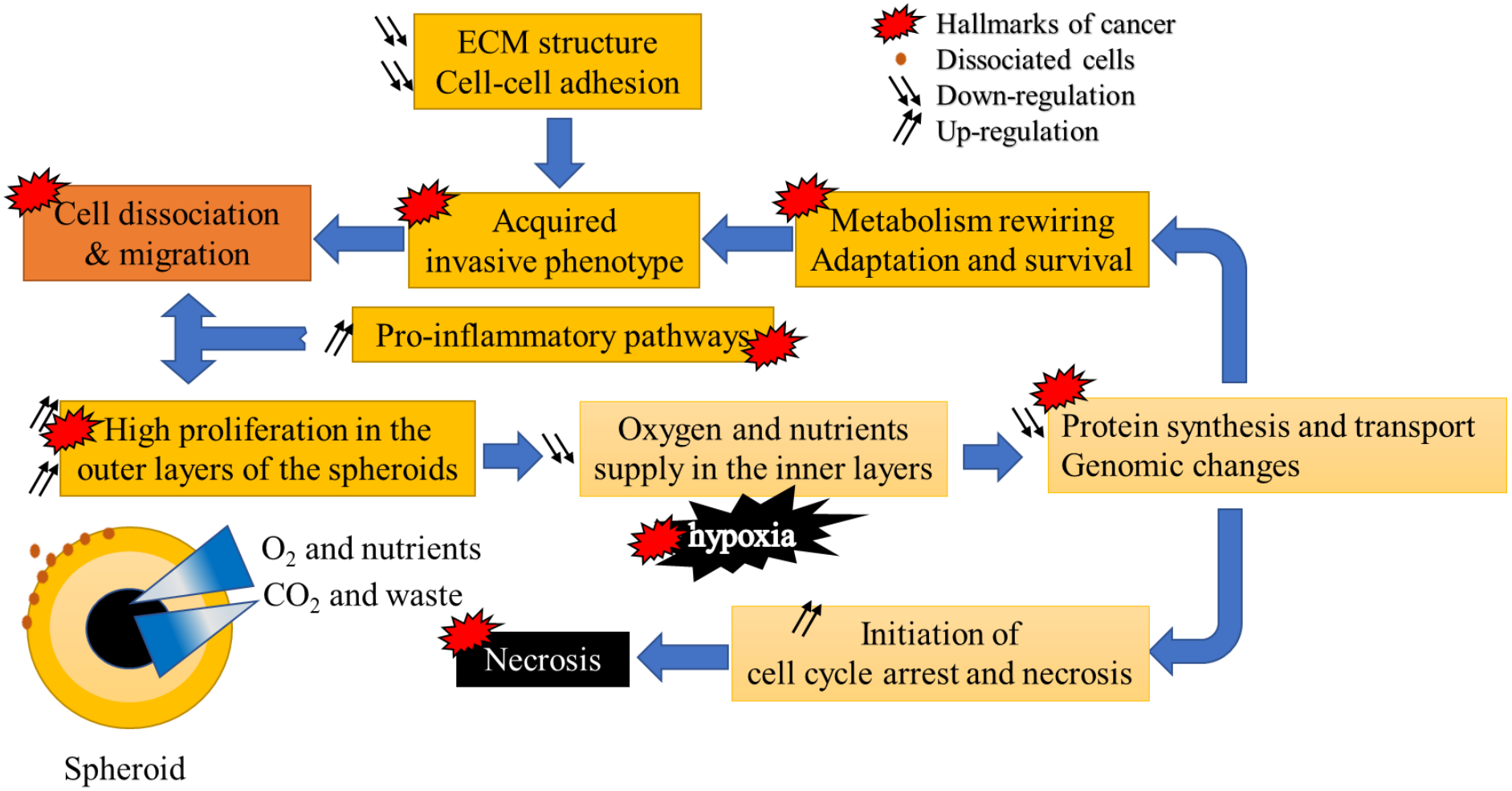

Figure 5.13 scheme summarising different biological processes and pathways activated and repressed when GBM spheroid were maintained in the flow system compared to the static conditions

Colours correspond to different layers of the spheroid. Matching colours were used to show hypothetical locations where pathways could be enriched

Chapter 6.
Discussion

GBM is the most aggressive form of brain cancer with a poor prognosis which has not improved significantly over the past twenty years. Clinically, it is classified as a grade IV astrocytoma. For primary GBM (about 90% of cases) predominantly affecting older people, to secondary malignancies occurring more often in younger people, the gold standard of treatment is surgery followed by chemoradiotherapy using TMZ. Despite the extensive research to improve survival rates, median survival after first diagnosis remains at 15 months with a 5-year survival rate still less than 5% (Baid et al., 2020). Recurrence after resection (occurring in nearly 80% of cases) with the development of resistance to TMZ are considered the main reasons for the worse prognosis of such tumour type. Therefore, new therapeutic targets to limit the resistance to TMZ and develop new drugs that work through different mechanisms are urgently required. To this end, translationally-relevant models are needed to reliably identify potential therapeutic targets that could improve the prognostic of GBM patients. The use of multicellular tumour spheroids (MCTS) cultured in a flow system has been receiving increased attention for the last decade, as these models can be developed to better mimic the *in vivo* tumour microenvironment (TME) more than the 3D static and monolayer culture models widely used over the past fifty years.

The work in this thesis focused on developing a GBM model for performing gene knockdown experiments in spheroids maintained in a microfluidic flow-based system. This study showed that the designed microfluidic chip was suitable for maintaining spheroids in a viable state for 7 days. During this time there were no major alterations of spheroid characteristics, and the RNA yield was significantly higher compared to the 3D static conditions for three independent genes (*PRMT2*, *RAB21* and *FUS*).

The increase of RNA yield could be the result of an enhanced proliferative activity of spheroids when maintained in the flow system as it was demonstrated by the transcriptome analysis of U87 spheroids showing the enrichment of pro-proliferative genes over all others. Whether this increased proliferative activity was an artefact of the device or that the device maintained the spheroids in a more optimal condition better representing the *in vivo* environment needs further work. With the significantly increased expression of targeted genes (*PRMT2* and *RAB21*) in the flow system compared to 3D static conditions, the microfluidic system was shown to be suitable for doing silencing experiments on targeted genes.

siRNA knockdown experiments on GBM spheroid model showed a significant gradual decrease of *PRMT2* and *RAB21* gene knockdown level, from 2D monolayer to 3D

static and finally the 3D flow culture system. These results could be explained by differences of microenvironment characteristics in each model. According to the literature review, the more the culture model tends to mimic the *in vivo* TME the more it exhibits similar responses (Park et al., 2015; Thippabhotla et al., 2019; Petreus et al., 2021). Therefore, the gradual increase in resistance to siRNA effect from 2D to 3D static to 3D flow system, could be mirroring the gradual increase of resistance to drug molecules seen in monolayer to 3D static sytems. The resistance to drug of cells cultured in 3D model compared to monolayer system is well documented and has been shown to be associated with the constitution and organization of MCTS (Gong et al., 2015; Kijanska & Kelm, 2016; Gopal et al., 2021). The theory is that the creation of barriers through the cell–cell and cell–ECM interactions in the MCTS model reduce the uptake of molecules and contributes to the development of chemoresistance (Pinto et al., 2020b).

Accordingly, previous studies reported the increase of chemoresistance of MCTS to clinically relevant doses in the flow system compared to the static (Das et al., 2013; Ip et al., 2016). The reasons for the reduced effect of siRNA on spheroids cultured in the flow system could, in part, be the same as those leading to the development of chemoresistance of cancer cells in the solid tumour under *in vivo* conditions. These factors include the cell-cell interactions barrier (Castells et al., 2012; Jo et al., 2018), the oxygen gradient and presence of hypoxia inside spheroids created by the flow system (Nunes et al., 2019), and finally the acidic environment created by glycolysis in the inner cells of spheroids in response to the limited supply of nutrients such as glucose or essential amino acids (Han & Kim, 2021).

Other reasons for the reduced knockdown in the flow system could be the poor uptake of siRNA molecules under shear stress conditions of the flow system (Ip et al., 2016a), or the dilution of siRNA inside cells of the spheroids cultured in the flow system, as a result of an enhanced cell proliferation (thus the amount of available siRNA may not be sufficient) compared to the static system which was confirmed by NGS analysis (Bartlett & Davis, 2006). Results of the current study showed that despite the effective gene silencing in 3D model using Accell siRNA technology, due to study limitations there was not enough evidence to conclude about optimal conditions for Accell siRNA silencing in the 3D flow system but highlight that the procedure is worthy of future work.

RNA sequencing analysis demonstrated that PDCs (G58 and G63) have a broadly similar gene expression pattern that is different from that of U87. While U87 presented homogenous gene enrichment which were mostly pro-proliferative, G58 and G63 presented

heterogeneity and complexity of different GO and KEGG terms. As was described earlier U87 appears to have lost many of the characteristics of the original tissue and has acquired a phenotype of an indefinite proliferation, while G58 and G63 retained most of the heterogeneity and complexity of the donor tissue. These findings demonstrate that, in contrast to primary cell lines, PDCs showed a heterogeneity in activated and deactivated pathways similar to what have been seen in GBM (Pearson & Regad, 2017) and other cancer tissues (Romera-Giner et al., 2021). Therefore, PDCs could be useful to better understand the cancer biology, discover reliable new therapeutic approaches by identifying biomarkers, and provide a trustable translational platform to study the correlation phenotype/genotype in term of drug response and cancer evolution.

Functional analysis demonstrated that in contrast to the static conditions, the flow system activate most of the biological mechanisms and pathways considered as hallmarks of cancer (Torrisi et al., 2022b). These include pathways and cellular functions involved in proliferation, inflammation, metabolism dysregulation, senescence, necrosis, and invasion. Accordingly, previous studies reported that the microfluidic system could be a relevant in vitro model to study different events of the metastatic cascade as it enhances the activation of different metastatic processes such as invasion, intra- and extravasation (Boussommier-Calleja et al., 2016). Recently, (Cho et al., 2021), demonstrated that the inflammatory cytokines enhance epithelial-mesenchymal transition (EMT) and further increase invasion property of breast cancer cells (MCF-7, MDA-MB-231, and SK-BR-3) when cultured in the microfluidic flow system.

The current study demonstrates that the microfluidic system is a suitable platform for doing gene silencing experiments, enables *invivo-like* behaviour of cells, which could allow more *accuracy* to study cellular response to treatment than other traditional culture systems (2D monolayer and 3D static). Previous studies have successfully used microfluidic systems in cancer diagnosis for detecting circulating tumour cells in early breast cancer (Guo et al., 2021; Krol et al., 2021), this study is the first to use the GBM model for doing knockdown experiments in a 3D flowing system. Recent applications of the microfluidic setup in cancer research led to improvement in understanding the biology of cancer, such as detection of a single cancer cell and metastatic events (Akgönüllü et al., 2021b) and discovering new therapeutic approaches such as reducing the side effects of systemic cancer treatment (Schirrmacher, 2019; Frankman et al., 2022).

6.1 Future work

The current study successfully optimised and established a flow system for the repression of gene expression using GBM model. However, the effectiveness of gene manipulation using this device needs a deeper investigation using genes where there is a better-established link with phenotype that can be easily assessed. It would be of interest to improve the gene knockdown level using the siRNA that could be achieved by testing other delivery methods for increasing siRNA intake, i.e. electroporation or sonication. There is the technical challenge to be overcome of integrating transfection methodologies with the microfluidic platform, however there is some work in this field (Chakrabarty et al., 2022).

Additionally, doing knockdown experiments in the current flow system using PDCs derived from GBM models will offer an opportunity to get reliable findings helping give a deeper insight into the tumour biology using a model closer to the *in vivo* character, where it is difficult to image some key events in the metastatic cascade such as intravasation and extravasation (Boussommier-Calleja et al., 2016; Mehta et al., 2022).

Finally, the investigation of the correlation in gene expression pattern and the activated versus repressed biological processes between PDCs (G58 and G63) and their tissue of origin will give another indication of whether the static or the flow system matches the real microenvironment of tumour. It is interesting to carry a further investigation of how much this flow system truly represents the *in vivo* conditions by using this model to study brain or other tumour types where normal as well as malignant tissues are available, e.g. colon.

The use of this device for culturing tumour tissues or coculturing tumour cells with endothelial or immune cells in an *in vivo*-like microenvironment could potentially offer insights into the contribution of BBB in GBM recurrence, TMZ resistance and may therefore be applicable to pre-clinical target validation studies.

6.2 Conclusion

This study has demonstrated that the microfluidic platform incorporating flow, can successfully maintain brain tumour spheroids for 7 days and can be used to repress gene expression. Work also showed that the microfluidic platform enhances the activation of *in vivo*-like biological processes and pathways considered as hallmarks of cancer. Future research studies using this microfluidic platform, to investigate spheroids and primary human tissues from GBM and other tumour type will give further evidence about the effectiveness of

the current flow system for mimicking the *in vivo* microenvironment, and hence, will help in understanding tumour biology and offer the possibility to discover new therapeutic options.

References

Abbott, N. J., Rönnbäck, L. & Hansson, E. (2006) Astrocyte-endothelial interactions at the blood-brain barrier. Nature Reviews. Neuroscience, 7 (1), 41-53.

Abe, H., Natsumeda, M., Okada, M., Watanabe, J., Tsukamoto, Y., Kanemaru, Y., Yoshimura, J., Oishi, M., Hashizume, R., Kakita, A. & Fujii, Y. (2020) MGMT expression contributes to temozolomide resistance in H3K27M-mutant diffuse midline gliomas. Frontiers in Oncology, (9). 1568.

Adamson, C., Kanu, O. O., Mehta, A. I., Di, C., Lin, N., Mattox, A. K. & Bigner, D. D. (2009) Glioblastoma multiforme: A review of where we have been and where we are going. Expert Opinion on Investigational Drugs, 18 (8), 1061-1083.

Aggarwal, B. B., Danda, D., Gupta, S. & Gehlot, P. (2009) Models for prevention and treatment of cancer: Problems vs promises. Biochemical Pharmacology, 78 (9), 1083-1094.

Agnihotri, S., Burrell, K. E., Wolf, A., Jalali, S., Hawkins, C., Rutka, J. T. & Zadeh, G. (2013) Glioblastoma, a brief review of history, molecular genetics, animal models and nov-el therapeutic strategies. Archivum Immunologiae Et Therapiae Experimentalis, 61 (1), 25-41.

Ahir, B. K., Ozer, H., Engelhard, H. H. & Lakka, S. S. (2017) MicroRNAMicroRNAs in glioblastoma pathogenesis and therapy: A comprehensive review. Critical Reviews in Oncology/Hematology, 120 22-33.

Ahn, S., Han, K., Park, Y., Bae, J. M., Kim, S. U., Jeun, S. & Yang, S. H. (2020) Cigarette smoking is associated with increased risk of malignant gliomas: A nationwide population-based cohort study. Cancers, 12 (5).

Aird, W. C. (2007) Phenotypic heterogeneity of the endothelium: II. representative vascular beds. Circulation Research, 100 (2), 174-190.

Akay, M., Hite, J., Avci, N. G., Fan, Y., Akay, Y., Lu, G. & Zhu, J. (2018) Drug screening of human GBM spheroids in brain cancer chip. Scientific Reports, 8 (1), 1-9.

Akgönüllü, S., Bakhshpour, M., Pişkin, A. K. & Denizli, A. (2021) Microfluidic systems for cancer diagnosis and applications. Micromachines, 12 (11).

Al Tameemi, W., Dale, T. P., Al-Jumaily, R. M. K. & Forsyth, N. R. (2019) Hypoxia-modified cancer cell metabolism. Frontiers in Cell and Developmental Biology, 7 4.

Aldape, K., Zadeh, G., Mansouri, S., Reifenberger, G. & von Deimling, A. (2015) Glioblastoma: Pathology, molecular mechanisms and markers. Acta Neuropathologica, 129 (6), 829-848.

Alexander, B. M., Pinnell, N., Wen, P. Y. & D'Andrea, A. (2012) Targeting DNA repair and the cell cycle in glioblastoma. Journal of Neuro-Oncology, 107 (3), 463-477.

Allahdini, F., Amirjamshidi, A., Reza-Zarei, M. & Abdollahi, M. (2010) Evaluating the prognostic factors effective on the outcome of patients with glioblastoma multiformis: Does maximal resection of the tumor lengthen the median survival? World Neurosurgery, 73 (2), 128-134; discussion e16.

Allen, M., Bjerke, M., Edlund, H., Nelander, S. & Westermark, B. (2016) Origin of the U87MG glioma cell line: Good news and bad news. Science Translational Medicine, 8 (354), 354re3.

Almeida, K. H. & Sobol, R. W. (2007) A unified view of base excision repair: Lesion-dependent protein complexes regulated by post-translational modification. DNA Repair, 6 (6), 695-711.

Almeida, P. G. C., Nani, J. V., Oses, J. P., Brietzke, E. & Hayashi, M. A. F. (2020) Neuroinflammation and glial cell activation in mental disorders. Brain, Behavior, & Immunity - Health, 2 100034.

Aloizou, A., Pateraki, G., Siokas, V., Mentis, A. A., Liampas, I., Lazopoulos, G., Kovatsi, L., Mitsias, P. D., Bogdanos, D. P., Paterakis, K. & Dardiotis, E. (2020) The role of MiRNA-21 in gliomas: Hope for a novel therapeutic intervention? Toxicology Reports, 7 1514-1530.

Alt, E. U., Barabadi, Z., Pfnür, A., Ochoa, J. E., Daneshimehr, F., Lang, L. M., Lin, D., Braun, S. E., Chandrasekar, B. & Izadpanah, R. (2018) TRAF3IP2, a novel therapeutic target in glioblastoma multiforme. Oncotarget, 9 (51), 29772-29788.

Alves, A. L. V., Gomes, I. N. F., Carloni, A. C., Rosa, M. N., da Silva, L. S., Evangelista, A. F., Reis, R. M. & Silva, V. A. O. (2021) Role of glioblastoma stem cells in cancer therapeutic resistance: A perspective on antineoplastic agents from natural sources and chemical derivatives. Stem Cell Research & Therapy, 12 (1), 206.

Amaral, A. J. R. & Pasparakis, G. (2016) Rapid formation of cell aggregates and spheroids induced by a “Smart” boronic acid copolymer. ACS Applied Materials & Interfaces, 8 (35), 22930-22941.

Amarzguioui, M. (2004) Improved siRNA-mediated silencing in refractory adherent cell lines by detachment and transfection in suspension. BioTechniques, 36 (5), 766-768, 770.

Amemiya, T., Hata, N., Mizoguchi, M., Yokokawa, R., Kawamura, Y., Hatae, R., Sangatsuda, Y., Kuga, D., Fujioka, Y., Takigawa, K., Akagi, Y., Yoshimoto, K., Iihara, K. & Miura, T. (2021) Mesenchymal glioblastoma-induced mature de-novo vessel formation of vascular endothelial cells in a microfluidic device. Molecular Biology Reports, 48 (1), 395-403.

An, Z., Aksoy, O., Zheng, T., Fan, Q. & Weiss, W. A. (2018) Epidermal growth factor receptor and EGFRvIII in glioblastoma: Signaling pathways and targeted therapies. Oncogene, 37 (12), 1561-1575.

Araque, A., Carmignoto, G. & Haydon, P. G. (2001) Dynamic signaling between astrocytes and neurons. Annual Review of Physiology, 63 795-813.

Araque, A., Parpura, V., Sanzgiri, R. P. & Haydon, P. G. (1999) Tripartite synapses: Glia, the unacknowledged partner. Trends in Neurosciences, 22 (5), 208-215.

Ariel D., S., Sivan, G., Ofer, P., Ayal, B. & Chaim, P. (2017) The blood brain barrier and neuropsychiatric lupus. Autoimmunity Reviews, 16 (6), 612-619.

Astolfi, M., Péant, B., Lateef, M. A., Rousset, N., Kendall-Dupont, J., Carmona, E., Monet, F., Saad, F., Provencher, D., Mes-Masson, A. -. & Gervais, T. (2016) Micro-dissected tumor tissues on chip: An ex vivo method for drug testing and personalized therapy. Lab on a Chip, 16 (2), 312-325.

Ayuso, J. M., Basheer, H. A., Monge, R., Sánchez-Álvarez, P., Doblaré, M., Shnyder, S. D., Vinader, V., Afarinkia, K., Fernández, L. J. & Ochoa, I. (2015) Study of the chemotactic response of multicellular spheroids in a microfluidic device. Plos One, 10 (10), e0139515.

Bachiller, S., Jiménez-Ferrer, I., Paulus, A., Yang, Y., Swanberg, M., Deierborg, T. & Boza-Serrano, A. (2018) Microglia in neurological diseases: A road map to brain-disease dependent-inflammatory response. Frontiers in Cellular Neuroscience, 12:488.

Bahreyni, A. & Luo, H. (2020) Advances in targeting cancer-associated genes by designed siRNA in prostate cancer. Cancers, 12 (12).

Baid, U., Rane, S. U., Talbar, S., Gupta, S., Thakur, M. H., Moiyadi, A. & Mahajan, A. (2020) Overall survival prediction in glioblastoma with radiomic features using machine learning. Frontiers in Computational Neuroscience, 14:61.

Bale, S. S., Manoppo, A., Thompson, R., Markoski, A., Coppeta, J., Cain, B., Haroutunian, N., Newlin, V., Spencer, A., Azizgolshani, H., Lu, M., Gosset, J., Keegan, P. & Charest, J. L. (2019) A thermoplastic microfluidic microphysiological system to recapitulate hepatic function and multicellular interactions. Biotechnology and Bioengineering, 116 (12), 3409-3420.

Ballabh, P., Braun, A. & Nedergaard, M. (2004) The blood–brain barrier: An overview: Structure, regulation, and clinical implications. Neurobiology of Disease, 16 (1), 1-13.

Banelli, B., Forlani, A., Allemanni, G., Morabito, A., Pistillo, M. P. & Romani, M. (2017) MicroRNAMicroRNA in glioblastoma: An overview. International Journal of Genomics, 2017 7639084.

Banerjee, K., Núñez, F. J., Haase, S., McClellan, B. L., Faisal, S. M., Carney, S. V., Yu, J., Alghamri, M. S., Asad, A. S., Candia, A. J. N., Varela, M. L., Candolfi, M., Lowenstein, P. R. & Castro, M. G. (2021) Current approaches for glioma gene therapy and virotherapy. Frontiers in Molecular Neuroscience, 14:62.

Banks, W. A., Kastin, A. J., Huang, W., Jaspan, J. B. & Maness, L. M. (1996) Leptin enters the brain by a saturable system independent of insulin. Peptides, 17 (2), 305-311.

Barbagallo, G. M. V., Altieri, R., Garozzo, M., Maione, M., Di Gregorio, S., Visocchi, M., Peschillo, S., Dolce, P. & Certo, F. (2020) High grade glioma treatment in elderly people: Is it different than in younger patients? analysis of surgical management guided by an intraoperative multimodal approach and its impact on clinical outcome. Frontiers in Oncology, 10 631255.

Barciszewska, A., Gurda, D., Głodowicz, P., Nowak, S. & Naskręt-Barciszewska, M. Z. (2015) A new epigenetic mechanism of temozolomide action in glioma cells. Plos One, 10 (8), e0136669.

Barnaby, S. N., Lee, A. & Mirkin, C. A. (2014) Probing the inherent stability of siRNA immobilized on nanoparticle constructs. Proceedings of the National Academy of Sciences of the United States of America, 111 (27), 9739-9744.

Bartlett, D. W. & Davis, M. E. (2006) Insights into the kinetics of siRNA-mediated gene silencing from live-cell and live-animal bioluminescent imaging. Nucleic Acids Research, 34 (1), 322-333.

Barzilai, A. (2013) The interrelations between malfunctioning DNA damage response (DDR) and the functionality of the neuro-glio-vascular unit. DNA Repair, 12 (8), 543-557.

Bassi, G., Panseri, S., Dozio, S. M., Sandri, M., Campodoni, E., Dapporto, M., Sprio, S., Tampieri, A. & Montesi, M. (2020) Scaffold-based 3D cellular models mimicking the heterogeneity of osteosarcoma stem cell niche. Scientific Reports, 10 (1), 1-12.

Batara, D. C. R., Choi, M., Shin, H., Kim, H. & Kim, S. (2021) Friend or foe: Paradoxical roles of autophagy in gliomagenesis. Cells, 10 (6), .

Batara, D. C. R., Choi, M., Shin, H., Kim, H. & Kim, S. (2021) Friend or foe: Paradoxical roles of autophagy in gliomagenesis. Cells, 10 (6), .

Bauer, H. & Traweger, A. (2016) Tight junctions of the blood-brain barrier - A molecular gatekeeper. CNS & Neurological Disorders Drug Targets, 15 (9), 1016-1029.

Bauer, M., Karch, R., Wulkersdorfer, B., Philippe, C., Nics, L., Klebermass, E., Weber, M., Poschner, S., Haslacher, H., Jäger, W., Tournier, N., Wadsak, W., Hacker, M., Zeitlinger, M. & Langer, O. (2019) A proof-of-concept study to inhibit ABCG2- and ABCB1-mediated efflux transport at the human blood-brain barrier. Journal of Nuclear Medicine: Official Publication, Society of Nuclear Medicine, 60 (4), 486-491.

Baumann, N. & Pham-Dinh, D. (2001) Biology of oligodendrocyte and myelin in the mammalian central nervous system. Physiological Reviews, 81 (2), 871-927.

Beauchesne, P., Bernier, V., Carnin, C., Taillandier, L., Djabri, M., Martin, L., Michel, X., Maire, J., Khalil, T., Kerr, C., Gorlia, T., Stupp, R. & Pedeux, R. (2010) Prolonged survival for patients with newly diagnosed, inoperable glioblastoma with 3-times daily ultrafractionated radiation therapy. Neuro-Oncology (Charlottesville, Va.), 12 (6), 595-602.

Beier, D., Schulz, J. B. & Beier, C. P. (2011) Chemoresistance of glioblastoma cancer stem cells--much more complex than expected. Molecular Cancer, 10 128.

Beiko, J., Suki, D., Hess, K. R., Fox, B. D., Cheung, V., Cabral, M., Shonka, N., Gilbert, M. R., Sawaya, R., Prabhu, S. S., Weinberg, J., Lang, F. F., Aldape, K. D., Sulman, E. P., Rao, G., McCutcheon, I. E. & Cahill, D. P. (2014) IDH1 mutant malignant astrocytomas are more amenable to surgical resection and have a survival benefit associated with maximal surgical resection. Neuro-Oncology, 16 (1), 81-91.

Berezhna, S. Y., Supekova, L., Supek, F., Schultz, P. G. & Deniz, A. A. (2006) siRNA in human cells selectively localizes to target RNA sites. Proceedings of the National Academy of Sciences of the United States of America, 103 (20), 7682-7687.

Bernacki, J., Dobrowolska, A., Nierwińska, K. & Małecki, A. (2008) Physiology and pharmacological role of the blood-brain barrier. Pharmacological Reports: PR, 60 (5), 600-622.

Bertuzzi, A., Fasano, A., Gandolfi, A. & Sinisgalli, C. (2010) Necrotic core in EMT6/ro tumour spheroids: Is it caused by an ATP deficit? Journal of Theoretical Biology, 262 (1), 142-150.

Bessis, A., Béchade, C., Bernard, D. & Roumier, A. (2007) Microglial control of neuronal death and synaptic properties. Glia, 55 (3), 233-238.

Bethesda, (. (2012) Temozolomide. In Anonymous LiverTox: Clinical and research information on drug-induced liver injury. Bethesda (MD): National Institute of Diabetes and Digestive and Kidney Diseases, .

Bette, S., Gempt, J., Huber, T., Delbridge, C., Meyer, B., Zimmer, C., Kirschke, J. S. & Boeckh-Behrens, T. (2017) FLAIR signal increase of the fluid within the resection cavity after glioma surgery: Generally valid as early recurrence marker? Journal of Neurosurgery, 127 (2), 417-425.

Betz, A. L. & Goldstein, G. W. (1978) Polarity of the blood-brain barrier: Neutral amino acid transport into isolated brain capillaries. Science (New York, N.Y.), 202 (4364), 225-227.

Bhattacharyya, D., Foote, R. S., Boulden, A. M. & Mitra, S. (1990) Physicochemical studies of human O6-methylguanine-DNA methyltransferase. European Journal of Biochemistry, 193 (2), 337-343.

Białkowska, K., Komorowski, P., Bryszewska, M. & Miłowska, K. (2020) Spheroids as a type of three-dimensional cell cultures-examples of methods of preparation and the most important application. International Journal of Molecular Sciences, 21 (17), .

Binder, S., Zipfel, I., Müller, C., Wiedemann, K., Schimmelpfennig, C., Pfeifer, G., Reiche, K., Hauschildt, S., Lehmann, J., Köhl, U., Horn, F. & Friedrich, M. (2021) The noncoding RNA LINC00152 conveys contradicting effects in different glioblastoma cells. Scientific Reports, 11 (1), 1-10.

Biró, O., Fóthi, Á, Alasztics, B., Nagy, B., Orbán, T. I. & Rigó, J. (2019) Circulating exosomal and argonaute-bound microRNAs in preeclampsia. Gene, 692 138-144.

Blake, A. J., Pearce, T. M., Rao, N. S., Johnson, S. M. & Williams, J. C. (2007) Multilayer PDMS microfluidic chamber for controlling brain slice microenvironment. Lab on a Chip, 7 (7), 842-849.

Blank, T. & Prinz, M. (2013) Microglia as modulators of cognition and neuropsychiatric disorders. Glia, 61 (1), 62-70.

Bobola, M. S., Emond, M. J., Blank, A., Meade, E. H., Kolstoe, D. D., Berger, M. S., Rostomily, R. C., Silbergeld, D. L., Spence, A. M. & Silber, J. R. (2004) Apurinic endonuclease activity in adult gliomas and time to tumor progression after alkylating agent-based chemotherapy and after radiotherapy. Clinical Cancer Research: An Official Journal of the American Association for Cancer Research, 10 (23), 7875-7883.

Bondy, M. L., Scheurer, M. E., Malmer, B., Barnholtz-Sloan, J. S., Davis, F. G., Il'yasova, D., Kruchko, C., McCarthy, B. J., Rajaraman, P., Schwartzbaum, J. A., Sadetzki, S., Schlehofer, B., Tihan, T., Wiemels, J. L., Wrensch, M. & Buffler, P. A. (2008) Brain tumor epidemiology: Consensus from the brain tumor epidemiology consortium. Cancer, 113 (7 Suppl), 1953-1968.

Bonifazi, P., D'Angelo, C., Zagarella, S., Zelante, T., Bozza, S., De Luca, A., Giovannini, G., Moretti, S., Iannitti, R. G., Fallarino, F., Carvalho, A., Cunha, C., Bistoni, F. & Romani, L. (2010) Intranasally delivered siRNA targeting PI3K/akt/mTOR inflammatory pathways protects from aspergillosis. Mucosal Immunology, 3 (2), 193-205.

Borawski, J., Lindeman, A., Buxton, F., Labow, M. & Gaither, L. A. (2007) Optimization procedure for small interfering RNA transfection in a 384-well format. J Biomol Screen, 12 (4), 546-559.

Boussommier-Calleja, A., Li, R., Chen, M. B., Wong, S. C. & Kamm, R. D. (2016) Microfluidics: A new tool for modeling cancer-immune interactions. Trends in Cancer, 2 (1), 6-19.

Bouzinab, K., Summers, H. S., Stevens, M. F. G., Moody, C. J., Thomas, N. R., Gershkovich, P., Weston, N., Ashford, M. B., Bradshaw, T. D. & Turyanska, L. (2020) Delivery of temozolomide and N3-propargyl analog to brain tumors using an apoferritin nanocage. ACS Applied Materials & Interfaces, 12 (11), 12609-12617.

Bowden, G. N., Kim, J. O., Faramand, A., Fallon, K., Flickinger, J. & Lunsford, L. D. (2020) Clinical dose profile of gamma knife stereotactic radiosurgery for extensive brain metastases. Journal of Neurosurgery, 134 (5), 1430-1434.

Bowden, S. G., Neira, J. A., Gill, B. J. A., Ung, T. H., Englander, Z. K., Zanazzi, G., Chang, P. D., Samanamud, J., Grinband, J., Sheth, S. A., McKhann, G. M., Sisti, M. B., Canoll, P., D'Amico, R. S. & Bruce, J. N. (2018) Sodium fluorescein facilitates guided sampling of diagnostic tumor tissue in nonenhancing gliomas. Neurosurgery, 82 (5), 719-727.

Bower, R., Green, V. L., Kuvshinova, E., Kuvshinov, D., Karsai, L., Crank, S. T., Stafford, N. D. & Greenman, J. (2017) Maintenance of head and neck tumor on-chip: Gateway to

Bradl, M. & Lassmann, H. (2010) Oligodendrocytes: Biology and pathology. Acta Neuropathologica, 119 (1), 37-53.

Bralten, L. B. C. & French, P. J. (2011) Genetic alterations in glioma. Cancers, 3 (1), 1129-1140.

Brandes, A. A., Franceschi, E., Paccapelo, A., Tallini, G., De Biase, D., Ghimenton, C., Danieli, D., Zunarelli, E., Lanza, G., Silini, E. M., Sturiale, C., Volpin, L., Servadei, F., Talacchi, A., Fioravanti, A., Pia Foschini, M., Bartolini, S., Pession, A. & Ermani, M. (2017) Role of MGMT methylation status at time of diagnosis and recurrence for patients with glioblastoma: Clinical implications. The Oncologist, 22 (4), 432-437.

Branter, J., Basu, S. & Smith, S. (2018) Tumour treating fields in a combinational therapeutic approach. Oncotarget, 9 (93), 36631-36644.

Brill, A., Dashevsky, O., Rivo, J., Gozal, Y. & Varon, D. (2005) Platelet-derived microparticles induce angiogenesis and stimulate post-ischemic revascularization. Cardiovascular Research, 67 (1), 30-38.

Brown, C. R., Gupta, S., Qin, J., Racie, T., He, G., Lentini, S., Malone, R., Yu, M., Matsuda, S., Shulga-Morskaya, S., Nair, A. V., Theile, C. S., Schmidt, K., Shahraz, A., Goel, V., Parmar, R. G., Zlatev, I., Schlegel, M. K., Nair, J. K., Jayaraman, M., Manoharan, M., Brown, D., Maier, M. A. & Jadhav, V. (2020) Investigating the pharmacodynamic durability of GalNAc-siRNA conjugates. Nucleic Acids Research, 48 (21), 11827-11844.

Brown, T. J., Brennan, M. C., Li, M., Church, E. W., Brandmeir, N. J., Rakszawski, K. L., Patel, A. S., Rizk, E. B., Suki, D., Sawaya, R. & Glantz, M. (2016) Association of the extent of resection with survival in glioblastoma: A systematic review and meta-analysis. JAMA Oncology, 2 (11), 1460-1469.

Browne, P. D., Nielsen, T. K., Kot, W., Aggerholm, A., Gilbert, M. T. P., Puetz, L., Rasmussen, M., Zervas, A. & Hansen, L. H. (2020) GC bias affects genomic and metagenomic reconstructions, underrepresenting GC-poor organisms. GigaScience, 9 (2), giaa008.

Browning, A. P., Sharp, J. A., Murphy, R. J., Gunasingh, G., Lawson, B., Burrage, K., Haass, N. K. & Simpson, M. (2021) Quantitative analysis of tumour spheroid structure. eLife, 10 .

Bustin, S. A. (2000) Absolute quantification of mRNA using real-time reverse transcription polymerase chain reaction assays. Journal of Molecular Endocrinology, 25 (2), 169-193.

Cahill, D. P., Levine, K. K., Betensky, R. A., Codd, P. J., Romany, C. A., Reavie, L. B., Batchelor, T. T., Futreal, P. A., Stratton, M. R., Curry, W. T., Iafrate, A. J. & Louis, D. N. (2007) Loss of the mismatch repair protein MSH6 in human glioblastomas is associated with tumor progression during temozolomide treatment. Clinical Cancer Research: An Official Journal of the American Association for Cancer Research, 13 (7), 2038-2045.

Cai, L., Qin, X., Xu, Z., Song, Y., Jiang, H., Wu, Y., Ruan, H. & Chen, J. (2019) Comparison of cytotoxicity evaluation of anticancer

Calcinotto, A., Kohli, J., Zagato, E., Pellegrini, L., Demaria, M. & Alimonti, A. (2019) Cellular senescence: Aging, cancer, and injury. Physiological Reviews, 99 (2), 1047-1078.

Cancer Genome Atlas Research Network (2008) Comprehensive genomic characterization defines human glioblastoma genes and core pathways. Nature, 455 (7216), 1061-1068.

cancer research uk (2021) Children's cancer statistics. Available online: https://www.cancerresearchuk.org [Accessed accessed oct 2021].

Carr, S. D., Green, V. L., Stafford, N. D. & Greenman, J. (2014) Analysis of radiation-induced cell death in head and neck squamous cell carcinoma and rat liver maintained in microfluidic devices. Otolaryngology--Head and Neck Surgery: Official Journal of American Academy of Otolaryngology-Head and Neck Surgery, 150 (1), 73-80.

Castells, M., Thibault, B., Delord, J. & Couderc, B. (2012) Implication of tumor microenvironment in chemoresistance: Tumor-associated stromal cells protect tumor cells from cell death. International Journal of Molecular Sciences, 13 (8), 9545-9571.

Caudle, R. M. (2006) Memory in astrocytes: A hypothesis. Theoretical Biology & Medical Modelling, 3 2.

Chan, J. A., Krichevsky, A. M. & Kosik, K. S. (2005) MicroRNAMicroRNA-21 is an antiapoptotic factor in human glioblastoma cells. Cancer Research, 65 (14), 6029-6033.

Chang, J. E., Khuntia, D., Robins, H. I. & Mehta, M. P. (2007) Radiotherapy and radiosensitizers in the treatment of glioblastoma multiforme. Clinical Advances in Hematology & Oncology: H&O, 5 (11), 894-915.

Chang, T. C., Mikheev, A. M., Huynh, W., Monnat, R. J., Rostomily, R. C. & Folch, A. (2014) Parallel microfluidic chemosensitivity testing on individual slice cultures. Lab on a Chip, 14 (23), 4540-4551.

Cheah, R., Srivastava, R., Stafford, N. D., Beavis, A. W., Green, V. & Greenman, J. (2017) Measuring the response of human head and neck squamous cell carcinoma to irradiation in a microfluidic model allowing customized therapy. International Journal of Oncology, 51 (4), 1227-1238.

Chen, F., Dong, M., Ge, M., Zhu, L., Ren, L., Liu, G. & Mu, R. (2013) The history and advances of reversible terminators used in new generations of sequencing technology. Genomics, Proteomics & Bioinformatics, 11 (1), 34-40.

Chen, G., Zhang, Y., Qadri, Y. J., Serhan, C. N. & Ji, R. (2018) Microglia in pain: Detrimental and protective roles in pathogenesis and resolution of pain. Neuron, 100 (6), 1292-1311.

Chen, L., Zeng, D., Xu, N., Li, C., Zhang, W., Zhu, X., Gao, Y., Chen, P. R. & Lin, J. (2019) Blood–Brain barrier- and Blood–Brain tumor barrier-penetrating peptide-derived targeted therapeutics for glioma and malignant tumor brain metastases. ACS Applied Materials & Interfaces, 11 (45), 41889-41897.

Chen, Y. & Liu, L. (2012) Modern methods for delivery of drugs across the blood-brain barrier. Advanced Drug Delivery Reviews, 64 (7), 640-665.

Chen, Y., Gao, D., Liu, H., Lin, S. & Jiang, Y. (2015) Drug cytotoxicity and signaling pathway analysis with three-dimensional tumor spheroids in a microwell-based microfluidic chip for drug screening. Analytica Chimica Acta, 898 85-92.

Chen, Y., Liu, T., Yu, C., Chiang, T. & Hwang, C. (2013) Effects of GC bias in next-generation-sequencing data on de novo genome assembly. PloS One, 8 (4), e62856.

chia, D. k., Davies, M. R. & Brazil, D. L. (2017) Pp13. chernobyl, brexit and brain tumours. Neuro-Oncology, 19 (suppl_1), i4-i4.

Cho, A., Jin, Y., An, Y., Kim, J., Choi, Y. S., Lee, J. S., Kim, J., Choi, W., Koo, D., Yu, W., Chang, G., Kim, D., Jo, S., Kim, J., Kim, S., Kim, Y., Kim, J. Y., Choi, N., Cheong, E., Kim, Y., Je, H. S., Kang, H. & Cho, S. (2021) Microfluidic device with brain extracellular matrix promotes structural and functional maturation of human brain organoids. Nature Communications, 12 (1), 1-23.

Cho, A., Jin, Y., An, Y., Kim, J., Choi, Y. S., Lee, J. S., Kim, J., Choi, W., Koo, D., Yu, W., Chang, G., Kim, D., Jo, S., Kim, J., Kim, S., Kim, Y., Kim, J. Y., Choi, N., Cheong, E., Kim, Y., Je, H. S., Kang, H. & Cho, S. (2021) Microfluidic device with brain extracellular matrix promotes structural and functional maturation of human brain organoids. Nature Communications, 12 (1), 1-23.

Choi, Y. Y., Kim, J., Lee, S. & Kim, D. (2016) Lab on a chip-based hepatic sinusoidal system simulator for optimal primary hepatocyte culture. Biomedical Microdevices, 18 (4), 58.

Choi, Y., Hyun, E., Seo, J., Blundell, C., Kim, H. C., Lee, E., Lee, S. H., Moon, A., Moon, W. K. & Huh, D. (2015) A microengineered pathophysiological model of early-stage breast cancer. Lab on a Chip, 15 (16), 3350-3357.

Choi, Y., McClain, M. A., LaPlaca, M. C., Frazier, A. B. & Allen, M. G. (2007) Three dimensional MEMS microfluidic perfusion system for thick brain slice cultures. Biomedical Microdevices, 9 (1), 7-13.

Christmann, M., Nagel, G., Horn, S., Krahn, U., Wiewrodt, D., Sommer, C. & Kaina, B. (2010) MGMT activity, promoter methylation and immunohistochemistry of pretreatment and recurrent malignant gliomas: A comparative study on astrocytoma and glioblastoma. International Journal of Cancer, 127 (9), 2106-2118.

Christoffersson, J., Meier, F., Kempf, H., Schwanke, K., Coffee, M., Beilmann, M., Zweigerdt, R. & Mandenius, C. (2018) A cardiac cell outgrowth assay for evaluating drug compounds using a cardiac spheroid-on-a-chip device. Bioengineering, 5 (2), .

Chung, C., Sweha, S. R., Pratt, D., Tamrazi, B., Panwalkar, P., Banda, A., Bayliss, J., Hawes, D., Yang, F., Lee, H., Shan, M., Cieslik, M., Qin, T., Werner, C. K., Wahl, D. R., Lyssiotis, C. A., Bian, Z., Shotwell, J. B., Yadav, V. N., Koschmann, C., Chinnaiyan, A. M., Blüml, S., Judkins, A. R. & Venneti, S. (2020) Integrated metabolic and epigenomic reprograming by H3K27M mutations in diffuse intrinsic pontine gliomas. Cancer Cell, 38 (3), 334-349.e9.

Chung, W., Allen, N. J. & Eroglu, C. (2015) Astrocytes control synapse formation, function and elimination. Cold Spring Harbor Perspectives in Biology, 7 (9), a020370.

Coffey, R. J., Lunsford, L. D. & Taylor, F. H. (1988) Survival after stereotactic biopsy of malignant gliomas. Neurosurgery, 22 (3), 465-473.

Collins, T., Pyne, E., Christensen, M., Iles, A., Pamme, N. & Pires, I. M. (2021) Spheroid-on-chip microfluidic technology for the evaluation of the impact of continuous flow on metastatic potential in cancer models in vitro. Biomicrofluidics, 15 (4), 044103.

Colonna, M. & Butovsky, O. (2017) Microglia function in the central nervous system during health and neurodegeneration. Annual Review of Immunology, 35 (1), 441-468.

Coomber, B. L. & Stewart, P. A. (1985) Morphometric analysis of CNS microvascular endothelium. Microvascular Research, 30 (1), 99-115.

Cordon-Cardo, C., O'Brien, J. P., Casals, D., Rittman-Grauer, L., Biedler, J. L., Melamed, M. R. & Bertino, J. R. (1989) Multidrug-resistance gene (P-glycoprotein) is expressed by endothelial cells at blood-brain barrier sites. Proceedings of the National Academy of Sciences of the United States of America, 86 (2), 695-698.

Cortés-Ríos, J., Zárate, A. M., Figueroa, J. D., Medina, J., Fuentes-Lemus, E., Rodríguez-Fernández, M., Aliaga, M. & López-Alarcón, C. (2020) Protein quantification by bicinchoninic acid (BCA) assay follows complex kinetics and can be performed at short incubation times. Analytical Biochemistry, 608 113904.

Costa, P. M., Cardoso, A. L., Nóbrega, C., Pereira de Almeida, Luís F., Bruce, J. N., Canoll, P. & Pedroso de Lima, Maria C. (2013) MicroRNAMicroRNA-21 silencing enhances the cytotoxic effect of the antiangiogenic drug sunitinib in glioblastoma. Human Molecular Genetics, 22 (5), 904-918.

Crespo, I., Vital, A. L., Gonzalez-Tablas, M., Patino, M. d. C., Otero, A., Lopes, M. C., de Oliveira, C., Domingues, P., Orfao, A. & Tabernero, M. D. (2015) Molecular and genomic alterations in glioblastoma multiforme. The American Journal of Pathology, 185 (7), 1820-1833.

Cui, X., Ma, C., Vasudevaraja, V., Serrano, J., Tong, J., Peng, Y., Delorenzo, M., Shen, G., Frenster, J., Morales, R. T., Qian, W., Tsirigos, A., Chi, A. S., Jain, R., Kurz, S. C., Sulman, E. P., Placantonakis, D. G., Snuderl, M. & Chen, W. (2020) Dissecting the immunosuppressive tumor microenvironments in glioblastoma-on-a-chip for optimized PD-1 immunotherapy. eLife, 9:e52253.

Cui, Y., Wang, Q., Wang, J., Dong, Y., Luo, C., Hu, G. & Lu, Y. (2012) Knockdown of AKT2 expression by RNA interference inhibits proliferation, enhances apoptosis, and increases chemosensitivity to the anticancer drug VM-26 in U87 glioma cells. Brain Research, 1469 1-9.

Cura, V. & Cavarelli, J. (2021) Structure, activity and function of the PRMT2 protein arginine methyltransferase. Life (Basel, Switzerland), 11 (11).

D'Alessio, A., Proietti, G., Sica, G. & Scicchitano, B. M. (2019) Pathological and molecular features of glioblastoma and its peritumoral tissue. Cancers, 11 (4).

Dadgar, N., Gonzalez-Suarez, A. M., Fattahi, P., Hou, X., Weroha, J. S., Gaspar-Maia, A., Stybayeva, G. & Revzin, A. (2020) A microfluidic platform for cultivating ovarian cancer spheroids and testing their responses to chemotherapies. Microsystems & Nanoengineering, 6 (1), 1-12.

Daneman, R. & Prat, A. (2015) The blood-brain barrier. Cold Spring Harbor Perspectives in Biology, 7 (1), a020412.

Daneman, R. (2012) The blood-brain barrier in health and disease. Annals of Neurology, 72 (5), 648-672.

Daneman, R., Zhou, L., Agalliu, D., Cahoy, J. D., Kaushal, A. & Barres, B. A. (2010) The mouse blood-brain barrier transcriptome: A new resource for understanding the development and function of brain endothelial cells. PloS One, 5 (10), e13741.

Dani, J. W., Chernjavsky, A. & Smith, S. J. (1992) Neuronal activity triggers calcium waves in hippocampal astrocyte networks. Neuron, 8 (3), 429-440.

Dar, S. A., Thakur, A., Qureshi, A. & Kumar, M. (2016) siRNAmod: A database of experimentally validated chemically modified siRNAs. Scientific Reports, 6 (1), 20031.

Das, D., Karthik, N. & Taneja, R. (2021) Crosstalk between inflammatory signaling and methylation in cancer. Frontiers in Cell and Developmental Biology, 0 .

Das, K. K. & Kumar, R. (2017) Pediatric glioblastoma. In Steven De Vleeschouwer (ed) Glioblastoma. Brisbane (AU): Codon Publications, .

Das, T., Meunier, L., Barbe, L., Provencher, D., Guenat, O., Gervais, T. & Mes-Masson, A. (2013) Empirical chemosensitivity testing in a spheroid model of ovarian cancer using a microfluidics-based multiplex platform. Biomicrofluidics, 7 (1), 11805.

Davalos, D., Grutzendler, J., Yang, G., Kim, J. V., Zuo, Y., Jung, S., Littman, D. R., Dustin, M. L. & Gan, W. (2005) ATP mediates rapid microglial response to local brain injury *in vivo*. Nature Neuroscience, 8 (6), 752-758.

Davis, M. E. (2016a) Glioblastoma: Overview of disease and treatment. Clinical Journal of Oncology Nursing, 20 (5), S2-S8.

Davis, M. E. (2018) Epidemiology and overview of gliomas. Seminars in Oncology Nursing, 34 (5), 420-429.

Dawson, A., Greenman, J., Bower, R. & Green, V. (2016) Microfluidics: The fur-free way towards personalised medicine in cancer therapy. 3 (1), 12-17.

de Boer, A. G. & Gaillard, P. J. (2007) Drug targeting to the brain. Annual Review of Pharmacology and Toxicology, 47 323-355.

Decarli, M. C., Amaral, R., Santos, D. P. d., Tofani, L. B., Katayama, E., Rezende, R. A., Silva, Jorge Vicente Lopes da, Swiech, K., Suazo, C. A. T., Mota, C., Moroni, L. & Moraes, Â M. (2021) Cell spheroids as a versatile research platform: Formation mechanisms, high throughput production, characterization and applications. Biofabrication, 13 (3), 032002.

Dehghannasiri, R., Olivieri, J. E., Damljanovic, A. & Salzman, J. (2021) Specific splice junction detection in single cells with SICILIAN. Genome Biology, 22 (1), 219.

Demeule, M., Currie, J., Bertrand, Y., Ché, C., Nguyen, T., Régina, A., Gabathuler, R., Castaigne, J. & Béliveau, R. (2008) Involvement of the low-density lipoprotein receptor-related protein in the transcytosis of the brain delivery vector angiopep-2. Journal of Neurochemistry, 106 (4), 1534-1544.

Dheda, K., Huggett, J. F., Bustin, S. A., Johnson, M. A., Rook, G. & Zumla, A. (2004) Validation of housekeeping genes for normalizing RNA expression in real-time PCR. BioTechniques, 37 (1), 112-119.

Diao, W., Tong, X., Yang, C., Zhang, F., Bao, C., Chen, H., Liu, L., Li, M., Ye, F., Fan, Q., Wang, J. & Ou-Yang, Z. (2019) Behaviors of glioblastoma cells in in vitro microenvironments. Scientific Reports, 9 (1), 1-9.

Ding, Z., Zhang, Z., Luo, D., Zhou, J., Zhong, J., Yang, J., Xiao, L., Shu, D. & Tan, H. (2015) Gene overexpression and RNA silencing tools for the genetic manipulation of the S-(+)-abscisic acid producing ascomycete botrytis cinerea. International Journal of Molecular Sciences, 16 (5), 10301-10323.

Dmytriw, A. A. & Pickett, G. E. (2013) Glioblastoma in a former chernobyl resident 24 years later. CMAJ : Canadian Medical Association Journal, 185 (13), 1154-1157.

Domingo-Musibay, E. & Galanis, E. (2015) What next for newly diagnosed glioblastoma? Future Oncology, 11 (24), 3273-3283.

Dong, F., Li, Q., Yang, C., Huo, D., Wang, X., Ai, C., Kong, Y., Sun, X., Wang, W., Zhou, Y., Liu, X., Li, W., Gao, W., Liu, W., Kang, C. & Wu, X. (2018) PRMT2 links histone H3R8 asymmetric dimethylation to oncogenic activation and tumorigenesis of glioblastoma. Nature Communications, 9 (1), 1-14.

Dong, S. X. M., Caballero, R., Ali, H., Roy, D. L. F., Cassol, E. & Kumar, A. (2020) Transfection of hard-to-transfect primary human macrophages with bax siRNA to reverse resveratrol-induced apoptosis. RNA Biology, 17 (6), 755-764.

Douple, E. B., Mabuchi, K., Cullings, H. M., Preston, D. L., Kodama, K., Shimizu, Y., Fujiwara, S. & Shore, R. E. (2011) Long-term radiation-related health effects in a unique human population: Lessons learned from the atomic bomb survivors of hiroshima and nagasaki. Disaster Medicine and Public Health Preparedness, 5 (0 1), S122-S133.

Du Rietz, H., Hedlund, H., Wilhelmson, S., Nordenfelt, P. & Wittrup, A. (2020) Imaging small molecule-induced endosomal escape of siRNA. Nature Communications, 11 (1), 1809.

Duivenvoorden, H. M., Brockwell, N. K., Nowell, C. J., Simpson, K. J. & Parker, B. S. (2021) High-content siRNA 3D co-cultures to identify myoepithelial cell-derived breast cancer suppressor proteins. Scientific Data, 8 (1), 147.

Eelen, G., de Zeeuw, P., Treps, L., Harjes, U., Wong, B. W. & Carmeliet, P. (2018) Endothelial cell metabolism. Physiological Reviews, 98 (1), 3-58.

Ehrenberg, K. R., Gao, J., Oppel, F., Frank, S., Kang, N., Kindinger, T., Dieter, S. M., Herbst, F., Möhrmann, L., Dubash, T. D., Schulz, E. R., Strakerjahn, H., Giessler, K. M., Weber, S., Oberlack, A., Rief, E., Strobel, O., Bergmann, F., Lasitschka, F., Weitz, J., Glimm, H. & Ball, C. R. (2019) Systematic generation of patient-derived tumor models in pancreatic cancer. Cells, 8 (2).

Eissa, N., Kermarrec, L., Hussein, H., Bernstein, C. N. & Ghia, J. (2017) Appropriateness of reference genes for normalizing messenger RNA in mouse 2,4-dinitrobenzene sulfonic acid (DNBS)-induced colitis using quantitative real time PCR. Scientific Reports, 7 (1), 42427.

Elbashir, S. M., Harborth, J., Lendeckel, W., Yalcin, A., Weber, K. & Tuschl, T. (2001) Duplexes of 21-nucleotide RNAs mediate RNA interference in cultured mammalian cells. Nature, 411 (6836), 494-498.

Erlich, Y., Mitra, P. P., delaBastide, M., McCombie, W. R. & Hannon, G. J. (2008) Alta-cyclic: A self-optimizing base caller for next-generation sequencing. Nature Methods, 5 (8), 679-682.

Esteller, M., Garcia-Foncillas, J., Andion, E., Goodman, S. N., Hidalgo, O. F., Vanaclocha, V., Baylin, S. B. & Herman, J. G. (2000) Inactivation of the DNA-repair gene MGMT and the clinical response of gliomas to alkylating agents. The New England Journal of Medicine, 343 (19), 1350-1354.

Fael Al-Mayhani, T. M., Ball, S. L. R., Zhao, J., Fawcett, J., Ichimura, K., Collins, P. V. & Watts, C. (2009) An efficient method for derivation and propagation of glioblastoma cell lines that conserves the molecular profile of their original tumours. Journal of Neuroscience Methods, 176 (2), 192-199.

Faivre, G., Pentsova, E., Demopoulos, A., Taillibert, S., Rosenblum, M. & Omuro, A. (2015) Clinical reasoning: Worsening neurologic symptoms in a brain tumor patient. Neurology, 85 (7), e57-e61.

Fan, X., Roberts, D. W., Schaewe, T. J., Ji, S., Holton, L. H., Simon, D. A. & Paulsen, K. D. (2017) Intraoperative image updating for brain shift following dural opening. Journal of Neurosurgery, 126 (6), 1924-1933.

Fan, Y., Nguyen, D. T., Akay, Y., Xu, F. & Akay, M. (2016) Engineering a brain cancer chip for high-throughput drug screening. Scientific Reports, 6 (1), 25062.

Feitelson, M. A., Arzumanyan, A., Kulathinal, R. J., Blain, S. W., Holcombe, R. F., Mahajna, J., Marino, M., Martinez-Chantar, M. L., Nawroth, R., Sanchez-Garcia, I., Sharma, D., Saxena, N. K., Singh, N., Vlachostergios, P. J., Guo, S., Honoki, K., Fujii, H., Georgakilas, A. G., Bilsland, A., Amedei, A., Niccolai, E., Amin, A., Ashraf, S. S., Boosani, C. S., Guha, G., Ciriolo, M. R., Aquilano, K., Chen, S., Mohammed, S. I., Azmi, A. S., Bhakta, D., Halicka, D., Keith, W. N. & Nowsheen, S. (2015) Sustained proliferation in cancer: Mechanisms and novel therapeutic targets. Seminars in Cancer Biology, 35 S25-S54.

Fellmann, C. & Lowe, S. W. (2014) Stable RNA interference rules for silencing. Nature Cell Biology, 16 (1), 10-18.

Felsberg, J., Thon, N., Eigenbrod, S., Hentschel, B., Sabel, M. C., Westphal, M., Schackert, G., Kreth, F. W., Pietsch, T., Löffler, M., Weller, M., Reifenberger, G. & Tonn, J. C. (2011) Promoter methylation and expression of MGMT and the DNA mismatch repair genes MLH1, MSH2, MSH6 and PMS2 in paired primary and recurrent glioblastomas. International Journal of Cancer, 129 (3), 659-670.

Feng, F., Huang, C., Xiao, M., Wang, H., Gao, Q., Chen, Z., Xu, X., Zhou, J., Li, F., Li, Y., Zhang, D., Chang, Y. & Jiang, X. (2020) Establishment and characterization of patient-derived primary cell lines as preclinical models for gallbladder carcinoma. Translational Cancer Research, 9 (3), 1698-1710.

Ferri, A., Stagni, V. & Barilà, D. (2020) Targeting the DNA damage response to overcome cancer drug resistance in glioblastoma. International Journal of Molecular Sciences, 21 (14), .

Fields, R. D. & Stevens-Graham, B. (2002) New insights into neuron-glia communication. Science (New York, N.Y.), 298 (5593), 556-562.

Fillebeen, C., Descamps, L., Dehouck, M. P., Fenart, L., Benaïssa, M., Spik, G., Cecchelli, R. & Pierce, A. (1999) Receptor-mediated transcytosis of lactoferrin through the blood-brain barrier. The Journal of Biological Chemistry, 274 (11), 7011-7017.

Fisher, J. L., Schwartzbaum, J. A., Wrensch, M. & Wiemels, J. L. (2007) Epidemiology of brain tumors. Neurologic Clinics, 25 (4), 867-890, vii.

Freeley, M., Derrick, E., Dempsey, E., Hoff, A., Davies, A., Leake, D., Vermeulen, A., Kelleher, D. & Long, A. (2015) RNAi screening with self-delivering, synthetic siRNAs for identification of genes that regulate primary human T cell migration. Journal of Biomolecular Screening, 20 (8), 943-956.

Freitas, F. C. P., Depintor, T. S., Agostini, L. T., Luna-Lucena, D., Nunes, F. M. F., Bitondi, M. M. G., Simões, Z. L. P. & Lourenço, A. P. (2019) Evaluation of reference genes for gene expression analysis by real-time quantitative PCR (qPCR) in three stingless bee species (hymenoptera: Apidae: Meliponini). Scientific Reports, 9 (1), 17692.

Friedlein, K., Bozhkov, Y., Hore, N., Merkel, A., Sommer, B., Brandner, S., Buchfelder, M., Savaskan, N. E. & Eyüpoglu, I. Y. (2015) A new functional classification system (FGA/B) with prognostic value for glioma patients. Scientific Reports, 5 (1), 12373.

Frimat, J. & Luttge, R. (2019) The need for physiological micro-nanofluidic systems of the brain. Frontiers in Bioengineering and Biotechnology, 0 .

Fröhlich, E., Bonstingl, G., Höfler, A., Meindl, C., Leitinger, G., Pieber, T. R. & Roblegg, E. (2013) Comparison of two in vitro systems to assess cellular effects of nanoparticles-containing aerosols. Toxicology in Vitro, 27-360 (1), 409-417.

Fu, C., Tseng, S., Yang, S., Hsu, L., Liu, C. & Chang, H. (2014) A microfluidic chip with a U-shaped microstructure array for multicellular spheroid formation, culturing and analysis. Biofabrication, 6 (1), 015009.

Fu, Y., Yang, J., Wang, X., Yang, P., Zhao, Y., Li, K., Chen, Y. & Xu, Y. (2018) Herbal compounds play a role in neuroprotection through the inhibition of microglial activation. Hindawi. Available online: https://www.hindawi.com/journals/jir/2018/9348046/ [Accessed Feb 7, 2020].

Fujisawa, H., Reis, R. M., Nakamura, M., Colella, S., Yonekawa, Y., Kleihues, P. & Ohgaki, H. (2000) Loss of heterozygosity on chromosome 10 is more extensive in primary (de novo) than in secondary glioblastomas. Laboratory Investigation; a Journal of Technical Methods and Pathology, 80 (1), 65-72.

Furukawa, K., Tanaka, M. & Oba, M. (2020) siRNA delivery using amphipathic cell-penetrating peptides into human hepatoma cells. Bioorganic & Medicinal Chemistry, 28 (8), 115402.

Gaillard, P. J., Appeldoorn, C. C. M., Rip, J., Dorland, R., van der Pol, Susanne M. A., Kooij, G., de Vries, H. E. & Reijerkerk, A. (2012) Enhanced brain delivery of liposomal methylprednisolone improved therapeutic efficacy in a model of neuroinflammation. Journal of Controlled Release: Official Journal of the Controlled Release Society, 164 (3), 364-369.

Galon, J., Pagès, F., Marincola, F. M., Angell, H. K., Thurin, M., Lugli, A., Zlobec, I., Berger, A., Bifulco, C., Botti, G., Tatangelo, F., Britten, C. M., Kreiter, S., Chouchane, L., Delrio, P., Arndt, H., Asslaber, M., Maio, M., Masucci, G. V., Mihm, M., Vidal-Vanaclocha, F., Allison, J. P., Gnjatic, S., Hakansson, L., Huber, C., Singh-Jasuja, H., Ottensmeier, C., Zwierzina, H., Laghi, L., Grizzi, F., Ohashi, P. S., Shaw, P. A., Clarke, B. A., Wouters, B. G., Kawakami, Y., Hazama, S., Okuno, K., Wang, E., O'Donnell-Tormey, J., Lagorce, C., Pawelec, G., Nishimura, M. I., Hawkins, R., Lapointe, R., Lundqvist, A., Khleif, S. N., Ogino, S., Gibbs, P., Waring, P., Sato, N., Torigoe, T., Itoh, K., Patel, P. S., Shukla, S. N., Palmqvist, R., Nagtegaal, I. D., Wang, Y., D'Arrigo, C., Kopetz, S., Sinicrope, F. A., Trinchieri, G., Gajewski, T. F., Ascierto, P. A. & Fox, B. A. (2012) Cancer classification using the immunoscore: A worldwide task force. Journal of Translational Medicine, 10 205.

Gan, H. K., Cvrljevic, A. N. & Johns, T. G. (2013) The epidermal growth factor receptor variant III (EGFRvIII): Where wild things are altered. The FEBS Journal, 280 (21), 5350-5370.

Garcia, J. H., Jain, S. & Aghi, M. K. (2021) Metabolic drivers of invasion in glioblastoma. Frontiers in Cell and Developmental Biology, 9 683276.

Garcia-Segura, L. M. & McCarthy, M. M. (2004) Minireview: Role of glia in neuroendocrine function. Endocrinology, 145 (3), 1082-1086.

GBD 2016 Brain and Other CNS Cancer Collaborators (2019) Global, regional, and national burden of brain and other CNS cancer, 1990-2016: A systematic analysis for the global burden of disease study 2016. The Lancet. Neurology, 18 (4), 376-393.

GBD 2017 DALYs and HALE Collaborators, Bisanzio, D., Shokraneh, F. & Williams, H. C. (2018) Global, regional, and national disability-adjusted life-years (DALYs) for 359 diseases and injuries and healthy life expectancy (HALE) for 195 countries and territories, 1990–2017: A systematic analysis for the global burden of disease study 2017. The Lancet, 392 (10159), 1859-1922.

Ge, J., Chen, Q., Liu, B., Wang, L., Zhang, S. & Ji, B. (2017a) Knockdown of Rab21 inhibits proliferation and induces apoptosis in human glioma cells. Cellular & Molecular Biology Letters, 22 30.

Gencturk, E., Mutlu, S. & Ulgen, K. O. (2017) Advances in microfluidic devices made from thermoplastics used in cell biology and analyses. United States: AIP Publishing LLC.

Genzen, J. R., Platel, J., Rubio, M. E. & Bordey, A. (2009) Ependymal cells along the lateral ventricle express functional P2X(7) receptors. Purinergic Signalling, 5 (3), 299-307.

Geramizadeh, B., Kohandel-Shirazi, M. & Soltani, A. (2021) A simple panel of IDH1 and P53 in differential diagnosis between low-grade astrocytoma and reactive gliosis. Clinical Pathology, 14 2632010X20986168.

Gerigk, M., Bulstrode, H., Shi, H. H., Tönisen, F., Cerutti, C., Morrison, G., Rowitch, D. & Huang, Y. Y. S. (2021) On-chip perivascular niche supporting stemness of patient-derived glioma cells in a serum-free, flowable culture. Lab on a Chip, 21 (12), 2343-2358.

Gerson, S. L. (2002) Clinical relevance of MGMT in the treatment of cancer. Journal of Clinical Oncology: Official Journal of the American Society of Clinical Oncology, 20 (9), 2388-2399.

Ghaffari, H., Grant, S. C., Petzold, L. R. & Harrington, M. G. (2020) Regulation of CSF and brain tissue sodium levels by the blood-CSF and blood-brain barriers during migraine. Frontiers in Computational Neuroscience, 0 .

Gheibi, P., Zeng, S., Son, K. J., Vu, T., Ma, A., Dall'Era, M. A., Yap, S. A., de Vere White, Ralph W., Pan, C. & Revzin, A. (2017) Microchamber cultures of bladder cancer: A platform for characterizing drug responsiveness and resistance in PDX and primary cancer cells. Scientific Reports, 7 (1), 12277.

Gielen, P. R., Aftab, Q., Ma, N., Chen, V. C., Hong, X., Lozinsky, S., Naus, C. C. & Sin, W. C. (2013) Connexin43 confers temozolomide resistance in human glioma cells by modulating the mitochondrial apoptosis pathway. Neuropharmacology, 75 539-548.

Gilbert, D. F., Mofrad, S. A., Friedrich, O. & Wiest, J. (2019) Proliferation characteristics of cells cultured under periodic versus static conditions. Cytotechnology, 71 (1), 443-452.

Gingrich, M. B. & Traynelis, S. F. (2000) Serine proteases and brain damage - is there a link? Trends in Neurosciences, 23 (9), 399-407.

Ginhoux, F. & Prinz, M. (2015) Origin of microglia: Current concepts and past controversies. Cold Spring Harbor Perspectives in Biology, 7 (8).

Gkretsi, V. & Stylianopoulos, T. (2018) Cell adhesion and matrix stiffness: Coordinating cancer cell invasion and metastasis. Frontiers in Oncology, 8 .

Goldmann, T. & Prinz, M. (2013) Role of microglia in CNS autoimmunity. Clinical & Developmental Immunology, 2013 208093.

Gong, X., Lin, C., Cheng, J., Su, J., Zhao, H., Liu, T., Wen, X. & Zhao, P. (2015) Generation of multicellular tumor spheroids with microwell-based agarose scaffolds for drug testing. PloS One, 10 (6), e0130348.

Gopal, S., Kwon, S., Ku, B., Lee, D. W., Kim, J. & Dordick, J. S. (2021) 3D tumor spheroid microarray for high-throughput, high-content natural killer cell-mediated cytotoxicity. Communications Biology, 4 (1), 1-14.

Gordon, R. & Woodruff, T. M. (2017) Chapter 3 - neuroinflammation as a therapeutic target in neurodegenerative diseases. In Veerle Baekelandt and Evy Lobbestael (eds) Disease-modifying targets in neurodegenerative disorders. Academic Press, 49-80.

GOSSELIN, R., SUTER, M. R., JI, R. & DECOSTERD, I. (2010) Glial cells and chronic pain. The Neuroscientist: A Review Journal Bringing Neurobiology, Neurology and Psychiatry, 16 (5), 519-531.

Grant, L. M., Kleiner, D. E., Conjeevaram, H. S., Vuppalanchi, R. & Lee, W. M. (2013) Clinical and histological features of idiosyncratic acute liver injury caused by temozolomide. Digestive Diseases and Sciences, 58 (5), 1415-1421.

Grasbon-Frodl, E. M., Kreth, F. W., Ruiter, M., Schnell, O., Bise, K., Felsberg, J., Reifenberger, G., Tonn, J. & Kretzschmar, H. A. (2007) Intratumoral homogeneity of MGMT promoter hypermethylation as demonstrated in serial stereotactic specimens from anaplastic astrocytomas and glioblastomas. International Journal of Cancer, 121 (11), 2458-2464.

Greten, F. R. & Grivennikov, S. I. (2019) Inflammation and cancer: Triggers, mechanisms, and consequences. Immunity, 51 (1), 27-41.

Grewal, J., Dellinger, C. A. & Yung, W. K. A. (2007) Fatal reactivation of hepatitis B with temozolomide. The New England Journal of Medicine, 356 (15), 1591-1592.

Grimes, D. R. & Currell, F. J. (2018) Oxygen diffusion in ellipsoidal tumour spheroids. Journal of the Royal Society Interface, 15 (145), 20180256.

Grosser, S., Lippoldt, J., Oswald, L., Merkel, M., Sussman, D. M., Renner, F., Gottheil, P., Morawetz, E. W., Fuhs, T., Xie, X., Pawlizak, S., Fritsch, A. W., Wolf, B., Horn, L., Briest, S., Aktas, B., Manning, M. L. & Käs, J. A. (2021) Cell and nucleus shape as an indicator of tissue fluidity in carcinoma. Physical Review. X, 11 (1), 011033.

Gu, J., Wang, J., Liu, X., Sai, K., Mai, J., Xing, F., Chen, Z., Yang, X., Lu, W., Guo, C., Liu, W., Xu, Y., Xie, S., Hu, C., Yan, G. & Zhu, W. (2021) IL-6 derived from therapy-induced senescence facilitates the glycolytic phenotype in glioblastoma cells. American Journal of Cancer Research, 11 (2), 458-478.

Gudbergsson, J. M., Kostrikov, S., Johnsen, K. B., Fliedner, F. P., Stolberg, C. B., Humle, N., Hansen, A. E., Kristensen, B. W., Christiansen, G., Kjær, A., Andresen, T. L. & Duroux, M. (2019) A tumorsphere model of glioblastoma multiforme with intratumoral heterogeneity for quantitative analysis of cellular migration and drug response. Experimental Cell Research, 379 (1), 73-82.

Guerra-Gomes, S., Sousa, N., Pinto, L. & Oliveira, J. F. (2018) Functional roles of astrocyte calcium elevations: From synapses to behavior. Frontiers in Cellular Neuroscience, 0 .

Guo, Q., Zhang, L., Liu, J., Li, Z., Li, J., Zhou, W., Wang, H., Li, J., Liu, D., Yu, X. & Zhang, J. (2021) Multifunctional microfluidic chip for cancer diagnosis and treatment. Nanotheranostics, 5 (1), 73-89.

Hachey, S. J. & Hughes, C. C. W. (2018) Applications of tumor chip technology. Lab on a Chip, 18 (19), 2893-2912.

Haemmig, S., Baumgartner, U., Glück, A., Zbinden, S., Tschan, M. P., Kappeler, A., Mariani, L., Vajtai, I. & Vassella, E. (2014) miR-125b controls apoptosis and temozolomide

resistance by targeting TNFAIP3 and NKIRAS2 in glioblastomas. Cell Death & Disease, 5 e1279.

Haiyong, H. (2018) RNA interference to knock down gene expression. Methods in Molecular Biology (Clifton, N.J.), 1706 293-302.

Hamilton, M. G., Roldán, G., Magliocco, A., McIntyre, J. B., Parney, I. & Easaw, J. C. (2011) Determination of the methylation status of MGMT in different regions within glioblastoma multiforme. Journal of Neuro-Oncology, 102 (2), 255-260.

Han, J. & Chen, Q. (2015) MiR-16 modulate temozolomide resistance by regulating BCL-2 in human glioma cells. International Journal of Clinical and Experimental Pathology, 8 (10), 12698-12707.

Han, J., Jun, Y., Kim, S. H., Hoang, H., Jung, Y., Kim, S., Kim, J., Austin, R. H., Lee, S. & Park, S. (2016) Rapid emergence and mechanisms of resistance by U87 glioblastoma cells to doxorubicin in an in vitro tumor microfluidic ecology. Proceedings of the National Academy of Sciences of the United States of America, 113 (50), 14283-14288.

Han, S. J., Kwon, S. & Kim, K. S. (2021) Challenges of applying multicellular tumor spheroids in preclinical phase. Cancer Cell International, 21 (1), 152.

Hanif, F., Muzaffar, K., Perveen, K., Malhi, S. M. & Simjee, S. U. (2017) Glioblastoma multiforme: A review of its epidemiology and pathogenesis through clinical presentation and treatment. Asian Pacific Journal of Cancer Prevention: APJCP, 18 (1), 3-9.

Hanisch, U. & Kettenmann, H. (2007) Microglia: Active sensor and versatile effector cells in the normal and pathologic brain. Nature Neuroscience, 10 (11), 1387-1394.

Hansen, A. J. (1985) Effect of anoxia on ion distribution in the brain. Physiological Reviews, 65 (1), 101-148.

Hansen, R. N., Zhang, Y., Seal, B., Ryan, K., Yong, C., Darilay, A. & Ramsey, S. D. (2020) Long-term survival trends in patients with unresectable stage III non-small cell lung cancer receiving chemotherapy and radiation therapy: A SEER cancer registry analysis. BMC Cancer, 20 276.

Hara, A., Kanayama, T., Noguchi, K., Niwa, A., Miyai, M., Kawaguchi, M., Ishida, K., Hatano, Y., Niwa, M. & Tomita, H. (2019) Treatment strategies based on histological targets against invasive and resistant glioblastoma. Hindawi. Available online: https://www.hindawi.com/journals/jo/2019/2964783/ [Accessed Feb 6, 2020].

Haroon, E., Miller, A. H. & Sanacora, G. (2017) Inflammation, glutamate, and glia: A trio of trouble in mood disorders. Neuropsychopharmacology (New York, N.Y.), 42 (1), 193-215.

Hartgerink, D., Swinnen, A., Roberge, D., Nichol, A., Zygmanski, P., Yin, F., Deblois, F., Hurkmans, C., Ong, C. L., Bruynzeel, A., Aizer, A., Fiveash, J., Kirckpatrick, J., Guckenberger, M., Andratschke, N., de Ruysscher, D., Popple, R. & Zindler, J. (2019) LINAC based stereotactic radiosurgery for multiple brain metastases: Guidance for clinical implementation. Acta Oncologica (Stockholm, Sweden), 58 (9), 1275-1282.

Haseloff, R. F., Dithmer, S., Winkler, L., Wolburg, H. & Blasig, I. E. (2015) Transmembrane proteins of the tight junctions at the blood-brain barrier: Structural and functional aspects. Seminars in Cell & Developmental Biology, 38 16-25.

Hassan, Z., Kumar, N. D., Reggiori, F. & Khan, G. (2021) How viruses hijack and modify the secretory transport pathway. Cells, 10 (10).

Hassell, B. A., Goyal, G., Lee, E., Sontheimer-Phelps, A., Levy, O., Chen, C. S. & Ingber, D. E. (2017) Human organ chip models recapitulate orthotopic lung cancer growth, therapeutic responses, and tumor dormancy In Vitro. Cell Reports (Cambridge), 21 (2), 508-516.

Hattersley, S. M., Dyer, C. E., Greenman, J. & Haswell, S. J. (2008) Development of a microfluidic device for the maintenance and interrogation of viable tissue biopsies. Lab on a Chip, 8 (11), 1842-1846.

Hattersley, S. M., Greenman, J. & Haswell, S. J. (2011) Study of ethanol induced toxicity in liver explants using microfluidic devices. Biomedical Microdevices, 13 (6), 1005-1014.

Hawkins, B. T. & Davis, T. P. (2005) The blood-brain barrier/neurovascular unit in health and disease. Pharmacological Reviews, 57 (2), 173-185.

He, C., Xu, K., Zhu, X., Dunphy, P. S., Gudenas, B., Lin, W., Twarog, N., Hover, L. D., Kwon, C., Kasper, L. H., Zhang, J., Li, X., Dalton, J., Jonchere, B., Mercer, K. S., Currier, D. G., Caufield, W., Wang, Y., Xie, J., Broniscer, A., Wetmore, C., Upadhyaya, S. A., Qaddoumi, I., Klimo, P., Boop, F., Gajjar, A., Zhang, J., Orr, B. A., Robinson, G. W., Monje, M., Freeman III, B. B., Roussel, M. F., Northcott, P. A., Chen, T., Rankovic, Z., Wu, G., Chiang, J., Tinkle, C. L., Shelat, A. A. & Baker, S. J. (2021) Patient-derived models recapitulate heterogeneity of molecular signatures and drug response in pediatric high-grade glioma. Nature Communications, 12 (1), 1-17.

He, W., Xu, H., Gou, H., Yuan, J., Liao, J., Chen, Y., Fan, S., Xie, B., Deng, S., Zhang, Y., Chen, J. & Zhao, M. (2017) CSFV infection up-regulates the unfolded protein response to promote its replication. Frontiers in Microbiology, 8 2129.

Healey, G. D., Lockridge, J. A., Zinnen, S., Hopkin, J. M., Richards, I. & Walker, W. (2014) Development of pre-clinical models for evaluating the therapeutic potential of candidate siRNA targeting STAT6. PLoS ONE, 9 (2), e90338.

Hegi, M. E., Diserens, A., Gorlia, T., Hamou, M., de Tribolet, N., Weller, M., Kros, J. M., Hainfellner, J. A., Mason, W., Mariani, L., Bromberg, J. E. C., Hau, P., Mirimanoff, R. O., Cairncross, J. G., Janzer, R. C. & Stupp, R. (2005) MGMT gene silencing and benefit from temozolomide in glioblastoma. The New England Journal of Medicine, 352 (10), 997-1003.

Herculano-Houzel, S. & Lent, R. (2005) Isotropic fractionator: A simple, rapid method for the quantification of total cell and neuron numbers in the brain. The Journal of Neuroscience: The Official Journal of the Society for Neuroscience, 25 (10), 2518-2521.

Heuser, V. D., Kiviniemi, A., Lehtinen, L., Munthe, S., Kristensen, B. W., Posti, J. P., Sipilä, J. O. T., Vuorinen, V., Carpén, O. & Gardberg, M. (2020) Multiple formin proteins participate in glioblastoma migration. BMC Cancer, 20 .

Hickerson, R. P., Flores, M. A., Leake, D., Lara, M. F., Contag, C. H., Leachman, S. A. & Kaspar, R. L. (2011) Use of self-delivery siRNAs to inhibit gene expression in an organotypic pachyonychia congenita model. Journal of Investigative Dermatology, 131 (5), 1037-1044.

Hira, V. V. V., Breznik, B., Vittori, M., Loncq de Jong, A., Mlakar, J., Oostra, R., Khurshed, M., Molenaar, R. J., Lah, T. & Van Noorden, Cornelis J. F. (2020) Similarities between stem cell niches in glioblastoma and bone marrow: Rays of hope for novel treatment strategies. Journal of Histochemistry & Cytochemistry, 68 (1), 33-57.

Hirschhaeuser, F., Menne, H., Dittfeld, C., West, J., Mueller-Klieser, W. & Kunz-Schughart, L. A. (2010) Multicellular tumor spheroids: An underestimated tool is catching up again. Journal of Biotechnology, 148 (1), 3-15.

Ho, W. Y., Yeap, S. K., Ho, C. L., Rahim, R. A. & Alitheen, N. B. (2012) Development of multicellular tumor spheroid (MCTS) culture from breast cancer cell and a high throughput screening method using the MTT assay. PloS One, 7 (9), e44640.

Hoarau-Véchot, J., Rafii, A., Touboul, C. & Pasquier, J. (2018) Halfway between 2D and animal models: Are 3D cultures the ideal tool to study cancer-microenvironment interactions? International Journal of Molecular Sciences, 19 (1), .

Hoerter, J. A. H., Krishnan, V., Lionberger, T. A. & Walter, N. G. (2011) siRNA-like double-stranded RNAs are specifically protected against degradation in human cell extract. PloS One, 6 (5), e20359.

Holland, E. C. (2000) Glioblastoma multiforme: The terminator. Proceedings of the National Academy of Sciences of the United States of America, 97 (12), 6242-6244.

horizondiscovery.com (2021) Accell siRNA transfection protocol. Available online: https://horizondiscovery.com/-/media/Files/Horizon/resources/Protocols/accell-delivery-protocol.pdf 2021].

Hu, B., Zhong, L., Weng, Y., Peng, L., Huang, Y., Zhao, Y. & Liang, X. (2020) Therapeutic siRNA: State of the art. Signal Transduction and Targeted Therapy, 5 (1), 1-25.

Huang, Q., Wu, L., Wang, Y. & Zhang, X. (2013) GOMA: Functional enrichment analysis tool based on GO modules. Chinese Journal of Cancer, 32 (4), 195-204.

Huang, X., Hussain, B. & Chang, J. (2021) Peripheral inflammation and blood-brain barrier disruption: Effects and mechanisms. CNS Neuroscience & Therapeutics, 27 (1), 36-47.

Humphrey, R. (1695) The anatomy of the brain. London: London: Sam Smith and Benjamin Walford, Printers to the Royal SocietyReturn to ref 56 in article.

Hunter, C., Smith, R., Cahill, D. P., Stephens, P., Stevens, C., Teague, J., Greenman, C., Edkins, S., Bignell, G., Davies, H., O'Meara, S., Parker, A., Avis, T., Barthorpe, S., Brackenbury, L., Buck, G., Butler, A., Clements, J., Cole, J., Dicks, E., Forbes, S., Gorton, M., Gray, K., Halliday, K., Harrison, R., Hills, K., Hinton, J., Jenkinson, A., Jones, D., Kosmidou, V., Laman, R., Lugg, R., Menzies, A., Perry, J., Petty, R., Raine, K., Richardson, D., Shepherd, R., Small, A., Solomon, H., Tofts, C., Varian, J., West, S., Widaa, S., Yates, A., Easton, D. F., Riggins, G., Roy, J. E., Levine, K. K., Mueller, W., Batchelor, T. T., Louis, D. N., Stratton, M. R., Futreal, P. A. & Wooster, R. (2006) A hypermutation phenotype and somatic MSH6 mutations in recurrent human malignant gliomas after alkylator chemotherapy. Cancer Research, 66 (8), 3987-3991.

Hwang, T., Mathios, D., McDonald, K. L., Daris, I., Park, S., Burger, P. C., Kim, S., Dho, Y., Carolyn, H., Bettegowda, C., Shin, J. H., Lim, M. & Park, C. (2019) Integrative analysis of DNA methylation suggests down-regulation of oncogenic pathways and reduced somatic mutation rates in survival outliers of glioblastoma. Acta Neuropathologica Communications, 7.

Iacob, G. & Dinca, E. B. (2009) Current data and strategy in glioblastoma multiforme. Journal of Medicine and Life, 2 (4), 386-393.

Iles, L. R. & Bartholomeusz, G. A. (2016) Three-dimensional spheroid cell culture model for target identification utilizing high-throughput RNAi screens. Methods in Molecular Biology (Clifton, N.J.), 1470 121-135.

Inskip, P. D., Tarone, R. E., Hatch, E. E., Wilcosky, T. C., Shapiro, W. R., Selker, R. G., Fine, H. A., Black, P. M., Loeffler, J. S. & Linet, M. S. (2001) Cellular-telephone use and brain tumors. The New England Journal of Medicine, 344 (2), 79-86.

Ip, C. K. M., Li, S., Tang, M. Y. H., Sy, S. K. H., Ren, Y., Shum, H. C. & Wong, A. S. T. (2016) Stemness and chemoresistance in epithelial ovarian carcinoma cells under shear stress. Scientific Reports, 6 (1), 26788.

Ishibazawa, A., Nagaoka, T., Takahashi, T., Yamamoto, K., Kamiya, A., Ando, J. & Yoshida, A. (2011) Effects of shear stress on the gene expressions of endothelial nitric oxide synthase, endothelin-1, and thrombomodulin in human retinal microvascular endothelial cells. Investigative Ophthalmology & Visual Science, 52 (11), 8496-8504.

Islam, Y., Leach, A. G., Smith, J., Pluchino, S., Coxonl, C. R., Sivakumaran, M., Downing, J., Fatokun, A. A., Teixidò, M. & Ehtezazi, T. (2020) Peptide based drug delivery systems to the brain. Nano Express, 1 (1), 012002.

Islam, Y., Leach, A. G., Smith, J., Pluchino, S., Coxonl, C. R., Sivakumaran, M., Downing, J., Fatokun, A. A., Teixidò, M. & Ehtezazi, T. (2020) Peptide based drug delivery systems to the brain. Nano Express, 1 (1), 012002.

Jackson, A. L. & Linsley, P. S. (2010) Recognizing and avoiding siRNA off-target effects for target identification and therapeutic application. Nature Reviews. Drug Discovery, 9 (1), 57-67.

Jacob, A. & Prekeris, R. (2015) The regulation of MMP targeting to invadopodia during cancer metastasis. Frontiers in Cell and Developmental Biology, 0 .

Jafari, M. & Ansari-Pour, N. (2019) Why, when and how to adjust your P values? Cell Journal (Yakhteh), 20 (4), 604-607.

Jäkel, S. & Dimou, L. (2017) Glial cells and their function in the adult brain: A journey through the history of their ablation. Frontiers in Cellular Neuroscience, 11 24.

Jastrzebska, K., Kucharczyk, K., Florczak, A., Dondajewska, E., Mackiewicz, A. & Dams-Kozlowska, H. (2014) Silk as an innovative biomaterial for cancer therapy. Reports of Practical Oncology and Radiotherapy, 20 (2), 87-98.

Jauregui-Huerta, F., Ruvalcaba-Delgadillo, Y., Gonzalez-Castañeda, R., Garcia-Estrada, J., Gonzalez-Perez, O. & Luquin, S. (2010) Responses of glial cells to stress and glucocorticoids. Current Immunology Reviews, 6 (3), 195-204.

Jensen, C. & Teng, Y. (2020) Is it time to start transitioning from 2D to 3D cell culture? Frontiers in Molecular Biosciences, 7, 33.

Jessen, K. R. (2004) Glial cells. The International Journal of Biochemistry & Cell Biology, 36 (10), 1861-1867.

Jiang, G., Li, L. -., Xin, Y., Zhang, L., Liu, Y. -. & Zheng, J. -. (2012) Strategies to improve the killing of tumors using temozolomide: Targeting the DNA repair protein MGMT. Current Medicinal Chemistry, 19 (23), 3886-3892.

Jiang, L., Schlesinger, F., Davis, C. A., Zhang, Y., Li, R., Salit, M., Gingeras, T. R. & Oliver, B. (2011) Synthetic spike-in standards for RNA-seq experiments. Genome Research, 21 (9), 1543-1551.

Jiang, Y., Yang, W., Zhang, J., Meng, F. & Zhong, Z. (2018) Protein toxin chaperoned by LRP-1-targeted virus-mimicking vesicles induces high-efficiency glioblastoma therapy *in vivo*. Advanced Materials (Deerfield Beach, Fla.), 30 (30), e1800316.

Jijiwa, M., Demir, H., Gupta, S., Leung, C., Joshi, K., Orozco, N., Huang, T., Yildiz, V. O., Shibahara, I., de Jesus, J. A., Yong, W. H., Mischel, P. S., Fernandez, S., Kornblum, H. I. & Nakano, I. (2011) CD44v6 regulates growth of brain tumor stem cells partially through the AKT-mediated pathway. PloS One, 6 (9), e24217.

Jiménez Calvente, C., Sehgal, A., Popov, Y., Kim, Y. O., Zevallos, V., Sahin, U., Diken, M. & Schuppan, D. (2015) Specific hepatic delivery of procollagen α1(I) small interfering RNA in lipid-like nanoparticles resolves liver fibrosis. Hepatology (Baltimore, Md.), 62 (4), 1285-1297.

Jiménez, A. J., Domínguez-Pinos, M., Guerra, M. M., Fernández-Llebrez, P. & Pérez-Fígares, J. (2014) Structure and function of the ependymal barrier and diseases associated with ependyma disruption. Tissue Barriers, 2 .

Jiménez-P, R., Martín-Cortázar, C., Kourani, O., Chiodo, Y., Cordoba, R., Domínguez-Franjo, M. P., Redondo, J. M., Iglesias, T. & Campanero, M. R. (2018) CDCA7 is a critical mediator of lymphomagenesis that selectively regulates anchorage-independent growth. Haematologica, 103 (10), 1669-1678.

Jin, U., Karki, K., Cheng, Y., Michelhaugh, S. K., Mittal, S. & Safe, S. (2019) The aryl hydrocarbon receptor is a tumor suppressor-like gene in glioblastoma. The Journal of Biological Chemistry, 294 (29), 11342-11353.

Jo, Y., Choi, N., Kim, K., Koo, H., Choi, J. & Kim, H. N. (2018) Chemoresistance of cancer cells: Requirements of tumor microenvironment-mimicking in vitro models in anti-cancer drug development. Theranostics, 8 (19), 5259-5275.

Johansson, C. B., Momma, S., Clarke, D. L., Risling, M., Lendahl, U. & Frisén, J. (1999) Identification of a neural stem cell in the adult mammalian central nervous system. Cell, 96 (1), 25-34.

Joo, T., Choi, J., Lee, J., Park, S. E., Jeon, Y., Jung, S. H. & Woo, H. G. (2019) SEQprocess: A modularized and customizable pipeline framework for NGS processing in R package. BMC Bioinformatics, 20 (1), 90.

Jovcevska, I. (2019) Genetic secrets of long-term glioblastoma survivors. Bosnian Journal of Basic Medical Sciences, 19 (2), 116-124.

JOVČEVSKA, I., KOČEVAR, N. & KOMEL, R. (2013) Glioma and glioblastoma - how much do we (not) know? Molecular and Clinical Oncology, 1 (6), 935-941.

Jung, T., Jung, S., Moon, K., Kim, I., Kang, S., Kim, Y., Park, C. & Lee, K. (2010) Changes of the O6-methylguanine-DNA methyltransferase promoter methylation and MGMT protein expression after adjuvant treatment in glioblastoma. Oncology Reports, 23 (5), 1269-1276.

Kadry, H., Noorani, B. & Cucullo, L. (2020) A blood-brain barrier overview on structure, function, impairment, and biomarkers of integrity. Fluids and Barriers of the CNS, 17 (1), 69.

Kaminsky, N., Bihari, O., Kanner, S. & Barzilai, A. (2016) Connecting malfunctioning glial cells and brain degenerative disorders. Genomics, Proteomics & Bioinformatics, 14 (3), 155-165.

Kanderi, T. & Gupta, V. (2022) Glioblastoma multiforme. In Anonymous StatPearls. Treasure Island (FL): StatPearls Publishing, .

Kanehisa, M., Araki, M., Goto, S., Hattori, M., Hirakawa, M., Itoh, M., Katayama, T., Kawashima, S., Okuda, S., Tokimatsu, T. & Yamanishi, Y. (2008) KEGG for linking genomes to life and the environment. Nucleic Acids Research, 36 (Database issue), 480.

Kanzawa, T., Germano, I. M., Komata, T., Ito, H., Kondo, Y. & Kondo, S. (2004) Role of autophagy in temozolomide-induced cytotoxicity for malignant glioma cells. Cell Death and Differentiation, 11 (4), 448-457.

Kapałczyńska, M., Kolenda, T., Przybyła, W., Zajączkowska, M., Teresiak, A., Filas, V., Ibbs, M., Bliźniak, R., Łuczewski, Ł & Lamperska, K. (2016) 2D and 3D cell cultures – a comparison of different types of cancer cell cultures. Archives of Medical Science, 14 (4), 910-919.

Katakowski, M., Buller, B., Wang, X., Rogers, T. & Chopp, M. (2010) Functional microRNA is transferred between glioma cells. Cancer Research, 70 (21), 8259-8263.

Katsigiannis, S., Krischek, B., Barleanu, S., Grau, S., Galldiks, N., Timmer, M., Kabbasch, C., Goldbrunner, R. & Stavrinou, P. (2019) Impact of time to initiation of radiotherapy on survival after resection of newly diagnosed glioblastoma. Radiation Oncology (London, England), 14 (1), 73.

Keime-Guibert, F., Chinot, O., Taillandier, L., Cartalat-Carel, S., Frenay, M., Kantor, G., Guillamo, J., Jadaud, E., Colin, P., Bondiau, P., Meneï, P., Loiseau, H., Bernier, V., Honnorat, J., Barrié, M., Mokhtari, K., Mazeron, J., Bissery, A. & Delattre, J. (2007) Radiotherapy for glioblastoma in the elderly. The New England Journal of Medicine, 356 (15), 1527-1535.

Khong, Y. M., Zhang, J., Zhou, S., Cheung, C., Doberstein, K., Samper, V. & Yu, H. (2007) Novel intra-tissue perfusion system for culturing thick liver tissue. Tissue Engineering, 13 (9), 2345-2356.

Kijanska, M. & Kelm, J. (2016) In vitro 3D spheroids and microtissues: ATP-based cell viability and toxicity assays Eli Lilly & Company and the National Center for Advancing Translational Sciences.

Kilroy, G., Burk, D. H. & Floyd, Z. E. (2009) High efficiency lipid-based siRNA transfection of adipocytes in suspension. Plos One, 4 (9), e6940.

Kim, H., Lee, S., Lim, J., Yoo, J. & Hwang, D. (2021) The epidermal growth factor receptor variant type III mutation frequently found in gliomas induces astrogenesis in human cere-bral organoids. Cell Proliferation, 54 (2), e12965.

Kim, H., Zheng, S., Amini, S. S., Virk, S. M., Mikkelsen, T., Brat, D. J., Grimsby, J., Sougnez, C., Muller, F., Hu, J., Sloan, A. E., Cohen, M. L., Van Meir, E. G., Scarpace, L., Laird, P. W., Weinstein, J. N., Lander, E. S., Gabriel, S., Getz, G., Meyerson, M., Chin, L., Barnholtz-Sloan, J. S. & Verhaak, R. G. W. (2015) Whole-genome and multisector exome sequencing of primary and post-treatment glioblastoma reveals patterns of tumor evolution. Genome Research, 25 (3), 316-327.

Kim, J. W., Kim, J. Y., Kim, J. E., Kim, S., Chung, H. & Park, C. (2014) HOXA10 is associated with temozolomide resistance through regulation of the homologous recombinant DNA repair pathway in glioblastoma cell lines. Genes & Cancer, 5 (5-6), 165-174.

Kim, S., Garg, H., Joshi, A. & Manjunath, N. (2009) Strategies for targeted nonviral deliv-ery of siRNAs *in vivo*. Trends in Molecular Medicine, 15 (11), 491-500.

Kim, T. Y., Kofron, C. M., King, M. E., Markes, A. R., Okundaye, A. O., Qu, Z., Mende, U. & Choi, B. (2018) Directed fusion of cardiac spheroids into larger heterocellular microtissues enables investigation of cardiac action potential propagation via cardiac fibroblasts. PLoS ONE, 13 (5), .

Kim, Y. (2013) Regulation of cell proliferation and migration in glioblastoma: New therapeutic approach. Frontiers in Oncology, 3 53.

Kim, Y., Park, J. & Choi, Y. K. (2019) The role of astrocytes in the central nervous system focused on BK channel and heme oxygenase metabolites: A review. Antioxidants, 8 (5), .

Kitange, G. J., Mladek, A. C., Carlson, B. L., Schroeder, M. A., Pokorny, J. L., Cen, L., Decker, P. A., Wu, W., Lomberk, G. A., Gupta, S. K., Urrutia, R. A. & Sarkaria, J. N. (2012) Inhibition of histone deacetylation potentiates the evolution of acquired temozolomide resistance linked to MGMT upregulation in glioblastoma xenografts. Clinical Cancer Research: An Official Journal of the American Association for Cancer Research, 18 (15), 4070-4079.

Kleinschmidt-Demasters, B. K., Kang, J. S. & Lillehei, K. O. (2006) The burden of radiation-induced central nervous system tumors: A single institution s experience. Journal of Neuropathology and Experimental Neurology, 65 (3), 204-216.

Korshunov, A., Sycheva, R. & Golanov, A. (2005) The prognostic relevance of molecular alterations in glioblastomas for patients age < 50 years. Cancer, 104 (4), 825-832.

Kreuter, J., Hekmatara, T., Dreis, S., Vogel, T., Gelperina, S. & Langer, K. (2007) Covalent attachment of apolipoprotein A-I and apolipoprotein B-100 to albumin nanoparticles enables drug transport into the brain. Journal of Controlled Release: Official Journal of the Controlled Release Society, 118 (1), 54-58.

Krol, I., Schwab, F. D., Carbone, R., Ritter, M., Picocci, S., De Marni, M. L., Stepien, G., Franchi, G. M., Zanardi, A., Rissoglio, M. D., Covelli, A., Guidi, G., Scarinci, D., Castro-Giner, F., Mazzarella, L., Doglioni, C., Borghi, F., Milani, P., Kurzeder, C., Weber, W. P. & Aceto, N. (2021) Detection of clustered circulating tumour cells in early breast cancer. British Journal of Cancer, 125 (1), 23-27.

Krol, J., Loedige, I. & Filipowicz, W. (2010) The widespread regulation of microRNAmicroRNA biogenesis, function and decay. Nature Reviews. Genetics, 11 (9), 597-610.

Kuang, J., Yan, X., Genders, A. J., Granata, C. & Bishop, D. J. (2018) An overview of technical considerations when using quantitative real-time PCR analysis of gene expression in human exercise research. PLoS ONE, 13 (5), .

Kukurba, K. R. & Montgomery, S. B. (2015) RNA sequencing and analysis. Cold Spring Harbor Protocols, 2015 (11), 951-969.

Kurosinski, P. & Götz, J. (2002) Glial cells under physiologic and pathologic conditions. Archives of Neurology, 59 (10), 1524-1528.

Ladomersky, E., Scholtens, D. M., Kocherginsky, M., Hibler, E. A., Bartom, E. T., Otto-Meyer, S., Zhai, L., Lauing, K. L., Choi, J., Sosman, J. A., Wu, J. D., Zhang, B., Lukas, R. V. & Wainwright, D. A. (2019) The coincidence between increasing age, immunosuppression, and the incidence of patients with glioblastoma. Frontiers in Pharmacology, 0 .

Lagies, S., Schlimpert, M., Neumann, S., Wäldin, A., Kammerer, B., Borner, C. & Peintner, L. (2020) Cells grown in three-dimensional spheroids mirror *in vivo* metabolic response of epithelial cells. Communications Biology, 3 (1), 1-10.

Lanese, A., Franceschi, E. & Brandes, A. A. (2018) The risk assessment in low-grade gliomas: An analysis of the european organization for research and treatment of cancer

(EORTC) and the radiation therapy oncology group (RTOG) criteria. Oncology and Therapy, 6 (2), 105-108.

Langhans, S. A. (2018) Three-dimensional in vitro cell culture models in drug discovery and drug repositioning. Frontiers in Pharmacology, 0 .

Lapointe, S., Perry, A. & Butowski, N. A. (2018) Primary brain tumours in adults. The Lancet, 392 (10145), 432-446.

Larionov, A., Krause, A. & Miller, W. (2005) A standard curve based method for relative real time PCR data processing. BMC Bioinformatics, 6 62.

Larjavaara, S., Mäntylä, R., Salminen, T., Haapasalo, H., Raitanen, J., Jääskeläinen, J. & Auvinen, A. (2007) Incidence of gliomas by anatomic location. Neuro-Oncology, 9 (3), 319-325.

Lauzier, A., Normandeau-Guimond, J., Vaillancourt-Lavigueur, V., Boivin, V., Charbonneau, M., Rivard, N., Scott, M. S., Dubois, C. M. & Jean, S. (2019) Colorectal cancer cells respond differentially to autophagy inhibition *in vivo*. Scientific Reports, 9 (1), 1-16.

Lawrence, J. E., Bammert, C. E., Jr, R. J. B., Rovin, R. A. & Winn, R. J. (2015) Targeting DNA repair mechanisms to treat glioblastoma IntechOpen.

Lee, D., Rötger, C., Appeldoorn, C. C. M., Reijerkerk, A., Gladdines, W., Gaillard, P. J. & Linker, R. A. (2014) Glutathione PEGylated liposomal methylprednisolone (2B3-201) attenuates CNS inflammation and degeneration in murine myelin oligodendrocyte glycoprotein induced experimental autoimmune encephalomyelitis. Journal of Neuroimmunology, 274 (1-2), 96-101.

Lee, S., No, D. Y., Kang, E., Ju, J., Kim, D. & Lee, S. (2013) Spheroid-based three-dimensional liver-on-a-chip to investigate hepatocyte-hepatic stellate cell interactions and flow effects. Lab on a Chip, 13 (18), 3529-3537.

Lehnardt, S. (2010) Innate immunity and neuroinflammation in the CNS: The role of microglia in toll-like receptor-mediated neuronal injury. Glia, 58 (3), 253-263.

Leite, D. M., Baskovic, B. Z., Civita, P., Neto, C., Gumbleton, M. & Pilkington, G. J. (2020) A human co-culture cell model incorporating microglia supports glioblastoma growth and migration, and confers resistance to cytotoxics. The FASEB Journal, 34 (1), 1710-1727.

Li, H., Peng, X., Zong, Q., Zhang, K., Wang, M., Liu, Y. & Han, G. (2016) Cigarette smoking and risk of adult glioma: A meta-analysis of 24 observational studies involving more than 2.3 million individuals. OncoTargets and Therapy, 9 3511-3523.

Li, J., Cai, J., Zhao, S., Yao, K., Sun, Y., Li, Y., Chen, L., Li, R., Zhai, X., Zhang, J. & Jiang, C. (2016) GANT61, a GLI inhibitor, sensitizes glioma cells to the temozolomide treatment. Journal of Experimental & Clinical Cancer Research: CR, 35 (1), 184.

Li, J., Liu, X., Crook, J. M. & Wallace, G. G. (2020) 3D printing of cytocompatible graphene/alginate scaffolds for mimetic tissue constructs. Frontiers in Bioengineering and Biotechnology, 8:824..

Li, Q., Chen, C., Kapadia, A., Zhou, Q., Harper, M. K., Schaack, J. & LaBarbera, D. V. (2011) 3D models of epithelial-mesenchymal transition in breast cancer metastasis: High-throughput screening assay development, validation, and pilot screen. Journal of Biomolecular Screening, 16 (2), 141-154.

Li, S., Zeng, A., Hu, Q., Yan, W., Liu, Y. & You, Y. (2017) miR-423-5p contributes to a malignant phenotype and temozolomide chemoresistance in glioblastomas. Neuro-Oncology, 19 (1), 55-65.

Li, Y., Liu, Y., Ren, J., Deng, S., Yi, G., Guo, M., Shu, S., Zhao, L., Peng, Y. & Qi, S. (2018) miR-1268a regulates ABCC1 expression to mediate temozolomide resistance in glioblastoma. Journal of Neuro-Oncology, 138 (3), 499-508.

Li, Y., Wei, Z., Dong, B., Lian, Z. & Xu, Y. (2016) Silencing of phosphoglucose isomerase/autocrine motility factor decreases U87 human glioblastoma cell migration. International Journal of Molecular Medicine, 37 (4), 998-1004.

Liddelow, S. A. (2011) Fluids and barriers of the CNS: A historical viewpoint. Fluids and Barriers of the CNS, 8 (1), 2.

Lim, W., Hoang, H., You, D., Han, J., Lee, J. E., Kim, S. & Park, S. (2018) Formation of size-controllable tumour spheroids using a microfluidic pillar array (μFPA) device. Analyst, 143 (23), 5841-5848.

Liu, G., Yuan, X., Zeng, Z., Tunici, P., Ng, H., Abdulkadir, I. R., Lu, L., Irvin, D., Black, K. L. & Yu, J. S. (2006) Analysis of gene expression and chemoresistance of CD133+ cancer stem cells in glioblastoma. Molecular Cancer, 5 67.

Liu, H., Li, Y., Mozhi, A., Zhang, L., Liu, Y., Xu, X., Xing, J., Liang, X., Ma, G., Yang, J. & Zhang, X. (2014) SiRNA-phospholipid conjugates for gene and drug delivery in cancer treatment. Biomaterials, 35 (24), 6519-6533.

Liu, H., Sun, Y., Zhang, Q., Jin, W., Gordon, R. E., Zhang, Y., Wang, J., Sun, C., Wang, Z. J., Qi, X., Zhang, J., Huang, B., Gui, Q., Yuan, H., Chen, L., Ma, X., Fang, C., Liu, Y., Yu, X. & Feng, S. (2021) Pro-inflammatory and proliferative microglia drive progression of glioblastoma. Cell Reports, 36 (11), 109718.

LIU, J., TANG, W., CHEN, G., LU, Y., FENG, C. & TU, X. M. (2016) Correlation and agreement: Overview and clarification of competing concepts and measures. Shanghai Archives of Psychiatry, 28 (2), 115-120.

Liu, Q., Zhang, H., Jiang, X., Qian, C., Liu, Z. & Luo, D. (2017) Factors involved in cancer metastasis: A better understanding to "seed and soil" hypothesis. Molecular Cancer, 16 (1), 176.

Liu, X., Fang, J., Huang, S., Wu, X., Xie, X., Wang, J., Liu, F., Zhang, M., Peng, Z. & Hu, N. (2021) Tumor-on-a-chip: From bioinspired design to biomedical application. Microsystems & Nanoengineering, 7 (1), 1-23.

Lo, E. H. & Rosenberg, G. A. (2009) The neurovascular unit in health and disease: Introduction. Stroke, 40 (3 Suppl), 2.

Loane, D. J. & Kumar, A. (2016) Experimental neurology. Experimental Neurology, 275 316-327.

Loo, J., Sicher, I., Goff, A., Kim, O., Clary, N., Alexeev, A., Sulchek, T., Zamarayeva, A., Han, S. & Calero-Garcia, M. (2021) Microfluidic transfection of mRNA into human primary lymphocytes and hematopoietic stem and progenitor cells using ultra-fast physical deformations. Scientific Reports, 11 (1), 1-11.

Lopez-Castejon, G., Luheshi, N. M., Compan, V., High, S., Whitehead, R. C., Flitsch, S., Kirov, A., Prudovsky, I., Swanton, E. & Brough, D. (2013) Deubiquitinases regulate the

activity of caspase-1 and interleukin-1β secretion via assembly of the inflammasome. The Journal of Biological Chemistry, 288 (4), 2721-2733.

Louis, D. N., Holland, E. C. & Cairncross, J. G. (2001) Glioma classification: A molecular reappraisal. The American Journal of Pathology, 159 (3), 779-786.

Louis, D. N., Perry, A., Reifenberger, G., von Deimling, A., Figarella-Branger, D., Cavenee, W. K., Ohgaki, H., Wiestler, O. D., Kleihues, P. & Ellison, D. W. (2016) The 2016 world health organization classification of tumors of the central nervous system: A summary. Acta Neuropathologica, 131 (6), 803-820.

Louis, D. N., Perry, A., Wesseling, P., Brat, D. J., Cree, I. A., Figarella-Branger, D., Ellison, D. W. (2021). The 2021 WHO classification of tumors of the central nervous system: A summary. Neuro-Oncology, 23(8), 1231-1251.

Low, S. Y. Y., Ho, Y. K., Too, H., Yap, C. T. & Ng, W. H. (2014) MicroRNAMicroRNA as potential modulators in chemoresistant high-grade gliomas. Journal of Clinical Neuroscience: Official Journal of the Neurosurgical Society of Australasia, 21 (3), 395-400.

Lu, C., Zhao, Y., Wong, H. L., Cai, J., Peng, L. & Tian, X. (2014) Current approaches to enhance CNS delivery of drugs across the brain barriers. International Journal of Nanomedicine, 9 2241-2257.

Luca, A., Calandra, C. & Luca, M. (2018) Molecular bases of alzheimer's disease and neurodegeneration: The role of neuroglia. Aging and Disease, 9 (6), 1134-1152.

Lukas, R. V., Wainwright, D. A., Ladomersky, E., Sachdev, S., Sonabend, A. M. & Stupp, R. (2019) Newly diagnosed glioblastoma: A review on clinical management. Oncology (Williston Park, N.Y.), 33 (3), 91-100.

Luo, H., Chen, Z., Wang, S., Zhang, R., Qiu, W., Zhao, L., Peng, C., Xu, R., Chen, W., Wang, H., Chen, Y., Yang, J., Zhang, X., Zhang, S., Chen, D., Wu, W., Zhao, C., Cheng, G., Jiang, T., Lu, D., You, Y., Liu, N. & Wang, H. (2015) C-myc-miR-29c-REV3L signalling pathway drives the acquisition of temozolomide resistance in glioblastoma. Brain: A Journal of Neurology, 138 (Pt 12), 3654-3672.

Lv, D., Hu, Z., Lu, L., Lu, H. & Xu, X. (2017) Three-dimensional cell culture: A powerful tool in tumor research and drug discovery. Oncology Letters, 14 (6), 6999-7010.

Lv, D., Yu, S., Ping, Y., Wu, H., Zhao, X., Zhang, H., Cui, Y., Chen, B., Zhang, X., Dai, J., Bian, X. & Yao, X. (2016) A three-dimensional collagen scaffold cell culture system for screening anti-glioma therapeutics. Oncotarget, 7 (35), 56904-56914.

Ma, Y. V., Middleton, K., You, L. & Sun, Y. (2018a) A review of microfluidic approaches for investigating cancer extravasation during metastasis. Microsystems & Nanoengineering, 4 (1), 17104.

Maher, E. A., Furnari, F. B., Bachoo, R. M., Rowitch, D. H., Louis, D. N., Cavenee, W. K. & DePinho, R. A. (2001) Malignant glioma: Genetics and biology of a grave matter. Genes & Development, 15 (11), 1311-1333.

Mahmoodi Chalbatani, G., Dana, H., Gharagouzloo, E., Grijalvo, S., Eritja, R., Logsdon, C. D., Memari, F., Miri, S. R., Rad, M. R. & Marmari, V. (2019) Small interfering RNAs (siRNAs) in cancer therapy: A nano-based approach. International Journal of Nanomedicine, 14 3111-3128.

Maletínská, L., Blakely, E. A., Bjornstad, K. A., Deen, D. F., Knoff, L. J. & Forte, T. M. (2000) Human glioblastoma cell lines: Levels of low-density lipoprotein receptor and low-density lipoprotein receptor-related protein. Cancer Research, 60 (8), 2300-2303.

Malik, S., Saltzman, W. M. & Bahal, R. (2021) Extracellular vesicles mediated exocytosis of antisense peptide nucleic acids. Molecular Therapy. Nucleic Acids, 25 302-315.

Manrique-Guzmán, S., Herrada-Pineda, T. & Revilla-Pacheco, F. (2017) Surgical management of glioblastoma. In Steven De Vleeschouwer (ed) Glioblastoma. Brisbane (AU): Codon Publications, .

Mansouri, A., Karamchandani, J. & Das, S. (2017) Molecular genetics of secondary glioblastoma. In Steven De Vleeschouwer (ed) Glioblastoma. Brisbane (AU): Codon Publications, .

Margison, G. P. & Santibáñez-Koref, M. F. (2002) O6-alkylguanine-DNA alkyltransferase: Role in carcinogenesis and chemotherapy. BioEssays: News and Reviews in Molecular, Cellular and Developmental Biology, 24 (3), 255-266.

Mark, C., Grundy, T. J., Strissel, P. L., Böhringer, D., Grummel, N., Gerum, R., Steinwachs, J., Hack, C. C., Beckmann, M. W., Eckstein, M., Strick, R., O'Neill, G. M. & Fabry, B. (2020) Collective forces of tumor spheroids in three-dimensional biopolymer networks. eLife, 9 e51912.

Marko, N. F., Toms, S. A., Barnett, G. H. & Weil, R. (2008) Genomic expression patterns distinguish long-term from short-term glioblastoma survivors: A preliminary feasibility study. Genomics, 91 (5), 395-406.

Matejuk, A. & Ransohoff, R. M. (2020) Crosstalk between astrocytes and microglia: An overview. Frontiers in Immunology, 0 .

Matellan, C. & del Río Hernández, Armando E. (2018) Cost-effective rapid prototyping and assembly of poly(methyl methacrylate) microfluidic devices. Scientific Reports, 8 .

Matellan, C., Del Río Hernández & Armando, E. (2018) Cost-effective rapid prototyping and assembly of poly(methyl methacrylate) microfluidic devices. Scientific Reports, 8 (1), 6971.

Matsuda, T. & Cepko, C. L. (2004) Electroporation and RNA interference in the rodent retina *in vivo* and in vitro. Proceedings of the National Academy of Sciences of the United States of America, 101 (1), 16-22.

McCord, M., Steffens, A., Javier, R., Kam, K., McCortney, K. & Horbinski, C. (2020) The efficacy of DNA mismatch repair enzyme immunohistochemistry as a screening test for hypermutated gliomas. Acta Neuropathologica Communications, 8 (1), 15.

Mehta, P., Rahman, Z., ten Dijke, P. & Boukany, P. E. (2022) Microfluidics meets 3D cancer cell migration. Trends in Cancer, .

Meng, Z. & Lu, M. (2017) RNA interference-induced innate immunity, off-target effect, or immune adjuvant? Frontiers in Immunology, 9.21345.

Merz, L., Höbel, S., Kallendrusch, S., Ewe, A., Bechmann, I., Franke, H., Merz, F. & Aigner, A. (2017) Tumor tissue slice cultures as a platform for analyzing tissue-penetration and biological activities of nanoparticles. European Journal of Pharmaceutics and Biopharmaceutics, 112 45-50.

Meshulam, L., Galron, R., Kanner, S., De Pittà, M., Bonifazi, P., Goldin, M., Frenkel, D., Ben-Jacob, E. & Barzilai, A. (2012) The role of the neuro-astro-vascular unit in the etiology of ataxia telangiectasia. Frontiers in Pharmacology, 3 157.

Messali, A., Villacorta, R. & Hay, J. W. (2014) A review of the economic burden of glioblastoma and the cost effectiveness of pharmacologic treatments. PharmacoEconomics, 32 (12), 1201-1212.

Meyers, J., Craig, J. & Odde, D. J. (2006) Potential for control of signaling pathways via cell size and shape. Current Biology: CB, 16 (17), 1685-1693.

Michael Jeffrey Viswanath Chidambara (2019) Characterisation of a novel microfluidic device for maintaining

Miller, D. S., Bauer, B. & Hartz, A. M. S. (2008) Modulation of P-glycoprotein at the blood-brain barrier: Opportunities to improve central nervous system pharmacotherapy. Pharmacological Reviews, 60 (2), 196-209.

Minghetti, L. & Levi, G. (1998) Microglia as effector cells in brain damage and repair: Focus on prostanoids and nitric oxide. Progress in Neurobiology, 54 (1), 99-125.

Minniti, G., Filippi, A. R., Osti, M. F. & Ricardi, U. (2017) Radiation therapy for older patients with brain tumors. Radiation Oncology (London, England), 12 .

Minniti, G., Lombardi, G. & Paolini, S. (2019) Glioblastoma in elderly patients: Current management and future perspectives. Cancers, 11 (3), .

Mirabelli, P., Coppola, L. & Salvatore, M. (2019) Cancer cell lines are useful model systems for medical research. Cancers, 11 (8), .

Mirzadeh, Z., Kusne, Y., Duran-Moreno, M., Cabrales, E., Gil-Perotin, S., Ortiz, C., Chen, B., Garcia-Verdugo, J. M., Sanai, N. & Alvarez-Buylla, A. (2017) Bi- and uniciliated ependymal cells define continuous floor-plate-derived tanycytic territories. Nature Communications, 8 13759.

Mitchell, P. S., Parkin, R. K., Kroh, E. M., Fritz, B. R., Wyman, S. K., Pogosova-Agadjanyan, E. L., Peterson, A., Noteboom, J., O'Briant, K. C., Allen, A., Lin, D. W., Urban, N., Drescher, C. W., Knudsen, B. S., Stirewalt, D. L., Gentleman, R., Vessella, R. L., Nelson, P. S., Martin, D. B. & Tewari, M. (2008) Circulating microRNAmicroRNAs as stable blood-based markers for cancer detection. Proceedings of the National Academy of Sciences of the United States of America, 105 (30), 10513-10518.

Mitra, S. (2007) MGMT: A personal perspective. DNA Repair, 6 (8), 1064-1070.

Mitragotri, S., Burke, P. A. & Langer, R. (2014) Overcoming the challenges in administering biopharmaceuticals: Formulation and delivery strategies. Nature Reviews. Drug Discovery, 13 (9), 655-672.

Mittapalli, R. K., Manda, V. K., Adkins, C. E., Geldenhuys, W. J. & Lockman, P. R. (2010) Exploiting nutrient transporters at the blood-brain barrier to improve brain distribution of small molecules. Therapeutic Delivery, 1 (6), 775-784.

Molenaar, R. J., Maciejewski, J. P., Wilmink, J. W. & van Noorden, Cornelis J. F (2018) Wild-type and mutated IDH1/2 enzymes and therapy responses. Oncogene, 37 (15), 1949-1960.

Molenaar, R. J., Maciejewski, J. P., Wilmink, J. W. & van Noorden, Cornelis J. F (2018) Wild-type and mutated IDH1/2 enzymes and therapy responses. Oncogene, 37 (15), 1949-1960.

Montaldi, A. P., Godoy, Paulo R. D. V. & Sakamoto-Hojo, E. T. (2015) APE1/REF-1 down-regulation enhances the cytotoxic effects of temozolomide in a resistant glioblastoma cell line. Mutation Research. Genetic Toxicology and Environmental Mutagenesis, 793 19-29.

Montazeri, M., Sanchez-Lopez, J. A., Caballero, I., Maslehat Lay, N., Elliott, S. & Fazeli, A. (2016) Interleukin-1 receptor antagonist mediates toll-like receptor 3-induced inhibition of trophoblast adhesion to endometrial cells in vitro. Human Reproduction (Oxford, England), 31 (9), 2098-2107.

Morgan, R. G., Chambers, A. C., Legge, D. N., Coles, S. J., Greenhough, A. & Williams, A. C. (2018) Optimized delivery of siRNA into 3D tumor spheroid cultures in situ. Scientific Reports, 8 (1), 1-10.

Moshksayan, K., Kashaninejad, N., Warkiani, M. E., Lock, J. G., Moghadas, H., Firoozabadi, B., Saidi, M. S. & Nguyen, N. (2018) Spheroids-on-a-chip: Recent advances and design considerations in microfluidic platforms for spheroid formation and culture. Sensors and Actuators. B, Chemical, 263 151-176.

Mota, B. & Herculano-Houzel, S. (2014) All brains are made of this: A fundamental building block of brain matter with matching neuronal and glial masses. Frontiers in Neuroanatomy, 8 127.

Mrugala, M. M. (2013) Advances and challenges in the treatment of glioblastoma: A clinician's perspective. Discovery Medicine, 15 (83), 221-230.

Müller Bark, J., Kulasinghe, A., Chua, B., Day, B. W. & Punyadeera, C. (2020) Circulating biomarkers in patients with glioblastoma. British Journal of Cancer, 122 (3), 295-305.

Müller Bark, J., Kulasinghe, A., Chua, B., Day, B. W. & Punyadeera, C. (2019) Circulating biomarkers in patients with glioblastoma. British Journal of Cancer, 1-11.

Munoz, J. L., Walker, N. D., Scotto, K. W. & Rameshwar, P. (2015) Temozolomide competes for P-glycoprotein and contributes to chemoresistance in glioblastoma cells. Cancer Letters, 367 (1), 69-75.

Murry, B. P., Blust, B. E., Singh, A., Foster, T. P. & Marchetti, D. (2006) Heparanase mechanisms of melanoma metastasis to the brain: Development and use of a brain slice model. Journal of Cellular Biochemistry, 97 (2), 217-225.

Nakajima, H., Kubo, T., Semi, Y., Itakura, M., Kuwamura, M., Izawa, T., Azuma, Y. & Takeuchi, T. (2012) Rapid, targeted, neuron-selective, *in vivo* knockdown following a single intracerebroventricular injection of a novel chemically modified siRNA in the adult rat brain. Journal of Biotechnology, 157 (2), 326-333.

Nakayama, T., Okada, N., Yoshikawa, M., Asaka, D., Kuboki, A., Kojima, H., Tanaka, Y. & Haruna, S. (2018) Assessment of suitable reference genes for RT–qPCR studies in chronic rhinosinusitis. Scientific Reports, 8 .

Napolitano, M., Vaz, G., Lawson, T. M., Docquier, M. -., van Maanen, A., Duprez, T. & Raftopoulos, C. (2014) Glioblastoma surgery with and without intraoperative MRI at 3.0T. Neuro-Chirurgie, 60 (4), 143-150.

Nazet, U., Schröder, A., Grässel, S., Muschter, D., Proff, P. & Kirschneck, C. (2019) Housekeeping gene validation for RT-qPCR studies on synovial fibroblasts derived from healthy and osteoarthritic patients with focus on mechanical loading. Plos One, 14 (12), e0225790.

Neal, J. T., Li, X., Zhu, J., Giangarra, V., Grzeskowiak, C. L., Ju, J., Liu, I. H., Chiou, S., Salahudeen, A. A., Smith, A. R., Deutsch, B. C., Liao, L., Zemek, A. J., Zhao, F., Karlsson, K., Schultz, L. M., Metzner, T. J., Nadauld, L. D., Tseng, Y., Alkhairy, S., Oh, C., Keskula, P., Mendoza-Villanueva, D., De La Vega, Francisco M., Kunz, P. L., Liao, J. C., Leppert, J.

T., Sunwoo, J. B., Sabatti, C., Boehm, J. S., Hahn, W. C., Zheng, G. X. Y., Davis, M. M. & Kuo, C. J. (2018) Organoid modeling of the tumor immune microenvironment. Cell, 175 (7), 1972-1988.e16.

Nelson, S. J. & Cha, S. (2003) Imaging glioblastoma multiforme. Cancer Journal (Sudbury, Mass.), 9 (2), 134-145.

Neves, K., Menezes Guimarães, D., Rayêe, D., Valério-Gomes, B., Meneses Iack, P., Lent, R. & Mota, B. (2019) The reliability of the isotropic fractionator method for counting total cells and neurons. Journal of Neuroscience Methods, 326 108392.

NICE (2018) Brain tumours (primary) and brain metastases in adults. Available online: https://www.nice.org.uk/guidance/NG99 2021].

Niculescu, A., Chircov, C., Bîrcă, A. C. & Grumezescu, A. M. (2021) Fabrication and applications of microfluidic devices: A review. International Journal of Molecular Sciences, 22 (4), .

Nieder, C., Grosu, A. L., Astner, S. & Molls, M. (2005) Treatment of unresectable glioblastoma multiforme. Anticancer Research, 25 (6C), 4605-4610.

Nimmerjahn, A., Kirchhoff, F. & Helmchen, F. (2005) Resting microglial cells are highly dynamic surveillants of brain parenchyma *in vivo*. Science (New York, N.Y.), 308 (5726), 1314-1318.

Nocera, A. D., Comín, R., Salvatierra, N. A. & Cid, M. P. (2018) Development of 3D printed fibrillar collagen scaffold for tissue engineering. Biomedical Microdevices, 20 (2), 26.

Noel, G., Huchet, A., Feuvret, L., Maire, J. P., Verrelle, P., Le Rhun, E., Aumont, M., Thillays, F., Sunyach, M. P., Henzen, C., Missohou, F., de Crevoisier, R., Bondiau, P. Y., Collin, P., Durando, X., Truc, G., Kerr, C., Bernier, V., Clavier, J., Atlani, D., D'Hombres, A., Vinchon-Petit, S., Lagrange, J. L. & Taillandier, L. (2012) Waiting times before initiation of radiotherapy might not affect outcomes for patients with glioblastoma: A french retrospective analysis of patients treated in the era of concomitant temozolomide and radiotherapy. Journal of Neuro-Oncology, 109 (1), 167-175.

Nomura, S., Tandon, N. N., Nakamura, T., Cone, J., Fukuhara, S. & Kambayashi, J. (2001) High-shear-stress-induced activation of platelets and microparticles enhances expression of cell adhesion molecules in THP-1 and endothelial cells. Atherosclerosis, 158 (2), 277-287.

Norden, A. D. & Wen, P. Y. (2006) Glioma therapy in adults. The Neurologist, 12 (6), 279-292.

Nunes, A. S., Barros, A. S., Costa, E. C., Moreira, A. F. & Correia, I. J. (2019) 3D tumor spheroids as in vitro models to mimic *in vivo* human solid tumors resistance to therapeutic drugs. Biotechnology and Bioengineering, 116 (1), 206-226.

Obermeier, B., Daneman, R. & Ransohoff, R. M. (2013) Development, maintenance and disruption of the blood-brain barrier. Nature Medicine, 19 (12), 1584-1596.

Oh, T. G., Bailey, P., Dray, E., Smith, A. G., Goode, J., Eriksson, N., Funder, J. W., Fuller, P. J., Simpson, E. R., Tilley, W. D., Leedman, P. J., Clarke, C. L., Grimmond, S., Dowhan, D. H. & Muscat, G. E. O. (2014) PRMT2 and RORγ expression are associated with breast cancer survival outcomes. Molecular Endocrinology, 28 (7), 1166-1185.

Ohgaki, H. & Kleihues, P. (2005) Population-based studies on incidence, survival rates, and genetic alterations in astrocytic and oligodendroglial gliomas. Journal of Neuropathology and Experimental Neurology, 64 (6), 479-489.

Ohgaki, H. & Kleihues, P. (2007) Genetic pathways to primary and secondary glioblastoma. The American Journal of Pathology, 170 (5), 1445-1453.

Ohgaki, H. (2009) Epidemiology of brain tumors. Methods in Molecular Biology (Clifton, N.J.), 472 323-342.

Ohtsuki, S. & Terasaki, T. (2007) Contribution of carrier-mediated transport systems to the blood-brain barrier as a supporting and protecting interface for the brain; importance for CNS drug discovery and development. Pharmaceutical Research, 24 (9), 1745-1758.

Ojemann, G., Ojemann, J., Lettich, E. & Berger, M. (2008) Cortical language localization in left, dominant hemisphere. an electrical stimulation mapping investigation in 117 patients. 1989. Journal of Neurosurgery, 108 (2), 411-421.

Okada, H., Kohanbash, G., Zhu, X., Kastenhuber, E. R., Hoji, A., Ueda, R. & Fujita, M. (2009) Immunotherapeutic approaches for glioma. Critical Reviews in Immunology, 29 (1), 1-42.

Oldrini, B., Vaquero-Siguero, N., Mu, Q., Kroon, P., Zhang, Y., Galán-Ganga, M., Bao, Z., Wang, Z., Liu, H., Sa, J. K., Zhao, J., Kim, H., Rodriguez-Perales, S., Nam, D., Verhaak, R. G. W., Rabadan, R., Jiang, T., Wang, J. & Squatrito, M. (2020) MGMT genomic rearrangements contribute to chemotherapy resistance in gliomas. Nature Communications, 11 (1), 1-10.

Olivier, C., Oliver, L., Lalier, L. & Vallette, F. M. (2020) Drug resistance in glioblastoma: The two faces of oxidative stress. Frontiers in Molecular Biosciences, 7 620677.

Oller-Salvia, B., Sánchez-Navarro, M., Giralt, E. & Teixidó, M. (2016) Blood-brain barrier shuttle peptides: An emerging paradigm for brain delivery. Chemical Society Reviews, 45 (17), 4690-4707.

Olubajo, F., Achawal, S. & Greenman, J. (2020) Development of a microfluidic culture paradigm for ex vivo maintenance of human glioblastoma tissue: A new glioblastoma model? Translational Oncology, 13 (1), 1-10.

Omuro, A. & DeAngelis, L. M. (2013) Glioblastoma and other malignant gliomas: A clinical review. Jama, 310 (17), 1842-1850.

Onchuru, T. O. & Kaltenpoth, M. (2019) Quantitative PCR primer design affects quantification of dsRNA-mediated gene knockdown. Ecology and Evolution, 9 (14), 8187-8192.

Oner, E., Kotmakci, M., Baird, A., Gray, S. G., Debelec Butuner, B., Bozkurt, E., Kantarci, A. G. & Finn, S. P. (2021) Development of EphA2 siRNA-loaded lipid nanoparticles and combination with a small-molecule histone demethylase inhibitor in prostate cancer cells and tumor spheroids. Journal of Nanobiotechnology, 19 .

Ong, L. J. Y., Islam, A., DasGupta, R., Iyer, N. G., Leo, H. L. & Toh, Y. (2017) A 3D printed microfluidic perfusion device for multicellular spheroid cultures. Biofabrication, 9 (4), 045005.

Osborn, M. F., Coles, A. H., Golebiowski, D., Echeverria, D., Moazami, M. P., Watts, J. K., Sena-Esteves, M. & Khvorova, A. (2018) Efficient gene silencing in brain tumors with hydrophobically modified siRNAs. Molecular Cancer Therapeutics, 17 (6), 1251-1258.

Ostrom, Q. T., Gittleman, H., Farah, P., Ondracek, A., Chen, Y., Wolinsky, Y., Stroup, N. E., Kruchko, C. & Barnholtz-Sloan, J. S. (2013) CBTRUS statistical report: Primary brain and

central nervous system tumors diagnosed in the united states in 2006-2010. Neuro-Oncology, 15 Suppl 2 ii1-56.

Pampaloni, F., Reynaud, E. G. & Stelzer, E. H. K. (2007) The third dimension bridges the gap between cell culture and live tissue. Nature Reviews. Molecular Cell Biology, 8 (10), 839-845.

Pan, W., Kastin, A. J., Zankel, T. C., van Kerkhof, P., Terasaki, T. & Bu, G. (2004) Efficient transfer of receptor-associated protein (RAP) across the blood-brain barrier. Journal of Cell Science, 117 (Pt 21), 5071-5078.

Pardridge, W. M. (1999) Blood-brain barrier biology and methodology. Journal of Neurovirology, 5 (6), 556-569.

Pardridge, W. M. (2005) The blood-brain barrier: Bottleneck in brain drug development. NeuroRx: The Journal of the American Society for Experimental NeuroTherapeutics, 2 (1), 3-14.

Park, C., Kim, J. E., Kim, J. Y., Song, S. W., Kim, J. W., Choi, S. H., Kim, T. M., Lee, S., Kim, I. H. & Park, S. (2012) The changes in MGMT promoter methylation status in initial and recurrent glioblastomas. Translational Oncology, 5 (5), 393-397.

Patra, B., Chen, Y., Peng, C., Lin, S., Lee, C. & Tung, Y. (2013) A microfluidic device for uniform-sized cell spheroids formation, culture, harvesting and flow cytometry analysis. Biomicrofluidics, 7 (5), 54114.

Pedraza, L., Laosa, O., Rodríguez-Mañas, L., Gutiérrez-Romero, D. F., Frías, J., Carnicero, J. A. & Ramírez, E. (2021) Drug induced liver injury in geriatric patients detected by a two-hospital prospective pharmacovigilance program: A comprehensive analysis using the roussel uclaf causality assessment method. Frontiers in Pharmacology, 0 .

Pekin, D., Skhiri, Y., Baret, J., Le Corre, D., Mazutis, L., Salem, C. B., Millot, F., El Harrak, A., Hutchison, J. B., Larson, J. W., Link, D. R., Laurent-Puig, P., Griffiths, A. D. & Taly, V. (2011) Quantitative and sensitive detection of rare mutations using droplet-based microfluidics. Lab on a Chip, 11 (13), 2156-2166.

Pelvig, D. P., Pakkenberg, H., Stark, A. K. & Pakkenberg, B. (2008) Neocortical glial cell numbers in human brains. Neurobiology of Aging, 29 (11), 1754-1762.

Perez-Catalan, N. A., Doe, C. Q. & Ackerman, S. D. (2021) The role of astrocyte-mediated plasticity in neural circuit development and function. Neural Development, 16 (1), 1.

Persidsky, Y., Ramirez, S. H., Haorah, J. & Kanmogne, G. D. (2006) Blood-brain barrier: Structural components and function under physiologic and pathologic conditions. Journal of Neuroimmune Pharmacology: The Official Journal of the Society on NeuroImmune Pharmacology, 1 (3), 223-236.

Petrackova, A., Vasinek, M., Sedlarikova, L., Dyskova, T., Schneiderova, P., Novosad, T., Papajik, T. & Kriegova, E. (2019) Standardization of sequencing coverage depth in NGS: Recommendation for detection of clonal and subclonal mutations in cancer diagnostics. Frontiers in Oncology, 0 .

Petreus, T., Cadogan, E., Hughes, G., Smith, A., Pilla Reddy, V., Lau, A., O'Connor, M. J., Critchlow, S., Ashford, M. & Oplustil O'Connor, L. (2021) Tumour-on-chip microfluidic platform for assessment of drug pharmacokinetics and treatment response. Communications Biology, 4 (1), 1-11.

Phillips, H. S., Kharbanda, S., Chen, R., Forrest, W. F., Soriano, R. H., Wu, T. D., Misra, A., Nigro, J. M., Colman, H., Soroceanu, L., Williams, P. M., Modrusan, Z., Feuerstein, B. G. & Aldape, K. (2006) Molecular subclasses of high-grade glioma predict prognosis, delineate a pattern of disease progression, and resemble stages in neurogenesis. Cancer Cell, 9 (3), 157-173.

Piccinini, F., Tesei, A., Arienti, C. & Bevilacqua, A. (2017) Cell counting and viability assessment of 2D and 3D cell cultures: Expected reliability of the trypan blue assay. Biological Procedures Online, 19 8.

Pinto, B., Henriques, A. C., Silva, P. M. A. & Bousbaa, H. (2020) Three-dimensional spheroids as in vitro preclinical models for cancer research. Pharmaceutics, 12 (12), .

Prasad, G. & Haas-Kogan, D. A. (2009) Radiation-induced gliomas. Expert Review of Neurotherapeutics, 9 (10), 1511-1517.

Prud'homme, G. J. (2007) Pathobiology of transforming growth factor β in cancer, fibrosis and immunologic disease, and therapeutic considerations. Laboratory Investigation, 87 (11), 1077-1091.

Purchiaroni, F., Begini, P., Minniti, G., Gallina, S., Delle Fave, G. & Marignani, M. (2014) Glioblastoma multiforme and hepatitis B: Do the right thing(s). European Review for Medical and Pharmacological Sciences, 18 (23), 3629-3631.

Qian, Z. M., Li, H., Sun, H. & Ho, K. (2002) Targeted drug delivery via the transferrin receptor-mediated endocytosis pathway. Pharmacological Reviews, 54 (4), 561-587.

Qin, Y., Musket, A., Kou, J., Preiszner, J., Tschida, B. R., Qin, A., Land, C. A., Staal, B., Kang, L., Tanner, K., Jiang, Y., Schweitzer, J. B., Largaespada, D. A. & Xie, Q. (2020) Overexpression of HGF/MET axis along with p53 inhibition induces de novo glioma formation in mice. Neuro-Oncology Advances, 2 (1), vdaa067.

Qiu, X., Huang, J., Westerhof, T. M., Lombardo, J. A., Henrikson, K. M., Pennell, M., Pourfard, P. P., Nelson, E. L., Nath, P. & Haun, J. B. (2018) Microfluidic channel optimization to improve hydrodynamic dissociation of cell aggregates and tissue. Scientific Reports, 8 (1), 2774.

Ramakrishnan, V., Akers, J., Nguyen, T., Wang, A., Adhikari, B., Hirshman, B., Li, J., Sarkaria, J., Hua, W., Ying, M., Nitta, M., Jiang, T., Carter, B. & Chen, C. C. (2018) Abstract 1956: miR-181d degradation mediated genetic heterogeneity and acquired resistance. Cancer Research, 78 (13 Supplement), 1956.

Rao, S. K., Pavicevic, Z., Du, Z., Kim, J., Fan, M., Jiao, Y., Rosebush, M., Samant, S., Gu, W., Pfeffer, L. M. & Nosrat, C. A. (2010) Pro-inflammatory genes as biomarkers and therapeutic targets in oral squamous cell carcinoma. The Journal of Biological Chemistry, 285 (42), 32512-32521.

Raposo, A. E. & Piller, S. C. (2018) Protein arginine methylation: An emerging regulator of the cell cycle. Cell Division, 13 3.

Regan, J. L., Schumacher, D., Staudte, S., Steffen, A., Haybaeck, J., Keilholz, U., Schweiger, C., Golob-Schwarzl, N., Mumberg, D., Henderson, D., Lehrach, H., Regenbrecht, C. R. A., Schäfer, R. & Lange, M. (2017) Non-canonical hedgehog signaling is a positive regulator of the WNT pathway and is required for the survival of colon cancer stem cells. Cell Reports, 21 (10), 2813-2828.

Regan, J. L., Schumacher, D., Staudte, S., Steffen, A., Lesche, R., Toedling, J., Jourdan, T., Haybaeck, J., Golob-Schwarzl, N., Mumberg, D., Henderson, D., Győrffy, B., Regenbrecht, C. R. A., Keilholz, U., Schäfer, R. & Lange, M. (2021) Identification of a nervous system gene expression signature in colon cancer stem cells reveals a role for neural crest regulators EGR2 and SOX2 in tumorigenesis. bioRxiv, 2021.02.02.428317.

Regazzo, G., Terrenato, I., Spagnuolo, M., Carosi, M., Cognetti, G., Cicchillitti, L., Sperati, F., Villani, V., Carapella, C., Piaggio, G., Pelosi, A. & Rizzo, M. G. (2016) A restricted signature of serum miRNAs distinguishes glioblastoma from lower grade gliomas. Journal of Experimental & Clinical Cancer Research: CR, 35 (1), 124.

Régina, A., Demeule, M., Ché, C., Lavallée, I., Poirier, J., Gabathuler, R., Béliveau, R. & Castaigne, J. -. (2008) Antitumour activity of ANG1005, a conjugate between paclitaxel and the new brain delivery vector angiopep-2. British Journal of Pharmacology, 155 (2), 185-197.

Reiber, H. (2001) Dynamics of brain-derived proteins in cerebrospinal fluid. Clinica Chimica Acta; International Journal of Clinical Chemistry, 310 (2), 173-186.

Reijnders, Maarten J. M. F. & Waterhouse, R. M. (2021) Summary visualizations of gene ontology terms with GO-figure! Frontiers in Bioinformatics, 0 .

Renovanz, M., Maurer, D., Lahr, H., Weimann, E., Deininger, M., Wirtz, C. R., Ringel, F., Singer, S. & Coburger, J. (2018) Supportive care needs in glioma patients and their caregivers in clinical practice: Results of a multicenter cross-sectional study. Frontiers in Neurology, 0 .

Reynolds, A., Leake, D., Boese, Q., Scaringe, S., Marshall, W. S. & Khvorova, A. (2004) Rational siRNA design for RNA interference. Nature Biotechnology, 22 (3), 326-330.

Reynolds, A., Leake, D., Boese, Q., Scaringe, S., Marshall, W. S. & Khvorova, A. (2004) Rational siRNA design for RNA interference. Nature Biotechnology, 22 (3), 326-330.

Rhee, S. Y., Wood, V., Dolinski, K. & Draghici, S. (2008) Use and misuse of the gene ontology annotations. Nature Reviews. Genetics, 9 (7), 509-515.

Riedmaier, I., Bergmaier, M. & Pfaffl, M. W. (2010) Comparison of two available platforms for determination of RNA quality. Null, 24 (4), 2154-2159.

Riffle, S., Pandey, R. N., Albert, M. & Hegde, R. S. (2017) Linking hypoxia, DNA damage and proliferation in multicellular tumor spheroids. BMC Cancer, 17 .

Rip, J., Schenk, G. J. & de Boer, A. G. (2009) Differential receptor-mediated drug targeting to the diseased brain. Expert Opinion on Drug Delivery, 6 (3), 227-237.

Robin, J. D., Ludlow, A. T., LaRanger, R., Wright, W. E. & Shay, J. W. (2016) Comparison of DNA quantification methods for next generation sequencing. Scientific Reports, 6 (1), 24067.

Rocha, H. L., Godet, I., Kurtoglu, F., Metzcar, J., Konstantinopoulos, K., Bhoyar, S., Gilkes, D. M. & Macklin, P. (2021) A persistent invasive phenotype in post-hypoxic tumor cells is revealed by fate mapping and computational modeling. iScience, 24 (9), 102935.

Rock, K., McArdle, O., Forde, P., Dunne, M., Fitzpatrick, D., O'Neill, B. & Faul, C. (2012) A clinical review of treatment outcomes in glioblastoma multiforme--the validation in a non-trial population of the results of a randomised phase III clinical trial: Has a more radical approach improved survival? The British Journal of Radiology, 85 (1017), 729.

Rodrigues, J. P., Prajapati, N., DeCoster, M. A., Poh, S. & Murray, T. A. (2021) Efficient LRP1-mediated uptake and low cytotoxicity of peptide L57 In Vitro shows its promise as CNS drug delivery vector. Journal of Pharmaceutical Sciences, 110 (2), 824-832.

Rodriguez, A. D., Horowitz, L. F., Castro, K., Kenerson, H., Bhattacharjee, N., Gandhe, G., Raman, A., Monnat, R. J., Yeung, R., Rostomily, R. C. & Folch, A. (2020) A microfluidic platform for functional testing of cancer drugs on intact tumor slices. Lab on a Chip, 20 (9), 1658-1675.

Rominiyi, O., Vanderlinden, A., Clenton, S. J., Bridgewater, C., Al-Tamimi, Y. & Collis, S. J. (2021) Tumour treating fields therapy for glioblastoma: Current advances and future directions. British Journal of Cancer, 124 (4), 697-709.

Ronaldson, P. T. & Davis, T. P. (2020) Regulation of blood-brain barrier integrity by microglia in health and disease: A therapeutic opportunity. Journal of Cerebral Blood Flow and Metabolism: Official Journal of the International Society of Cerebral Blood Flow and Metabolism, 40 (1_suppl), S6-S24.

Roux, E., Bougaran, P., Dufourcq, P. & Couffinhal, T. (2020) Fluid shear stress sensing by the endothelial layer. Frontiers in Physiology, 11 861.

Roy, S., Coldren, C., Karunamurthy, A., Kip, N. S., Klee, E. W., Lincoln, S. E., Leon, A., Pullambhatla, M., Temple-Smolkin, R. L., Voelkerding, K. V., Wang, C. & Carter, A. B. (2018) Standards and guidelines for validating next-generation sequencing bioinformatics pipelines: A joint recommendation of the association for molecular pathology and the college of american pathologists. The Journal of Molecular Diagnostics, 20 (1), 4-27.

Roy, S., LaFramboise, W. A., Nikiforov, Y. E., Nikiforova, M. N., Routbort, M. J., Pfeifer, J., Nagarajan, R., Carter, A. B. & Pantanowitz, L. (2016) Next-generation sequencing informatics: Challenges and strategies for implementation in a clinical environment. Archives of Pathology & Laboratory Medicine, 140 (9), 958-975.

Ruan, H., Chai, Z., Shen, Q., Chen, X., Su, B., Xie, C., Zhan, C., Yao, S., Wang, H., Zhang, M., Ying, M. & Lu, W. (2018) A novel peptide ligand RAP12 of LRP1 for glioma targeted drug delivery. Journal of Controlled Release: Official Journal of the Controlled Release Society, 279 306-315.

Ruigrok, M. J. R., Maggan, N., Willaert, D., Frijlink, H. W., Melgert, B. N., Olinga, P. & Hinrichs, W. L. J. (2017) siRNA-mediated RNA interference in precision-cut tissue slices prepared from mouse lung and kidney. The AAPS Journal, 19 (6), 1855-1863.

Ruigrok, M. J. R., Xian, J., Frijlink, H. W., Melgert, B. N., Hinrichs, W. L. J. & Olinga, P. (2018) siRNA-mediated protein knockdown in precision-cut lung slices. European Journal of Pharmaceutics and Biopharmaceutics, 133 339-348.

Ruppen, J., Cortes-Dericks, L., Marconi, E., Karoubi, G., Schmid, R. A., Peng, R., Marti, T. M. & Guenat, O. T. (2014) A microfluidic platform for chemoresistive testing of multicellular pleural cancer spheroids. Lab on a Chip, 14 (6), 1198-1205.

Ruppen, J., Wildhaber, F. D., Strub, C., Hall, S. R. R., Schmid, R. A., Geiser, T. & Guenat, O. T. (2015) Towards personalized medicine: Chemosensitivity assays of patient lung cancer cell spheroids in a perfused microfluidic platform. Lab on a Chip, 15 (14), 3076-3085.

Ryan, S., Baird, A., Vaz, G., Urquhart, A. J., Senge, M., Richard, D. J., O'Byrne, K. J. & Davies, A. M. (2016) Drug discovery approaches utilizing three-dimensional cell culture. Assay and Drug Development Technologies, 14 (1), 19-28.

Sá, A. C. C., Sadee, W. & Johnson, J. A. (2018) Whole transcriptome profiling: An RNA-Seq primer and implications for pharmacogenomics research. Clinical and Translational Science, 11 (2), 153-161.

Saadeh, F. S., Mahfouz, R. & Assi, H. I. (2018) EGFR as a clinical marker in glioblastomas and other gliomas. The International Journal of Biological Markers, 33 (1), 22-32.

Sahay, G., Querbes, W., Alabi, C., Eltoukhy, A., Sarkar, S., Zurenko, C., Karagiannis, E., Love, K., Chen, D., Zoncu, R., Buganim, Y., Schroeder, A., Langer, R. & Anderson, D. G. (2013) Efficiency of siRNA delivery by lipid nanoparticles is limited by endocytic recycling. Nature Biotechnology, 31 (7), 653-658.

Sajid, M. I., Moazzam, M., Kato, S., Yeseom Cho, K. & Tiwari, R. K. (2020) Overcoming barriers for siRNA therapeutics: From bench to bedside. Pharmaceuticals (Basel, Switzerland), 13 (10), .

Sanai, N., Tramontin, A. D., Quiñones-Hinojosa, A., Barbaro, N. M., Gupta, N., Kunwar, S., Lawton, M. T., McDermott, M. W., Parsa, A. T., Verdugo, J. M., Berger, M. S. & Alvarez-Buylla, A. (2004) Unique astrocyte ribbon in adult human brain contains neural stem cells but lacks chain migration. Nature, 427 (6976), 740-744.

Sanmillan, J. L., Fernández-Coello, A., Fernández-Conejero, I., Plans, G. & Gabarrós, A. (2017) Functional approach using intraoperative brain mapping and neurophysiological monitoring for the surgical treatment of brain metastases in the central region. Journal of Neurosurgery, 126 (3), 698-707.

Sanson, M., Marie, Y., Paris, S., Idbaih, A., Laffaire, J., Ducray, F., El Hallani, S., Boisselier, B., Mokhtari, K., Hoang-Xuan, K. & Delattre, J. (2009) Isocitrate dehydrogenase 1 codon 132 mutation is an important prognostic biomarker in gliomas. Journal of Clinical Oncology, 27 (25), 4150-4154.

Sant, S. & Johnston, P. A. (2017) The production of 3D tumor spheroids for cancer drug discovery. Drug Discovery Today. Technologies, 23 27-36.

Santo, V. E., Estrada, M. F., Rebelo, S. P., Abreu, S., Silva, I., Pinto, C., Veloso, S. C., Serra, A. T., Boghaert, E., Alves, P. M. & Brito, C. (2016) Adaptable stirred-tank culture strategies for large scale production of multicellular spheroid-based tumor cell models. Journal of Biotechnology, 221 118-129.

Saunders, N. R., Dreifuss, J., Dziegielewska, K. M., Johansson, P. A., Habgood, M. D., Møllgård, K. & Bauer, H. (2014) The rights and wrongs of blood-brain barrier permeability studies: A walk through 100 years of history. Frontiers in Neuroscience, 8 404.

Schaich, M., Kestel, L., Pfirrmann, M., Robel, K., Illmer, T., Kramer, M., Dill, C., Ehninger, G., Schackert, G. & Krex, D. (2009) A MDR1 (ABCB1) gene single nucleotide polymorphism predicts outcome of temozolomide treatment in glioblastoma patients. Annals of Oncology: Official Journal of the European Society for Medical Oncology, 20 (1), 175-181.

Schirmer, M., D'Amore, R., Ijaz, U. Z., Hall, N. & Quince, C. (2016) Illumina error profiles: Resolving fine-scale variation in metagenomic sequencing data. BMC Bioinformatics, 17 125.

Schiroli, D., Gómara, M. J., Maurizi, E., Atkinson, S. D., Mairs, L., Christie, K. A., Cobice, D. F., McCrudden, C. M., Nesbit, M. A., Haro, I. & Moore, T. (2019) Effective *In vivo* topical delivery of siRNA and gene silencing in intact corneal epithelium using a modified cell-penetrating peptide. Molecular Therapy. Nucleic Acids, 17 891-906.

Schirrmacher, V. (2019) From chemotherapy to biological therapy: A review of novel concepts to reduce the side effects of systemic cancer treatment (review). International Journal of Oncology, 54 (2), 407-419.

Schrauder, M. G., Strick, R., Schulz-Wendtland, R., Strissel, P. L., Kahmann, L., Loehberg, C. R., Lux, M. P., Jud, S. M., Hartmann, A., Hein, A., Bayer, C. M., Bani, M. R., Richter, S., Adamietz, B. R., Wenkel, E., Rauh, C., Beckmann, M. W. & Fasching, P. A. (2012) Circulating micro-RNAs as potential blood-based markers for early stage breast cancer detection. PloS One, 7 (1), e29770.

Schwartzbaum, J. A., Fisher, J. L., Aldape, K. D. & Wrensch, M. (2006) Epidemiology and molecular pathology of glioma. Nature Clinical Practice. Neurology, 2 (9), 494-503; quiz 1 p following 516.

Scott, J., Tsai, Y., Chinnaiyan, P. & Yu, H. M. (2011) Effectiveness of radiotherapy for elderly patients with glioblastoma. International Journal of Radiation Oncology, Biology, Physics, 81 (1), 206-210.

Segura, I., De Smet, F., Hohensinner, P. J., Ruiz de Almodovar, C. & Carmeliet, P. (2009) The neurovascular link in health and disease: An update. Trends in Molecular Medicine, 15 (10), 439-451.

Serrano-Heras, G., Castro-Robles, B., Romero-Sánchez, C. M., Carrión, B., Barbella-Aponte, R., Sandoval, H. & Segura, T. (2020) Involvement of N-methylpurine DNA glycosylase in resistance to temozolomide in patient-derived glioma cells. Scientific Reports, 10 (1), 1-10.

Shan, H., Chu, Y., Chang, P., Yang, L., Wang, Y., Zhu, S., Zhang, M. & Tao, L. (2017) Neuroprotective effects of hydrogen sulfide on sodium azide induced autophagic cell death in PC12 cells. Molecular Medicine Reports, 16 (5), 5938-5946.

Shan, Z., Tian, R., Zhang, M., Gui, Z., Wu, J., Ding, M., Zhou, X. & He, J. (2016) miR128-1 inhibits the growth of glioblastoma multiforme and glioma stem-like cells via targeting BMI1 and E2F3. Oncotarget, 7 (48), 78813-78826.

Shankar, G. M., Balaj, L., Stott, S. L., Nahed, B. & Carter, B. S. (2017) Liquid biopsy for brain tumors. Expert Review of Molecular Diagnostics, 17 (10), 943-947.

Sharifi Tabar, M., Hesaraki, M., Esfandiari, F., Sahraneshin Samani, F., Vakilian, H. & Baharvand, H. (2015) Evaluating electroporation and lipofectamine approaches for transient and stable transgene expressions in human fibroblasts and embryonic stem cells. Cell Journal, 17 (3), 438-450.

Sharma, S., Salehi, F., Scheithauer, B. W., Rotondo, F., Syro, L. V. & Kovacs, K. (2009) Role of MGMT in tumor development, progression, diagnosis, treatment and prognosis. Anticancer Research, 29 (10), 3759-3768.

Shen, H., Cai, S., Wu, C., Yang, W., Yu, H. & Liu, L. (2021) Recent advances in three-dimensional multicellular spheroid culture and future development. Micromachines, 12 (1), .

Shin, H., Lee, S., Hong, H. J., Lim, Y. C., Koh, W. & Lim, J. (2018) Stem cell properties of human clonal salivary gland stem cells are enhanced by three-dimensional priming culture in nanofibrous microwells. Stem Cell Research & Therapy, 9 (1), 74.

Shinsato, Y., Furukawa, T., Yunoue, S., Yonezawa, H., Minami, K., Nishizawa, Y., Ikeda, R., Kawahara, K., Yamamoto, M., Hirano, H., Tokimura, H. & Arita, K. (2013) Reduction of MLH1 and PMS2 confers temozolomide resistance and is associated with recurrence of glioblastoma. Oncotarget, 4 (12), 2261-2270.

Shtam, T. A., Kovalev, R. A., Varfolomeeva, E. Y., Makarov, E. M., Kil, Y. V. & Filatov, M. V. (2013) Exosomes are natural carriers of exogenous siRNA to human cells in vitro. Cell Communication and Signaling: CCS, 11 88.

Shu, D., Shu, Y., Haque, F., Abdelmawla, S. & Guo, P. (2011) Thermodynamically stable RNA three-way junction for constructing multifunctional nanoparticles for delivery of therapeutics. Nature Nanotechnology, 6 (10), 658-667.

Silantyev, A. S., Falzone, L., Libra, M., Gurina, O. I., Kardashova, K. S., Nikolouzakis, T. K., Nosyrev, A. E., Sutton, C. W., Mitsias, P. D. & Tsatsakis, A. (2019) Current and future trends on diagnosis and prognosis of glioblastoma: From molecular biology to proteomics. Cells, 8 (8), .

Silber, J. R., Blank, A., Bobola, M. S., Mueller, B. A., Kolstoe, D. D., Ojemann, G. A. & Berger, M. S. (1996) Lack of the DNA repair protein O6-methylguanine-DNA methyltransferase in histologically normal brain adjacent to primary human brain tumors. Proceedings of the National Academy of Sciences of the United States of America, 93 (14), 6941-6946.

Silber, J. R., Bobola, M. S., Blank, A., Schoeler, K. D., Haroldson, P. D., Huynh, M. B. & Kolstoe, D. D. (2002) The apurinic/apyrimidinic endonuclease activity of Ape1/ref-1 contributes to human glioma cell resistance to alkylating agents and is elevated by oxidative stress. Clinical Cancer Research: An Official Journal of the American Association for Cancer Research, 8 (9), 3008-3018.

Silva-Alvarez, C., Carrasco, M., Balmaceda-Aguilera, C., Pastor, P., García, María de los Angeles, Reinicke, K., Aguayo, L., Molina, B., Cifuentes, M., Medina, R. & Nualart, F. (2005) Ependymal cell differentiation and GLUT1 expression is a synchronous process in the ventricular wall. Neurochemical Research, 30 (10), 1227-1236.

Singh, A., Trivedi, P. & Jain, N. K. (2018) Advances in siRNA delivery in cancer therapy. Artificial Cells, Nanomedicine, and Biotechnology, 46 (2), 274-283.

Sioud, M. (2020) Optimized siRNA delivery into primary immune cells using electroporation. Methods in Molecular Biology (Clifton, N.J.), 2115 119-131.

Siracusa, R., Fusco, R. & Cuzzocrea, S. (2019) Astrocytes: Role and functions in brain pathologies. Frontiers in Pharmacology, 9, 1245 .

Smith, C. & Ironside, J. W. (2007) Diagnosis and pathogenesis of gliomas. Current Diagnostic Pathology, 13 (3), 180-192.

Sodunke, T. R., Turner, K. K., Caldwell, S. A., McBride, K. W., Reginato, M. J. & Noh, H. M. (2007a) Micropatterns of matrigel for three-dimensional epithelial cultures. Biomaterials, 28 (27), 4006-4016.

Sodunke, T. R., Turner, K. K., Caldwell, S. A., McBride, K. W., Reginato, M. J. & Noh, H. M. (2007) Micropatterns of matrigel for three-dimensional epithelial cultures. Biomaterials, 28 (27), 4006-4016.

Soulet, D. & Rivest, S. (2008) Microglia. Current Biology, 18 (12), R506-R508.

Soutschek, J., Akinc, A., Bramlage, B., Charisse, K., Constien, R., Donoghue, M., Elbashir, S., Geick, A., Hadwiger, P., Harborth, J., John, M., Kesavan, V., Lavine, G., Pandey, R. K., Racie, T., Rajeev, K. G., Röhl, I., Toudjarska, I., Wang, G., Wuschko, S., Bumcrot, D., Koteliansky, V., Limmer, S., Manoharan, M. & Vornlocher, H. (2004) Therapeutic silencing

of an endogenous gene by systemic administration of modified siRNAs. Nature, 432 (7014), 173-178.

Soutschek, J., Akinc, A., Bramlage, B., Charisse, K., Constien, R., Donoghue, M., Elbashir, S., Geick, A., Hadwiger, P., Harborth, J., John, M., Kesavan, V., Lavine, G., Pandey, R. K., Racie, T., Rajeev, K. G., Röhl, I., Toudjarska, I., Wang, G., Wuschko, S., Bumcrot, D., Koteliansky, V., Limmer, S., Manoharan, M. & Vornlocher, H. (2004) Therapeutic silencing of an endogenous gene by systemic administration of modified siRNAs. Nature, 432 (7014), 173-178.

Sözmen, A. B. & Arslan Yildiz, A. (2021) Cost-effective and rapid prototyping of PMMA microfluidic device via polymer-assisted bonding. Microfluidics and Nanofluidics, 25 (8), 66.

Spassky, N., Merkle, F. T., Flames, N., Tramontin, A. D., García-Verdugo, J. M. & Alvarez-Buylla, A. (2005) Adult ependymal cells are postmitotic and are derived from radial glial cells during embryogenesis. The Journal of Neuroscience: The Official Journal of the Society for Neuroscience, 25 (1), 10-18.

Stevens, B. (2003) Glia: Much more than the neuron's side-kick. Current Biology, 13 (12), R469-R472.

Stevens, B. (2003) Glia: Much more than the neuron's side-kick. Current Biology, 13 (12), R469-R472.

Stojcheva, N., Schechtmann, G., Sass, S., Roth, P., Florea, A., Stefanski, A., Stühler, K., Wolter, M., Müller, N. S., Theis, F. J., Weller, M., Reifenberger, G. & Happold, C. (2016) MicroRNAMicroRNA-138 promotes acquired alkylator resistance in glioblastoma by targeting the bcl-2-interacting mediator BIM. Oncotarget, 7 (11), 12937-12950.

Stoyanov, G. S., Dzhenkov, D., Ghenev, P., Iliev, B., Enchev, Y. & Tonchev, A. B. (2018) Cell biology of glioblastoma multiforme: From basic science to diagnosis and treatment. Medical Oncology (Northwood, London, England), 35 (3), 27.

Stoyanov, G. S., Lyutfi, E., Georgieva, R., Georgiev, R., Dzhenkov, D. L., Petkova, L., Ivanov, B. D., Kaprelyan, A. & Ghenev, P. (2022) Reclassification of glioblastoma multiforme according to the 2021 world health organization classification of central nervous system tumors: A single institution report and practical significance. Cureus, 14 (2), e21822.

Stringer, B. W., Day, B. W., D'Souza, R. C. J., Jamieson, P. R., Ensbey, K. S., Bruce, Z. C., Lim, Y. C., Goasdoué, K., Offenhäuser, C., Akgül, S., Allan, S., Robertson, T., Lucas, P., Tollesson, G., Campbell, S., Winter, C., Do, H., Dobrovic, A., Inglis, P., Jeffree, R. L., Johns, T. G. & Boyd, A. W. (2019) A reference collection of patient-derived cell line and xenograft models of proneural, classical and mesenchymal glioblastoma. Scientific Reports, 9 (1), 4902.

Stummer, W., Pichlmeier, U., Meinel, T., Wiestler, O. D., Zanella, F. & Reulen, H. (2006) Fluorescence-guided surgery with 5-aminolevulinic acid for resection of malignant glioma: A randomised controlled multicentre phase III trial. The Lancet. Oncology, 7 (5), 392-401.

Stupp, R., Hegi, M. E., Mason, W. P., van den Bent, Martin J., Taphoorn, M. J. B., Janzer, R. C., Ludwin, S. K., Allgeier, A., Fisher, B., Belanger, K., Hau, P., Brandes, A. A., Gijtenbeek, J., Marosi, C., Vecht, C. J., Mokhtari, K., Wesseling, P., Villa, S., Eisenhauer, E., Gorlia, T., Weller, M., Lacombe, D., Cairncross, J. G. & Mirimanoff, R. (2009) Effects of radiotherapy with concomitant and adjuvant temozolomide versus radiotherapy alone on survival in glioblastoma in a randomised phase III study: 5-year analysis of the EORTC-NCIC trial. The Lancet. Oncology, 10 (5), 459-466.

Stupp, R., Mason, W. P., van den Bent, Martin J., Weller, M., Fisher, B., Taphoorn, M. J. B., Belanger, K., Brandes, A. A., Marosi, C., Bogdahn, U., Curschmann, J., Janzer, R. C., Ludwin, S. K., Gorlia, T., Allgeier, A., Lacombe, D., Cairncross, J. G., Eisenhauer, E. & Mirimanoff, R. O. (2005) Radiotherapy plus concomitant and adjuvant temozolomide for glioblastoma. The New England Journal of Medicine, 352 (10), 987-996.

Sun, M. Z., Oh, T., Ivan, M. E., Clark, A. J., Safaee, M., Sayegh, E. T., Kaur, G., Parsa, A. T. & Bloch, O. (2015) Survival impact of time to initiation of chemoradiotherapy after resection of newly diagnosed glioblastoma. Journal of Neurosurgery, 122 (5), 1144-1150.

Sun, Q., Pei, C., Li, Q., Dong, T., Dong, Y., Xing, W., Zhou, P., Gong, Y., Zhen, Z., Gao, Y., Xiao, Y., Su, J. & Ren, H. (2018) Up-regulation of MSH6 is associated with temozolomide resistance in human glioblastoma. Biochemical and Biophysical Research Communications, 496 (4), 1040-1046.

Sun, S., Lee, D., Lee, N. P., Pu, J. K. S., Wong, S. T. S., Lui, W. M., Fung, C. F. & Leung, G. K. K. (2012) Hyperoxia resensitizes chemoresistant human glioblastoma cells to temozolomide. Journal of Neuro-Oncology, 109 (3), 467-475.

Sylvester, D., Hattersley, S. M., Stafford, N., Haswell, S. & Greenman, J. (2012) Development of microfluidic-based analytical methodology for studying the effects of chemotherapy agents on cancer tissue.

Tabata, H. (2015) Diverse subtypes of astrocytes and their development during corticogenesis. Frontiers in Neuroscience, 0 .

Tabei, Y., Kobayashi, K., Saito, K., Shimizu, S., Suzuki, K., Sasaki, N., Shiokawa, Y. & Nagane, M. (2021) Survival in patients with glioblastoma at a first progression does not correlate with isocitrate dehydrogenase (IDH)1 gene mutation status. Japanese Journal of Clinical Oncology, 51 (1), 45-53.

Tamimi, A. F. & Juweid, M. (2017) Epidemiology and outcome of glioblastoma. In Steven De Vleeschouwer (ed) Glioblastoma. Brisbane (AU): Codon Publications, .

Tan, A. C., Ashley, D. M., López, G. Y., Malinzak, M., Friedman, H. S. & Khasraw, M. (2020) Management of glioblastoma: State of the art and future directions. CA: A Cancer Journal for Clinicians, 70 (4), 299-312.

Taniguchi, T., Endo, K., Tanioka, H., Sasaoka, M., Tashiro, K., Kinoshita, S. & Kageyama, M. (2020) Novel use of a chemically modified siRNA for robust and sustainable *in vivo* gene silencing in the retina. Scientific Reports, 10 (1), 1-9.

Taylor, O. G., Brzozowski, J. S. & Skelding, K. A. (2019) Glioblastoma multiforme: An overview of emerging therapeutic targets. Frontiers in Oncology, 0 .

Tentori, L. & Graziani, G. (2009) Recent approaches to improve the antitumor efficacy of temozolomide. Current Medicinal Chemistry, 16 (2), 245-257.

Thiebaut, F., Tsuruo, T., Hamada, H., Gottesman, M. M., Pastan, I. & Willingham, M. C. (1989) Immunohistochemical localization in normal tissues of different epitopes in the multidrug transport protein P170: Evidence for localization in brain capillaries and crossreactivity of one antibody with a muscle protein. The Journal of Histochemistry and Cytochemistry: Official Journal of the Histochemistry Society, 37 (2), 159-164.

Thier, K., Calabek, B., Tinchon, A., Grisold, W. & Oberndorfer, S. (2016) The last 10 days of patients with glioblastoma: Assessment of clinical signs and symptoms as well as treatment. American Journal of Hospice and Palliative Medicine®, 33 (10), 985-988.

Thomas Charles Collins (2019) Developing a novel spheroid-on-chip microfluidic

Tian, M., Ma, W., Chen, Y., Yu, Y., Zhu, D., Shi, J. & Zhang, Y. (2018) Impact of gender on the survival of patients with glioblastoma. Bioscience Reports, 38 (6), .

Tian, T., Mingyi, M., Qiu, X. & Qiu, Y. (2016) MicroRNAMicroRNA-101 reverses temozolomide resistance by inhibition of GSK3β in glioblastoma. Oncotarget, 7 (48), 79584-79595.

Tichopad, A., Didier, A. & Pfaffl, M. W. (2004) Inhibition of real-time RT-PCR quantification due to tissue-specific contaminants. Molecular and Cellular Probes, 18 (1), 45-50.

Tomczak, A., Mortensen, J. M., Winnenburg, R., Liu, C., Alessi, D. T., Swamy, V., Vallania, F., Lofgren, S., Haynes, W., Shah, N. H., Musen, M. A. & Khatri, P. (2018) Interpretation of biological experiments changes with evolution of the gene ontology and its annotations. Scientific Reports, 8 (1), 5115.

Toriello, N. M., Douglas, E. S., Thaitrong, N., Hsiao, S. C., Francis, M. B., Bertozzi, C. R. & Mathies, R. A. (2008) Integrated microfluidic bioprocessor for single-cell gene expression analysis. Proceedings of the National Academy of Sciences of the United States of America, 105 (51), 20173-20178.

Torrisi, F., Alberghina, C., D'Aprile, S., Pavone, A. M., Longhitano, L., Giallongo, S., Tibullo, D., Di Rosa, M., Zappalà, A., Cammarata, F. P., Russo, G., Ippolito, M., Cuttone, G., Li Volti, G., Vicario, N. & Parenti, R. (2022) The hallmarks of glioblastoma: Heterogeneity, intercellular crosstalk and molecular signature of invasiveness and progression. Biomedicines, 10 (4), .

Townsley, B. T., Covington, M. F., Ichihashi, Y., Zumstein, K. & Sinha, N. R. (2015) BrAD-seq: Breath adapter directional sequencing: A streamlined, ultra-simple and fast library preparation protocol for strand specific mRNA library construction. Frontiers in Plant Science, 0 .

Traxl, A., Mairinger, S., Filip, T., Sauberer, M., Stanek, J., Poschner, S., Jäger, W., Zoufal, V., Novarino, G., Tournier, N., Bauer, M., Wanek, T. & Langer, O. (2019) Inhibition of ABCB1 and ABCG2 at the mouse blood-brain barrier with marketed drugs to improve brain delivery of the model ABCB1/ABCG2 substrate [11C]erlotinib. Molecular Pharmaceutics, 16 (3), 1282-1293.

Trevisan, B., Morsi, A., Aleman, J., Rodriguez, M., Shields, J., Meares, D., Farland, A. M., Doering, C. B., Spencer, H. T., Atala, A., Skardal, A., Porada, C. D. & Almeida-Porada, G. (2021) Effects of shear stress on production of FVIII and vWF in a cell-based therapeutic for hemophilia A. Frontiers in Bioengineering and Biotechnology, 9 639070.

Trujillo-de Santiago, G., Flores-Garza, B. G., Tavares-Negrete, J. A., Lara-Mayorga, I. M., González-Gamboa, I., Zhang, Y. S., Rojas-Martínez, A., Ortiz-López, R. & Álvarez, M. M. (2019) The tumor-on-chip: Recent advances in the development of microfluidic systems to recapitulate the physiology of solid tumors. Materials, 12 (18), .

Tsai, H., Yang, K., Wu, M., Chen, J. & Tseng, C. (2019) The effects of different dynamic culture systems on cell proliferation and osteogenic differentiation in human mesenchymal stem cells. International Journal of Molecular Sciences, 20 (16), .

Tsaryk, R., Yucel, N., Leonard, E. V., Diaz, N., Bondareva, O., Odenthal-Schnittler, M., Arany, Z., Vaquerizas, J. M., Schnittler, H. & Siekmann, A. F. (2022) Shear stress switches

the association of endothelial enhancers from ETV/ETS to KLF transcription factor binding sites. Scientific Reports, 12 (1), 1-15.

Tsuji, n. & Tamai, n. (1999) Carrier-mediated or specialized transport of drugs across the blood-brain barrier. Advanced Drug Delivery Reviews, 36 (2-3), 277-290.

Uchenunu, O., Pollak, M., Topisirovic, I. & Hulea, L. (2018) Oncogenic kinases and perturbations in protein synthesis machinery and energetics in neoplasia. Journal of Molecular Endocrinology, 62 (2), R83-R103.

Uddin, M. S., Kabir, M. T., Mamun, A. A., Sarwar, M. S., Nasrin, F., Emran, T. B., Alanazi, I. S., Rauf, A., Albadrani, G. M., Sayed, A. A., Mousa, S. A. & Abdel-Daim, M. M. (2021) Natural small molecules targeting NF-κB signaling in glioblastoma. Frontiers in Pharmacology, 12 703761.

Udvardi, M. K., Czechowski, T. & Scheible, W. (2008) Eleven golden rules of quantitative RT-PCR. The Plant Cell, 20 (7), 1736-1737.

Ujifuku, K., Mitsutake, N., Takakura, S., Matsuse, M., Saenko, V., Suzuki, K., Hayashi, K., Matsuo, T., Kamada, K., Nagata, I. & Yamashita, S. (2010) miR-195, miR-455-3p and miR-10a(*) are implicated in acquired temozolomide resistance in glioblastoma multiforme cells. Cancer Letters, 296 (2), 241-248.

Unger, C., Lokmer, N., Lehmann, D. & Axmann, I. M. (2019) Detection of phenol contamination in RNA samples and its impact on qRT-PCR results. Analytical Biochemistry, 571 49-52.

Vaira, V., Fedele, G., Pyne, S., Fasoli, E., Zadra, G., Bailey, D., Snyder, E., Faversani, A., Coggi, G., Flavin, R., Bosari, S. & Loda, M. (2010) Preclinical model of organotypic culture for pharmacodynamic profiling of human tumors. Proceedings of the National Academy of Sciences of the United States of America, 107 (18), 8352-8356.

van Midwoud, P. M. & Sturla, S. J. (2013) Improved efficacy of acylfulvene in colon cancer cells when combined with a nuclear excision repair inhibitor. Chemical Research in Toxicology, 26 (11), 1674-1682.

van Midwoud, P. M., Verpoorte, E. & Groothuis, G. M. M. (2011) Microfluidic devices for in vitro studies on liver drug metabolism and toxicity. Integrative Biology, 3 (5), 509-521.

Vein, A. A. (2008) Science and fate: Lina stern (1878–1968), A neurophysiologist and biochemist. Journal of the History of the Neurosciences, 17 (2), 195-206.

Vertrees, R. A., Jordan, J. M., Solley, T. & Goodwin, T. J. (2009) Tissue culture models. Basic Concepts of Molecular Pathology, 2 159-182.

Vigneswaran, K., Neill, S. & Hadjipanayis, C. G. (2015) Beyond the world health organization grading of infiltrating gliomas: Advances in the molecular genetics of glioma classification. Annals of Translational Medicine, 3 (7), 95.

Vinci, M., Gowan, S., Boxall, F., Patterson, L., Zimmermann, M., Court, W., Lomas, C., Mendiola, M., Hardisson, D. & Eccles, S. A. (2012) Advances in establishment and analysis of three-dimensional tumor spheroid-based functional assays for target validation and drug evaluation. BMC Biology, 10 29.

Virga, J., Szivos, L., Hortobágyi, T., Chalsaraei, M. K., Zahuczky, G., Steiner, L., Tóth, J., Reményi-Puskár, J., Bognár, L. & Klekner, A. (2019) Extracellular matrix differences in glioblastoma patients with different prognoses. Oncology Letters, 17 (1), 797-806.

Vogelbaum, M. A. (2012) Does extent of resection of a glioblastoma matter? Clinical Neurosurgery, 59 79-81.

von Bartheld, C. S., Bahney, J. & Herculano-Houzel, S. (2016) The search for true numbers of neurons and glial cells in the human brain: A review of 150 years of cell counting. The Journal of Comparative Neurology, 524 (18), 3865-3895.

Walid, M. S. (2008) Prognostic factors for long-term survival after glioblastoma. The Permanente Journal, 12 (4), 45-48.

Wan, J. & Lu, H. (2020) Enabling high-throughput single-animal gene-expression studies with molecular and micro-scale technologies. Lab on a Chip, 20 (24), 4528-4538.

Wan, L., Neumann, C. A. & LeDuc, P. R. (2020) Tumor-on-a-chip for integrating a 3D tumor microenvironment: Chemical and mechanical factors. Lab on a Chip, 20 (5), 873-888.

Wang, J., Zhang, X., Li, X., Zhang, Y., Hou, T., Wei, L., Qu, L., Shi, L., Liu, Y., Zou, L. & Liang, X. (2016) Anti-gastric cancer activity in three-dimensional tumor spheroids of bufadienolides. Scientific Reports, 6 (1), 24772.

Wang, K., Kievit, F. M., Chiarelli, P. A., Stephen, Z. R., Lin, G., Silber, J. R., Ellenbogen, R. G. & Zhang, M. (2021) siRNA nanoparticle suppresses drug-resistant gene and prolongs survival in an orthotopic glioblastoma xenograft mouse model. Advanced Functional Materials, 31 (6), .

Wei, S. C. & Yang, J. (2016) Forcing through tumor metastasis: The interplay between tissue rigidity and epithelial-mesenchymal transition. Trends in Cell Biology, 26 (2), 111-120.

Wei, Y. C., Chen, F., Zhang, T., Chen, D. Y., Jia, X., Wang, J. B., Guo, W. & Chen, J. (2014) Vascular smooth muscle cell culture in microfluidic devices. Biomicrofluidics, 8 (4), 046504.

Weissenrieder, J., Reed, J., Green, M., Moldovan, G., Koubek, E., Neighbors, J. & Hohl, R. (2020) The dopamine D2 receptor contributes to the spheroid formation behavior of U87 glioblastoma cells. Pharmacology, 105 (1-2), 19-27.

Weiswald, L., Bellet, D. & Dangles-Marie, V. (2015) Spherical cancer models in tumor biology. Neoplasia (New York, N.Y.), 17 (1), 1-15.

Wekerle, H. (2002) Immune protection of the brain--efficient and delicate. The Journal of Infectious Diseases, 186 Suppl 2 140.

Wesolowski, J. R., Rajdev, P. & Mukherji, S. K. (2010) Temozolomide (temodar). AJNR. American Journal of Neuroradiology, 31 (8), 1383-1384.

Westergaard, E. & Brightman, M. W. (1973) Transport of proteins across normal cerebral arterioles. The Journal of Comparative Neurology, 152 (1), 17-44.

Wilson, T. A., Karajannis, M. A. & Harter, D. H. (2014) Glioblastoma multiforme: State of the art and future therapeutics. Surgical Neurology International, 5 64.

Winkler, J., Abisoye-Ogunniyan, A., Metcalf, K. J. & Werb, Z. (2020) Concepts of extracellular matrix remodelling in tumour progression and metastasis. Nature Communications, 11 (1), 1-19.

Wolburg, H., Noell, S., Mack, A., Wolburg-Buchholz, K. & Fallier-Becker, P. (2009) Brain endothelial cells and the glio-vascular complex. Cell and Tissue Research, 335 (1), 75-96.

Woo, P. Y. M., Li, Y., Chan, A. H. Y., Ng, S. C. P., Loong, H. H. F., Chan, D. T. M., Wong, G. K. C. & Poon, W. (2019) A multifaceted review of temozolomide resistance mechanisms in glioblastoma beyond O-6-methylguanine-DNA methyltransferase. Glioma, 2 (2), 68.

Wu, T., Hu, E., Xu, S., Chen, M., Guo, P., Dai, Z., Feng, T., Zhou, L., Tang, W., Zhan, L., Fu, X., Liu, S., Bo, X. & Yu, G. (2021) clusterProfiler 4.0: A universal enrichment tool for interpreting omics data. The Innovation, 2 (3), 100141.

Wu, W., Hodges, E., Redelius, J. & Höög, C. (2004) A novel approach for evaluating the efficiency of siRNAs on protein levels in cultured cells. Nucleic Acids Research, 32 (2), e17.

Xi, G., Mania-Farnell, B., Lei, T. & Tomita, T. (2016) Histone modification as a drug resistance driver in brain tumors. Oncol Transl Med, (2), 216-26.

Xia, H., Avci, N. G., Akay, Y., Esquenazi, Y., Schmitt, L. H., Tandon, N., Zhu, J. & Akay, M. (2020) Temozolomide in combination with NF-κB inhibitor significantly disrupts the glioblastoma multiforme spheroid formation. IEEE Open Journal of Engineering in Medicine and Biology, 1 9-16.

Xu, H., Li, Z., Yu, Y., Sizdahkhani, S., Ho, W. S., Yin, F., Wang, L., Zhu, G., Zhang, M., Jiang, L., Zhuang, Z. & Qin, J. (2016) A dynamic *in vivo*-like organotypic blood-brain barrier model to probe metastatic brain tumors. Scientific Reports, 6 (1), 36670.

Xu, Y., Shi, T., Xu, A. & Zhang, L. (2016) 3D spheroid culture enhances survival and therapeutic capacities of MSCs injected into ischemic kidney. Journal of Cellular and Molecular Medicine, 20 (7), 1203-1213.

Xu-Welliver, M. & Pegg, A. E. (2002) Degradation of the alkylated form of the DNA repair protein, O6 -alkylguanine-DNA alkyltransferase. Carcinogenesis, 23 (5), 823-830.

Yamada, Y., Yoshida, C., Hamada, K., Kikkawa, Y. & Nomizu, M. (2020) Development of three-dimensional cell culture scaffolds using laminin peptide-conjugated agarose microgels. Biomacromolecules, 21 (9), 3765-3771.

Yan, H., Parsons, D. W., Jin, G., McLendon, R., Rasheed, B. A., Yuan, W., Kos, I., Batinic-Haberle, I., Jones, S., Riggins, G. J., Friedman, H., Friedman, A., Reardon, D., Herndon, J., Kinzler, K. W., Velculescu, V. E., Vogelstein, B. & Bigner, D. D. (2009) IDH1 and IDH2 mutations in gliomas. The New England Journal of Medicine, 360 (8), 765-773.

Yang, F., He, Z., Duan, H., Zhang, D., Li, J., Yang, H., Dorsey, J. F., Zou, W., Nabavizadeh, S. A., Bagley, S. J., Abdullah, K., Brem, S., Zhang, L., Xu, X., Byrne, K. T., Vonderheide, R. H., Gong, Y. & Fan, Y. (2021) Synergistic immunotherapy of glioblastoma by dual targeting of IL-6 and CD40. Nature Communications, 12 (1), 1-15.

Yang, J., Liu, M., Hong, D., Zeng, M. & Zhang, X. (2021) The paradoxical role of cellular senescence in cancer. Frontiers in Cell and Developmental Biology, 9 722205.

Yang, X., Li, K., Zhang, X., Liu, C., Guo, B., Wen, W. & Gao, X. (2018) Nanofiber membrane supported lung-on-a-chip microdevice for anti-cancer drug testing. Lab on a Chip, 18 (3), 486-495.

Yang, Y., Liu, X., Zheng, J., Xue, Y., Liu, L., Ma, J., Wang, P., Yang, C., Wang, D., Shao, L., Ruan, X. & Liu, Y. (2020) Interaction of BACH2 with FUS promotes malignant progression of glioma cells via the TSLNC8–miR-10b-5p–WWC3 pathway. Molecular Oncology, 14 (11), 2936-2959.

Yeung, Y. T., McDonald, K. L., Grewal, T. & Munoz, L. (2013) Interleukins in glioblastoma pathophysiology: Implications for therapy. British Journal of Pharmacology, 168 (3), 591-606.

Yip, S., Miao, J., Cahill, D. P., Iafrate, A. J., Aldape, K., Nutt, C. L. & Louis, D. N. (2009) MSH6 mutations arise in glioblastomas during temozolomide therapy and mediate

temozolomide resistance. Clinical Cancer Research: An Official Journal of the American Association for Cancer Research, 15 (14), 4622-4629.

Yoshida, J. (1996) Molecular neurosurgery using gene therapy to treat malignant glioma. Nagoya Journal of Medical Science, 59 (3-4), 97-105.

Yoshikawa, T., Uchimura, E., Kishi, M., Funeriu, D. P., Miyake, M. & Miyake, J. (2004) Transfection microarray of human mesenchymal stem cells and on-chip siRNA gene knockdown. Journal of Controlled Release: Official Journal of the Controlled Release Society, 96 (2), 227-232.

Yu, J., Yu, H., Yan, J., Wu, X., Yang, L., Dai, J., Ma, M., Tang, H., Xu, T., Chi, Z., Si, L., Sheng, X., Cui, C., Guo, J. & Kong, Y. (2018) Methylation of O6-methylguanine DNA methyltransferase promoter is a predictive biomarker in chinese melanoma patients treated with alkylating agents. Translational Cancer Research, 7 (3), 495-505.

Yu, Q. & Stamenković, I. (2004) Transforming growth factor-beta facilitates breast carcinoma metastasis by promoting tumor cell survival. Clinical & Experimental Metastasis, .

Yuan, A. L., Ricks, C. B., Bohm, A. K., Lun, X., Maxwell, L., Safdar, S., Bukhari, S., Gerber, A., Sayeed, W., Bering, E. A., Pedersen, H., Chan, J. A., Shen, Y., Marra, M., Kaplan, D. R., Mason, W., Goodman, L. D., Ezhilarasan, R., Kaufmann, A. B., Cabral, M., Robbins, S. M., Senger, D. L., Cahill, D. P., Sulman, E. P., Cairncross, J. G. & Blough, M. D. (2018) ABT-888 restores sensitivity in temozolomide resistant glioma cells and xenografts. Plos One, 13 (8), e0202860.

Yung, T. K. F., Chan, K. C. A., Mok, T. S. K., Tong, J., To, K. & Lo, Y. M. D. (2009) Single-molecule detection of epidermal growth factor receptor mutations in plasma by microfluidics digital PCR in non-small cell lung cancer patients. Clinical Cancer Research: An Official Journal of the American Association for Cancer Research, 15 (6), 2076-2084.

Yuste, J. E., Tarragon, E., Campuzano, C. M. & Ros-Bernal, F. (2015) Implications of glial nitric oxide in neurodegenerative diseases. Frontiers in Cellular Neuroscience, 9, 253254 .

Zagzag, D., Lukyanov, Y., Lan, L., Ali, M. A., Esencay, M., Mendez, O., Yee, H., Voura, E. B. & Newcomb, E. W. (2006) Hypoxia-inducible factor 1 and VEGF upregulate CXCR4 in glioblastoma: Implications for angiogenesis and glioma cell invasion. Laboratory Investigation; a Journal of Technical Methods and Pathology, 86 (12), 1221-1232.

Zahir-Jouzdani, F., Mottaghitalab, F., Dinarvand, M. & Atyabi, F. (2018) siRNA delivery for treatment of degenerative diseases, new hopes and challenges. Journal of Drug Delivery Science and Technology, 45 428-441.

Zaklina, S. and Christina Yamada, (2018), Dharmacon™ accell™ siRNA reagents:

Zhang, H., Liu, X., Li, T. & Han, X. (2014) Miscible organic solvents soak bonding method use in a PMMA multilayer microfluidic device.

Zhang, P., Xia, Q., Liu, L., Li, S. & Dong, L. (2020) Current opinion on molecular characterization for GBM classification in guiding clinical diagnosis, prognosis, and therapy. Frontiers in Molecular Biosciences, 7: 562798.

Zhang, W., Lin, S., Wang, C., Hu, J., Li, C., Zhuang, Z., Zhou, Y., Mathies, R. A. & Yang, C. J. (2009) PMMA/PDMS valves and pumps for disposable microfluidics. Lab on a Chip, 9 (21), 3088-3094.

Zhang, W., Zhang, J., Hoadley, K., Kushwaha, D., Ramakrishnan, V., Li, S., Kang, C., You, Y., Jiang, C., Song, S. W., Jiang, T. & Chen, C. C. (2012) miR-181d: A predictive

glioblastoma biomarker that downregulates MGMT expression. Neuro-Oncology, 14 (6), 712-719.

Zhang, Y. & Pardridge, W. M. (2001) Rapid transferrin efflux from brain to blood across the blood-brain barrier. Journal of Neurochemistry, 76 (5), 1597-1600.

Zhao, S., Ye, Z. & Stanton, R. (2020) Misuse of RPKM or TPM normalization when comparing across samples and sequencing protocols. Rna, 26 (8), 903-909.

Zhu, P., Du, X. L., Lu, G. & Zhu, J. (2017) Survival benefit of glioblastoma patients after FDA approval of temozolomide concomitant with radiation and bevacizumab: A population-based study. Oncotarget, 8 (27), 44015-44031.

Zhu, Z., Geng, Y., Yuan, Z., Ren, S., Liu, M., Meng, Z. & Pan, D. (2019) A bubble-free microfluidic device for easy-to-operate immobilization, culturing and monitoring of zebrafish embryos. Micromachines, 10 (3), .

Zhuang, Y., Grainger, J. M., Vedell, P. T., Yu, J., Moyer, A. M., Gao, H., Fan, X., Qin, S., Liu, D., Kalari, K. R., Goetz, M. P., Boughey, J. C., Weinshilboum, R. M. & Wang, L. (2021) Establishment and characterization of immortalized human breast cancer cell lines from breast cancer patient-derived xenografts (PDX). Npj Breast Cancer, 7 (1), 1-12.

Ziółkowska-Suchanek, I. (2021) Mimicking tumor hypoxia in non-small cell lung cancer employing three-dimensional in vitro models. Cells, 10 (1).

Zlokovic, B. V. (2008) The blood-brain barrier in health and chronic neurodegenerative disorders. Neuron, 57 (2), 178-201.

Zoetemelk, M., Rausch, M., Colin, D. J., Dormond, O. & Nowak-Sliwinska, P. (2019) Short-term 3D culture systems of various complexity for treatment optimization of colorectal carcinoma. Scientific Reports, 9 (1), 1-14.

Zou, P., Xu, H., Chen, P., Yan, Q., Zhao, L., Zhao, P. & Gu, A. (2013) IDH1/IDH2 mutations define the prognosis and molecular profiles of patients with gliomas: A meta-analysis. PloS One, 8 (7), e68782.

Appendix 1

1. Full Sequencing data error rate distribution for all samples

Trials	U87-pr	U87-po
1	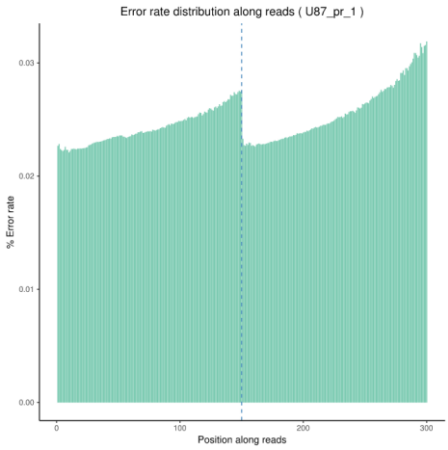	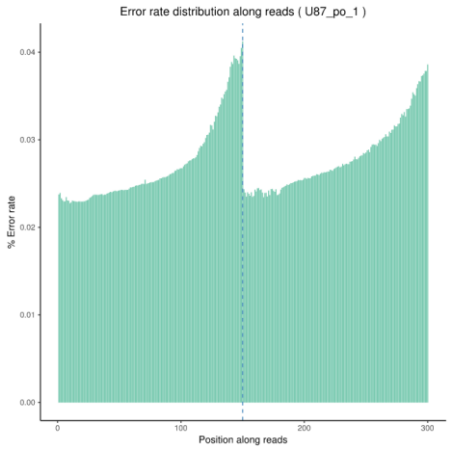
2	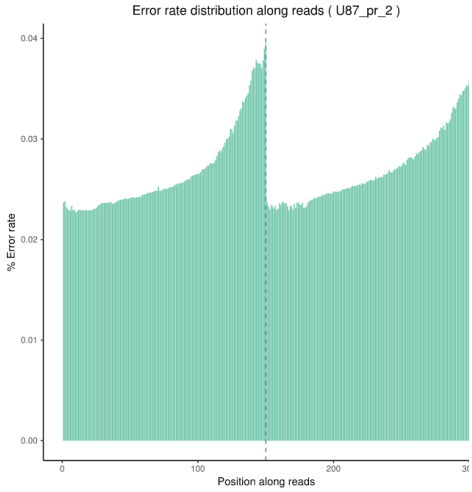	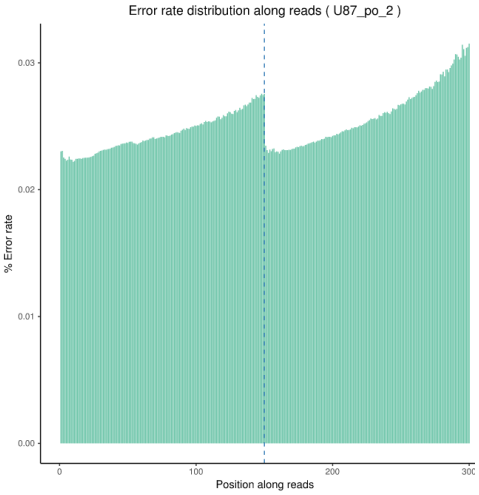

3

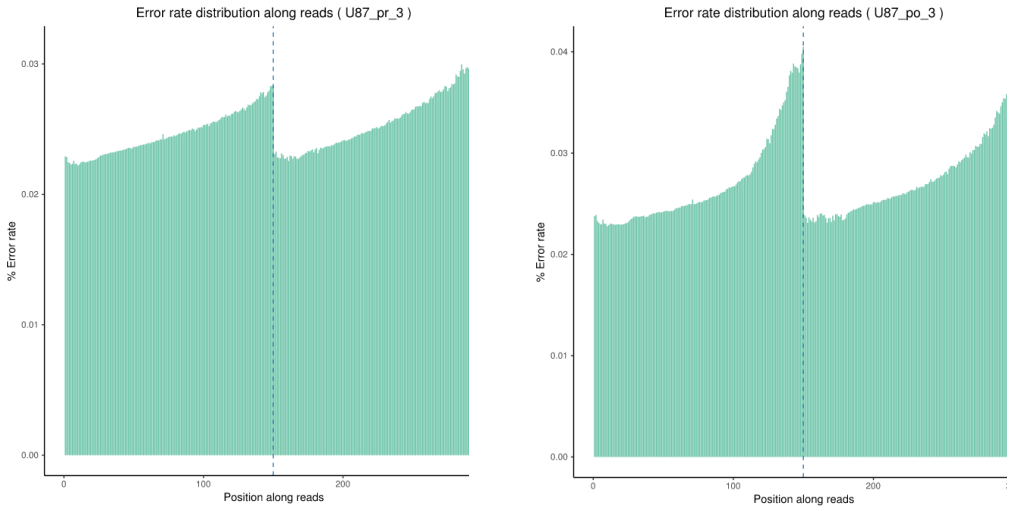

Figure 1 Sequencing data error rate distribution for U87 cell line. The x-axis shows the base position along with each sequencing read and the y-axis shows the base error rate. The left side of the vertical dashed line is for read 1, the right side is for read 2.

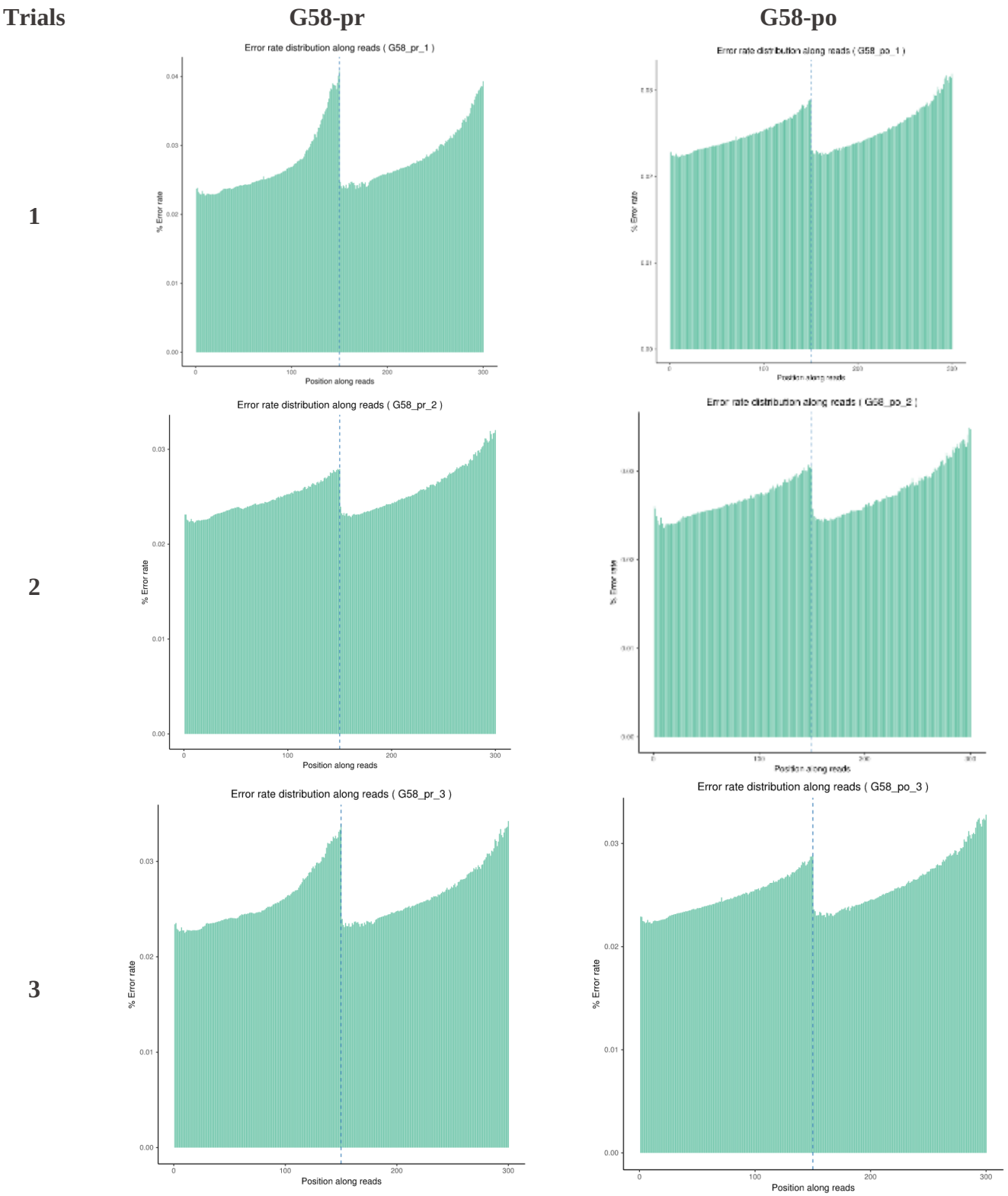

Figure 2 Sequencing data error rate distribution for G58 cell line. The x-axis shows the base position along with each sequencing read and the y-axis shows the base error rate. The left side of the vertical dashed line is for read 1, the right side is for read 2.

1

2

3

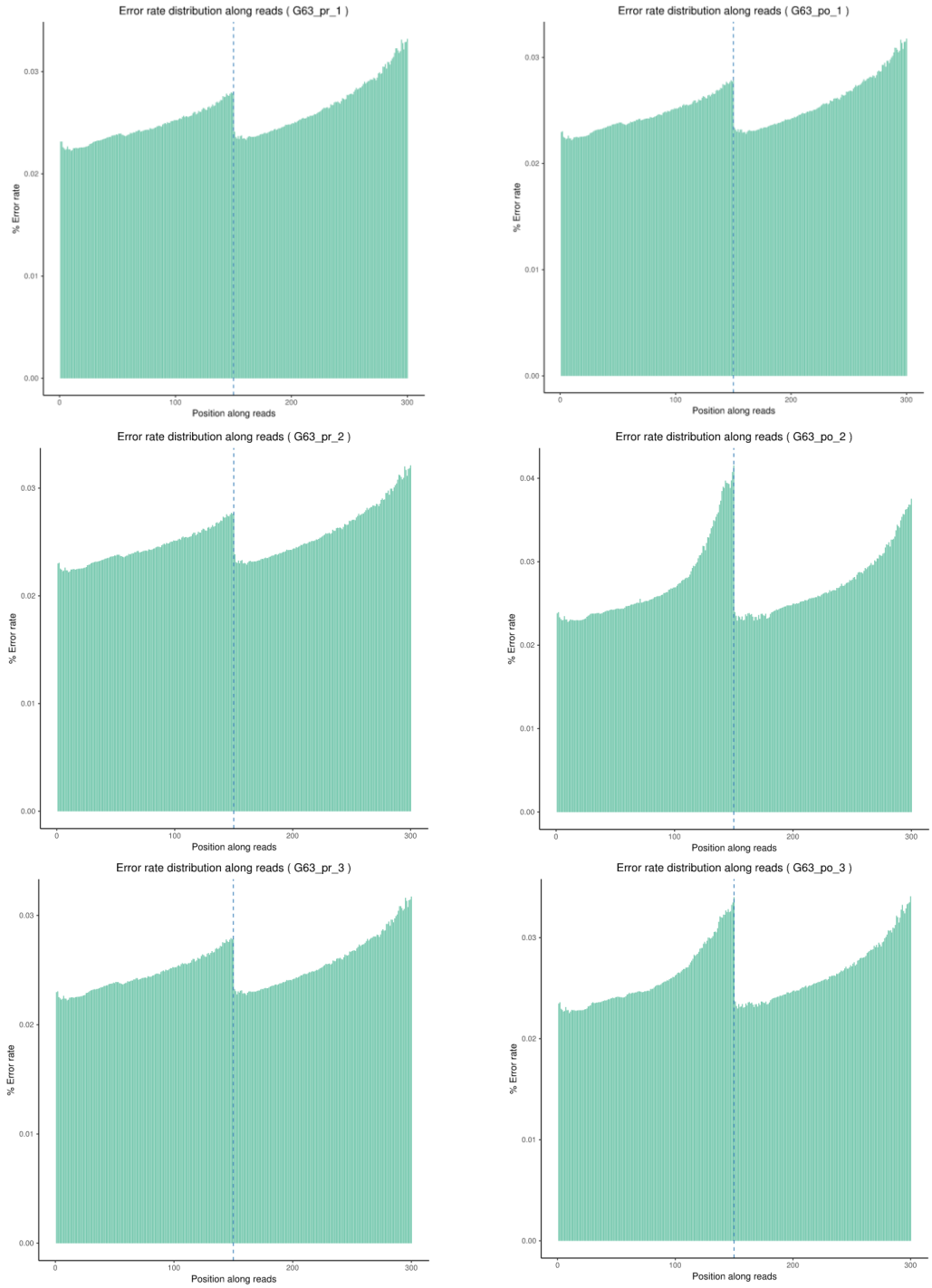

Figure 3 Sequencing data error rate distribution for G63 cell line. The x-axis shows the base position along with each sequencing read and the y-axis shows the base error rate. The left side of the vertical dashed line is for read 1, the right side is for read 2.

2. Full GC content distribution for all samples

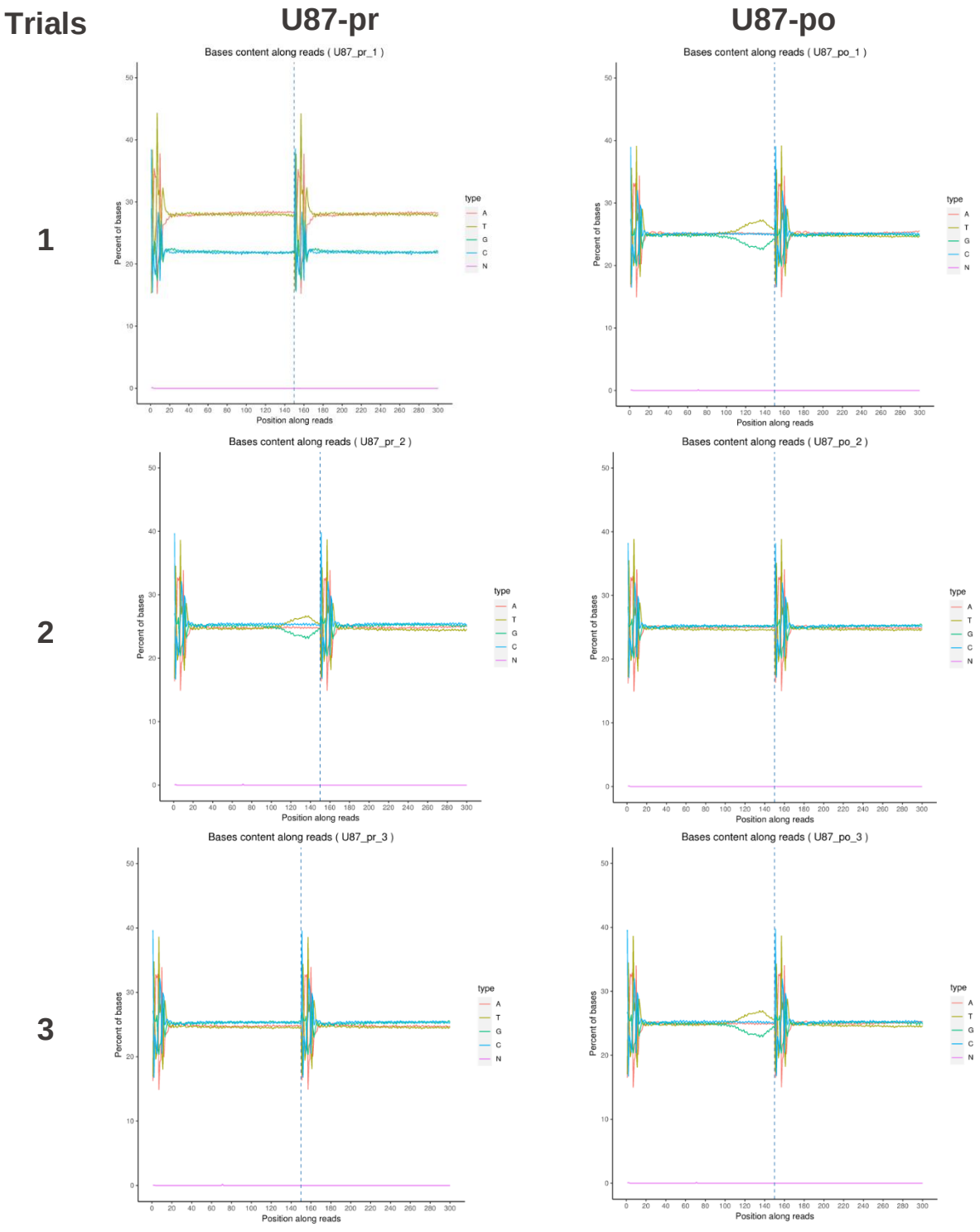

Figure 4 GC content distribution for U87 cell line The x-axis shows each base position within a read, and the y-axis shows the percentage of each base, with each base represented by a different colour. The left side of the vertical dashed line is the GC-content of read 1, the right side is the GC-content of read 2.

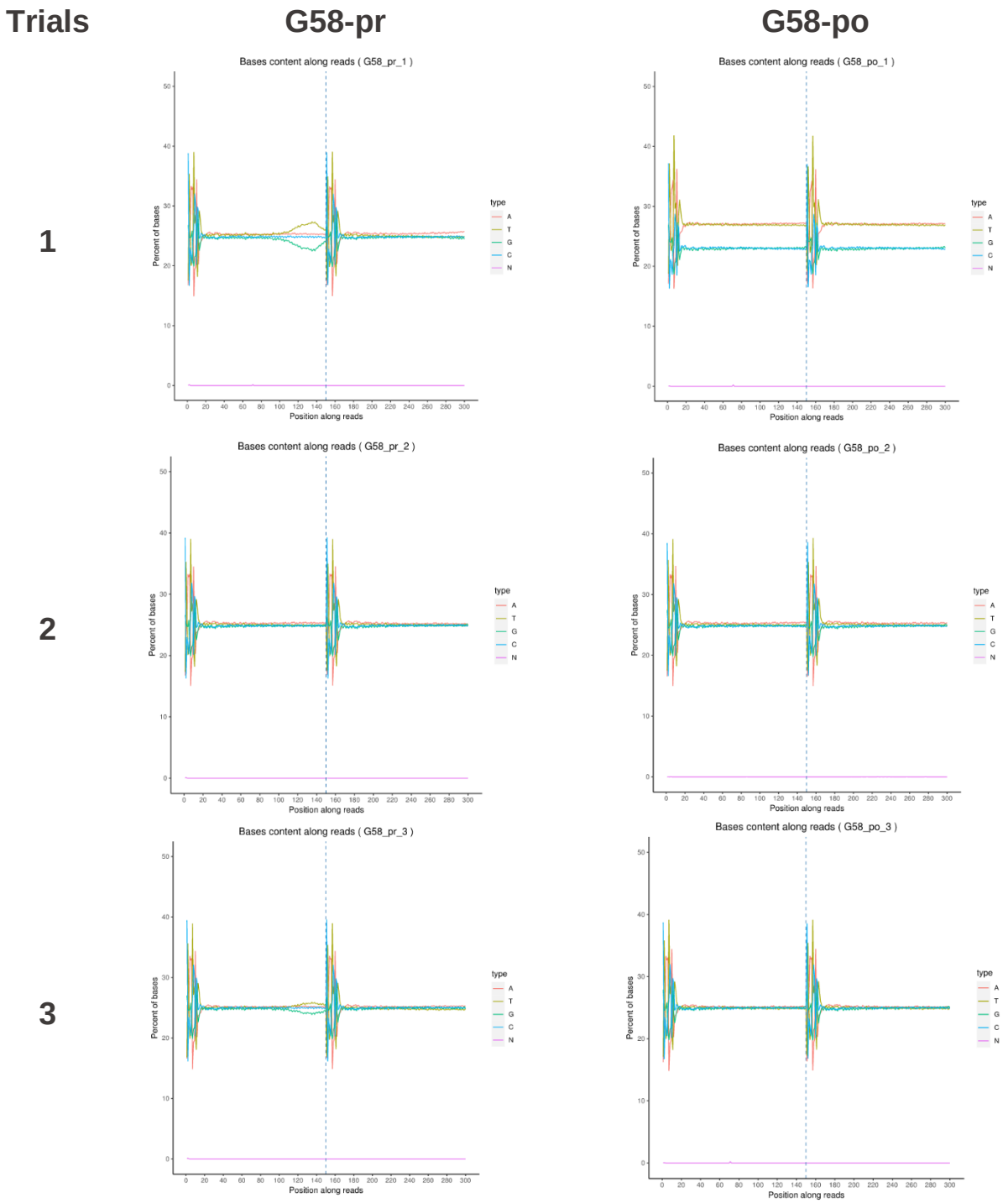

Figure 5 GC content distribution for G58 cell line The x-axis shows each base position within a read, and the y-axis shows the percentage of each base, with each base represented by a different colour. The left side of the vertical dashed line is the GC-content of read 1, the right side is the GC-content of read 2.

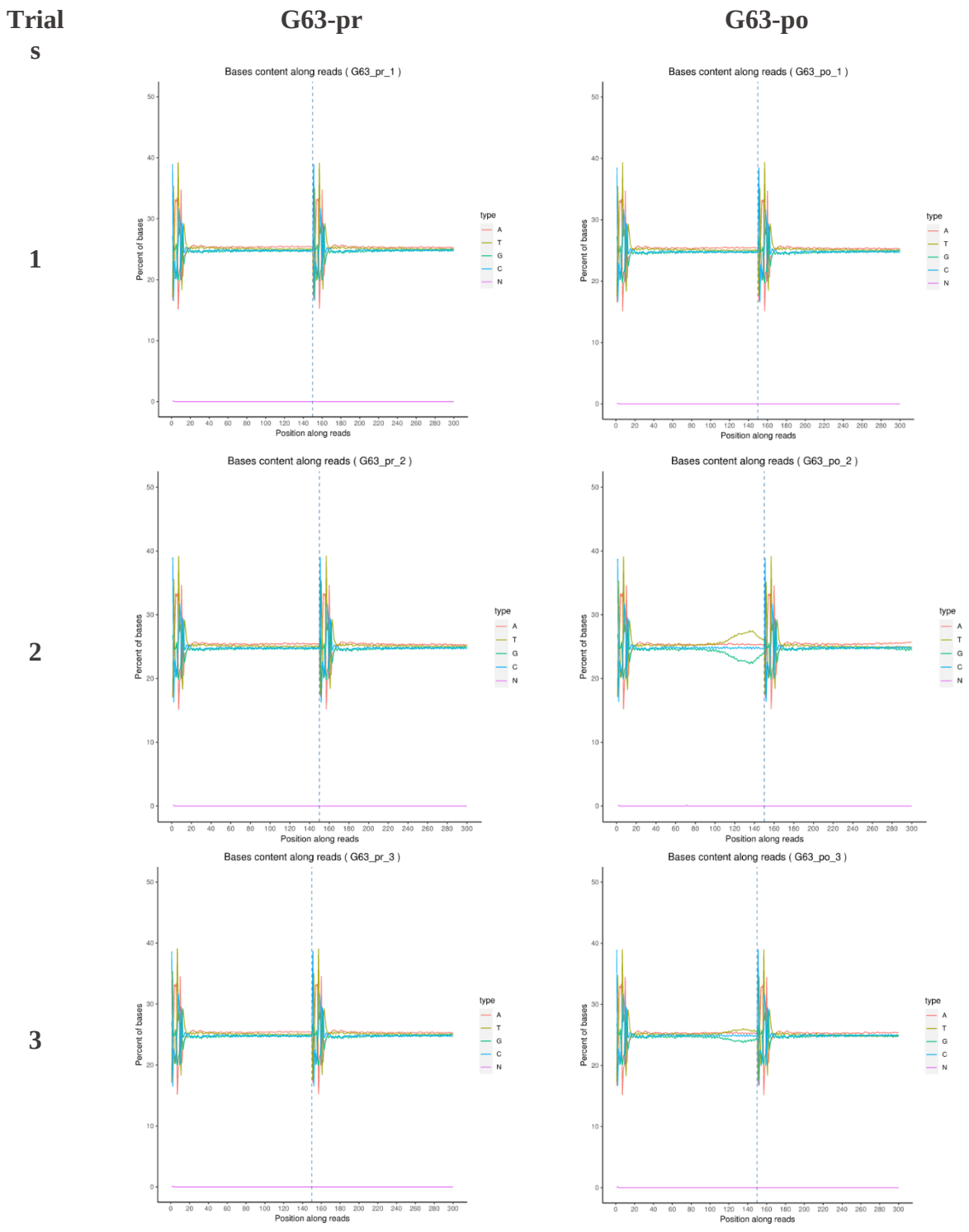

Figure 6 GC content distribution for G63 cell line The x-axis shows each base position within a read, and the y-axis shows the percentage of each base, with each base represented by a different colour. The left side of the vertical dashed line is the GC-content of read 1, the right side is the GC-content of read 2.

3. Full sample sequencing data filtering for all samples

Trials	U87-pr	U87-po
1	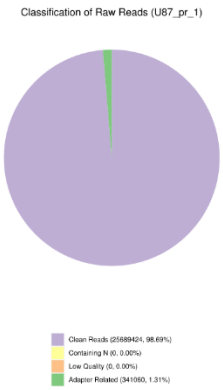	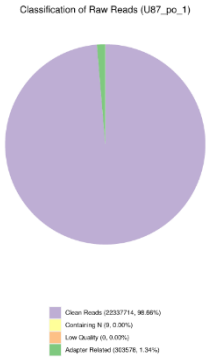
2	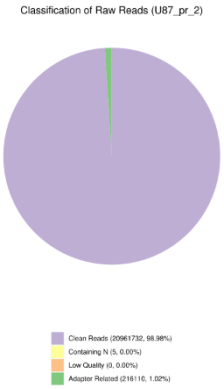	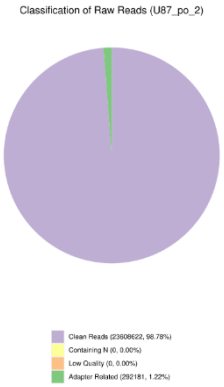
3	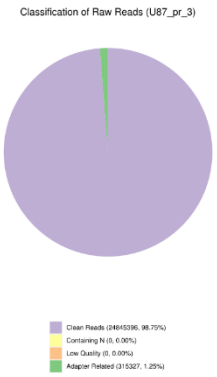	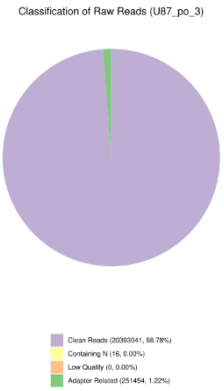

Figure 7 Sample Sequencing Data Filtering for U87 cell line Proportions of the different colours in the graph represent the proportion of different components. **Adapter related**: (reads containing adapter) / (total raw reads). **Containing N**: (reads with more than 10% N) / (total raw reads). **Low quality**: (reads of low quality) / (total raw reads). **Clean reads**: (clean reads) / (total raw reads).

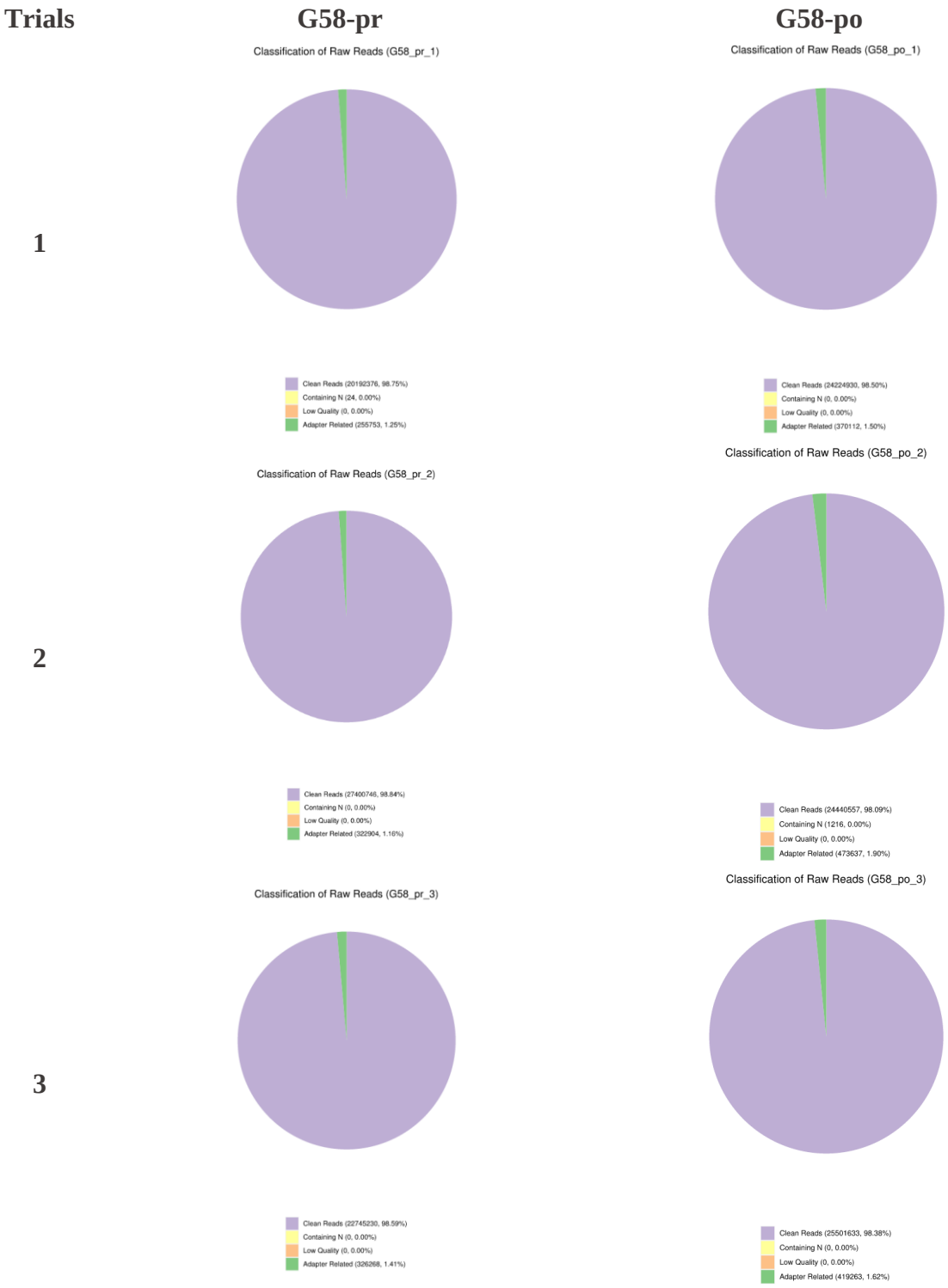

Figure 8 Sample Sequencing Data Filtering for G58 cell line. Proportions of the different colours in the graph represent the proportion of different components. **Adapter related**: (reads containing adapter) / (total raw reads). **Containing N**: (reads with more than 10% N) / (total raw reads). **Low quality**: (reads of low quality) / (total raw reads). **Clean reads**: (clean reads) / (total raw reads).

Trials	G63-pr	G63-po
1	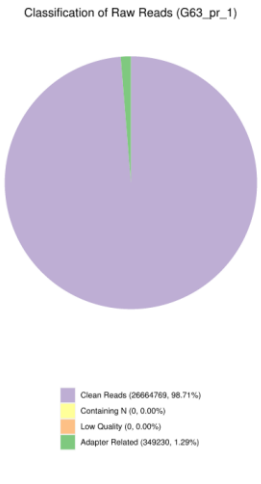	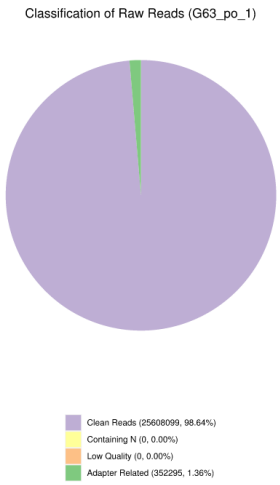
2	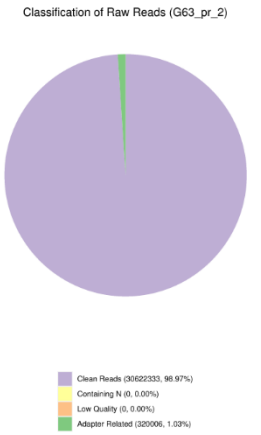	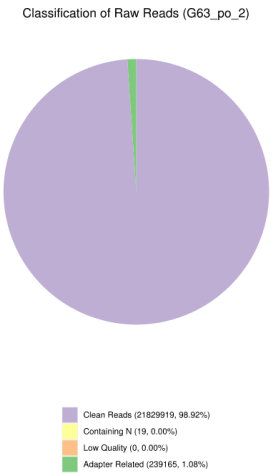
3	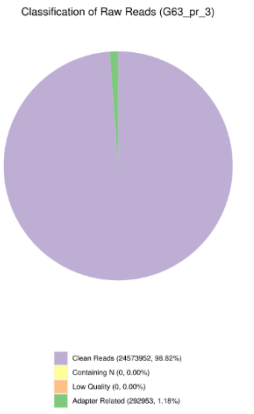	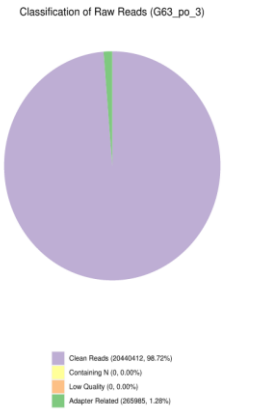

Figure 9 Sample Sequencing Data Filtering for G63 cell line. Proportions of the different colours in the graph represent the proportion of different components. Adapter related: (reads containing adapter) / (total raw reads). Containing N: (reads with more than 10% N) / (total raw reads). Low quality: (reads of low quality) / (total raw reads). Clean reads: (clean reads) / (total raw reads).

4. Full GC content distribution for all samples

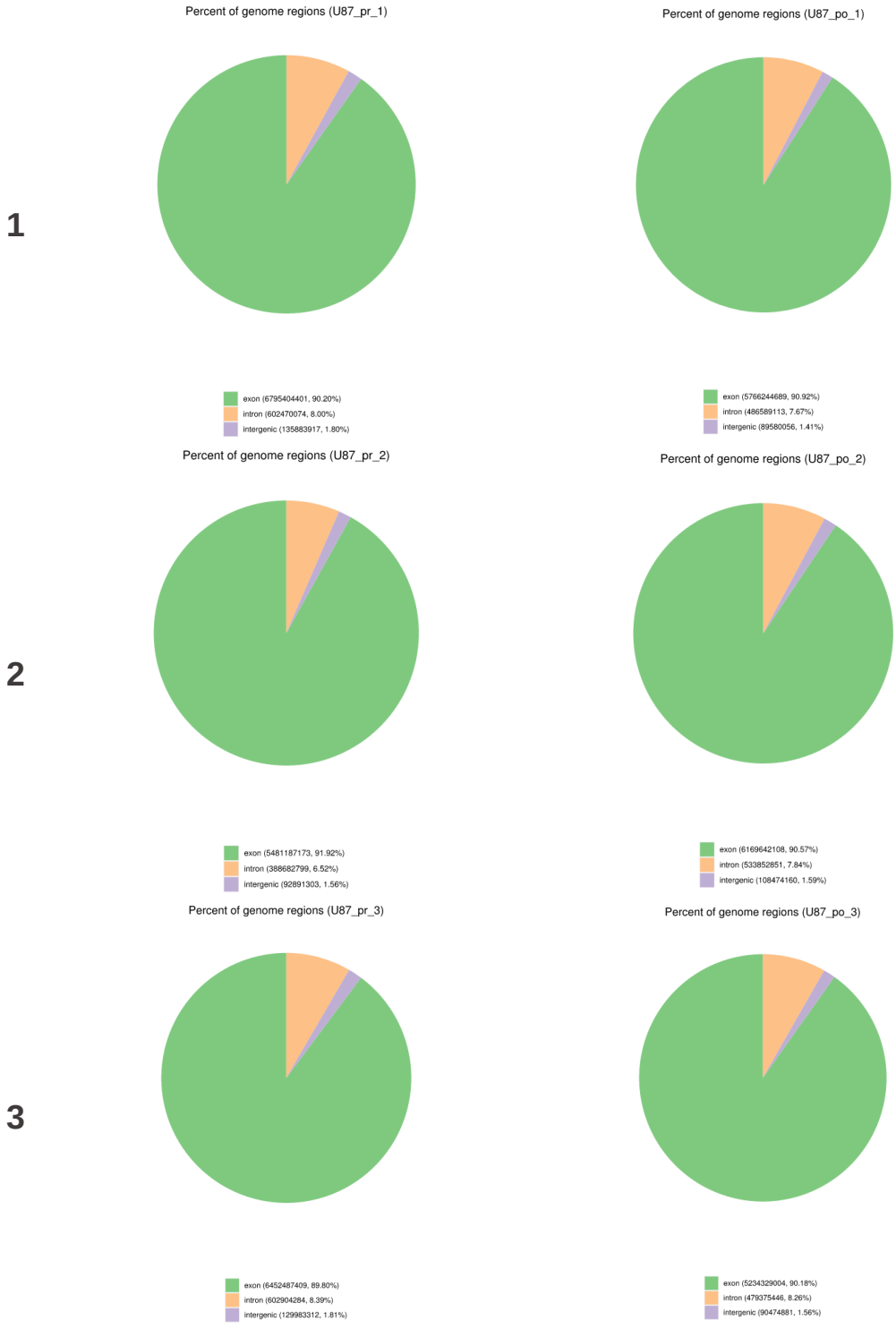

Figure 10 ratio of sequencing reads types in the genomic region for U87 cell line. The ratios of the different colours in the figure represent the ratio of reads to different regions**. Exon**: The number of reads aligned to exon regions of the genome and its proportion in clean reads. **Intron**: The number of reads aligned to intron regions of the genome and its proportion in clean reads. **Intergenic**: The number of reads aligned to intergenic regions of the genome and its proportion in clean reads.

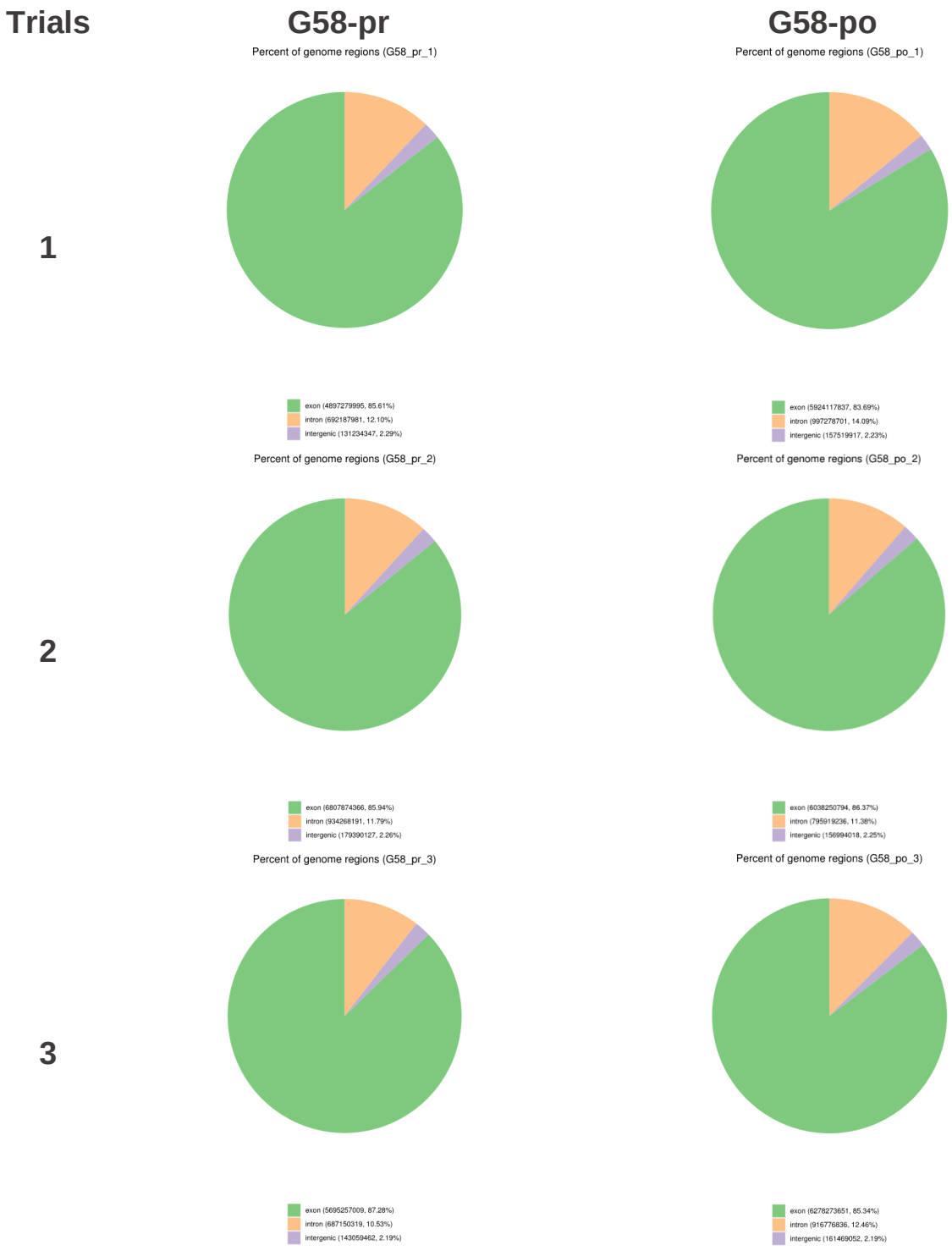

Figure 11 ratio of sequencing reads types in the genomic region for G58 cell line. The ratios of the different colours in the figure represent the ratio of reads to different regions**. Exon**: The number of reads aligned to exon regions of the genome and its proportion in clean reads. **Intron**: The number of reads aligned to intron regions of the genome and its proportion in clean reads. **Intergenic**: The number of reads aligned to intergenic regions of the genome and its proportion in clean reads.

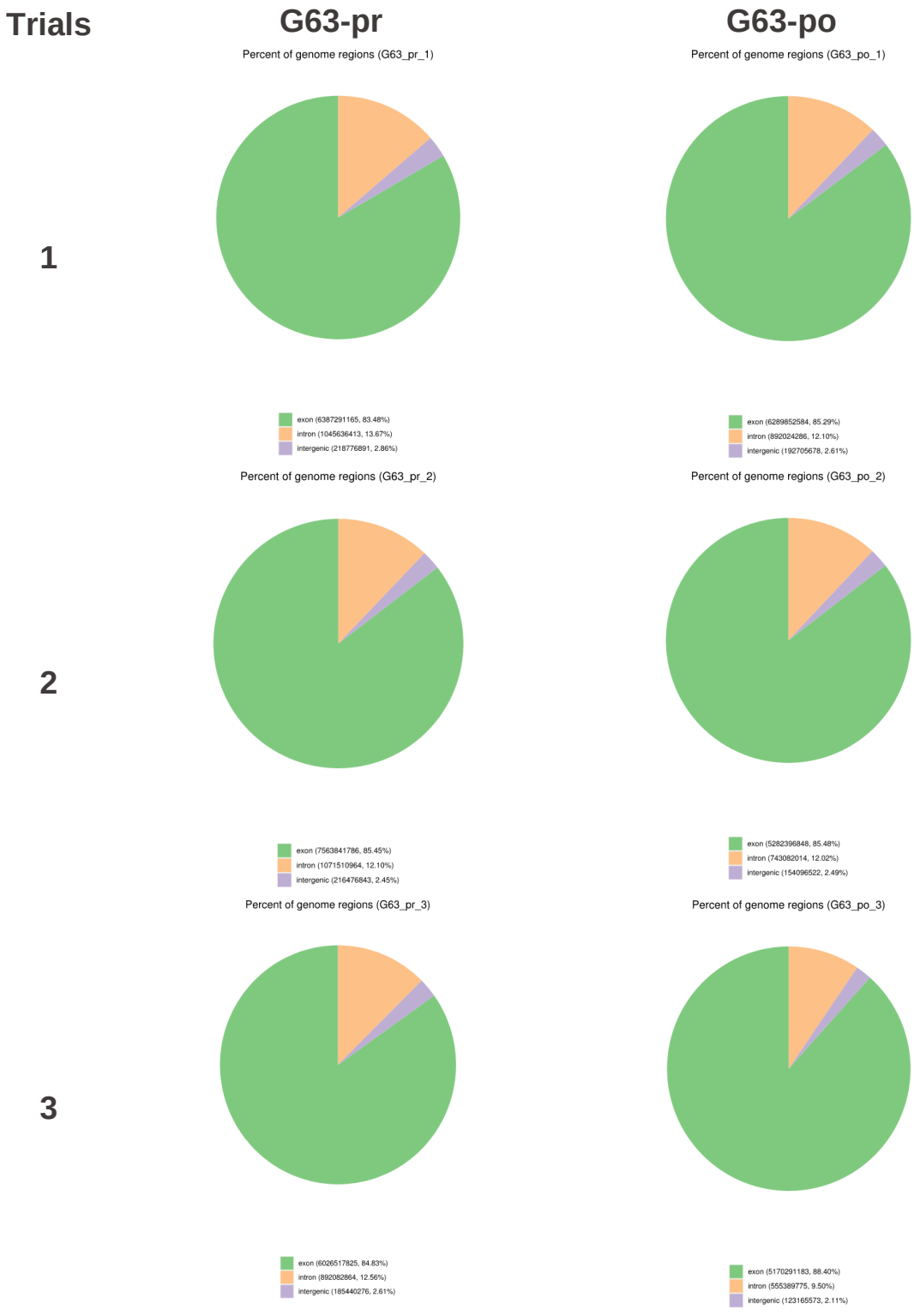

Figure 12 ratio of sequencing reads types in the genomic region for G63 cell line. The ratios of the different colours in the figure represent the ratio of reads to different regions**. Exon**: The number of reads aligned to exon regions of the genome and its proportion in clean reads. **Intron**: The number of reads aligned to intron regions of the genome and its proportion in clean reads. **Intergenic**: The number of reads aligned to intergenic regions of the genome and its proportion in clean reads.

Appendix 2

Table 1 Summary of quality control of RNA samples provided by Novogene

Sample Name	Nucleic Acid ID	Concentration(ng/ul)	Volume(ul)	Total amount(ug)	RIN	Sample QC Results
U87-pr-1	EKRN210015491-1A	380	15	5.7	9.5	Pass
U87-pr-2	EKRN210015492-1A	614	22	13.508	9.2	Pass
U87-pr-3	EKRN210015493-1A	448	18	8.064	9.3	Pass
U87-po-1	EKRN210015494-1A	465	19	8.835	9.4	Pass
U87-po-2	EKRN210015495-1A	482	21	10.122	9.3	Pass
U87-po-3	EKRN210015496-1A	626	24	15.024	9.1	Pass
G58-pr-1	EKRN210015497-1A	205	23	4.715	9.3	Pass
G58-pr-2	EKRN210015498-1A	130	26	3.38	9.3	Pass
G58-pr-3	EKRN210015499-1A	187	25	4.675	9.3	Pass
G58-po-1	EKRN210015500-1A	56	22	1.232	9.2	Pass
G58-po-2	EKRN210015501-1A	117	26	3.042	9.3	Pass
G58-po-3	EKRN210015502-1A	159	24	3.816	7	Pass
G63-pr-1	EKRN210015503-1A	129	18	2.322	9.4	Pass
G63-pr-2	EKRN210015504-1A	38	8	0.304	9.6	Hold*
G63-pr-3	EKRN210015505-1A	75	24	1.8	8.8	Pass
G63-po-1	EKRN210015506-1A	40	18	0.72	8.6	Pass
G63-po-2	EKRN210015507-1A	111	21	2.331	9.3	Pass
G63-po-3	EKRN210015508-1A	105	20	2.1	9.3	Pass

*For **G63-pr-2** sample a second Quality control check was done and the sample passed it successfully

Table 2 Summary of sample and reference genome comparisons.

sample	total_reads	total_map	unique_map	multi_map	positive_map	negative_map	proper_map
U87_pr_1	51378848	50298684(97.9%)	49202073(95.76%)	1096611(2.13%)	24592287(47.86%)	24609786(47.9%)	48325754(94.06%)
U87_po_1	44675428	42390527(94.89%)	41459873(92.8%)	930654(2.08%)	20679289(46.29%)	20780584(46.51%)	40045512(89.64%)
U87_pr_2	41923464	39846617(95.05%)	38929941(92.86%)	916676(2.19%)	19427781(46.34%)	19502160(46.52%)	37715308(89.96%)
U87_po_2	47217244	45498173(96.36%)	44442405(94.12%)	1055768(2.24%)	22203901(47.02%)	22238504(47.1%)	43411088(91.94%)
U87_pr_3	49690792	47992752(96.58%)	46853030(94.29%)	1139722(2.29%)	23408902(47.11%)	23444128(47.18%)	45811090(92.19%)
U87_po_3	40786082	38790415(95.11%)	37943530(93.03%)	846885(2.08%)	18930234(46.41%)	19013296(46.62%)	36700710(89.98%)
G58_pr_1	40384752	38235724(94.68%)	37361619(92.51%)	874105(2.16%)	18634671(46.14%)	18726948(46.37%)	36028280(89.21%)
G58_po_1	48449860	47273813(97.57%)	46184762(95.32%)	1089051(2.25%)	23077455(47.63%)	23107307(47.69%)	45256888(93.41%)
G58_pr_2	54801492	52913515(96.55%)	51643391(94.24%)	1270124(2.32%)	25797546(47.07%)	25845845(47.16%)	50379456(91.93%)
G58_po_2	48881114	46716687(95.57%)	45553862(93.19%)	1162825(2.38%)	22749526(46.54%)	22804336(46.65%)	44216870(90.46%)
G58_pr_3	45490460	43598909(95.84%)	42556197(93.55%)	1042712(2.29%)	21243125(46.7%)	21313072(46.85%)	41304230(90.8%)
G58_po_3	51003266	49144383(96.36%)	47958313(94.03%)	1186070(2.33%)	23960250(46.98%)	23998063(47.05%)	46727636(91.62%)
G63_pr_1	53329538	51117956(95.85%)	49829571(93.44%)	1288385(2.42%)	24889744(46.67%)	24939827(46.77%)	48498196(90.94%)
G63_po_1	51216198	49263830(96.19%)	48065002(93.85%)	1198828(2.34%)	24011353(46.88%)	24053649(46.96%)	46854542(91.48%)
G63_pr_2	61244666	59125729(96.54%)	57710685(94.23%)	1415044(2.31%)	28830466(47.07%)	28880219(47.16%)	56282970(91.9%)
G63_po_2	43659838	41302888(94.6%)	40338322(92.39%)	964566(2.21%)	20122288(46.09%)	20216034(46.3%)	38924010(89.15%)
G63_pr_3	49147904	47455825(96.56%)	46311127(94.23%)	1144698(2.33%)	23131488(47.07%)	23179639(47.16%)	45145882(91.86%)
63_po_3	40880824	39078534(95.59%)	38157056(93.34%)	921478(2.25%)	19050755(46.6%)	19106301(46.74%)	37043830(90.61%)

Table 3: most enriched up-regulated KEGG pathways in G58 and G63 showing the enrichment of ferroptosis and necroptosis pathways

G58			
Rank	**Gene description**	**GeneRatio**	**padj**
17	Transcriptional misregulation in cancer	36/661	3.70E-05
18	Pathways in cancer	78/661	3.95E-05
23	Ferroptosis	13/661	0.000122
27	Viral carcinogenesis	34/661	0.00025
28	Small cell lung cancer	21/661	0.000285
31	Necroptosis	26/661	0.002394

G63			
Rank	**Gene description**	**GeneRatio**	**padj**
12	Ferroptosis	9/433	0.001334
13	Synaptic vesicle cycle	11/433	0.001337
14	mTOR signaling pathway	18/433	0.007072
15	Pathogenic Escherichia coli infection	9/433	0.007545
16	p53 signaling pathway	11/433	0.009012
17	Thyroid cancer	7/433	0.010486
18	Fluid shear stress and atherosclerosis	16/433	0.015907

Rank: rank among the most enriched pathways

Appendix 3

Table 1 Top 10 up regulated DEGs expressed by U87 cell line cultured in microfluidic system vs those cultured in 3D static model.

log2Fold Change	padj	Gene_ name	Gene _chr	Gene_ biotype	Gene_description
3.125171	1.65E-27	LCP1	13	gene_biotype	Lymphocyte cytosolic protein 1
4.068218	6.36E-27	LINC02392	12	protein_coding	Long intergenic non-protein coding RNA 2392
3.573153	8.72E-18	AC005077.4	7	lincRNA	Hypothetical protein LOC285908 (LOC285908) pseudogene
2.917758	9.77E-18	RPLP0P2	11	Processed pseudogene	Ribosomal protein lateral stalk subunit P0 pseudogene 2
2.456538	4.80E-17	TCF7	5	transcribed_ processed pseudogene	Transcription factor 7
2.050031	1.50E-15	NOV	8	protein_coding	Nephroblastoma overexpressed
3.342713	4.32E-14	CRYM	16	protein_coding	Crystallin mu
2.267075	5.13E-14	PNLIPRP3	10	protein_coding	Pancreatic lipase related protein 3
3.491114	6.81E-13	FOLR3	11	protein_coding	Folate receptor 3
1.991428	1.62E-12	NOCT	4	protein_coding	Nocturnin

Table 2 Top 10 down regulated DEGs expressed by U87 cell line cultured in microfluidic system vs those cultured in 3D static model.

log2FoldChange	padj	gene_name	Gene _chr	gene_biotype	gene_description
-3.59641	7.25E-27	HLA-DRA	6	protein_coding	Major histocompatibility complex, class II, DR alpha
-3.99419	9.53E-26	HLA-DQA1	6	protein_coding	Major histocompatibility complex, class II, DQ alpha 1
-3.89081	9.86E-20	SLC14A1	18	protein_coding	Solute carrier family 14 member 1 (Kidd blood group)
-2.5387	3.12E-19	CD74	5	protein_coding	CD74 molecule
-2.06116	2.15E-15	HLA-DPA1	6	protein_coding	Major histocompatibility complex, class II, DP alpha 1
-2.09802	2.15E-15	TMEM132B	12	protein_coding	Transmembrane protein 132B
-3.066	4.67E-14	CHRDL1	X	protein_coding	Chordin like 1
-2.46741	4.69E-14	EREG	4	protein_coding	Epiregulin
-1.85873	1.90E-13	SERPINA1	14	protein_coding	Serpin family A member 1
-1.98656	1.86E-12	SPARC	5	protein_coding	Secreted protein acidic and cysteine rich

Table 3 Top 10 up regulated DEGs expressed by G58 cell line cultured in microfluidic system vs those cultured in 3D static model.

log2FoldChange	padj	gene_name	gene_chr	gene_biotype	gene_description
1.615551	1.61E-08	NPTX1	17	protein_coding	Neuronal pentraxin 1
1.41151	1.61E-08	TFRC	3	protein_coding	Transferrin receptor
1.428234	1.56E-06	SERPINE1	7	protein_coding	Serpin family E member 1
1.480181	2.28E-06	ETS2	21	protein_coding	ETS proto-oncogene 2, transcription factor
4.287175	2.93E-06	C15orf48	15	protein_coding	Chromosome 15 open reading frame 48
2.684659	2.99E-06	AC016831.6	7	lincRNA	Novel transcript
3.630081	6.10E-06	GBP5	1	protein_coding	Guanylate binding protein 5
1.56856	7.81E-06	NQO1	16	protein_coding	NAD(P)H quinone dehydrogenase 1
1.709418	5.36E-05	FTH1P7	13	processed_pseudogene	Ferritin heavy chain 1 pseudogene 7
1.906299	8.76E-05	NOCT	4	protein_coding	Nocturnin

Table 4 Top 10 down regulated DEGs expressed by G58 cell line cultured in microfluidic system vs those cultured in 3D static model.

log2FoldChange	padj	gene_name	Gene_chr	gene_biotype	gene_description
-1.58624	1.56E-06	TMEM176A	7	protein_coding	Transmembrane protein 176A
-1.55269	1.56E-06	LINC01105	2	processed_transcript	Long intergenic non-protein coding RNA 1105
-2.05035	1.56E-06	AP004608.1	11	processed_transcript	uncharacterized LOC283177
-1.31828	2.28E-06	CLEC18B	16	protein_coding	C-type lectin domain family 18 member B
-1.3927	2.28E-06	TMEM176B	7	protein_coding	Transmembrane protein 176B
-1.24773	8.47E-06	CSMD1	8	protein_coding	CUB and Sushi multiple domains 1
-0.88311	1.82E-05	AEBP1	7	protein_coding	AE binding protein 1
-1.30023	3.07E-05	HOPX	4	protein_coding	HOP homeobox
-1.19796	3.86E-05	SSPO	7	protein_coding	SCO-spondin
-0.80772	4.19E-05	TXNIP	1	protein_coding	Thioredoxin interacting protein

Table 5 Top 10 up regulated DEGs expressed by G63 cell line cultured in microfluidic system vs those cultured in 3D static model.

log2FoldChange	padj	Gene_name	Gene_chr	Gene_biotype	Gene_description
1.816055	3.73E-23	SLC7A11	4	protein_coding	Solute carrier family 7-member 11
1.844362	6.46E-19	NQO1	16	protein_coding	NAD(P)H quinone dehydrogenase 1
1.518169	6.57E-15	OSGIN1	16	protein_coding	Oxidative stress induced growth inhibitor 1
2.801816	6.83E-09	RFPL1S	22	antisense	RFPL1 antisense RNA 1
1.29252	7.95E-07	NMRAL2P	3	transcribed_ unprocessed_pseudogene	NmrA like redox sensor 2, pseudogene
0.987813	1.23E-06	TXNRD1	12	protein_coding	Thioredoxin reductase 1
0.995276	3.87E-06	SLC1A5	19	protein_coding	Solute carrier family 1 member 5
1.379285	5.15E-06	THBS1	15	protein_coding	Thrombospondin 1
0.79537	5.43E-06	SQSTM1	5	protein_coding	Sequestosome 1
0.754022	1.70E-05	ODC1	2	protein_coding	Ornithine decarboxylase 1

Table 6 Top 10 down regulated DEGs expressed by G63 cell line cultured in microfluidic system vs those cultured in 3D static model.

log2FoldChange	padj	Gene_name	Gene_chr	Gene_biotype	Gene_description
-1.39757	6.83E-09	FAM181B	11	protein_coding	Family with sequence similarity 181 member B
-1.02957	2.68E-07	CHI3L1	1	protein_coding	Chitinase 3 like 1
-0.87422	4.52E-07	GAD1	2	protein_coding	Glutamate decarboxylase 1
-1.25069	2.94E-06	FAM131B	7	protein_coding	Family with sequence similarity 131 member B
-1.05818	5.46E-06	ASTN1	1	protein_coding	Astrotactin 1
-1.21781	1.44E-05	DPP6	7	protein_coding	Dipeptidyl peptidase like 6
-1.13455	1.49E-05	AC092645.1	2	TEC	TEC
-1.38725	1.62E-05	SSPO	7	protein_coding	SCO-spondin
-1.33756	1.62E-05	HOPX	4	protein_coding	HOP homeobox
-0.77083	3.21E-05	TARBP1	1	protein_coding	TAR (HIV-1) RNA binding protein 1

log2FoldChange: The ratio of gene expression level between the treatment group and the control group of a comparison combination was processed by the shrinkage model of the differential analysis software, and finally the logarithm was taken with 2 as the base.
pvalue: Pvalue in hypergenometric test of compare group.
padj: The corrected pvalue of multiple hypothesis test of compare group.
gene_name: gene name.
gene_chr: The name of the chromosome where the gene is located.
gene_biotype: Gene type,such as coding protein genes,long non-coding genes,etc.
gene_description: Gene description.